CIVIL ENGINEERING STUDIES

STRUCTURAL RESEARCH SERIES NO. 268

A MODEL TO SIMULATE THE RESPONSE OF CONCRETE TO MULTI-AXIAL LOADING

by

HEDLEY E. H. ROY

METE A. SOZEN

UNIVERSITY OF ILLINOIS

URBANA, ILLINOIS

JUNE, 1963

A MODEL TO SIMULATE THE RESPONSE OF CONCRETE TO MULTI-AXIAL LOADING

by

Hedley E. H. Roy

and

Mete A. Sozen

University of Illinois

Urbana, Illinois

June 1963

TABLE OF CONTENTS

TABLE OF CONTENTS (Cont'd)

LIST OF TABLES

LIST OF FIGURES

LIST OF FIGURES (Cont'd)

LIST OF FIGURES (Cont'd)

LIST OF FIGURES (Cont'd)

LIST OF FIGURES (Cont'd)

LIST OF FIGURES (Cont'd)

LIST OF FIGURES (Cont'd)

1. INTRODUCTION

1.1 Object

The object of the thesis is twofold: to develop a theoretical explanation of some of the phenomena observed in tests of concrete under different stress conditions; and to present the results of a test program which was conducted on a series of axially-loaded prisms with longitudinal and transverse reinforcement.

The theory which was developed gave a good representation of the behavior of unconfined concrete throughout the entire range of the load-deflection curve. Accordingly, it was possible to explain the factors responsible for the failure of concrete under this type of loading condition. In addition, the theory was extended to the case of confined compression to illustrate the effect of different types of confinement.

1.2 Outline of Studies

(a) Theory

Following a review of some of the existing theories of failure which have been applied to concrete, a description is given of the development of a model which is assumed to be representative of the structure of cement paste. The basic unit of the resulting model consists of non-deforming spheres, cubically arranged, and interconnected by elastic struts. Based on observations of the beha .or of concrete, load-strain relations for the component struts of the model are derived, and the behavior of the resulting matrix is then studied.

The first loading condition which is investigated is that of unconfined compression of concrete. The proposed model is subjected to continuously increasing compressive strain and the resulting load-strain relations are derived and compared with those obtained from tests of concrete. Observations about the behavior of concrete, which are implied by that of the model, are discussed.

In a similar manner, the model is subjected to axial compression and simultaneous uniform lateral confining pressure. The behavior of the model is compared with that of concrete tested under triaxial compression, and the theoretical results are projected to practical conditions after a consideration of the structure of concrete.

Finally, the model is applied to the case of axially-loaded concrete which is confined laterally by means of rectangular transverse reinforcement. Since this type of reinforcement produces nonuniform transverse pressure, the theoretical solution is obtained by investigating a network of struts, formed by stacking a number of the individual cubes together to form the total structure.

The results for the condition of uniform lateral confinement are compared with those for the condition of rectangular transverse reinforcement, and the reasons for the differences between these two cases are discussed.

(b) Experimental Investigation

A description is given of a series of tests conducted on square, axially-loaded columns confined by rectangular ties. A total of 60 specimens were tested, all of which had dimensions of 5 by 5 by 25 in., and nominal concrete strength of 3000 psi. The series included 15 plain concrete prisms as control specimens, and the volumetric ratio of the transverse reinforcement in the remaining 45 specimens was kept constant at 0.02.

The variables used in the tests were the spacing and stiffness of the transverse reinforcement, and the amount and stiffness of longitudinal reinforcement.

1.3 Acknowledgments

The work described in this report was carried out in the Structural Research Laboratory of the Department of Civil Engineering, University of Illinois.

The tests were made as part of a research project on moment-rotation characteristics of reinforced concrete members sponsored by the Portland Cement Association.

This report is based on a doctoral dissertation prepared by H. E. H. Roy, Fellow in Civil Engineering, under the direction of Dr. M. A. Sozen, Associate Professor of Civil Engineering.

2. FAILURE THEORIES

2.1 Introductory Remarks

In order to draw intelligent conclusions from test results and in order to project these results beyond the limitations of the test conditions, it is necessary to have a theory of failure for the material concerned. In Section 2.2, a brief discussion is presented of the observed load-deformation characteristics of concrete. A number of theories have been developed to explain various facets of the observed phenomena, but they have been found to have, at best, a limited application. In the following sections, some of these theories will be outlined and their limitations discussed. Particular attention will be given to the theory proposed by Erling Reinius (1)* since it appears to agree quite closely with the structure and many aspects of the behavior of concrete.

2.2 Stress-Strain Relationships for Concrete

(a) Unconfined Concrete

Figure 2.1 shows typical load-strain relations for unconfined normal weight aggregate concrete subjected to axial compression (2). The strain at maximum load usually ranges from 0.0015 to 0.0025. For strains less than that at maximum load, the curve can be approximated by a parabola. Special testing equipment is required to obtain the portion of the curve beyond peak load, since there is a sudden release in energy after the maximum load is reached.

---

* Numbers in parentheses refer to entries in the list of references.

(b) Confined Concrete

An extensive test program was conducted by Richart, Brandtzaeg and Brown (3) to study the behavior of concrete under combined compressive stress. Some of their results are summarized in Fig. 2.2. They found that lateral confining pressures produce an increase in strength and also in deformation at and beyond peak load.

The equation derived by the authors expressing the strength of concrete under triaxial compression is

$$f_1 = f'_c + 4.1\ f_2 \tag{2.1}$$

where f_1 = strength of confined concrete

f'_c = strength of unconfined concrete

f_2 = confining pressure

(c) Spirally Reinforced Concrete

Richart, Brandtzaeg and Brown (4) also tested a series of columns reinforced with spiral steel. They found that the concrete enclosed by the spiral behaves similarly to that subjected to lateral confining pressure, and that Eq. 2.1 could also be used to determine the strength of these spirally reinforced columns. The value of f_2 was determined by assuming that the lateral force induced in the spiral was equivalent to a lateral pressure uniformly distributed across the diameter.

(d) Columns with Rectilinear Lateral Reinforcement

Tests carried out by Szulczynski (5) on rectangular columns reinforced with separate (rectangular) ties showed that this type of reinforcement also produces some increase in strength and considerable increase in ductility. Figures 2.3 and 2.4 summarize some of the results obtained in these tests. In these graphs, curves 1 refer to plain concrete specimens, curves 2 to specimens with No.2 ties at 2-in. spacing and curves 3 to specimens with No. 3 ties at 2-in. spacing.

The variables used were amount of lateral reinforcement, strength of concrete and shape of cross section. The proposed equation of the strength of rectangularly-tied columns was

$$f_1 = f''_c + 1.8\ f_2 \tag{2.2}$$

where f_1 = unit strength in compression

f''_c = unit strength of prism without reinforcement

f_2 = lateral confining pressure,

determined as the average stress across a line joining the mid-point of two adjacent sides.

2.3 Review of Concrete Failure Theories

A number of authors (1,3,6) have presented summaries and critical analyses of failure theories which are applicable to concrete under various stress conditions. Usually, these theories are concerned with predicting the value of the maximum stress which concrete can withstand under some loading condition. Very little emphasis is given to the behavior of the material up to and beyond maximum load.

The stress-strain curves shown in Fig. 2.1 represent an important aspect of the behavior of concrete, since unconfined compression is the most basic stress condition to which concrete can be subjected. Reinius (1) succeeded in deriving the portion of the unconfined compression curves up to maximum load. However, it would be very desirable to have a means of predicting these stress-strain curves for strains beyond maximum load, since the behavior in this region is an inherent characteristic of concrete.

The maximum stress and maximum strain theories are based on the assumption that failure is dependent on stresses or strains in one principal direction only. However, tests have shown that the strength of concrete is a function of the loading conditions in all three principal directions. The results of the tests by Richart, Brandtzaeg and Brown (3) illustrate this fact very clearly. The maximum strain theory may be applied to cases in which one of the stresses is considerably greater than the others. In reinforced concrete beams, for example, failure in flexure is said to take place when the strain at the extreme fiber in compression reaches a limiting value. In general, however, this theory cannot be applied to concrete.

Various authors have proposed maximum energy theories. Examples of theories of this type are the total energy theory, proposed by Beltrami and Haigh; the energy of distortion theory, introduced by Huber, von Mises and Hencky; and the theory of Tresca. The maximum energy theories assume that the material has a distinct yield point, and so apply mainly to ductile materials, and cannot be used for concrete.

Griffith (7) derived a theory of failure for brittle materials, based on tests of glass. His theory was derived for the condition of an infinite brittle body, stretched by a uniform stress at infinity. He assumed that this body contained at least one small crack, and that this crack would propagate when the rate of release of strain energy, due to the formation of the crack, was equal to the rate of absorption of energy in the formation of new surfaces. Griffith's theory is based on the behavior of the material at the microscopic level, and so is difficult to apply to relatively large specimens with nonuniform stress distributions.

Shear or sliding failure theories have been applied quite extensively to concrete. These theories assume that failure takes place by sliding along some critical plane. The most general of the shear failure theories is Mohr's theory, which states that the shearing stress and simultaneous normal stress on the sliding plane satisfy a given relationship. Mohr's theory may be expressed by the equation

$$\tau = f(\sigma) \qquad (2.3)$$

where τ = the shearing stress at failure

σ = the normal stress on the plane of sliding

Coulomb's theory is a particular case of Mohr's theory, and assumes that the relation between τ and σ is linear.

All the shear failure theories are based on the same general assumption, which is that failure is dependent on the major and minor principal stresses, and is independent of the intermediate principal stress. However, some experiments have produced results which conflict with this assumption to a certain extent.

Karman (8) and Böker (9) conducted tests on marble in which the intermediate stress was varied. They tested cylinders subjected to small lateral pressures ($\sigma_2 = \sigma_3$) and large end pressures (σ_1), thus producing a small value of the intermediate principal stress; and they also subjected cylinders to large lateral pressures and small end pressures, producing a high intermediate stress.

The resulting Mohr's circle envelopes for the failure of these specimens are shown in Fig. 2.5. The solid curve is the failure envelope for the condition of high intermediate stress, and the broken curve is that for the condition of low intermediate stress.

It can be seen from Fig. 2.5 that variations in the intermediate principal stress produced strength differences of approximately ten percent. On the basis of these results, Böker (9) concluded that Mohr's theory was invalidated, and that the intermediate stress should not be disregarded.

Reinius (1) tested concrete prisms under combined axial compression and one-directional lateral confining pressure. The confining pressures ranged up to 15 percent of the axial pressure. The resulting strength increase was approximately equal to the magnitude of the lateral pressure, and hence the strength was dependent on the intermediate principal stress.

The results of these tests, and others conducted by Wåstlund (10), and Bellamy (11), imply that Mohr's theory is not correct. However, the influence of the intermediate principal stress is not sufficiently great to be critical for applications to concrete.

A drawback of Mohr's theory is that in some instances, as in the case of columns confined by rectangular ties, one or more of the principal stresses may vary over the cross section, and may also be difficult or even impossible to determine.

Brandtzaeg (3) developed a theory based on the assumption that concrete is composed of a number of nonisotropic elements, each of which has a fixed failure plane along which sliding failure may occur. In addition to the possibility of a plastic sliding failure, it is assumed that the material may fail by splitting whenever the tensile stress in any direction reaches a limiting value σ_t. Hence, Brandtzaeg's theory states that failure is caused by simultaneous "splitting" and "disorganizing" effects, the former being of primary importance. The presence of an external lateral restraint replaces much of the lateral tension in the elastic elements. Brandtzaeg's theory is applicable only up to the point at which splitting failure occurs.

2.4 Bresler and Pister

Many investigators have noted that all three principal stresses are important for the condition of failure. This fact is taken into account in the octahedral shearing stress theory, which is equivalent to the energy of distortion theory and so subject to the same limitations. The octahedral shearing stress is determined by the equation

$$\tau_o = \frac{1}{3}\left[(\sigma_1-\sigma_2)^2 + (\sigma_2-\sigma_3)^2 + (\sigma_3-\sigma_1)^2\right]^{1/2} \qquad (2.4)$$

where σ_1, σ_2 and σ_3 are the three principal stresses.

Bresler and Pister (12) developed a theory using stress invariants rather than principal stresses. The three stress invariants I_1, I_2 and I_3 are defined as follows:

$$\begin{aligned} I_1 &= \sigma_1 + \sigma_2 + \sigma_3 \\ I_2 &= \sigma_1\sigma_2 + \sigma_2\sigma_3 + \sigma_3\sigma_1 \\ I_3 &= \sigma_1\sigma_2\sigma_3 \end{aligned} \qquad (2.5)$$

In formulating their theory, they made use of a "mean normal stress" σ_a and "mean shearing stress" τ_a, developed by Novozhilov and obtained as follows.

Considering an infinitesimal spherical element of unit volume, the state of stress at any point on the surface can be expressed in terms of a shearing stress τ_s and a normal stress σ_s. The "mean stresses" are obtained by averaging these stresses over the spherical surface

$$\text{i.e.} \quad \sigma_a = \text{Lim}_{s\to 0} \frac{1}{S}\int_s \sigma_s \, ds$$

$$\tau_a = \text{Lim}_{s\to 0} \left[\frac{1}{S}\int_s \tau_s^{\,2} \, ds\right]^{1/2} \qquad (2.6)$$

which leads to

$$\sigma_a = \frac{1}{3}\,(\sigma_1+\sigma_2+\sigma_3) = \frac{1}{3}\, I_1$$

$$\tau_a = \frac{1}{\sqrt{15}}\left[(\sigma_1-\sigma_2)^2 + (\sigma_2-\sigma_3)^2 + (\sigma_3-\sigma_1)^2\right]^{1/2} \qquad (2.7)$$

$$= \sqrt{\frac{2}{15}}\,(I_1^{\,2}-3I_2)^{1/2}$$

It can be seen that the "mean shearing stress" is equal to a constant times the octahedral shearing stress. The "mean stresses" do not contain the third stress invariant I_3, but Novozhilov has shown that its effect is almost negligible.

Bresler and Pister carried out tests on hollow concrete cylinders subjected to various combinations of torsion and axial load. They attempted to interpret their data by two trial functions involving σ_a and τ_a as follows:

a linear function

$$\frac{\tau_a}{f'_c} = A_1 + B_1\left(\frac{\sigma_a}{f'_c}\right) \qquad (2.8)$$

and a quadratic function

$$\frac{\tau_a}{f'_c} = A_2 + B_2\left(\frac{\sigma_a}{f'_c}\right) + C_2\left(\frac{\sigma_a}{f'_c}\right)^2 \qquad (2.9)$$

The coefficients A_1, B_1, A_2, B_2 and C_2 were obtained empirically from the test results, and depended on the size of test specimen.

In an effort to test the validity of this theory, Oran (13), tried to apply it to the results of the tests by Richart, Brandtzaeg and Brown (3), Series 2, 3A and 3B. The results are shown in Fig. 2.6, and Eqs. 2.8 and 2.9, developed by Bresler and Pister, have been plotted on the same graph for comparison.

Figure 2.6 illustrates that the theory by Bresler and Pister is not able to represent faithfully the phenomena observed over the whole range of the tests by Richart et al. Not only do the specific curves derived by Bresler and Pister fail to agree with the test results, but also each series of tests produces a different curve, which suggests that the parameters σ_a/f'_c and τ_a/f'_c cannot properly be applied to the tests.

2.5 McHenry and Karni

McHenry and Karni (14) carried out tests on 91 hollow cylinders which were 24 in. high and had 14-in. outside diameters and 10-in. inside diameters. The specimens were subjected to a combination of internal pressure and axial compression. The maximum tensile stress produced by the internal pressure was between 7 and 12 percent of the compressive strength of the cylinders.

The general trend of the results was that either stress produced a reduction in the maximum value of the other stress. The very approximate relation between the stresses which was mentioned by the authors was that when either stress was at a value of 50 percent of the strength for that stress alone, the other stress was reduced by 50 percent.

The authors attempted to analyze the results in a manner similar to that of Bresler and Pister (12). They plotted the relationship between the octahedral normal stress and the octahedral shearing stress at failure, and found it to be essentially linear, except near conditions of simple compressive and simple tensile stresses.

No single relationship between the octahedral stresses could be applied to the whole range of the tests. This fact, together with the data presented in Fig. 2.6, results in the conclusion that failure theories which are dependent on a relation between the octahedral stresses, or similar parameters, are invalid for concrete.

2.6 Reinius

Studies of the structure of cement paste indicate (15,16) that it is composed of cement particles in various stages of hydration, interconnected by cement "gel," a porous substance containing solid, needle-like crystals. The crystals are microscopic in size and are randomly-oriented. Based on this information, Reinius (1) developed a model which he assumed to be representative of the structure of concrete, and by means of which he was able to explain some of the observed properties of concrete.

(a) The Model

Figure 2.7 shows a diagram of the Reinius model. It consists of a number of identical spheres (analogous to the unhydrated cement grains in cement paste) arranged in a body-centered cubic. The basic unit is a cube with a sphere at each corner and one in the center. The center-to-center spacing of the spheres in closest proximity to each other is assumed to be a distance a; hence the length of one side of the cube is $2a/\sqrt{3}$.

The spheres are interconnected by a number of rods, analogous to the needle-like crystals in the gel. The rods are homogeneous, elastic, have a constant modulus of elasticity, and are capable of carrying both tensile and compressive forces. They are attached to the spheres by means of pinned connections.

It is assumed that the bonds between spheres of spacing a can carry transverse as well as longitudinal stresses. Accordingly, they are represented by four rods intersecting at point A. Each rod is assumed to have length ℓ_4 and area A_4. Two of the rods, AB and AC, lie in the vertical plane passing through the centers of the spheres. The other two rods, AD and AE, lie in a plane also passing through the centers of the spheres, but perpendicular to plane ABC. The angle of inclination of the rods is denoted by β as indicated in Fig. 2.7.

It is further assumed that the bonds between spheres of spacing $2a/\sqrt{3}$ cannot carry transverse stresses. Hence, they are represented by single rods. These rods have lengths ℓ_1, ℓ_2 and ℓ_3 and areas A_1, A_2 and A_3, and carry forces P_1, P_2 and P_3 in the x, y and z directions, respectively.

The area of a face of the cube is considered to be unity. Hence, external pressures of intensity P_x, P_y and P_z, in the directions of the corresponding principal axes, can be represented by forces P_x, P_y and P_z acting on each sphere in the appropriate external face of the structure. Similarly, forces P_1, P_2 and P_3 represent internal pressures in the x, y, and z directions, respectively.

Reinius proportioned the areas and lengths of the rods, together with angle β, so as to obtain a value of approximately 0.15 for Poisson's ratio, ν, under unrestrained loading in one direction. The results are:

$$A_1 = A_2 = A_3 = 4A_4$$
$$\ell_1 = \ell_2 = \ell_3 = 1.5\ell_4 \quad (2.10)$$
$$\beta = 55^\circ$$
$$\nu = 0.144$$

Reinius next determined the forces in each rod when the structure is subjected to uniaxial pressure P_x, P_y or P_z and is unrestrained in the other two directions. The results are summarized in Table 1. The sign convention used is that compression is positive and tension negative.

The effect of unrestrained loading can be seen more readily by referring to the two-dimensional model shown in Fig. 2.8a. Under the action of force F, vertical strut PS and diagonal struts PQ and PR will be subjected to compressive stresses. In order to maintain static equilibrium, strut QR must then go into tension. The force in strut QR corresponds to forces P_1 and P_2 in the Reinius model under pressure P_z, while the force in PS corresponds to P_3 and forces PQ or PR correspond to the system of forces P_{AB}, P_{AC}, P_{AD} and P_{AE}.

(b) Theory of Failure

When concrete cubes or cylinders are tested under compression, failure is accompanied by tension cracks which are usually parallel to the direction of loading. Rupture and cracking can be attributed to the failure of the cement crystals under tension or of the bond between these crystals and the aggregate or cement particles.

It seems probable that when concrete is loaded, the weakest tension crystals will break first, and in so doing will subject other compression crystals to increased stress. This process can be illustrated by the use of

Fig. 2.8b. If strut QR breaks, the total force F must then be carried by strut PS and hence additional load is transferred to the system of struts STUV. As the load is increased, the next weakest crystals, or their bonds, will fail. Thus, the number of tension failures and the transverse expansion will be accelerated with increasing load.

If failure in tension is prevented, rupture of the concrete will occur as a result of failure of the crystals under compression.

In explaining the failure phenomenon by means of the Reinius model, the behavior of the whole concrete mass can be studied by considering a single cube. As can be seen from Table 1, under unrestrained loading P_z, rods 1, 2 and AB (Fig. 2.7) are subjected to approximately equal tensile stresses, since areas A_1 and A_2 are equal to $4A_4$. The failure of various tensile crystals throughout the structure can be simulated by reducing the area of rods 1, 2 and AB as the load is increased, while keeping the rod lengths, the modulus of elasticity E and the angle β constant.

Reinius first assumed that as the tensile crystals break, the compression crystals can withstand the resulting increased stress without failing. The resulting rod stresses and deformations are given in Table 2 for tension rod areas equal to 1.0, 0.75, 0.50, 0.25, and 0.10 times their original values.

In order to relate rod areas to the magnitude of P_z, Reinius selected relative values of P_z so that the resulting curve for transverse deformation vs load was similar to that obtained from the tests of Richart, Brandtzaeg and Brown (4). The results obtained by this means are shown by the solid curves in Fig. 2.9.

Reinius noted that at high compressive stresses, the theoretical
ere much less than the corresponding test results. He reasoned
difference was due to the fact that some compression crystals
aking before complete tension failure occurred in the transverse
. Since rod 3 is the most highly-stressed compression rod in the
assumed that it reduced in area at the same rate as the tension
le the remaining compression rods remained unchanged. The results
lculations are given in Table 3, and the derived stress-strain
e the broken curves shown in Fig. 2.9. These curves agree quite
with test results.

Explanation of Observed Phenomena

Using the model and failure theory outlined above, Reinius
several properties of concrete which have been observed in test
For the most part these explanations were qualitative.

Various experimenters have observed that if concrete is subjected
ted loading, the maximum load in each case being nearly as great as
ngth of the specimen, the unloading curves have considerable curvature
e reloading curve is nearly linear up to a high percentage of peak
typical graph of stress vs strain for repeated loading of a concrete
is shown in Fig. 2.10. It should be noted that the initial tangent
ecrease with each successive loading, but in each case are greater
secant modulus of the previous peak load.

The Reinius theory would seem to imply that both unloading and
g curves would be linear and would follow the initial loading secant

modulus line. However, Reinius explained the observed effect by postulating that during unloading, crystals which had previously broken in compression now carry tension, with a resulting nonlinear unloading curve. Upon reloading, less crystals are effective than in the initial curve, hence the modulus of elasticity is less. The linear reloading curve is due to the fact that the majority of the effective crystals are those which were not broken during the initial loading.

Another concrete property explained by Reinius is the occurrence of oblique fracture surfaces during compression tests. Reinius suggested that these failure surfaces initiate at a cavity on the lateral surface. The presence of the cavity causes the horizontal tension members to begin breaking in a diagonal line through the specimen.

Reinius also made tests on 51 prisms loaded to failure while lateral pressures of up to 15 percent of the axial pressure were applied in one direction only. He found that the increase in strength was on the order of the magnitude of lateral pressure. The explanation given for this strength increase was that a rearrangement of the rod stresses takes place in the model. Reinius tabulated rod stresses for a model with $P_y = 0.5\ P_z$, and $P_x = 0$. He made arbitrary assumptions for the new rod areas under this loading, and found that besides the expected reduction in stress for the horizontal members in the y-direction, there was also a decrease in the tensions in the x-direction.

In a similar manner, the fact that concrete under three-dimensional compression has greater strength than under one-dimensional compression can be explained by the resulting reduction in tensile stresses. In spiral columns, for example, if the spiral reinforcement is sufficiently strong, failure in lateral tension can be prevented completely. Rupture thus results from a failure of the compression crystals.

Reinius made another series of tests on concrete cubes which had a precompression applied in the y-direction. After removal of this stress, the cubes were loaded to failure in the z-direction. He found that the modulus of elasticity for these cubes was lower than for similar cubes with no preloading. Also ϵ_x was less, and ϵ_y was greater than the transverse deformation of cubes with no lateral precompression.

Reinius' explanation for these results was that when P_y is applied, more failures take place in the y-direction than in the x- and z-directions. Hence, the effective area is less in the y-direction, giving greater ϵ_y values.

(d) Observations Concerning the Reinius Theory

Reinius has made an important contribution to plain and reinforced concrete technology. His model and failure theory are based on observations of the structure and behavior of concrete and provide an explanation for many concrete properties.

Unfortunately, the Reinius theory possesses some limitations. In the first place there is an inconsistency regarding the failure theory of compression rods. As the rods break with increasing load, a greater percentage of P_z is transferred to the three diagonal compression members, particularly rod AC. Thus, these three rods carry a greater proportion of a greater load; however, the failure theory assumes that these rods do not break.

Tests of plain concrete have shown that at strains beyond maximum load there is a gradual decrease in load with considerable increase in strain. However, the Reinius theory would produce only the increasing portion of the load-strain curve, with no explanation for the behavior beyond maximum load.

Another limitation of the Reinius theory is in its explanation of the effect of confining pressure on the strength and deformation of concrete. In tests by Richart, Brandtzaeg and Brown (3), for example, strains as high as 0.06 and stresses as great as 24,600 psi were obtained for confined concrete.

In attempting to explain the effect of confining pressure by means of the Reinius model, it is more convenient to consider strain as the independent variable rather than load. Since the struts are assumed to have constant modulus of elasticity, the relation of strut area to magnitude of load could also be considered as a relation between strut area and strain. To obtain the load-strain curve for unconfined concrete, Reinius assumed that the area of the vertical struts (rods 3) was almost zero at maximum load and that the maximum load occurred at a vertical strain, ϵ_z, of approximately 0.002. Hence, in order to be consistent, the same reduction in area must be assumed at this strain regardless of the magnitude of confining pressure. It is obvious, therefore, that these vertical struts are completely ineffectual at the high strains obtained in tests of confined concrete.

A similar observation can be made with respect to increase in strength due to confinement. The vertical pressure is the sum of the stresses in the vertical struts and the vertical component of the stresses in the diagonal struts. As has already been pointed out, since the vertical struts are virtually ineffective at high strains, the total load must therefore be carried by the diagonal struts.

The only way these difficulties can be resolved using the Reinius model is by assuming that the diagonal struts are capable of withstanding almost limitless strain and almost infinite stress. However, this explanation is inconsistent with the assumptions made concerning the behavior of the vertical struts.

2.5 Baker

Baker (16) developed a two-dimensional lattice by means of which he studied some of the properties of concrete. A diagram of the lattice is shown in Fig. 2.11.

Baker assumed that the arrangement of the aggregate in concrete causes the formation of structural rings, which transmit load around the enclosed mortar. The deformation of these rings under the action of external pressure induces tension in the mortar, perpendicular to the direction of the applied pressure. Square ABCD in Fig. 2.11 represents a typical unit of the concrete structure. The diagonal members AB, AC, BD and CD are assumed to be analogous to a structural ring, which is subjected to compressive stresses as a result of the applied pressure p. Member BC is stressed in tension to maintain equilibrium, and accordingly represents the tensile stress in the mortar. The vertical shortening of the model induces compression in member AD, analogous to the direct compressive stresses in mortar.

The modulus of elasticity of the rings is assumed to be greater than that of the mortar, since the former are composed to a large extent of densely-packed aggregate, more or less in contact.

Baker suggested that lattices similar to that shown in Fig. 2.11 may be developed on a smaller scale, owing to transfer of pressure between sand grains, and that microscopic lattices may also be formed by the particles of cement grout. However, he concluded that the governing influence in concrete as a whole must be the stresses developed by pressure spanning the voids between the stones, and that the compressive strength of concrete is primarily a function of the tensile strength of the mortar.

Baker investigated the behavior of an elastic model similar to the diagram shown in Fig. 2.11. The model was constructed of draper's elastic, and the areas of the diagonal members were half that of the horizontal and vertical members. The lattice was given an initial prestress, to prevent any members from becoming compressed during tests.

The model was subjected to loads equivalent to external pressure in concrete, and the effect of end restraint on the behavior of the members was studied. In addition, a study was made of the formation of cracks in concrete, and their influence on the force distribution among the lattice members. This model investigation supported the previous conclusion that tensile forces are of primary importance in the compressive strength of concrete.

3. DEVELOPMENT OF A NEW FAILURE THEORY

3.1 Introductory Remarks

The development of a theory to describe the behavior of concrete under various conditions of loading is described in this chapter. The basic concept of the Reinius model, that is, a lattice of struts representing the needle-like crystals of the cement gel, seemed to be a logical basis on which to formulate a failure theory, since this concept agrees favorably with the observed structure of concrete.

One of the disadvantages of the Reinius model is that it is rather complicated to work with, because of the complex arrangement of the diagonal struts. Also, the model provides very little resistance to torsion in comparison to its direct shear resistance. Accordingly, some modification to the Reinius model is desirable. In addition, the failure theory should be such that it has an intelligible origin, and does not require direct matching of test results in order to determine the rod areas under various loading conditions.

Several tentative models were conceived and discarded before the final one was obtained, and some of these will be outlined below. In all cases the models are assumed to represent the structure of cement paste. They consist of nondeforming spheres, analogous to unhydrated cement grains, interconnected by elastic rods or struts, analogous to the needle-like crystals of the cement gel. The rods are assumed to be attached to the spheres by pinned connections.

In the following discussion of the preliminary models, only the final results of the relationship among the strut areas will be given. A description of the method used to calculate these area relations is outlined in Section 3.3, and the calculations for each model are given in Appendix B.

3.2 Preliminary Models

(a) Tetrahedron

Since a tetrahedron is the simplest stable three-dimensional structure which can be constructed from pin-connected struts, it seemed to be a good choice for a failure model. The tetrahedral model is shown in Fig. 3.1.

In order to produce a structure with the same behavior in all three principal directions, the areas of all struts must be equal. This is also logical when one considers that the strut lengths are all equal, and so the crystals which "grow" between cement grains should produce equal areas.

The value of Poisson's ratio for this model is 0.22. Although this value is somewhat high, it is within the range of test results. However, the fact that the same value of Poisson's ratio is obtained, regardless of the choice of strut areas, is a limitation, since values of ν as low as 0.1 have been obtained from tests of concrete.

Another disadvantage of the model is its shape. In the first place, the model is not conducive to the use of Cartesian coordinates, which would be very desirable, particularly when applied to rectangular members. In addition, if a number of single tetrahedrons is stacked together, they tend to produce structures which are also tetrahedral in shape. For this reason it is not possible to subdivide a rectangular structure into a number of tetrahedral units, unless the relative size of the units is so small that the analysis of the resulting network of struts becomes extremely laborious.

The final limitation of the model may be illustrated by means of Fig. 3.1. Under the action of load P, the inclined struts AB, AC and AD are subjected to compression, and the struts in the horizontal plane, BC, CD and BD are in tension. The magnitude of the compressive forces is three times that of the tensile forces. However, the compressive strength of concrete is approximately ten times as great as its tensile strength. This results in the condition that the maximum value of load P, and the behavior of the structure as a whole for strains beyond that at maximum load, is virtually independent of the strength of the compression struts, since no further load can be resisted by a unit if one of its tensile struts breaks. Since it is not reasonable to conclude that cement crystals under compression have almost no effect on the behavior of concrete subjected to compressive stress, the tetrahedral model does not produce reasonable results.

For the reasons outlined above, it was concluded that the tetrahedral model could not be used as a means of representing the structure of concrete.

(b) Body-Centered Cubic Models

The next trial model considered was one in which the spheres were situated in a body-centered cubic arrangement, as shown in Fig. 3.2. This is similar to the Reinius model except that, for simplicity, each group of four diagonal struts has been replaced by a single strut. The model has the disadvantage that it possesses no resistance to torsion, but it was thought that if it produced reasonable results for other types of loading, it could be modified to provide torsional resistance.

The notation used is similar to that employed by Reinius: The areas of struts in the x, y and z directions are A_1, A_2 and A_3 respectively and their lengths are L_1; the inclined or diagonal struts have length L_4 and area A_4. In order that the model will behave similarly if subjected to unrestrained loading in any of the three directions, x, y or z, the areas A_1, A_2 and A_3 must be equal. As was pointed out in the discussion of the tetrahedral model, this conclusion is also logical on the basis of crystal growth.

As a first approximation, the diameters of the spheres were assumed to be negligible with respect to their center-to-center spacing. Hence $L_4 = \sqrt{3}/2\ L_1$. The value of A_4 was then computed in order to give a Poisson's ratio of 0.15 under unrestrained compression. The result of this calculation is that $A_4 = 0.555\ A_1$. However, since L_4 is less than L_1, it follows from the concept of crystal growth, that A_4 should be greater than A_1. Accordingly the model does not produce a reasonable result, and must be discarded.

The next approach which was followed was to assume that the spheres were of finite diameter. This produces the result that the ratio L_4/L_1 is unknown, but less than $\sqrt{3}/2$, since the spheres are all of equal diameter. Again assuming that Poisson's ratio is 0.15 for unrestrained compression, the quantity $\frac{A_1}{A_4}\frac{L_4}{L_1}$ can be shown to be equal to 1.56. If $L_4/L_1 < \sqrt{3}/2$ then

$A_1/A_4 > 1.81$. As in the previous case this result is illogical in terms of crystal growth.

3.3 The Cubic Model

The model which was finally adopted is shown in Fig. 3.3. This model was formed by assuming a sphere at each corner of a cube, connected by struts along each edge of the cube, in the x, y, and z directions. In addition, on each cube face the spheres are connected by intersecting diagonal struts. The sphere diameters are assumed to be negligible compared with their spacing, so that the length of each strut is equal to the distance between the centers of the spheres to which it is connected. All struts are assumed to be homogeneous and elastic, to have constant modulus of elasticity E, and to have equal stress-strain properties in both tension and compression.

Struts in the x, y, and z directions are numbered 1, 2, and 3, respectively. Their lengths are L_1, L_2, and L_3 and their areas are A_1, A_2, and A_3, respectively. The forces in struts 1, 2, and 3 are P_1, P_2, and P_3, respectively. The diagonal struts in the vertical planes (parallel to planes xz and yz) are numbered 4. They have lengths L_4 and areas A_4, and transmit forces P_4. The diagonal struts in the horizontal planes (parallel to the xy plane) are numbered 5 and have lengths L_5, areas A_5, and forces P_5.

Since the spheres are assumed to be arranged in a cube, the relations among the strut lengths are:

$$L_1 = L_2 = L_3 \qquad (3.1)$$
$$L_4 = L_5 = \sqrt{2}\, L_1$$

As was mentioned in Section 3.2a, the relation of the strut areas must be such that the structure has the same behavior in all three principal directions. Also, from a consideration of the concept of crystal growth, struts of equal length should have equal areas. Accordingly, it follows that:

$$A_1 = A_2 = A_3$$
$$A_4 = A_5 \qquad (3.2)$$

The only remaining unknown is the relation between areas A_1 and A_4. This was determined so as to produce an initial value of Poisson's ratio (before any crystals begin to break) of 0.15, under unrestrained compression in the z direction. Since the model is statically indeterminate, the calculation of the relation between A_1 and A_4 involves equations of equilibrium and compatibility, as well as considerations of symmetry.

Each cube is considered to be a separate unit or "building block." These units are stacked together in a dense, face-to-face arrangement to form the total structure. Thus, the total area of each strut in the interior of the structure in the x, y, and z directions is $4A_1$, while that of the interior diagonal struts is $2A_4$. Because of symmetry, the behavior of the whole structure under unrestrained compression may be determined by a study of a single cube. It is further assumed that the area of each face of the cube is unity, so that a stress in the structure in the x, y, or z directions may be represented by a single force of the same magnitude and direction, applied to the exterior of the cube.

The notation used is as follows:

tensile forces and deflections	+ ve
compressive forces and deflections	- ve
applied compressive stress P_z	- ve

(a) Equilibrium Equations

Principles of equilibrium require that $\Sigma F_x = 0$. Therefore,

$$P_1 + \frac{1}{\sqrt{2}} P_4 + \frac{1}{\sqrt{2}} P_5 = 0 \tag{3.3}$$

From symmetry in the horizontal direction,

$$P_1 = P_2 \tag{3.4}$$

Also, $\Sigma F_z = 0$,

$$P_z = 4P_3 + \frac{8}{\sqrt{2}} P_4 \tag{3.5}$$

(b) Compatibility Equations

The deflection of any strut is given by,

$$\Delta_i = \frac{P_i L_i}{A_i E} \quad (i = 1,2,\ldots,5) \tag{3.6}$$

The deflected position of the model is shown in Fig. 3.4. It has been drawn assuming positive values of Δ_1 and Δ_2 and a negative value of Δ_3. However, the assumed directional sense of Δ_i does not affect the determination of the compatibility relations. The assumptions which do affect the compatibility relations are that the deflections are sufficiently small that they do not cause changes in geometry, and that the deflected positions of struts 1, 2, and 3 are parallel to their initial positions.

From Fig. 3.4 it can be seen that

$$\Delta_5 = \frac{1}{\sqrt{2}} \Delta_1 + \frac{1}{\sqrt{2}} \Delta_2 \tag{3.7}$$

and

$$\Delta_4 = \frac{1}{\sqrt{2}} \Delta_1 + \frac{1}{\sqrt{2}} \Delta_3 \tag{3.8}$$

Using the relationship

$$\epsilon_i = \frac{\Delta_i}{L_i}, \quad (i = 1,2,\ldots 5) \tag{3.9}$$

Equations 3.7 and 3.8 can be rewritten in terms of strains by combining them with Eqs. 3.1, 3.2, 3.4, and 3.6.

Hence,

$$\epsilon_5 = \epsilon_1 = \epsilon_2 \tag{3.10}$$

and

$$\epsilon_4 = \frac{1}{2} (\epsilon_1 + \epsilon_3) \tag{3.11}$$

(c) Determination of Relation Between A_1 and A_4

The equilibrium and compatibility equations which have been derived can be used to develop a general expression for Poisson's ratio in terms of A_1 and A_4 and, accordingly, to compute the relation between A_1 and A_4.

Rewriting Eq. 3.8 by means of Eq. 3.6 and using the length and area relations of Eqs. 3.1 and 3.2, the force in strut 4 may be expressed as:

$$P_4 = \frac{A_4}{2A_1} (P_1 + P_3) \tag{3.12}$$

Similarly, from Eq. 3.7 the force in strut 5 is given as:

$$P_5 = \frac{A_4}{A_1} P_1 \tag{3.13}$$

Combining Eqs. 3.3 and 3.13 the relation between P_1 and P_4 becomes:

$$P_1 = - \frac{A_1}{\sqrt{2}\, A_1 + A_4} P_4 \tag{3.14}$$

Also, by combining Eqs. 3.12 and 3.14, P_3 may be expressed in terms of P_4.

$$P_3 = \frac{A_1}{A_4} \frac{(2\sqrt{2}\, A_1 + 3A_4)}{(\sqrt{2}\, A_1 + A_4)} P_4 \tag{3.15}$$

The equation for Poisson's ratio, ν, is

$$\nu = \frac{-\epsilon_x}{\epsilon_z} = \frac{-\epsilon_1}{\epsilon_3} = \frac{-P_1}{P_3} \tag{3.16}$$

Now, substituting Eqs. 3.14 and 3.15 in Eq. 3.16,

$$\nu = \frac{A_4}{2\sqrt{2}\, A_1 + 3A_4} \tag{3.17}$$

Assuming $\nu = 0.15$, the relation between A_1 and A_4 becomes

$$A_1 = 1.30\ A_4 \tag{3.18}$$

This result is reasonable from a consideration of crystal growth, since L_1 is less than L_4.

The model which has thus been determined is capable of withstanding torsion and direct shear as well as external tension, compression, and bending moments. These facts, together with its agreement with observations concerning the structure and behavior of concrete, imply that the model should produce a reasonable failure theory.

3.4 The Failure Theory

Observations described by Reinius (1) and others (14,15) have shown that the structure of cement paste is extremely heterogeneous. A complex network of randomly-oriented crystals of various sizes connect cement grains in all stages of hydration. Therefore, it seems probable that the crystals will exhibit a great variation in strength, because of a number of factors such as their size, strength of bond to the surrounding elements, and angle of inclination to the loading direction.

Random distributions such as the strength of cement crystals occur very often in nature. Statisticians, in an effort to describe such distributions mathematically, have had considerable success with the so-called "normal curve" or "Gaussian Curve" (17). The general equation of this curve is

$$y = \frac{1}{\sigma\sqrt{2\pi}} e^{-\frac{(x-\bar{x})^2}{2\sigma^2}} \qquad (3.19)$$

and a plot of the curve is shown in Fig. 3.5 for the particular values $\sigma = 1$, $\bar{x} = 2$. The quantity y, the height of the curve at any point along the x-axis, is known as the "probability density" or "frequency density" of the particular value of x involved. $\bar{x}$ is the mean value of x for the distribution, and σ is the "standard deviation," a measure of the probability of encountering values of x different from $\bar{x}$.

It appears reasonable to apply the normal distribution curve to the problem of crystal strength variation. Accordingly, if the curve is used to relate strain and the number of crystals which break under load, the variable x corresponds to a function of strain, and y corresponds to the number of crystals which break at a particular strain.

Since the struts of the failure model represent crystals in the cement paste, crystal breakages are represented by a reduction in area in the appropriate model strut. In applying the normal curve to the model, therefore, the variable y must correspond to a strut area, while x corresponds to strain or a function of strain.

For use with the failure model, it is more convenient to work with the normal curve equation in the form

$$y = 50\, e^{-k\,(x-\bar{x})^2} \qquad (3.20)$$

The constant 50 is used because at $x = \bar{x}$, 50 percent of the crystals are assumed to have been broken. The percent strut area remaining, A, then becomes

$$A = 100 - y \; , \quad x < \bar{x}$$
$$A = y \qquad\quad , \quad x \geq \bar{x} \tag{3.21}$$

The final derivation of the failure theory for the cement paste now reduces to the determination of constants k and $\bar{x}$ and variable x. Since tests of concrete and cement paste have shown that their strength is considerably less in tension than in compression, it seems obvious that two equations are required, one for tension struts and one for compression struts. This conclusion does not produce any departure from the logical derivation of the failure theory, even though the struts are assumed to have equal stress-strain properties in both tension and compression. The strength of tension crystals is largely dependent on the effectiveness of their bonds to the surrounding elements, while that of the compression crystals has no such dependency.

In preliminary attempts to derive the area-strain equations for the struts, it was assumed that x was proportional to tensile or compressive strain. The constants k and $\bar{x}$ were then determined as described below.

As shown in Fig. 2.1, when concrete specimens are loaded under compression to high strains (2), the load-carrying capacity is practically zero at a strain of 0.01. Hence, in the area-strain equation for compression struts, the value of A should be nearly zero at $\epsilon = 0.01$. Also, before any load is applied to the strut ($\epsilon = 0$), it seems reasonable to assume that A should be approximately 100. Based on these upper and lower limits, the value of $\bar{x}$ was assumed to be at $\epsilon = 0.005$. The choice of k then determines the exact value of A at the upper and lower bounds.

The load in the strut is given by the equation $P = AE\epsilon$, where E is assumed to be constant. Figure 3.6 shows the compression strut load-strain relation for a range in k from 0.05 to 0.5. It can be seen that the maximum load occurs in the vicinity of $x = \bar{x}$.

As a first approximation, the value of k was assumed to be 0.1. The relation between area and strain for the compression struts is thus given by the equation

$$y = 50e^{-0.1\,(x - 5)^2} \tag{3.22}$$

where $x = \epsilon \times 10^3$

$A(\%) = 100 - y \;, \; x < 5$

$A = y \;, \; x \geq 5$

Since the tensile strength of concrete is approximately 10 percent of its compressive strength, and since the maximum load occurs at approximately $x = \bar{x}$, the value of $\bar{x}$ for the tension struts was assumed to be 0.5. In order to produce an area-strain or load-strain relation which is similar to that for the compression struts, the value of k must be 10. Hence, the tension strut area-strain relation may be expressed:

$$y = 50e^{-10(x - 0.5)^2} \tag{3.23}$$

where $x = \epsilon \times 10^3$

$A(\%) = 100 - y \;, \; x < 0.5$

$A = y \;, \; x \geq 0.5$

These failure theories for tension and compression struts were then applied to the model shown in Fig. 3.3, for the condition of unrestrained compression in the z-direction. The resulting load-strain curve is shown in Fig. 3.7. The broken curve has been plotted by assuming continuously increasing horizontal strains (ϵ_x and ϵ_y), and deriving the related vertical strains (ϵ_z) and vertical stress (P_z). The solid curve represents the corresponding load-strain relation for the condition of continuously increasing vertical strain.

The unusual shape of the curve in the vicinity of $\epsilon_z = 2 \times 10^{-3}$ is an inherent characteristic of the general area-strain equation, and is not dependent on the particular choice of values for the constants k and $\bar{x}$. These constants were assigned a wide range of values in the equations for both the tension and compression struts, but the results in each case were similar to that shown in Fig. 3.7.

The reason for this phenomenon can be illustrated by considering the compatibility and equilibrium equations for the model shown in Fig. 3.3. From Eq. 3.11,

$$\epsilon_z = 2\epsilon_4 - \epsilon_x$$

where ϵ_z = strain in member 3

ϵ_4 = strain in member 4

ϵ_x = strain in member 1

and the equilibrium equation involving P_1 and P_4, obtained from Eqs. 3.14 and 3.18, is

$$P_4 = -2.18 \; P_1$$

As is described in Chapter 4, this relation between P_1 and P_4 is constant for all strains, since it depends on the relation between A_1 and A_5, which vary at the same rate throughout the entire range of strains.

The relation between P_1 and ϵ_x is similar to that shown for compression struts in Fig. 3.6. Thus, for values of ϵ_x below maximum load in strut 1, P_1 increases with increasing ϵ_x. To satisfy equilibrium P_4 must increase at the same rate, and this increase will be accompanied by an increase in ϵ_4 and a decrease in A_4. However, for horizontal strains beyond the maximum value of P_1, P_4 will begin decreasing while A_4 remains constant. Hence the relation between $\epsilon_4 = P_4/A_4$ and ϵ_x in this region will be similar to that between P_1 and ϵ_x.

The compatibility equation may be written in incremental form as:

$$\Delta\epsilon_z = 2\Delta\epsilon_4 - \Delta\epsilon_x$$

It can be seen, therefore, that for absolute increases in ϵ_z $(\Delta\epsilon_z \leq 0)$, the condition

$$\Delta\epsilon_4 \leq 1/2\ \Delta\epsilon_x$$

must be satisfied. However, the shape of the P_1 vs. ϵ_x curve in the region beyond peak load is such that

$$\Delta\epsilon_4 > 1/2\ \Delta\epsilon_x\ ,$$

so that increases in ϵ_x produce decreases in the absolute value of ϵ_z, as shown in Fig. 3.7.

To produce reasonable results, therefore, the tension strut load-strain curve must be "flatter" beyond peak load than that given by the assumed theory. Values of k and $\bar{x}$ which produce sufficiently flat curves yield the result that A is approximately equal to 50 at $\epsilon = 0$, which is unreasonable.

A similar difficulty is encountered concerning the compression strut theory. The curves of Fig. 3.6 do not agree with the test results shown in Fig. 2.1. The load drops off much more rapidly beyond maximum load than test results indicate.

In order to resolve these inconsistencies while still maintaining the normal distribution concept, it was decided to use a "skewed" curve of the form

$$y = 50e^{-k(z - \bar{z})^2} \tag{3.24}$$

where $z = \ln x = \ln(\epsilon \times 10^3)$

The physical significance of this logarithmic transformation is that very weak crystals are more common than very strong crystals.

The principles governing the choice of constants k and $\bar{z}$ were similar to those outlined for the previous theory.

The compression strut area relation is given by the equation

$$y = 50e^{-1.3(z - 0.588)^2} \tag{3.25}$$

where $z = \ln(\epsilon \times 10^3)$

$$A(\%) = 100 - y, \quad \epsilon < 1.8 \times 10^{-3}$$

$$A = y, \quad \epsilon \geq 1.8 \times 10^{-3}$$

The load-strain relation corresponding to this equation is shown in Fig. 3.8. As can be seen, the shape of the curve for strains beyond peak load agrees quite favorably with test results.

The area-strain equation for the tension struts is

$$y = 50e^{-0.5(z + 1.61)^2} \tag{3.26}$$

where $z = \ln (\epsilon \times 10^3)$

$$A(\%) = 100 - y \; , \; \epsilon < 0.2 \times 10^{-3}$$

$$A = y \; , \; \epsilon \geq 0.2 \times 10^{-3}$$

The resulting tension load vs. strain curve is shown in Fig. 3.9.

4. UNCONFINED CONCRETE

4.1 Introductory Remarks

Using the model and failure criteria described in Chapter 3, it is possible to develop a theoretical load-strain relation for concrete subjected to unconfined compression. Since the model is assumed to represent cement paste, the relationships derived from it will be of necessity independent of the quality of aggregate in the concrete. However, failure of the model is dependent primarily on the strength of the tension members. The only tension resistance in unconfined concrete is provided by the paste, so that the shape of the theoretical load-deflection curve should agree quite closely with the shape of measured curves.

As in the case of the calculations outlined in Chapter 3 to determine the strut area relation, the load-strain curves for the concrete structure as a whole can be developed by considering a single cube.

4.2 Derivation of Theoretical Load-Strain Curves

In determining the load-strain relations for the model, it was assumed that before any load is applied to the structure, struts 1, 2, and 3 have an area A. The corresponding initial area of struts 4 and 5, from Eq. 3.18, is 0.769 A. As load is applied to the structure, Eqs. 3.2 and 3.18 are no longer valid, since the struts will break at varying rates. The strut areas must therefore be computed from the area-strain relations given by Eqs. 3.25 and 3.26.

Laboratory tests of a compression member are usually conducted by applying continuously increasing compressive strains to the specimen, and recording the corresponding loads. The difficulty in applying incremental compressive strains to the theoretical model, however, is that for a given value of compressive strain, the resulting forces in the struts cannot be determined directly. The force distribution among the struts is dependent on their areas, which change with changing strains. Hence, for any assumed value of vertical strain $\epsilon_z = \epsilon_3$, the related strains in struts 1, 2, 4, and 5 can be determined only by a trial and error approach. In order to overcome this difficulty, it was noted that test results of unconfined compression specimens indicate that continuously increasing compressive strains induce increasing tensile strains in the direction perpendicular to the applied load. It should therefore be possible to apply incremental horizontal tensile strains to the model and calculate the related vertical strains and loads. By this method the problem can be solved directly for each assumed strain value.

The method of deriving the load-strain relations is described here. The first step is to assume a value of ϵ_x. Then, from Eq. 3.10 it may be noted that

$$\epsilon_5 = \epsilon_1 = \epsilon_2 = \epsilon_x$$

so that the relation of areas A_1, A_2, and A_5 will be constant for any value of ϵ_x:

$$\frac{A_5}{A_1} = \frac{A_5}{A_2} = 0.769 \tag{4.1}$$

Equation 3.13 may now be rewritten

$$P_5 = \frac{A_5}{A_1} P_1 = 0.769 \ P_1 \tag{4.2}$$

Substituting Eq. 4.2 in Eq. 3.3

$$P_4 = -2.18 \ P_1 \tag{4.3}$$

From Fig. 3.9, the value of P_1 may be found, and the corresponding value of P_4 may be obtained from Eq. 4.3. Using Fig. 3.8 and the computed value of P_4, the quantity ϵ_4 is then determined. Finally, ϵ_3 is derived from Eq. 3.11 and P_3 is then obtained from Fig. 3.8.

All the unknown quantities have now been determined, and the vertical stress P_z is computed from Eq. 3.5. When the above procedure is repeated for successively increasing values of ϵ_x, the entire curves of load vs. deflection and load vs. horizontal strain may be obtained.

The theoretical relationship between load and vertical strain is shown in Fig. 4.1, and that between load and horizontal strain is shown in Fig. 4.2. The maximum value of P_z is 5.37 AE x 10^{-3}.

4.3 Discussion of Theoretical Results

The theoretical load-deflection curve shown in Fig. 4.1 agrees very favorably with test results. The ascending portion of the curve is very nearly linear up to approximately 40 percent of maximum load. Beyond this point, the slope of the curve decreases at an increasing rate until the maximum load is reached. These properties are in agreement with observations made by Richart, Brandtzaeg and Brown (4). The maximum load is reached at a vertical strain of 0.0018, which is also well within the range of test results.

The descending portion of the curve, at strains greater than that at maximum load, is convex until the load has reduced to about 80 percent of its maximum, and beyond this point it becomes concave. This phenomenon also agrees with test results, as may be illustrated by a comparison with the curves shown in Fig. 2.1.

The theoretical curve for load vs. transverse strain, shown in Fig. 4.2, also agrees with the test results recorded by Richart, Brandtzaeg and Brown (4). The transverse tensile strain increases at a rather slow rate with increasing load until approximately 80 percent of maximum load has been reached. As the load is increased beyond this point, the transverse strains increase at an accelerating rate up to maximum load. As vertical compression is increased beyond maximum load, the transverse strain increases very rapidly. The value of the strain at maximum load is about 0.0009, while after only a 5 percent decrease in load it has reached a value of nearly 0.0023.

The ratio ϵ_x/ϵ_z at maximum load is about 0.5, which is somewhat lower than the values observed by Richart, Brandtzaeg and Brown (4). However, this fact does not suggest a limitation in the failure theory, since in the vicinity of maximum load, cracking caused by transverse strains is extensive. For this reason it is almost impossible to obtain accurate measurements of the transverse strains.

The failure theory provides a very good insight into the behavior of concrete under unconfined compression. The compressive load P_z is resisted by compressive forces in members 3 and 4. Forces P_4 in turn induce transverse tensions in members 1, 2, and 5, and with increasing P_z, these tension forces cause a reduction in areas A_1, A_2, and A_3 which is analogous to failures in the horizontal cement crystals of the prototype. In the vicinity of maximum load, these tension struts have reduced in area to such an extent that further increases in strain produce a reduction in tensile forces P_1, P_2, and P_5. To maintain equilibrium, there is a corresponding reduction in P_4, so that a greater proportion of P_z is resisted by the vertical struts. If vertical compression is continued, struts 3 will also be strained beyond their maximum capacities, and beyond this point the value of P_z will decrease very rapidly.

The quantitative demonstration described in this chapter shows that the observed behavior of unconfined concrete under axial compression can be simulated by the model developed in Chapter 3. What is of significance in the use of this model is that the shape of the load-deflection curve is predicted throughout the whole range of loading.

The effect of aggregate properties on the load-deflection curve can be recognized by combining the known compression-strain properties of the aggregates with the response of the matrix. However, it should be pointed out that the use of different qualities of aggregate will not alter the general shape of the curves in Figs. 4.1 and 4.2. A useful device by which the effect of the aggregate may be incorporated in the model itself is to assume that the strength and modulus of elasticity of the aggregate is included in the unknown quantities A and E of the model. However, this device has the disadvantage that the physical significance of the model, as being representative of cement paste, is destroyed. For this reason, it is preferable to assume the aggregate properties to act in series with the model.

The results of the model analysis suggest that the behavior of unconfined concrete for strains beyond maximum load is nearly independent of the tension crystals. An examination of Table B1, which gives values of strut areas A_1 and A_3 at various increments of axial strain ϵ_z, reveals that at maximum load, A_1 has been reduced to 16.2 percent of its original value, while A_3 has been reduced by only 50 percent. The load-strain relations for strains beyond this point are almost entirely dictated by the behavior of the compression elements in the concrete, in particular by the behavior of the vertical cement crystals. The close agreement of this descending portion of the load-strain curve with test results is also an indication that the model describes the actual behavior of concrete.

5. CONFINED CONCRETE

5.1 Introductory Remarks

The behavior of concrete under compressive stress and simultaneous lateral confining pressures is of considerable practical and theoretical interest. Therefore, it is desirable to extend the failure theory to this loading condition.

Tests on concrete subjected to combined compressive stresses (3) have shown that its strength may be increased greatly by the action of confining pressures. If the failure theory is to be of value in predicting the behavior of concrete, it should produce a corresponding strength increase. It is also particularly important to apply the theory to the case of concrete confined by rectilinear reinforcement, in order to interpret the results of the test program described in Appendix A and the tests by Szulczynski (5). Specifically, it should be possible, by means of the theory, to explain the difference between the effectiveness of rectangular and spiral transverse reinforcement.

As has been described in Chapter 4, the strength of the model under unconfined compression is largely dependent on the strength of the horizontal struts, which are in tension. Since lateral confinement reduces the horizontal tensile strains and so increases the effectiveness of these struts, it should thereby cause an increase in the maximum value of P_z.

However, it is not possible by means of the theory as outlined in Chapters 3 and 4 to explain the very large increases in strength and deformation which have been observed in tests (3). From Eq. 3.5 it can be seen that

P_z is a function of forces P_3 and P_4 only. The maximum value of P_3, as determined by means of Eq. 3.25, and shown qualitatively in Fig. 3.8, is $1.094\ AE \times 10^{-3}$. Similarly, the maximum value of P_4 is $0.842\ AE \times 10^{-3}$. Hence, from Eq. 3.5, the maximum theoretical value of P_z is $9.15\ AE \times 10^{-3}$. This represents an increase of only approximately 70 percent over the value of $P_z = 5.37\ AE \times 10^{-3}$, derived in Chapter 4 for the case of unconfined compression. As shown in Fig. 2.2, strength increases of much greater magnitude have been obtained in tests on confined concrete.

Also, referring to Fig. 3.8, it can be seen that the maximum value of P_3 is reached at a strain, ϵ_z, of about 2.75×10^{-3}. If ϵ_z is increased beyond this value, a reduction in P_z will result. However, in the tests by Richart, Brandtzaeg and Brown (3), the maximum load was reached at strains as high as 60×10^{-3}.

The difficulties described above can be overcome by a consideration of the structure of concrete. The over-all structure is composed of a great many solid particles of aggregate and unhydrated cement grains, bonded together by the cement paste. In the initial state, before any load is applied to the structure, the spacing of these solid particles is extremely varied. Some particles are contiguous, while in other parts of the structure the closest spacing may be several particle diameters. As load is applied to the structure, and the cement crystals begin breaking, an increasing number of particles will come in contact with each other, thus permitting a direct load transfer which is dependent of the strength of the cement crystals.

Since for unconfined compression, the strength appears to be mainly a function of horizontal tensile forces, these grain-to-grain contacts are relatively unimportant. In the case of confined compression, however, the large strains produced will cause a much greater incidence of direct grain contact, so that the solid particles play a much greater role in the behavior of the concrete mass as a whole. In addition, the confining pressures permit load to be carried by the structure even when no cement crystals are effective, thus creating a condition which is independent of the struts in the failure model.

In order to explain the behavior of confined concrete, it seems apparent that a study must first be made of the behavior of solid particles under similar loading conditions.

5.2 Behavior of Granular Media Under Combined Compressive Stresses

A number of investigations have been made of the behavior of an array of granular particles in contact. Duffy and Mindlin (18) calculated incremental stress-strain relations for a face-centered cubic arrangement of elastic, identical spheres in contact. Thurston and Deresiewicz (19) enlarged on these results and studied the problem of three-dimensional compression applied to this model.

Thurston and Deresiewicz assumed the face-centered cubic model to be subjected to equal confining pressures in the three principal directions, following which uniaxial compression was applied to failure. They found that failure occurred due to a "twinning" process, in which one layer of spheres was displaced through an adjacent parallel layer, thereby forcing apart the spheres in this adjacent layer. The failure stress associated with this loading condition is given by the equation

$$\frac{\sigma_a^*}{\sigma_o^{(o)}} = \frac{\sqrt{6} + 8f}{\sqrt{6} - 4f} \tag{5.1}$$

where σ_a^* = failure stress

$\sigma_o^{(o)}$ = initial isotropic pressure

f = coefficient of friction of spheres

Thurston and Deresiewicz also derived total load-strain relations for the loading condition described above. The results are shown in Fig. 5.1, which is a graph relating additional (dimensionless) stress and strain in the direction of uniaxial compression. In Fig. 5.1, the following notation is used:

σ_o = additional isotropic stress

σ_a = additional axial pressure applied in the z-direction

$\sigma_o^{(o)}$ = initial isotropic pressure

For the particular case of $\sigma_o = 0$, the graph shows the relation between axial and confining pressures.

Although the magnitudes of the pressures are extremely small, it is of interest to study the general shape of the curves in Fig. 5.1. It can be seen that the stiffness of the structure increases with increasing strain. This behavior is a result of the ideal nature of the model. The spheres are of equal size, arranged in the densest manner possible, and are assumed to deform elastically until the failure stress is reached.

Although the investigations of Thurston and Deresiewicz provide an insight into the behavior of an ideal granular medium, their results cannot be applied to real aggregates such as occur in concrete. In a material such as sand, for example, the size and orientation of the particles may be extremely random. In addition, under the action of compressive stresses, local and general failures of the grains take place.

Some typical results of drained triaxial tests on fine sand (20,21) are shown in Fig. 5.2. The curves in Fig. 5.2 show the relation between $(\sigma_1 - \sigma_3)$ and axial compressive strain, where

σ_1 = axial pressure

σ_3 = lateral confining or consolidation pressure.

As in the case of the results shown in Fig. 5.1, the magnitudes of the pressures are small. However, the qualitative stress-strain relations are of great importance in providing an understanding of the behavior of the aggregate and cement grains in concrete. As can be seen, the stiffness decreases with increasing strain. Also, as might be expected, dense sands are much stiffer than loose sands.

Before the behavior of confined concrete can be interpreted, the effect of confinement on the model must be investigated. The results of this investigation, together with the observed stress-strain relations of aggregate particles should then enable the desired conclusions about the behavior to be made.

5.3 Combined Axial Compression and Uniform Transverse Pressure

The first condition of confining pressure which was studied was that which occurs in spirally-reinforced columns, in which vertical compressions induce horizontal confining pressures, p_c, which increase with increasing strains. Since for any given value of vertical strain, the value of p_c is the same for all points in the structure, the over-all behavior can again be determined by studying the behavior of a single cube.

For the assumed loading condition, the compatibility equations, and the equilibrium equations 3.4 and 3.5, are still valid. However, Eq. 3.3 must be modified to include the effect of p_c.

Referring to Fig. 5.3a, it is seen that pressure p_c may be represented by a force of $p_c/4$ at each corner of the cube. It was decided to express the calculations in terms of the equivalent force H, as shown in Fig. 5.3b, since confining pressure due to rectangular ties must later be represented in this manner, as will be discussed in Section 5.4. Hence, the value of H becomes

$$H = \frac{\sqrt{2}}{4}\, p_c = 0.354\ p_c \qquad (5.2)$$

H is assumed to be positive in the direction shown in Fig. 5.3b.

For equilibrium of forces in the x-direction,

$$P_1 + \frac{1}{\sqrt{2}} P_4 + \frac{1}{\sqrt{2}} P_5 + \frac{1}{\sqrt{2}} H = 0 \qquad (5.3)$$

The method of determining the load-strain relations was similar to that outlined in Chapter 4. It was again assumed that the independent variable was ϵ_x, which was increased in successive increments over the entire desired range.

From Eqs. 5.3, 3.13, and 3.18

$$P_4 = -(H + 2.18\ P_1) \tag{5.4}$$

In order to compute the value of H, it was assumed that the spiral steel had an ideal elasto-plastic stress-strain relation, and that its yield stress was 50,000 psi. Assuming $E = 30 \times 10^6$ psi, the value of strain at yield = 1.67×10^{-3}. In accordance with these assumptions, the value of H increases linearly with ϵ_x, reaching its maximum value at $\epsilon_x = 1.67 \times 10^{-3}$. Beyond this strain, H remains constant.

Accordingly, the value of H is given by the equation

$$\begin{aligned} H &= H_{max} \times \frac{\epsilon_x \times 10^3}{1.67}, & \epsilon_x &< 1.67 \times 10^{-3} \\ H &= H_{max}, & \epsilon_x &\geq 1.67 \times 10^{-3} \end{aligned} \tag{5.5}$$

Using Eqs. 5.4 and 5.5, together with the area-strain relations given in Eqs. 3.25 and 3.26, the load-deflection relation can be determined. The result of these calculations is shown in Fig. 5.4 for an assumed maximum value of p_c of $0.1\ f'_c = 0.537\ AE \times 10^{-3}$. The maximum load is $6.7\ AE \times 10^{-3}$, or 124.5 percent of the calculated maximum load for unconfined concrete in Chapter 4, and the value of H_{max} in Eq. 5.5 is $19\ AE \times 10^{-5}$.

5.4 Combined Axial Compression and Concentrated Transverse Forces

The final confining pressure condition investigated was that which occurs in columns confined by rectangular ties. Since this type of transverse reinforcement provides little lateral restraint along the sides of the column, for ties of the size normally used in practice, it was assumed that the effect of the ties could be represented by a single horizontal force at each corner, as shown in Fig. 5.3b.

The value of p_c is no longer constant over the cross section, as it was in the previous case, and, hence, the problem cannot be solved by considerations of a single cube. The method of solution which was followed was to divide the cross section into successively finer grids, which is equivalent to assuming successively smaller cube sizes with respect to the size of the column. Denoting the number of cubes along each side of the column by n, the load-deflection relation was determined for values of n = 1, as shown in Fig. 5.3b; n = 2, as in Fig. 5.5; n = 3, as in Fig. 5.6; and n = 4, as in Fig. 5.7.

For the sake of simplicity, the axial spacing of the ties was assumed not to be a variable. To achieve this condition, it was considered that the force H was applied as a line load, of intensity 2H, over the entire length of the specimen. In all cases the cubes were assumed to have a dimension of one unit, with the result that the magnitude of H was increased linearly with the value of n, in order to produce the same relative effect.

As can be seen, the shape of the cross section was not varied, the only condition studied being that of a square column.

In order to compare the effect of spiral reinforcement with that of rectangular ties, it was assumed that the average stress across an axial section remained constant so that for n = 1, the value of H_{max} in Eq. 5.5 is 19 AE x 10^{-5}, and for n = 2, H_{max} = 38 AE x 10^{-5}.

(a) n = 1

For the case of n = 1, the conditions are identical to that for the spirally reinforced column, as investigated in Section 5.3. The resulting load-deflection curve is therefore as shown in Fig. 5.4, and the value of the maximum load is 124.5 percent of the maximum load for unconfined concrete.

(b) n = 2

Referring to Fig. 5.5, it can be seen that, because of symmetry, it is only necessary to study the behavior of cube ABCD in order to determine that of the whole structure.

The value of H_{max} in Eq. 5.5 is 38 AE x 10^{-5}.

The notation used for the struts is indicated in Fig. 5.5. The diagonal struts in the vertical planes containing AB and AC are designated 4A, and those in the vertical planes containing BD and CD are called 4B. All vertical members are denoted by the numeral 3.

For any stage of loading, it was assumed that the value of ϵ_z was constant over the entire cross section. Under these conditions, for a given value of ϵ_z, there are only two unknown horizontal deflections: the deflection of B along a line connecting B and D; and the deflection of A along a line connecting A and D.

The equation for equilibrium of forces in the z-direction is

$$P_z = 4P_3 + 2\sqrt{2}\ (P_{4A} + P_{4B}) \qquad (5.6)$$

The equations of compatibility and the remaining equilibrium equations relating members 1A, 2A, 3, 4A and 5A are those which were used in Section 5.3. The corresponding equations relating members 1B, 2B, 3, 4B and 5B are those which were used in Chapter 4 for unconfined compression. Accordingly, it can be seen that the load-strain relations for the 2 by 2 grid can be obtained by combining the case of unrestrained compression with the case of compression plus hydrostatic confining pressure.

The procedure followed was to first plot a graph of P_{4B} vs. ϵ_z from the results of Chapter 4, and next to plot a graph of P_{4A} vs. ϵ_z, obtained by following the procedure of Section 5.3 with $H_{max} = 38\ AE \times 10^{-5}$. Now, for an assumed value of ϵ_z, the value of P_3 was obtained by means of Eq. 3.25 and the values of P_{4A} and P_{4B} were obtained from the graphs referred to above. Finally, P_z was determined from Eq. 5.6. The load-deflection curve, shown in Fig. 5.8, was determined by working with successive increments of ϵ_z.

The calculated value of the maximum load is 115 percent of the maximum load for unconfined concrete.

(c) <u>n = 3</u>

A diagram of the 3 by 3 grid system is shown in Fig. 5.6. As in the case of the 2 by 2 grid, because of symmetry, it is only necessary to consider one quadrant of the structure. In addition, the notation of the horizontal struts in the y-direction was adopted as a result of conditions of symmetry in the horizontal plane. The diagonal struts in the vertical planes containing 1A, 1B, 1C, and 1D are denoted by 4A, 4B, 4C, and 4D, respectively, and all vertical struts are denoted by 3.

The calculations involved in computing the load-deflection relation are given in Appendix B. Only a general description of the method will be described in this section. For a given value of ϵ_z, constant over the whole cross section, there are four unknown horizontal deflections. Using these deflections, it is possible to determine four compatibility equations involving the eight struts 1A to 1D and 5A to 5D. Also, from Eq. 3.11 four additional compatibility equations can be derived relating struts 1A to 1D, 4A to 4D, and 3. Finally, four equations of horizontal equilibrium can be written.

The equations were solved in the following manner: The four equilibrium equations were rewritten in terms of areas and strains. Next, the eight compatibility equations were substituted into the equilibrium equations in order to obtain four equations involving only the strains ϵ_{xA}, ϵ_{xB}, ϵ_{xC} and ϵ_{xD} as basic unknowns, together with the 12 unknown strut areas. For each assumed value of ϵ_z, these four equations were then solved by a trial and error procedure as described in the following paragraph.

The first step in the solution of the equations was to assume values for ϵ_{xA}, ϵ_{xB}, ϵ_{xC}, and ϵ_{xD}. Next, from the compatibility equations, the remaining eight unknown strains were determined. From the area-strain relations of Eqs. 3.25 and 3.26, the 12 related areas were determined. These areas were inserted in the four equilibrium equations, which were then solved to compute values of ϵ_{xA}, ϵ_{xB}, ϵ_{xC}, and ϵ_{xD}. If the resulting values did not compare favorably with the assumed values, the procedure was repeated until convergence was obtained.

The main purpose in determining the load-deflection relations under the action of corner confining loads was to compare the resulting maximum load with that obtained for "spirally-reinforced" concrete. Accordingly, in the 3 by 3 and 4 by 4 grids, the loads were not determined for ϵ_z values greater than that at maximum load.

The load-deflection curve for the 3 by 3 grid is shown in Fig. 5.9, and the maximum value of P_z is 108.8 percent of the maximum load for unconfined concrete.

(d) n = 4

The notation used in this system is shown in Fig. 5.7. The method of solution is as outlined in Section 5.4c except that six equations of horizontal equilibrium are required, as well as 12 compatibility equations. These equations, as well as the details of the solution, are given in Appendix B, and the resulting load-deflection curve is shown in Fig. 5.10.

The maximum value of P_z is 107.5 percent of the maximum load for unconfined concrete.

5.5 General Discussion

The relation between the maximum load carried by the model and the size of grid is shown in Fig. 5.11 for values of n from 1 to 4. The result for n = 1 is that of the condition of spiral reinforcement. The shape of the curve at $n = 4$ indicates that this value of n is sufficient to determine the effect of rectangular reinforcement on the model. The increase in the theoretical maximum load caused by rectangular reinforcement is approximately 7 percent.

(a) Spiral Reinforcement

Spiral reinforcement produces an increase in the theoretical maximum load of 24.5 percent over the maximum load of unconfined concrete. The corresponding increase observed in tests (4) would be 41 percent for the assumed value of $p_c = 0.1\ f'_c$, as can be seen from Eq. 2.1. This difference is shown in Fig. 5.4, in which the strength given by Eq. 2.1 has been plotted as a broken line. The lack of agreement between the model and test results is not surprising since it was pointed out in Section 5.1 that the upper bound on the value of P_z for the model is 9.15 AE $\times 10^{-3}$, or 70 percent greater than the unconfined strength. It seems apparent that the gap between the model and test results becomes greater with increasing magnitude of p_c.

It was further suggested in Section 5.1 that the difference between the behavior of the model and that of concrete is attributable to direct load transfer between the solid particles existing in concrete. The relatively high strains which concrete must undergo in order to develop the strength of the spiral cause most of the cement crystals to fracture, and force the solid particles into contact. As the strains increase, these granular contacts become increasingly important, and require the use of curves such as Fig. 5.2 to express the behavior of concrete.

The explanation given above is not unrealistic. Indeed, it is inherent in the derivation of the model, which is assumed to represent the crystals of cement paste. As these crystals break at high strains, the model must withdraw more and more from participation in the over-all behavior of the concrete.

In the tests conducted by Richart, Brandtzaeg and Brown (4), a spirally-reinforced column was subjected to several repetitions of maximum loading. The spiral was then removed and the unreinforced core was loaded to its capacity. The strength of the core was 1040 psi, or approximately half the strength of the plain columns which were tested in the same series.

The phenomenon described in the previous paragraph is not incompatible with the model. As the model is subjected to axial compression, the diagonal struts in the plane parallel to the direction of loading (struts 4) do not fail completely. The loads carried by these struts are limited by the amount of horizontal force provided by the tension struts and transverse reinforcement. Accordingly, their reduction in area is limited to that required to produce their maximum load-carrying capacity, or approximately 40 percent of their original area. Under the action of the axial strain, the axes of these diagonal struts rotate into a position more nearly perpendicular to the loading direction. Hence, when the load is removed, these struts, which are still bonded to the adjacent cement particles, are capable of providing the tension resistance necessary to produce unconfined compression strength.

Hanson (23) conducted a series of tests on lightweight concrete under combined stresses. The test series included specimens with normal weight aggregate for comparison. The magnitude of the lateral stress ranged from zero to one-third of the unconfined compressive strength of the specimens. Hanson found that under the usual range of stresses found in structures, the strength of the lightweight concretes was approximately equal to that of normal weight concrete having the same unconfined compressive strength. At higher magnitudes of combined compressive stresses, however, the strength of the lightweight concretes was 65 to 90 percent of that of the corresponding normal weight concrete.

The results of Hanson's tests agree with the behavior of the model. For low magnitudes of confining pressure, a relatively small percentage of the aggregate particles are in direct contact, so that the strength is mainly a function of the cement paste. At higher values of combined compressive stresses, many more of the aggregate particles come into contact, and since the strength of lightweight aggregate is less than that of normal weight aggregate, the concrete as a whole will show a similar decrease in strength.

(b) Rectangular Transverse Reinforcement

The strength of the model restrained by means of rectangular transverse reinforcement is approximately 7 percent greater than the theoretical strength of unconfined concrete, as can be seen from Fig. 5.11. This strength increase is only 28.5 percent of the corresponding increase for spirally-reinforced concrete, and demonstrates the lower efficiency of rectangular reinforcement as a means of providing lateral confinement for concrete.

The reason for this reduced efficiency is that, whereas spiral reinforcement confines all the horizontal tension members in the structure, rectangular reinforcement provides little restraint for those portions of the concrete remote from the corners. This explanation can be illustrated by referring to Fig. 5.12, which shows a plan view of the 4 by 4 grid. The solid lines represent the deflected position of the model confined by rectangular reinforcement, at the point of maximum load ($\epsilon_z = 0.0025$). The broken lines indicate the deflected position of the unconfined model, at the same value of vertical strain. The original position of the model is not shown.

It can be seen that a bulging of the structure has taken place near the middle of each side of the column, while the corners have been compressed horizontally with respect to the unconfined model. Since the broken lines represent the condition of the unconfined specimen at a vertical strain beyond that at its maximum load, the tension struts are almost completely ineffective at this point. It follows, therefore, that the structure of the confined model is also extremely disintegrated in the exterior portions midway between the corners.

The above observations agree with the test results of Szulczynski (5), in which it was observed that considerable surface spalling of the concrete took place near maximum load. It was also noted in these tests that vertical "arches" were formed, which spanned between the ties. These arches could also be explained by means of the model, in a manner similar to that described above. The concrete between the ties receives little lateral confinement, and the resulting high tensile strains cause a break-down in the structure.

6. TEST RESULTS

6.1 Outline of Tests

The variables considered in the test series were as follows:

(1) Spacing of transverse reinforcement, which ranged in 2-in. increments from 2 to 8 in.

(2) Bending stiffness of transverse reinforcement. This was varied by using both No. 2 and No. 3 bars as ties.

(3) Amount of longitudinal reinforcement. The longitudinal reinforcement ratio, p', ranged from 0 to 1.8 percent.

(4) Bending stiffness of longitudinal reinforcement, which was a secondary variable because of the different tie spacings used.

A total of 60 test specimens were cast; all specimens were 5 by 5 in. in cross section, and 25 in. long. The specimens were cast in groups of four, each group being composed of one plain specimen; one specimen with ties only; one specimen with ties plus 4-No. 2 longitudinal bars; and one specimen with ties plus 4-No. 3 longitudinal bars. All the specimens with ties in any one group had identical tie arrangements. In all cases the ties were fabricated with outside dimensions of 5 by 5 in. The volumetric ratio of the transverse reinforcement was 2 percent for all the specimens with ties.

In order to maintain consistent concrete strengths, the aggregates were oven-dried before each batch was mixed, and the amounts of aggregate, cement, and water were carefully weighed. As a result, the variation in strength throughout the test series was relatively small.

A detailed description of the materials, as well as the casting and testing procedure, is given in Appendix A.

6.2 Behavior of Test Specimens

The load-deflection relations obtained from the tests are included in Appendix A (Figs. A.4 to A.34). The general shape of the curves is similar for all tied columns, being essentially linear up to a load of between 60 and 75 percent of maximum load. Beyond this point, the slope of the curve decreases with increasing deflection until maximum load is reached. The average over-all strain at maximum load, computed by dividing the total deflection by the specimen length, ranged from 0.0027 to 0.0053, with approximately 75 percent of the values being between 0.003 and 0.004.

The plain specimens behaved in a similar manner to the tied specimens up to about 75 percent of maximum load. However, the strains did not increase as rapidly with increases in load beyond this point. The average over-all strain at maximum load ranged between 0.0021 and 0.0027 for the plain specimens. Since the stiffness of the testing machine was not sufficient to absorb the sudden release of energy at maximum load in the plain specimens, a sudden fracture occurred, and it was not possible to record strains beyond that at maximum load.

The load in the tied specimens decreased rather rapidly with increasing strains beyond maximum load. Rather extensive spalling occurred when the load had reduced to about 50 percent of its maximum value. In the specimens of Series 1, which had No. 2 ties at 2-in. spacing, and the specimens of Series 2, which had 2-No. 2 ties at 4-in. spacing, fracture of one of the ties occurred after the load had reduced to about 30 percent of maximum. In the remaining specimens, fracture of the ties did not occur, and testing was discontinued at about 10 percent of maximum load.

Crushing in the specimens of Series 1 usually occurred over a length of 4 to 6 in., and the zone of crushing was very nearly horizontal in most cases. For the specimens of larger tie spacing, however, the zone of crushing usually was inclined at an angle of 45° to 60° to the vertical, and for the majority of these specimens the failure zone extended from the middle of a tie space on one side of the specimen to the middle of an adjacent space on the other side. Because of the inclined failure zone, most of the specimens with 4-, 6-, and 8-in. tie spacings began to exhibit sliding along this failure surface, producing relatively large vertical deflections in many cases.

The definition of strain as applied to reinforced concrete requires some discussion. In general, strain is defined by the relation

$$\text{strain} = \text{deformation/length.}$$

However, the appropriate legnth to be used in applying this relation is not always apparent. In the case of axially-loaded columns, the total shortening is usually the most important deformation, and hence the critical strain would appear to be the average strain throughout the length. If most of the crushing takes place over a relatively small region, however, the values of average strain at the same load level in similar columns of different lengths will vary considerably. For this reason, if the results of one condition are to be applied to other conditions, it is necessary to compute the local strain at the crushing zone.

An important application of reinforced concrete columns is their use in monolithic beam and column construction. To analyze this type of structure, it is important to know the strain at the beam-column connection, particularly if the analysis is based on the principles of ultimate capacity.

From the above comments, it can be seen that it is very desirable in tests of columns to obtain local strain values. In an effort to determine the strain of the test specimens over the failure region, deflection dials were mounted on the specimens over two continuous 2-in. gage lengths. For the specimens in which crushing occurred outside this 4-in. gage length, the strain at the failure zone was computed by subtracting from the total deflection the deflection of the uncrushed portion of the specimen, and dividing the difference by the height of the crushed region. The deflection of the uncrushed portion was computed by calculating the strain obtained from the mounted dials, and assuming that this strain was constant over the total length of the specimen outside the failure zone. In most cases, the deflection dials which measured deformations of the uncrushed part of the specimen showed a decrease in strain for that portion of the test which was carried on after maximum load had been reached. This phenomenon was due to the fact that the load on the specimen was decreasing, and demonstrated that the total axial deformation was occurring only in the crushed region.

Figures A.35 to A.57 show the relation between load and strain in the crushed region for the columns with ties. The strain in the zone of crushing when the net load had reduced to 50 percent of its maximum value for the specimens with No. 2 ties at 2-in. spacing ranged from 0.017 to 0.042 with a mean of 0.032; for the specimens with 2-No. 2 ties at 4-in. spacing ranged from 0.015 to 0.027 with a mean of 0.020; for the specimens with No. 3 ties at 4-in. spacing ranged from 0.015 to 0.023 with a mean of 0.018; for the specimens with 3-No. 2 ties at 6-in. spacing ranged from 0.013 to 0.023 with a mean of 0.018; and for the specimens with 4-No. 2 ties at 8-in. spacing ranged from 0.005 to 0.015 with a mean of 0.009.

6.3 Effect of Variables

(a) Amount of Transverse Reinforcement

The effect of the amount of transverse reinforcement on the strength and ductility of axially loaded columns is illustrated in Figs. 2.3 and 2.4. In each case, curve 1 shows the stress-strain relation for a plain concrete specimen; curve 2 refers to a specimen with No. 2 ties at 2-in. spacing; and curve 3 refers to a specimen with No. 3 ties at 2-in. spacing. The stresses used in plotting the curves are gross stresses, obtained by dividing the axial load by the gross area of the cross section. The strains are average longitudinal deformations, based on the total shortening of the columns.

It can be seen from Figs. 2.3 and 2.4 that the use of ties did not affect the gross strength of the specimens appreciably. However, the ties did produce considerable improvement in ductility. As can be seen from the graphs, at large strains, the larger the amount of transverse reinforcement, the greater the percentage of maximum load which was maintained.

(b) Tie Spacing

The curves of Fig. 6.1 show load-strain relations for tie spacings of 2, 4, 6, and 8 in. In all cases the transverse reinforcement ratio was equal to 2 percent and the cross-sectional dimensions of the columns were 5 by 5 in. The load used for the ordinate of the graph was the relative gross strength, obtained by dividing the load on the specimen by the maximum load of the plain specimen in the same series. The strains were the local strains at the failure zone.

Figure 6.1 illustrates that the ductility decreased with increasing tie spacing, when the transverse reinforcement ratio was kept constant.

(c) Longitudinal Reinforcement

Figure 6.2 shows the effect of longitudinal reinforcement. The solid curves refer to specimens with longitudinal steel ratio, p', equal to 0, 0.8 and 1.8 percent, and with transverse reinforcement ratio, p'', constant at 2 percent. The broken curves have been plotted by subtracting from the total load-strain curves the load carried by the longitudinal bars.

Longitudinal reinforcement was included in the specimens to see if it helped confine the concrete in combination with the ties. However, it had no significant effect on concrete strength or ductility. This is illustrated by the fact that the broken curves compare well with that for the specimen with no longitudinal steel.

(d) Concrete Strength

An examination of Figs. 2.3 and 2.4 reveals that concrete strength has no marked influence on the strain at maximum load. However, for strains beyond maximum load, the higher strength concrete results in a decrease in ductility.

(e) Shape of Cross Section

The curves of Fig. 2.3 refer to 5 by 5 in. columns, and those of Fig. 2.4 refer to 5 by 10 in. columns. In order to compare the behavior of these two column sizes, it is necessary to compare curves 2 of Fig. 2.3 with curves 3 of Fig. 2.4, since these have very nearly equal values of the volumetric ratio, p''. On the basis of this comparison, the shape of cross section appears to have no significant effect on either strength or ductility.

(f) Stiffness of Longitudinal Reinforcement

The stiffness of the longitudinal reinforcement, as demonstrated by the effectiveness of a given size of longitudinal bar at different tie spacings, had apparently no influence on the results. This was as expected, since it was pointed out in Section 6.3c that longitudinal reinforcement had little effect on strength or ductility in specimens with a 2-in. tie spacing.

(g) Stiffness of Ties

The specimens of Series 2 had 2-No. 2 ties at a 4-in. spacing, while those of Series 3 had 1-No. 3 tie at a 4-in. spacing. It was hoped that by a comparison of these two series, the effect of tie stiffness on the results could be determined. However, the only difference which could be observed was that in Series 2, fracture of one of the ties usually occurred at high strains, while in no case did one of the No. 3 ties break.

6.4 Discussion of Test Results

(a) Strength

The use of ties had no significant effect on the gross strength of the test specimens. The maximum load of the tied specimens with no longitudinal reinforcement was an average of 101 percent of the plain specimen strength, with a range from 97 to 107 percent. The maximum net load of the specimens with No. 2 vertical bars, computed by subtracting the load carried by the bars from the total load, was an average of 97 percent of the plain specimen strength. The range in values for these specimens was from 90 to 102 percent. The maximum net load of the specimens with No. 3 vertical bars was 96 percent of the plain specimen strength, with a range from 91 to 102 percent. The latter averages do not include the results from specimen 1232, which failed by local fracture at the end.

The results summarized in the previous paragraph illustrate that the gross strength of the specimens, calculated on the basis of the total cross-sectional area, was not greatly affected by the ties. The gross strength is often thought of as the useful strength, since it ordinarily has the most significance in practice. However, it is also of interest to investigate the net strength, or the strength of the concrete confined by the ties. It is only by an investigation on this basis that an accurate concept can be obtained of the real effect of ties on the behavior of concrete. In addition, the net strength is important in order to compare the results of various test programs.

In the tests carried out by Szulczynski (5), the net strength was calculated by dividing the maximum load by the concrete area within the ties. The increase in unit strength, Δf_c, was then defined as the difference between the net strength and the strength of the plain specimen of the same set. The relation between Δf_c and the effectiveness of the transverse reinforcement was expressed by means of an assumed lateral stress, f_2, defined as follows:

$$f_2 = \frac{p'' f''_y}{(\frac{b}{h} + \frac{h}{b})} \qquad (6.1)$$

where p'' = volumetric ratio of the transverse reinforcement

f''_y = yield stress of the transverse reinforcement

b = width of the enclosed section

h = depth of the enclosed section.

The equation

$$\Delta f_c = 1.8 f_2 \tag{6.2}$$

represented a reasonable lower bound to the data of Szulczynski's tests, and the equation

$$\Delta f_c = 1.4 f_2 \tag{6.3}$$

described the lower bound to all the results in the tests.

The results of the model analysis described in Chapter 5 can be used to develop an equation similar to Eqs. 6.2 and 6.3. It was observed in Section 5.5b that the theoretical strength increase produced by rectangular transverse reinforcement was only 28.5 percent of that produced by spiral reinforcement. Although it was pointed out that the absolute magnitude of the theoretical strength increases did not agree with test results, it seems reasonable to assume that the relative effects of the two types of transverse reinforcement are valid. The modification of the results in terms of granular contacts applies to both the spiral and rectangular cases. On the basis of this reasoning, it may be assumed that rectangular ties are approximately 30 percent as efficient as spiral reinforcement.

The strength increase caused by spiral reinforcement, as observed in tests (4), and expressed in Eq. 2.1, is given by the relationship

$$\Delta f_c = 4.1 f_2 \tag{6.4}$$

The corresponding strength increase caused by rectangular ties, obtained by combining the results of the model analysis with Eq. 6.4, may be expressed

$$\Delta f_c = 1.2 f_2 \tag{6.5}$$

The increase in unit strength, Δf_c, observed in the test results described in this chapter, is plotted as a function of f_2 (Eq. 6.1) in Figs. 6.3, 6.4 and 6.5. Broken lines corresponding to Eqs. 6.2 and 6.3, and a solid line corresponding to Eq. 6.5, have been shown on the same graphs for comparison.

Figure 6.3 shows the strength increases for the specimens with ties and no longitudinal reinforcement. The open circles refer to specimens with No. 2 bars as ties, and the solid circles refer to specimens with No. 3 bars as ties. It is seen that the strength increases for the test series are less than that in the tests by Szulczynski, since five of the results fall below the line representing Eq. 6.3. The line representing Eq. 6.5 gives a lower bound to all the test results, and suggests that the results of the model analysis of Chapter 5 are realistic.

The increases in strength for the specimens with No. 2 and No. 3 longitudinal bars are indicated in Figs. 6.4 and 6.5 respectively. These results are somewhat lower than those plotted in Fig. 6.3. A possible explanation for this reduction in strength is that the load which is assumed to be carried by the bars is greater than its correct value. However, if this is the case, the discrepancy cannot be due to buckling of the bars, since the results of Fig. 6.5 are at least as low as those of Fig. 6.4. In addition, the two lowest results of Fig. 6.5 are for specimens with tie spacings of 2 and 8 in., which implies that the unsupported length of the bars is not a critical factor.

Another possible reason for the strength difference is that the bars reduce the efficiency of the adjacent concrete. It seems likely that the concrete at the corners of the specimen, outside the bars, will spall off very easily, and this weakening effect may extend some distance from the bars.

(b) Deformation

The most important variables affecting the deformation of the specimens were the amount and spacing of the ties. Increasing the amount, or decreasing the spacing of the transverse reinforcement, while holding the other variables constant, produced an increase in ductility. From the tests of Szulczynski (5), it appeared that increasing the concrete strength produced some decrease in ductility beyond maximum load. The remaining variables - shape of cross section, stiffness of transverse reinforcement, and amount and stiffness of longitudinal reinforcement - had little or no effect on the ductility.

The tests have demonstrated that the use of rectangular ties can improve the behavior of concrete in compression to a great extent. In the specimens with ties at 2-in. spacing, the average strain at fracture, based on the total shortening of the specimen, ranged from 0.025 to 0.046, with a mean value of 0.034.

6.5 Stress-Strain Relationship Obtained From Test Results

In order to apply the test results to geometrical and loading conditions which are different from those in the test program, it is very desirable to define the stress-strain relation in terms of the most important variables. A study of Figs. 6.1 and 6.2 reveals that the relation between the stress of the concrete enclosed by the ties and the strain in the failure region can be expressed conservatively by means of two straight lines, as shown in Fig. 6.6. The position of line AB is fixed, where B represents the maximum net strength, which is equal to the unconfined compressive strength, and occurs at a strain of 0.002. The slope of line BD varies, depending on the amount and spacing of the transverse reinforcement, and can be determined by studying the variation in strain at point C, the point at which the stress has reduced to 50 percent of its maximum value.

It was pointed out in Section 6.4 that the main variables affecting the ductility of the specimens were the amount and spacing of the transverse reinforcement. Accordingly, the value of ϵ_{50}, the strain corresponding to point C in Fig. 6.6, will be expressed in terms of the parameters p'' and s/h, where p'' is the volumetric ratio of the transverse reinforcement, defined as the ratio between the volume of the ties and the volume enclosed by the outside dimensions of the ties; s is the center-to-center spacing of the ties, and h is the smaller value of the outside dimensions of the ties.

The relation between ϵ_{50} and s/h for the test series is shown in Fig. 6.7. It can be seen from Fig. 6.7 that the equation

$$\epsilon_{50} = 0.015 \frac{h}{s} \qquad (6.6)$$

agrees very closely with the test data.

The influence of the volumetric ratio p'' on the variation of ϵ_{50} is more difficult to define accurately, since the amount of available data relating these variables is rather limited. A study of the tests by Szulczynski (5), the results of which are illustrated in Figs. 2.3 and 2.4, seems to indicate that the relation between ϵ_{50} and p'' is linear. Accordingly, since the results shown in Fig. 6.7 correspond to a value of p'' equal to 0.02, the stress-strain relationship for concrete confined by rectangular transverse reinforcement may be expressed by the equation

$$\epsilon_{50} = 0.75 \frac{p''h}{s} \qquad (6.7)$$

7. SUMMARY

7.1 The Failure Theory

In order to explain some aspects of the behavior of concrete, a failure theory was developed based on observations of the structures of concrete and cement paste. Cement paste is composed of a number of solid particles interconnected by slender crystals, the cement gel. Accordingly, an analogous model was derived in a manner similar to that introduced by Reinius (1), by assuming a cubic arrangement of identical, nondeformable spheres, interconnected by elastic struts, as shown in Fig. 3.3. The areas of the struts were proportioned so as to produce a value of Poisson's ratio of 0.15 in the initial stages of uniaxial compression of the model.

As concrete is loaded, the cement crystals in both tension and compression begin breaking at various locations in the concrete mass. The number of such crystal fractures increases with increasing load until eventually further increases in deformation result in a decrease in load. Since crystal failures in the concrete mass are equivalent to a reduction in the area of the appropriate strut in the model, equations relating area and strain were developed for the struts. The random nature of the crystal strengths suggested the use of the normal distribution curve or Gaussian curve to express these area-strain relations. In order to produce reasonable results it was necessary to use skewed curves for both the tension and compression struts, which implies that extremely weak crystals are more common than extremely strong crystals.

The area-strain equation for the compression struts was

$$y = 50e^{-1.3(z - 0.588)^2} \tag{7.1}$$

where $z = \ln (\epsilon \times 10^3)$

$$A(\%) = 100 - y \ , \ \epsilon < 1.8 \times 10^{-3}$$

$$A = y \qquad , \ \epsilon \geq 1.8 \times 10^{-3}$$

and that for the tension struts was

$$y = 50e^{-0.5(z + 1.61)^2} \qquad (7.2)$$

where $z = \ln (\epsilon \times 10^3)$

$$A(\%) = 100 - y, \ \epsilon < 0.2 \times 10^{-3}$$

$$A = y \qquad , \ \epsilon \geq 0.2 \times 10^{-3}$$

7.2 Application of the Failure Theory to Concrete Under Uniaxial Stresses

The model, together with the area-strain relations of its struts, was then used to explain the load-strain relations of concrete subjected to both unconfined and confined compression. The resulting load-deflection curve for unconfined compression (Fig. 4.1) agreed very favorably with curves obtained from tests, and the behavior of the model provided a basis for explaining the phenomenon of failure in concrete under this loading condition. A description of this failure process will be given in the following paragraph.

Under the action of gradually increasing vertical compressive strain, a plain concrete specimen which has no lateral restraint will begin developing horizontal tensile strains. These tensile strains are caused by the action of cement crystals which are inclined at an angle to the direction of compression, and which create horizontal forces to maintain static equilibrium. In the absence of external horizontal compression on the specimen, these induced horizontal forces must be resisted by tensile stresses in horizontal cement crystals. The incidence of crystal fractures accelerates with increasing compressive strain until finally the tension crystals reach their maximum load-carrying capacity. The maximum compressive load then occurs after a small further increase in strain. For strains beyond that at which the capacity of the tension crystals is reached, a greater proportion of the applied compression is resisted by the vertical crystals, and eventually the number of compression failures is so extensive that the load decreases rather rapidly with increasing strain.

7.3 Application of The Failure Theory to Concrete Under Triaxial Stresses

An explanation of the behavior of confined concrete depends on a consideration of solid particles in the concrete, as well as the cement crystals. From the preceding description of the failure of unconfined concrete, it can be seen that the initiation of failure for this loading condition is a function of the strength in tension of the horizontal cement crystals. For this reason, when concrete is subjected to lateral confining pressures in addition to axial compression, the strength is increased, and is more dependent on the compressive strength of the cement crystals.

The structure of concrete is composed of a number of solid particles, both unhydrated cement grains and granules of aggregate. The spacing of these particles varies considerably throughout the concrete, but as compression of the concrete progresses, and the cement crystals break, an increasing number of the solid particles are forced into contact. At very high strains, in the presence of sufficient confinement, virtually all the load will be carried by direct grain-to-grain contact. A description of the behavior of confined concrete can accordingly be given by the derived model and failure theory at low strains, but as the strain increases, the behavior is more nearly a function of the load-strain relations of confined aggregate.

The failure theory was also used to illustrate the difference between the strength and ductility of spirally-reinforced columns and of columns with rectangular ties. The theoretical strength of spiral columns was appreciably greater because all horizontal tension members were confined by the action of the spiral. In the case of tied columns, however, the confining effect of the ties was produced by concentrated horizontal loads at the corners of the column. Accordingly, many of the horizontal struts remote from the corner received little or no confining pressure.

7.4 Experimental Program

In order to compare the theoretical behavior of tied columns with that occurring in practice, a test program was carried out on axially-loaded columns with rectangular ties.

A total of 60 specimens were tested, all having dimensions of 5 by 5 by 25 in. The main variables considered in the test program were the spacing and bending stiffness of the ties, and the amount and stiffness of the longitudinal reinforcement. The results of these tests indicated that the use of ties did not affect the gross strength of the columns appreciably, but did produce considerable increase in ductility.

From a consideration of the test results of these 60 specimens, together with the results of 30 specimens tested by Szulczynski (5), the following conclusions can be made regarding the behavior of axially-loaded tied columns: Rectangular ties have no significant effect on the gross strength of columns, but do produce an increase in deformation capacity. The ductility of tied columns increases with increasing amount or decreasing spacing of the ties, if the other variables are kept constant. The ductility is decreased somewhat with increases in concrete strength. Other variables, such as flexural stiffness of transverse reinforcement, amount and flexural stiffness of longitudinal reinforcement, and shape of cross section have little or no effect on the behavior.

An important application of rectangular ties is their use as stirrups in reinforced concrete beams. Since the principles of limit design require considerable ductility of the members concerned, and also since ductility is extremely important in providing resistance to dynamic loading, favorable deformation qualities are very desirable in reinforced concrete. The results of the theoretical and experimental investigations outlined above imply that sufficient ductility can be obtained by using properly-designed rectangular ties.

REFERENCES

1. Reinius, Erling, "A Theory of the Deformation and the Failure of Concrete," Cement and Concrete Association, London, Translation No. 63. (Translated from the Swedish and reprinted from "Betong," 1955, No. 1.)

2. Ramaley, D. and D. McHenry, "Stress-Strain Curves for Concrete Strained Beyond the Ultimate Load," Laboratory Report No. SP-12, U. S. Bureau of Reclamation, March 1947.

3. Richart, F. E., A. Brandtzaeg, and R. L. Brown, "A Study of the Failure of Concrete Under Combined Compressive Stresses," University of Illinois Engineering Experiment Station Bulletin No. 185, 1928.

4. Richart, F. E., A. Brandtzaeg, and R. L. Brown, "The Failure of Plain and Spirally Reinforced Concrete in Compression," University of Illinois Engineering Experiment Station Bulletin No. 190, 1929.

5. Szulczynski, Tadeusz and M. A. Sozen, "Load-Deformation Characteristics of Concrete Prisms with Rectilinear Transverse Reinforcement," University of Illinois Structural Research Series No. 224, September 1961.

6. Seely, F. B. and J. O. Smith, "Advanced Mechanics of Materials," John Wiley and Sons, Inc., Second Edition, pp. 69-94.

7. Griffith, A. A., "The Phenomena of Rupture and Flow in Solids," Philosophical Transactions, Royal Society of London, Vol. 221, Series A, 1920, pp. 163-198. (See also, Griffith, A. A., "The Theory of Rupture," Proceedings, First International Congress for Applied Mechanics, Delft, 1924.)

8. von Karman, Th., "Festigkeitsversuche unter allseitigem Druck," Mitteilungen über Forschungsarbeiten auf dem Gebiete des Ingenieurwesens, Vol. 118, 1912.

9. Böker, Robert, "Die Mechanik der bleibenden Formänderung in kristallinisch aufgebauten Körpern," Mitteilungen über Forschungsarbeiten auf dem Gebiete des Ingenieurwesens, Vol. 175 and 176, 1915.

10. Wästlund, G., "Nya rön angående betongens grundläggande hållfasthetsegenskaper," Betong, Vol. 22, No. 3, 1937, pp. 189-205.

11. Bellamy, C. J., "Strength of Concrete Under Combined Stress," Proceedings, ACI, Vol. 58, October 1961.

12. Bresler, B. and K. S. Pister, "Failure of Plain Concrete Under Combined Stresses," Proceedings, ASCE, Vol. 81, Separate No. 674, April 1955. (See also, Bresler, B. and K. S. Pister, "Strength of Concrete Under Combined Stresses," Proceedings, ACI, Vol. 55, September 1958.)

13. Oran, Cenap, "Theories of Failure," Term Paper for Theoretical and Applied Mechanics Department Course No. 427, University of Illinois, 1957.

14. McHenry, D. and J. Karni, "Strength of Concrete Under Combined Tensile and Compressive Stress," Proceedings, ACI, Vol. 54, April 1958.

15. Boutet, D., "Réflexions sur les bétons en général et sur les bétons de ciment en particulier," Travaux, Vol. 34, No. 183, 1950.

16. Bernal, J. D., J. W. Jeffery, and H. F. W. Taylor, "Crystallographic Research on the Hydration of Portland Cement," Magazine of Concrete Research, Vol. 4, No. 11, 1952.

17. Baker, A. L. L., "An Analysis of Deformation and Failure Characteristics of Concrete," Magazine of Concrete Research, Vol. 11, No. 33, 1959.

18. Holmes, M. C., "An Outline of Probability and its Uses," Edwards Brothers, Inc., Ann Arbor, Michigan.

19. Duffy, J. and R. D. Mindlin, "Stress-Strain Relations and Vibrations of a Granular Medium," Journal of Applied Mechanics, Vol. 24, 1957.

20. Thurston, C. W. and H. Deresiewicz, "Analysis of a Compression Test of a Model of a Granular Medium," Journal of Applied Mechanics, Vol. 26, 1959.

21. Bjerrum, L., S. Kringstad, and O. Kummeneje, "The Shear Strength of a Fine Sand," Fifth International Conference on Soil Mechanics and Foundation Engineering, Vol. 1, 1961.

22. Peck, R. B., W. E. Hanson, and T. W. Thornburn, "Foundation Engineering," John Wiley and Sons, Inc., 1954, pp. 68-95.

23. Hanson, J. A., "Strength of Structural Lightweight Concrete Under Combined Stress," Journal of the PCA Research and Development Laboratories, Vol. 5, No. 1, January 1963.

TABLE 1

ROD FORCES UNDER UNIAXIAL PRESSURE - REINIUS MODEL

Pressure	P_1	P_2	P_3	P_{AB}	P_{AC}	P_{AD}	P_{AE}
P_z	-0.051	-0.051	0.351	-0.013	0.057	0.022	0.022
P_y	-0.051	0.351	-0.051	0.040	0.004	0.053	-0.009
P_x	0.351	-0.051	-0.051	0.040	0.004	-0.009	0.053

Values given are coefficients of P_z in the first line, of P_y in the second line, and of P_x in the third line.

TABLE 2

PRELIMINARY REINIUS FAILURE THEORY

Effective Area Of Rods 1, 2, and AB In Relation to Original Area	$P_1 = P_2$	P_3	$\epsilon_x = \epsilon_y$	ϵ_z	$\nu = \frac{\epsilon_x}{\epsilon_z}$
100 %	$-0.051\ P_z$	$0.351\ P_z$	$-0.051\ K^*$	0.351 K	0.14
75 %	$-0.048\ P_z$	$0.355\ P_z$	-0.064 K	0.355 K	0.18
50 %	$-0.043\ P_z$	$0.362\ P_z$	-0.086 K	0.362 K	0.24
25 %	$-0.033\ P_z$	$0.377\ P_z$	-0.132 K	0.377 K	0.35
10 %	$-0.020\ P_z$	$0.399\ P_z$	-0.195 K	0.399 K	0.50

* $K = P_z/AE$, where A = original area of struts 1, 2, 3.

TABLE 3

FINAL REINIUS FAILURE THEORY

Effective Area of Rods 1, 2, 3, And AB in Relation to Original Area	$P_1 = P_2$	P_3	$\epsilon_x = \epsilon_y$	ϵ_z	$\nu = \frac{\epsilon_x}{\epsilon_z}$
100 %	$-0.051\ P_z$	$0.351\ P_z$	$-0.051\ K^*$	$0.351\ K$	0.14
75 %	$-0.059\ P_z$	$0.324\ P_z$	$-0.078\ K$	$0.432\ K$	0.18
50 %	$-0.067\ P_z$	$0.284\ P_z$	$-0.135\ K$	$0.568\ K$	0.24
25 %	$-0.076\ P_z$	$0.217\ P_z$	$-0.305\ K$	$0.867\ K$	0.35
10 %	$-0.069\ P_z$	$0.142\ P_z$	$-0.689\ K$	$1.416\ K$	0.49

* $K = P_z/AE$, where A = original area of struts 1, 2, 3.

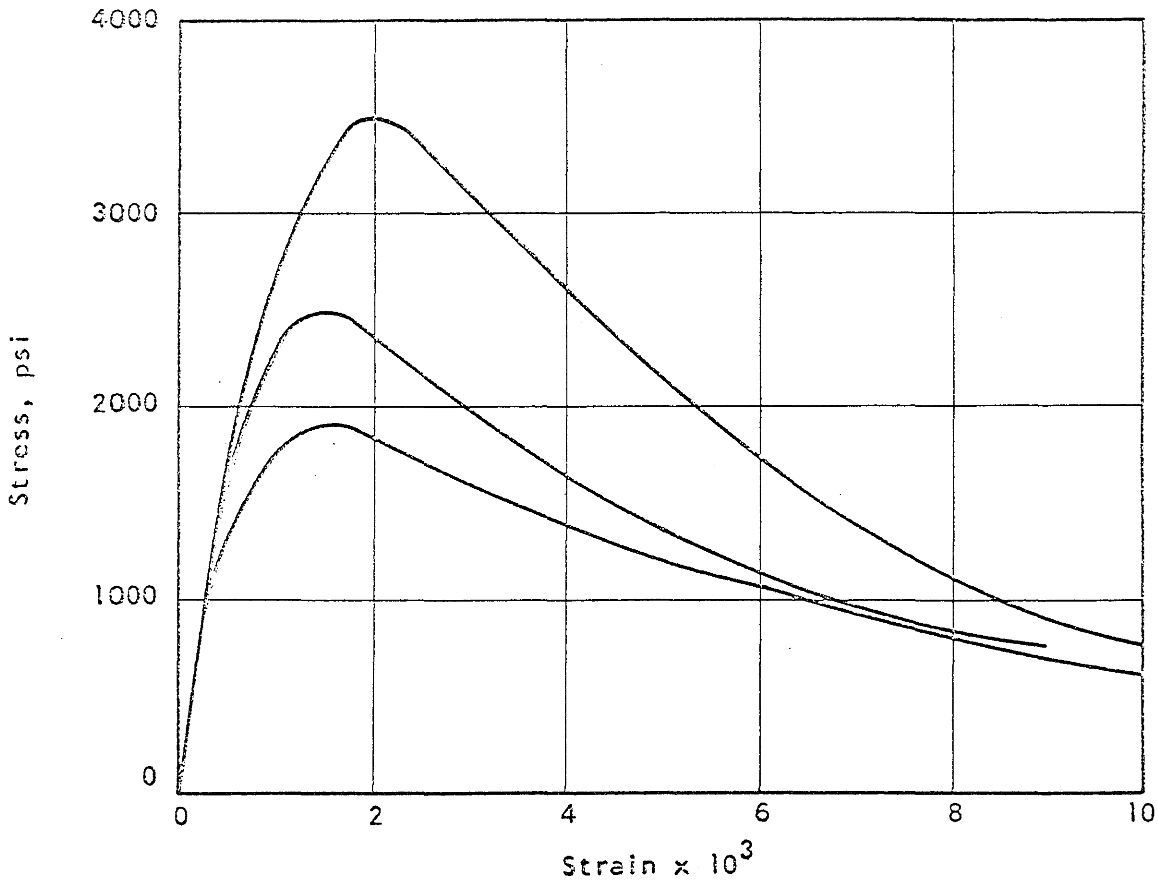

FIG. 2.1 STRESS-STRAIN CURVES MEASURED FROM 3 BY 6-IN. CYLINDERS (Reference 2)

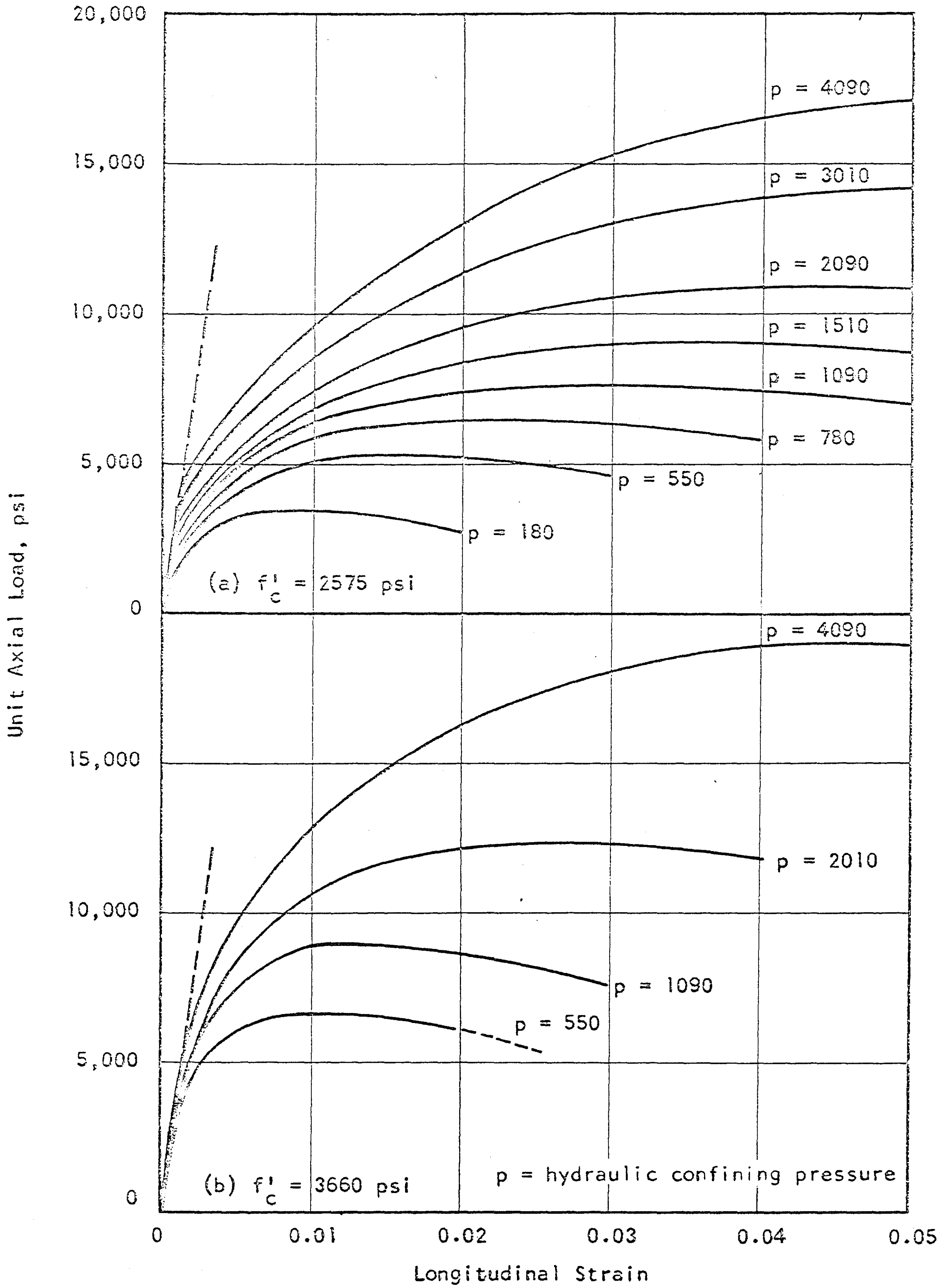

FIG. 2.2 STRESS-STRAIN CURVES MEASURED FROM 4 BY 8-IN. CYLINDERS UNDER LATERAL HYDRAULIC PRESSURE (Reference 3)

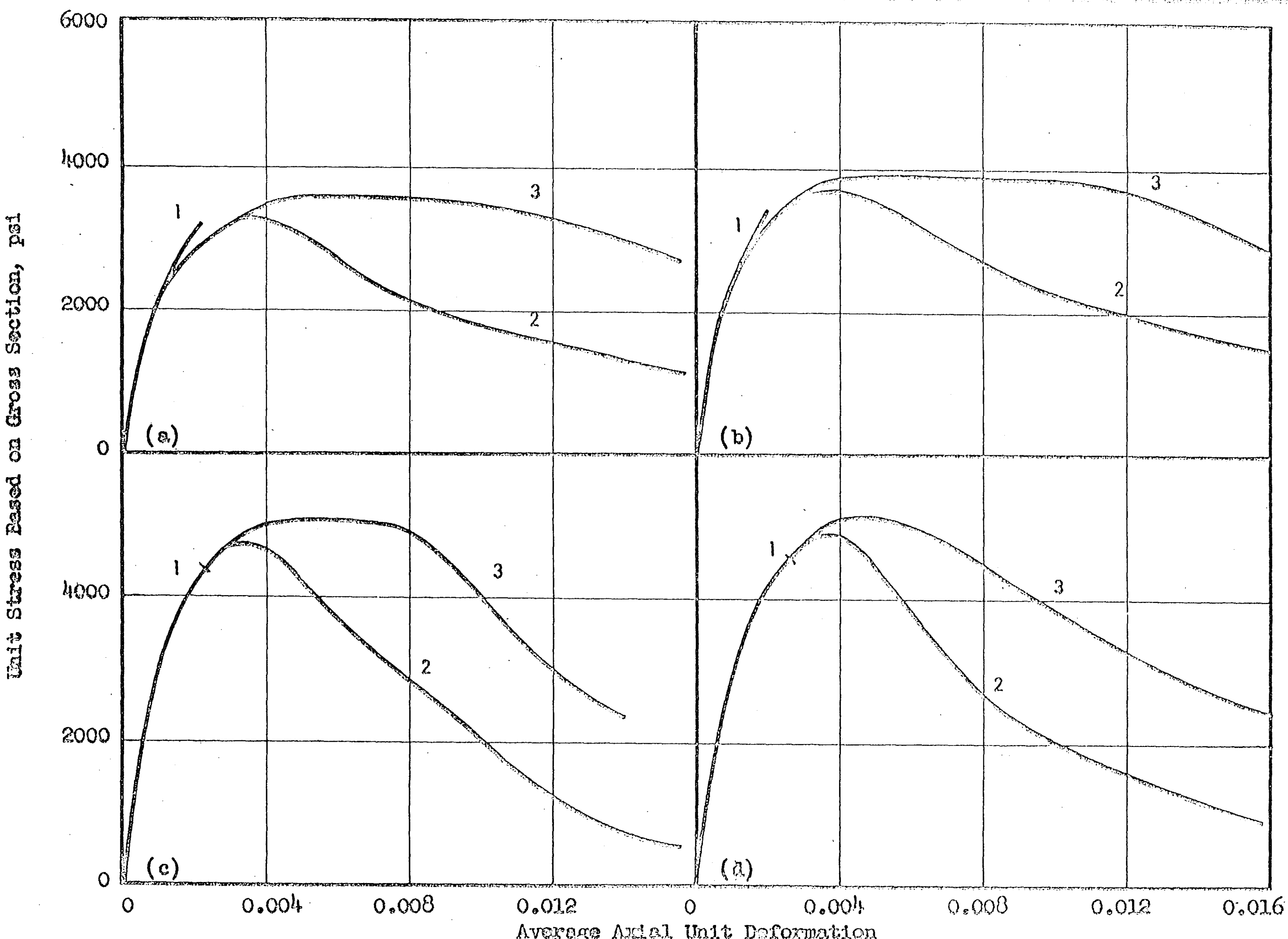

FIG. 2.3 LOAD-DEFORMATION CURVES MEASURED FROM 5 BY 5 BY 25-IN. PRISMS (Reference 5).

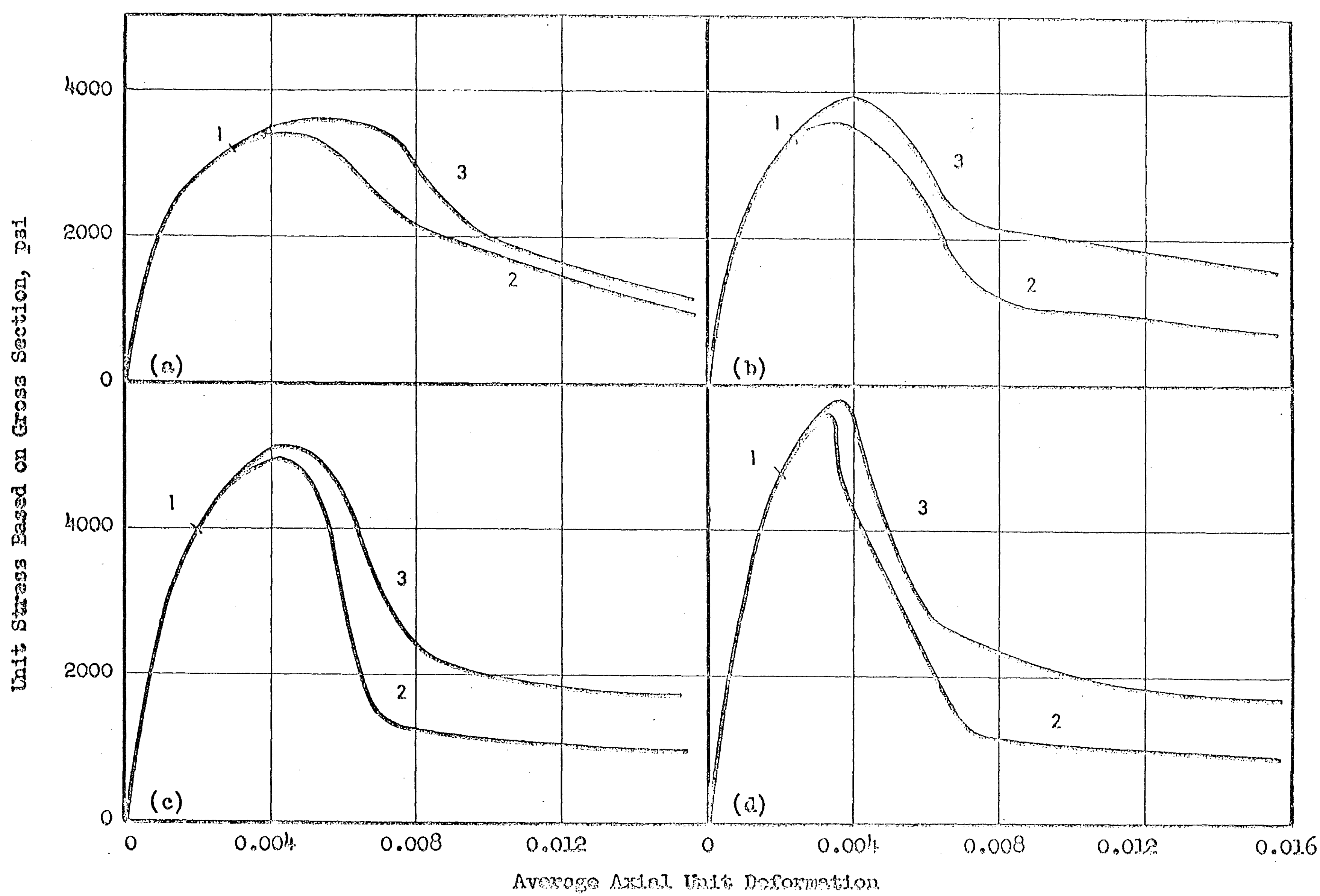

FIG. 2.4 LOAD-DEFORMATION CURVES MEASURED FROM 5 BY 10 BY 25-IN. PRISMS (Reference 5)

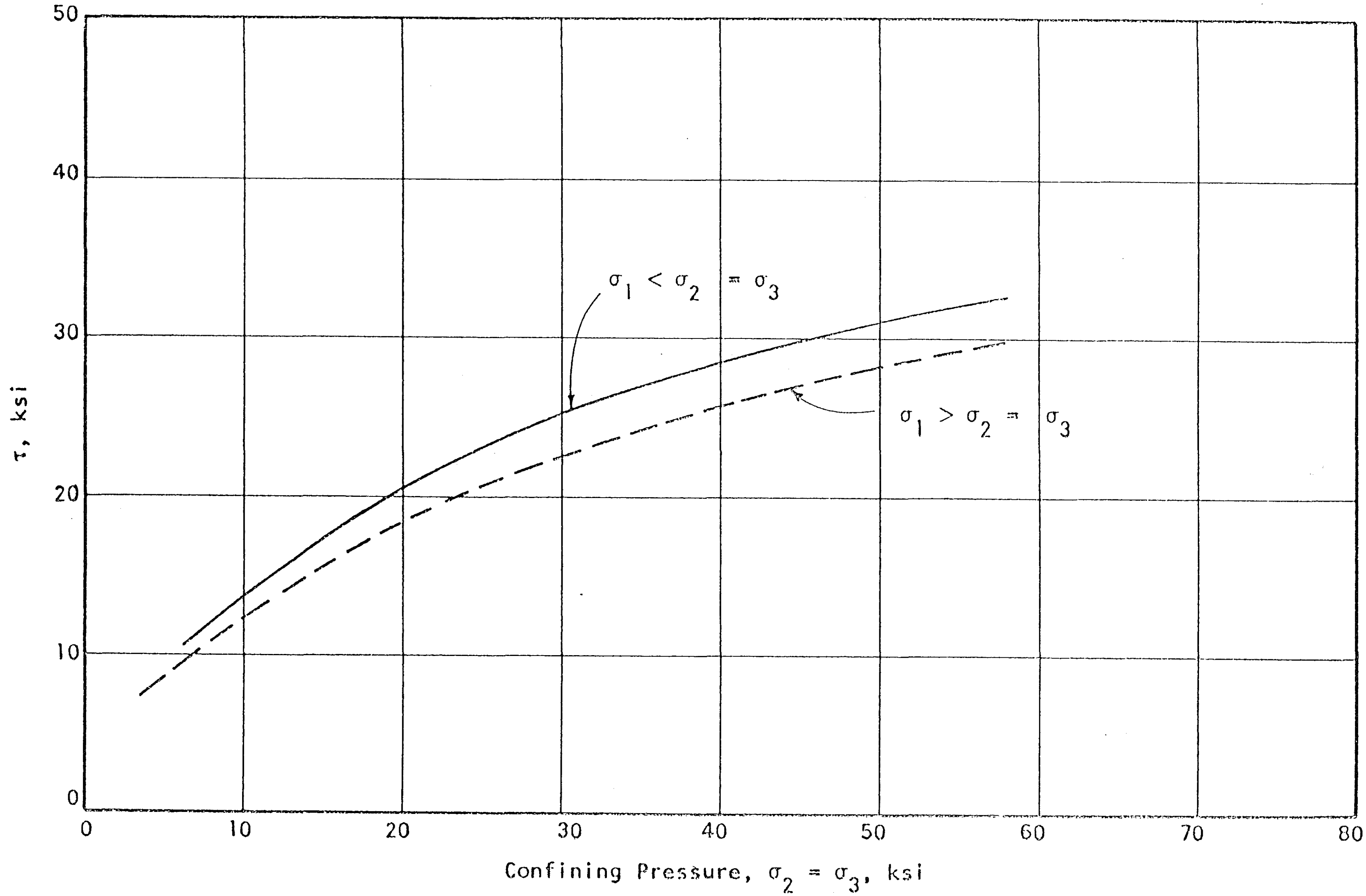

FIG. 2.5 MOHR'S CIRCLE ENVELOPES - KARMAN AND BOKER TESTS (Reference 9)

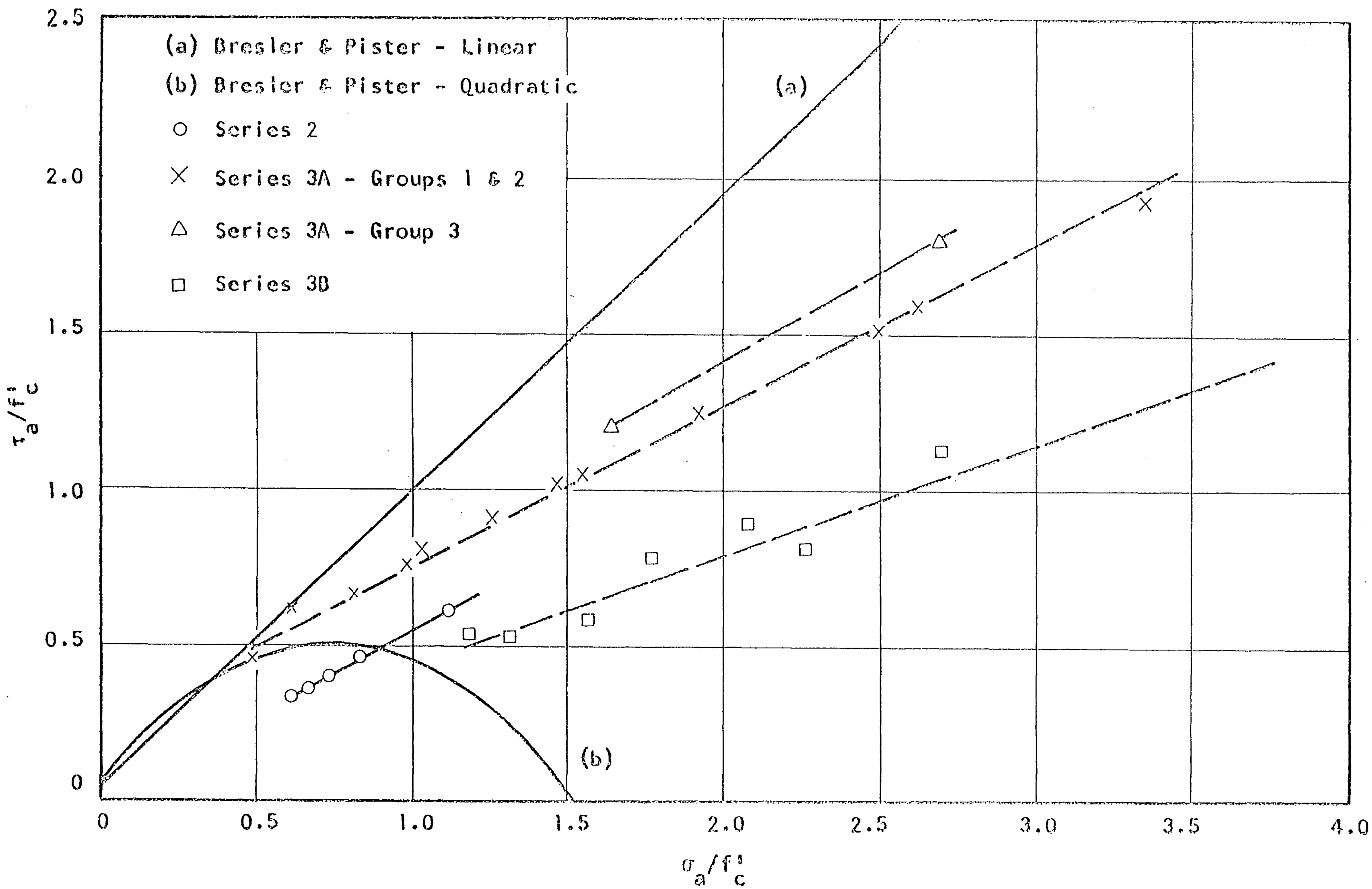

FIG. 2.6 COMPARISON OF THE LINEAR AND QUADRATIC FUNCTIONS PROPOSED BY BRESLER AND PISTER WITH TEST DATA FROM RICHART, BRANDTZAEG, AND BROWN (References 3 and 12)

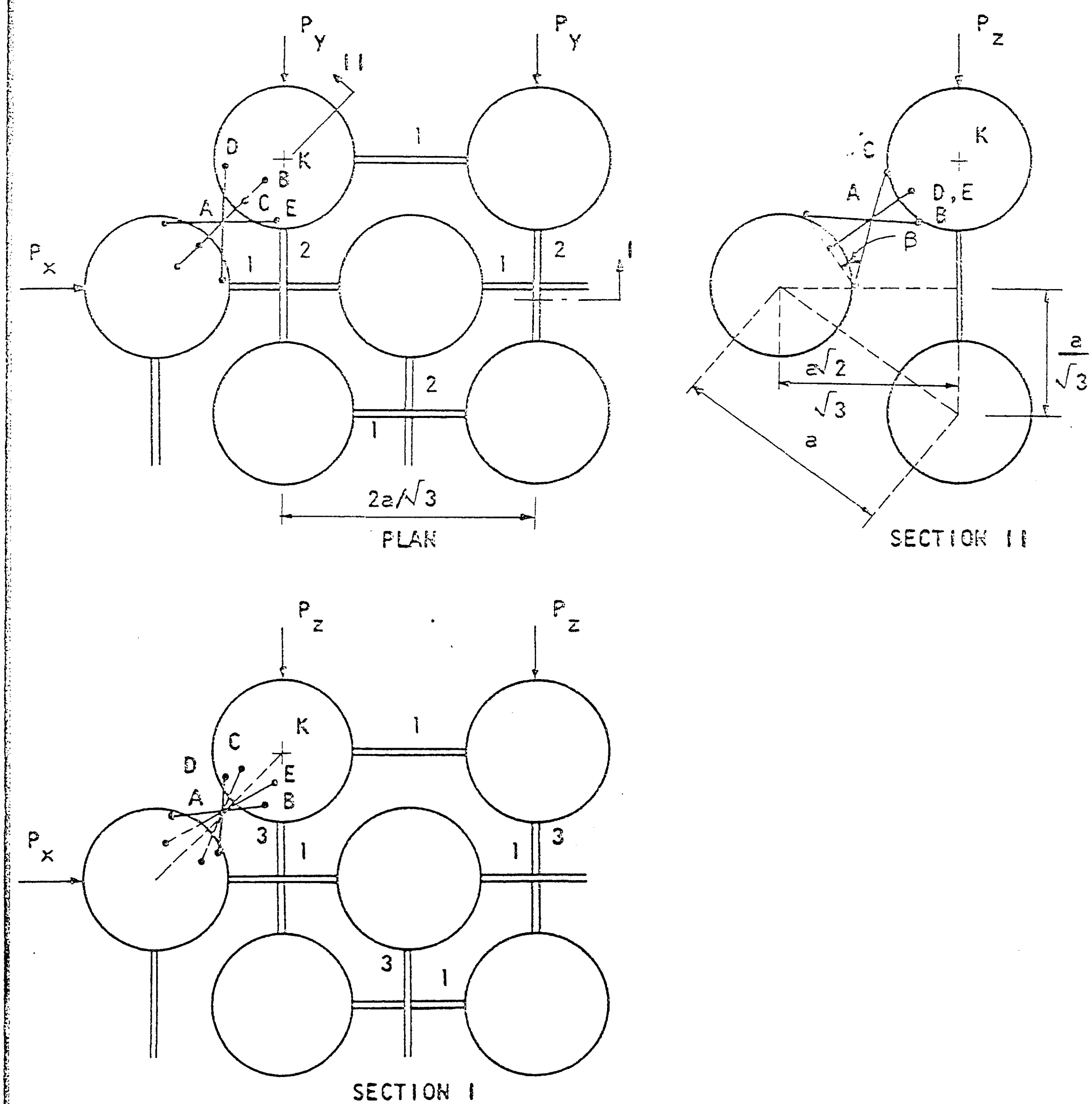

FIG. 2.7 REINIUS' MODEL
(Reference 1)

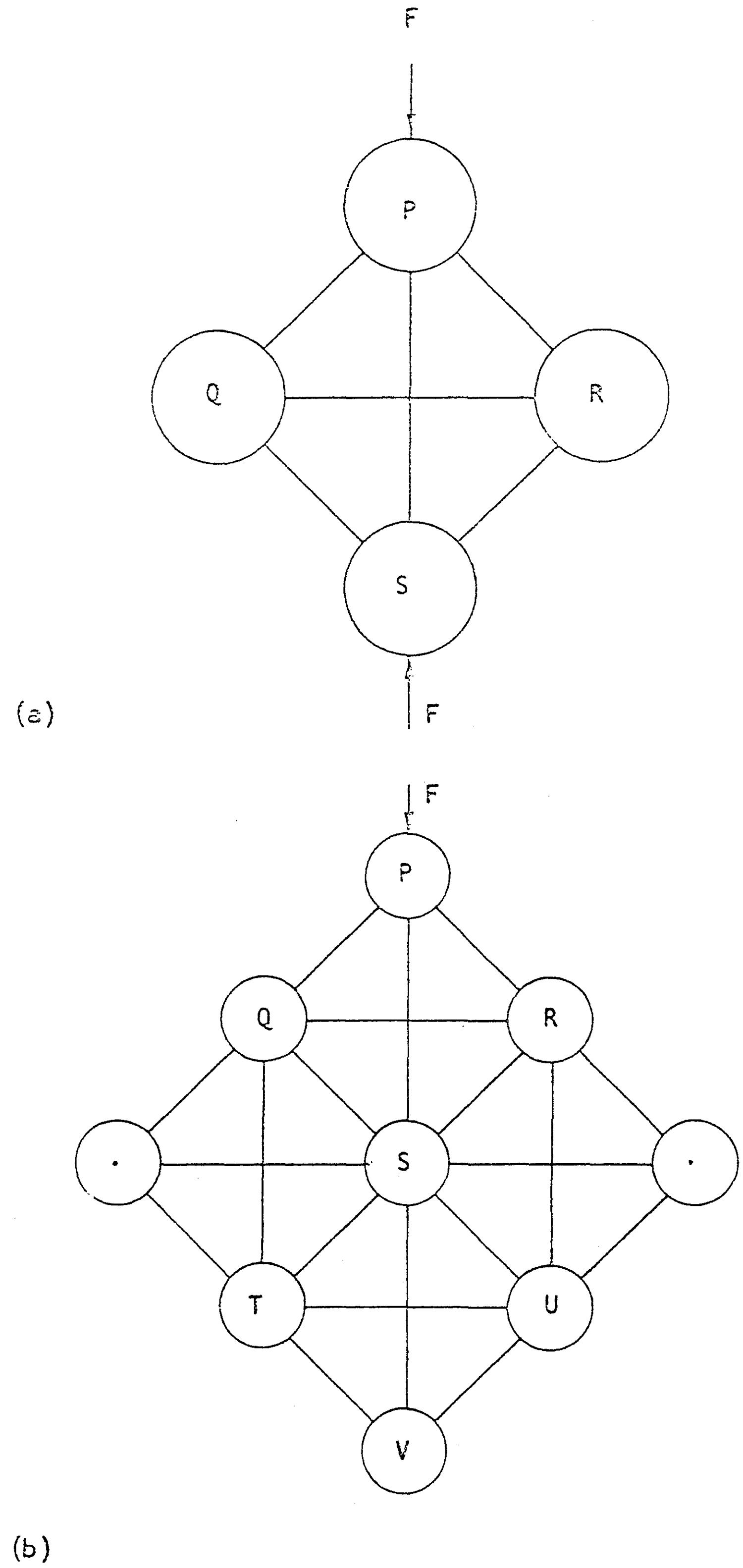

FIG. 2.8 TWO-DIMENSIONAL MODEL

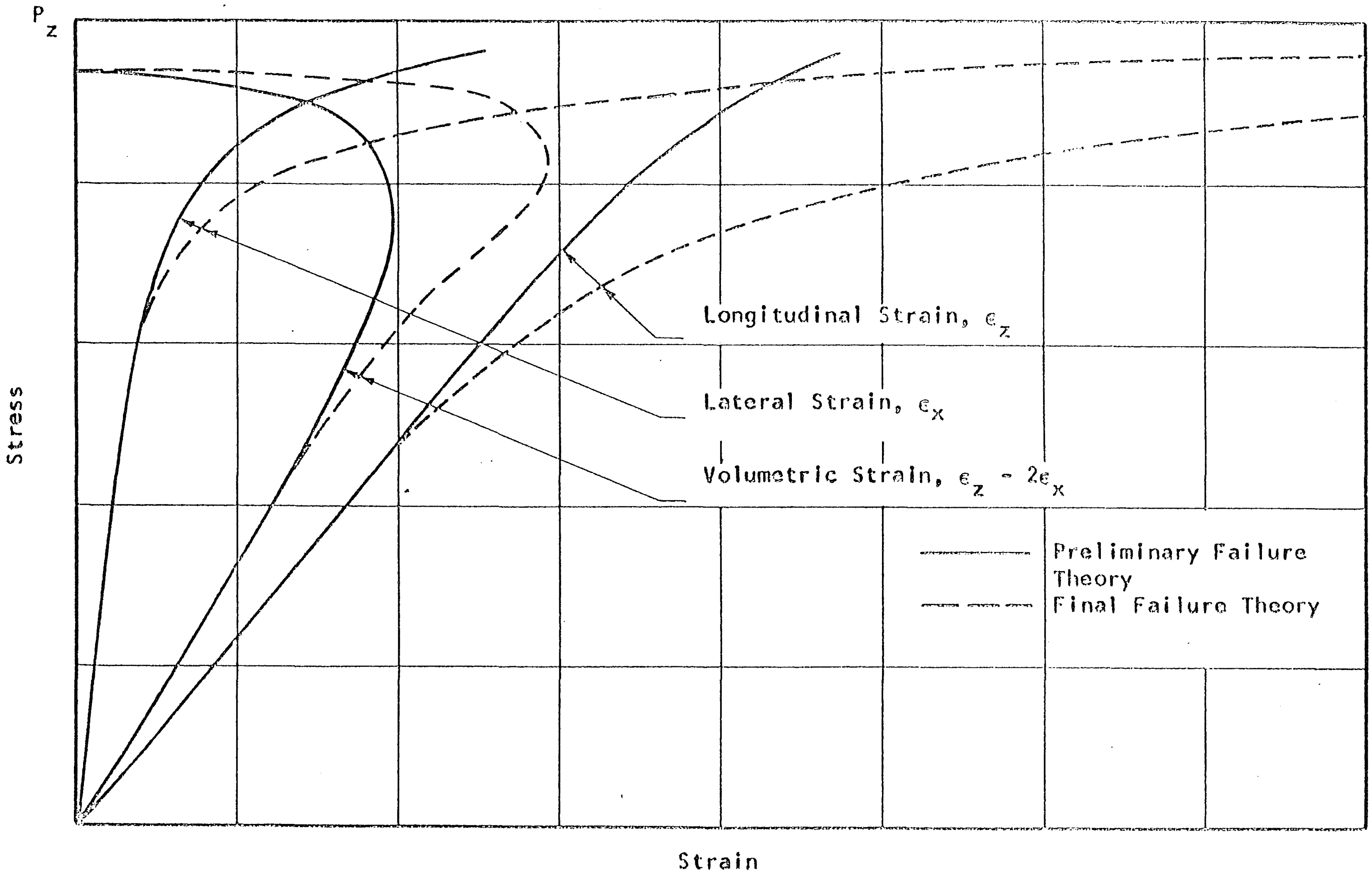

FIG. 2.9 STRESS-STRAIN CURVES, REINIUS' THEORY (Reference 1)

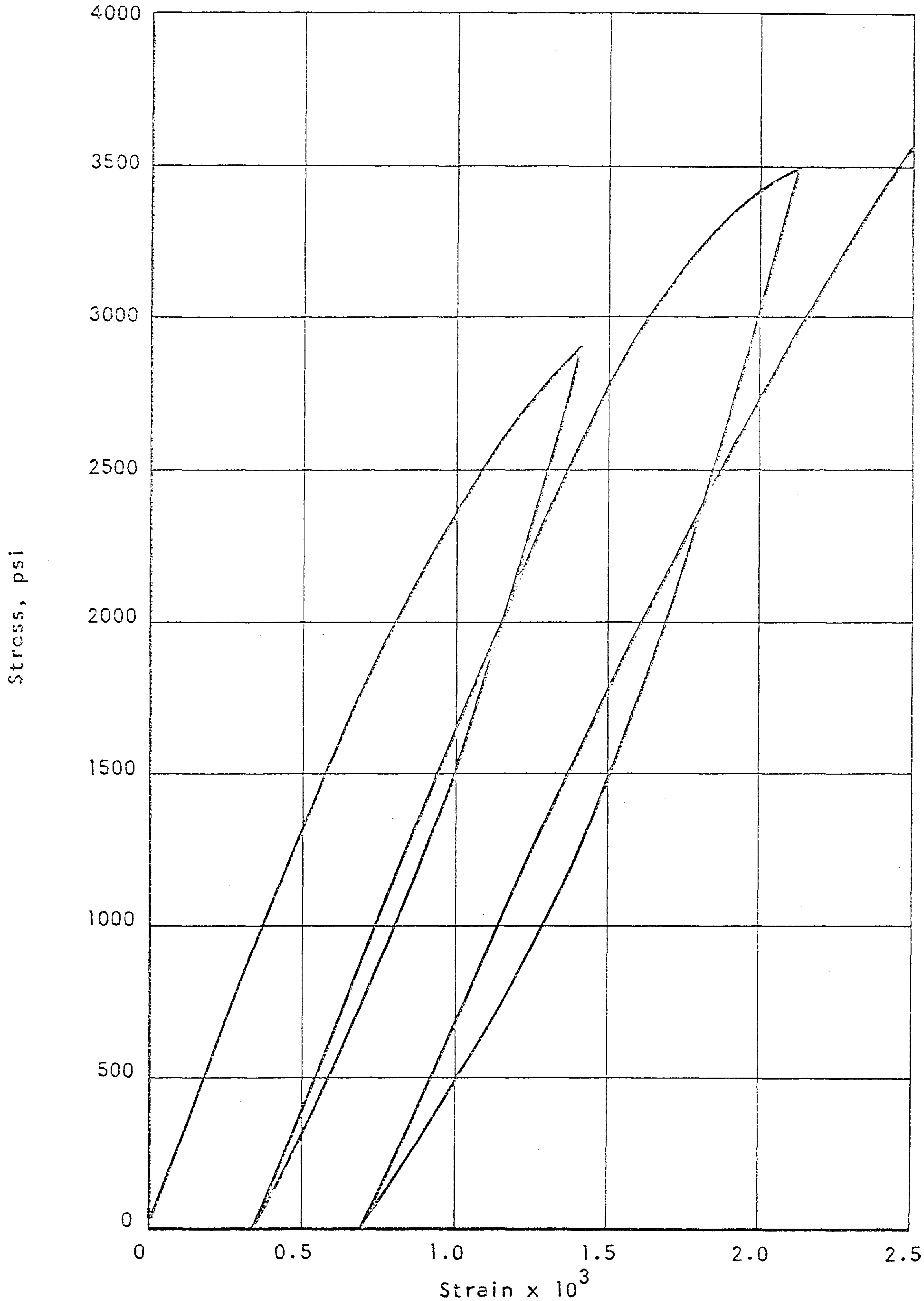

FIG. 2.10 UNCONFINED CONCRETE UNDER REPEATED LOADING

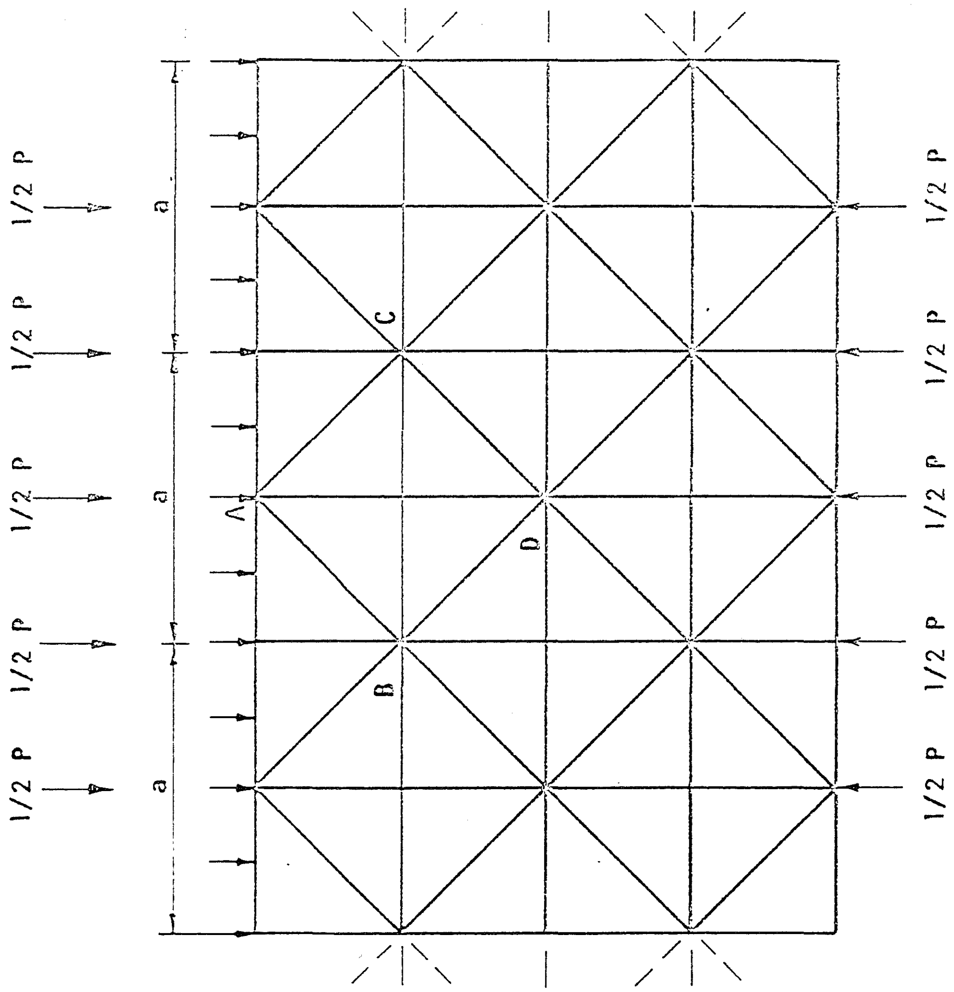

FIG. 2.11 BAKER'S LATTICE (Reference 17)

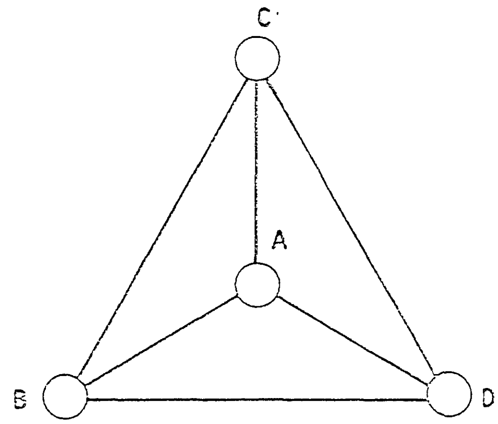

Plan

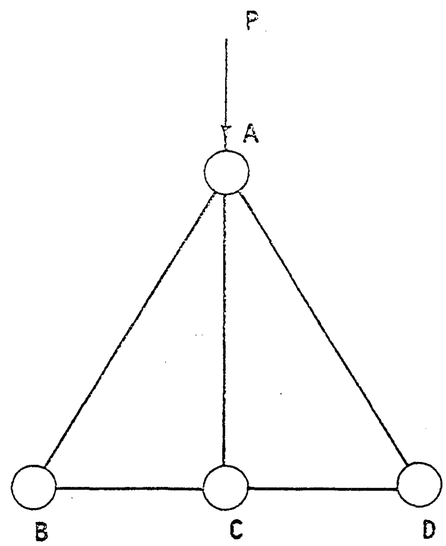

Elevation

FIG. 3.1 TETRAHEDRAL MODEL

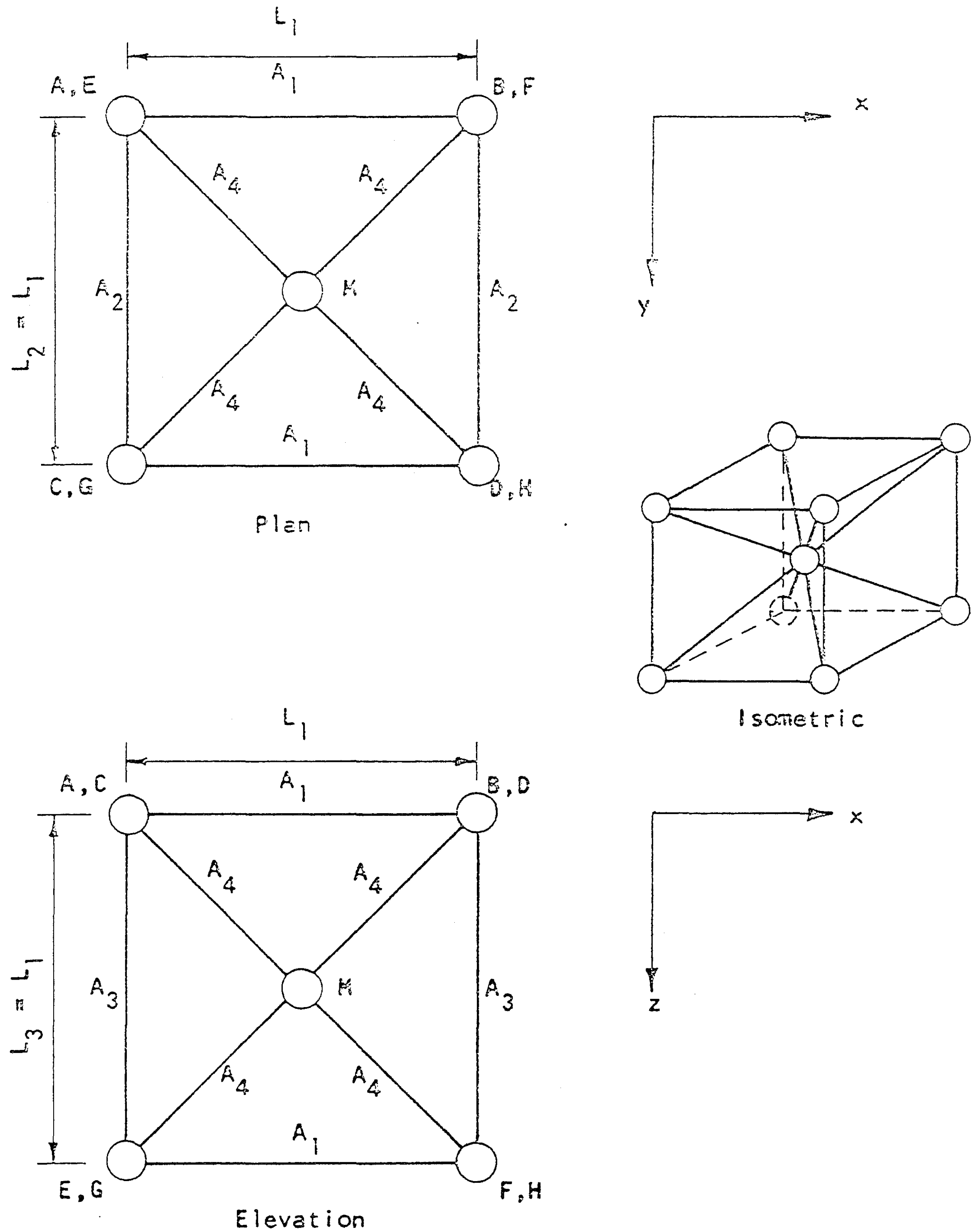

FIG. 3.2 BODY-CENTERED CUBIC MODEL

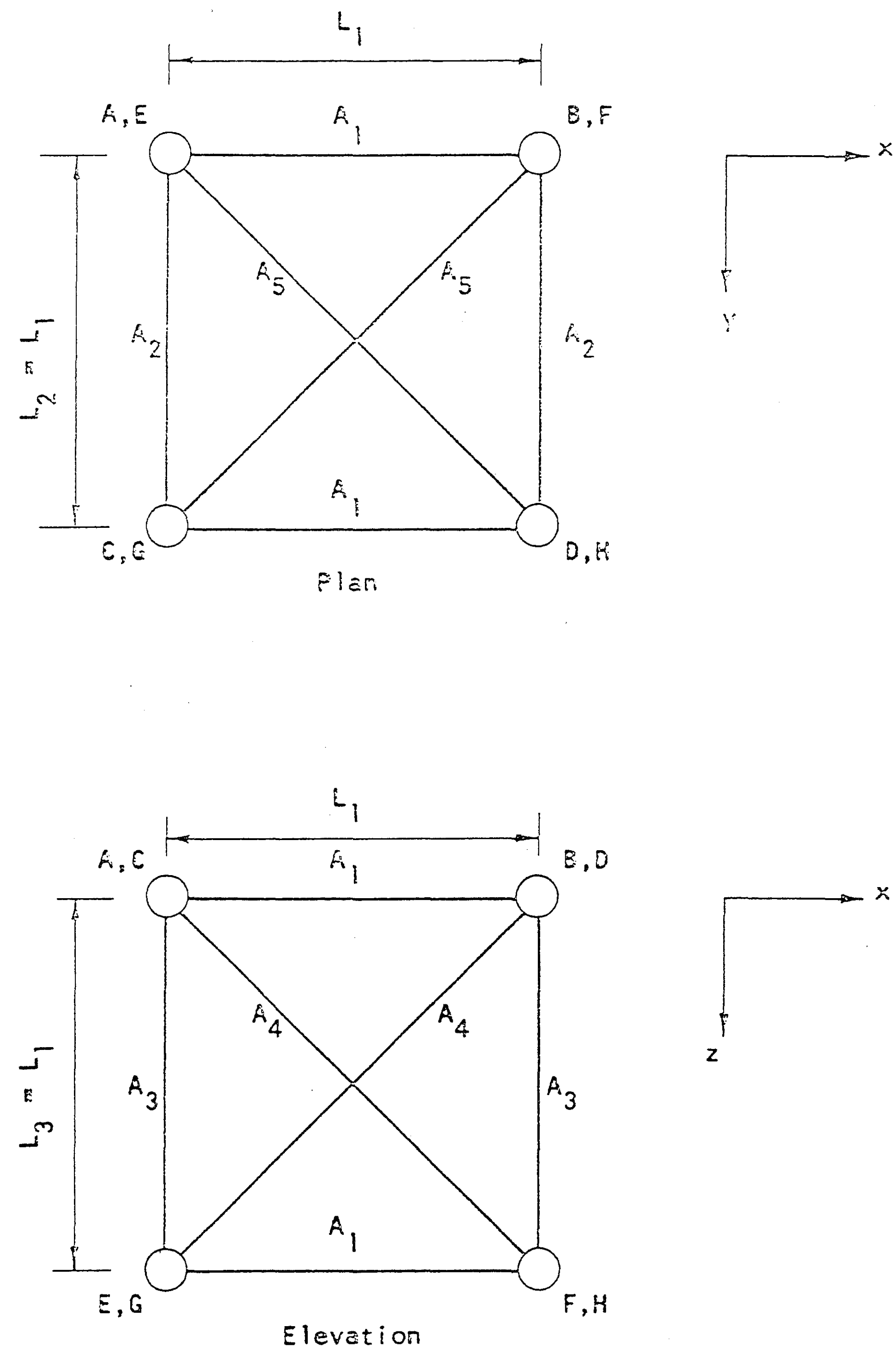

FIG. 3.3a PROPOSED CUBIC MODEL

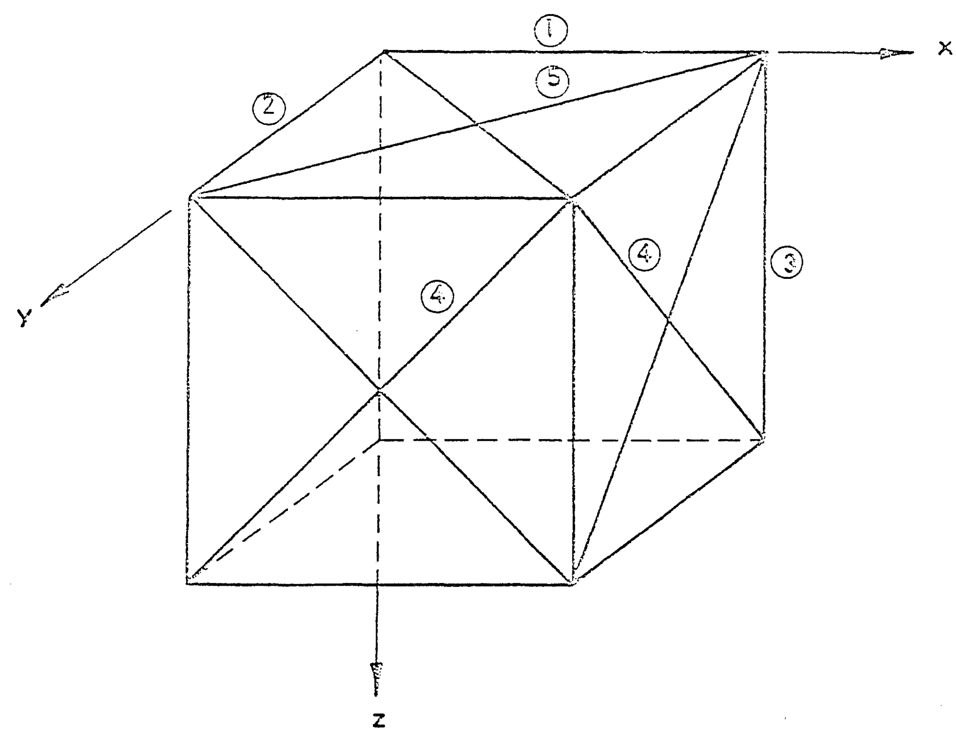

FIG. 3.3b ISOMETRIC DIAGRAM OF PROPOSED CUBIC MODEL

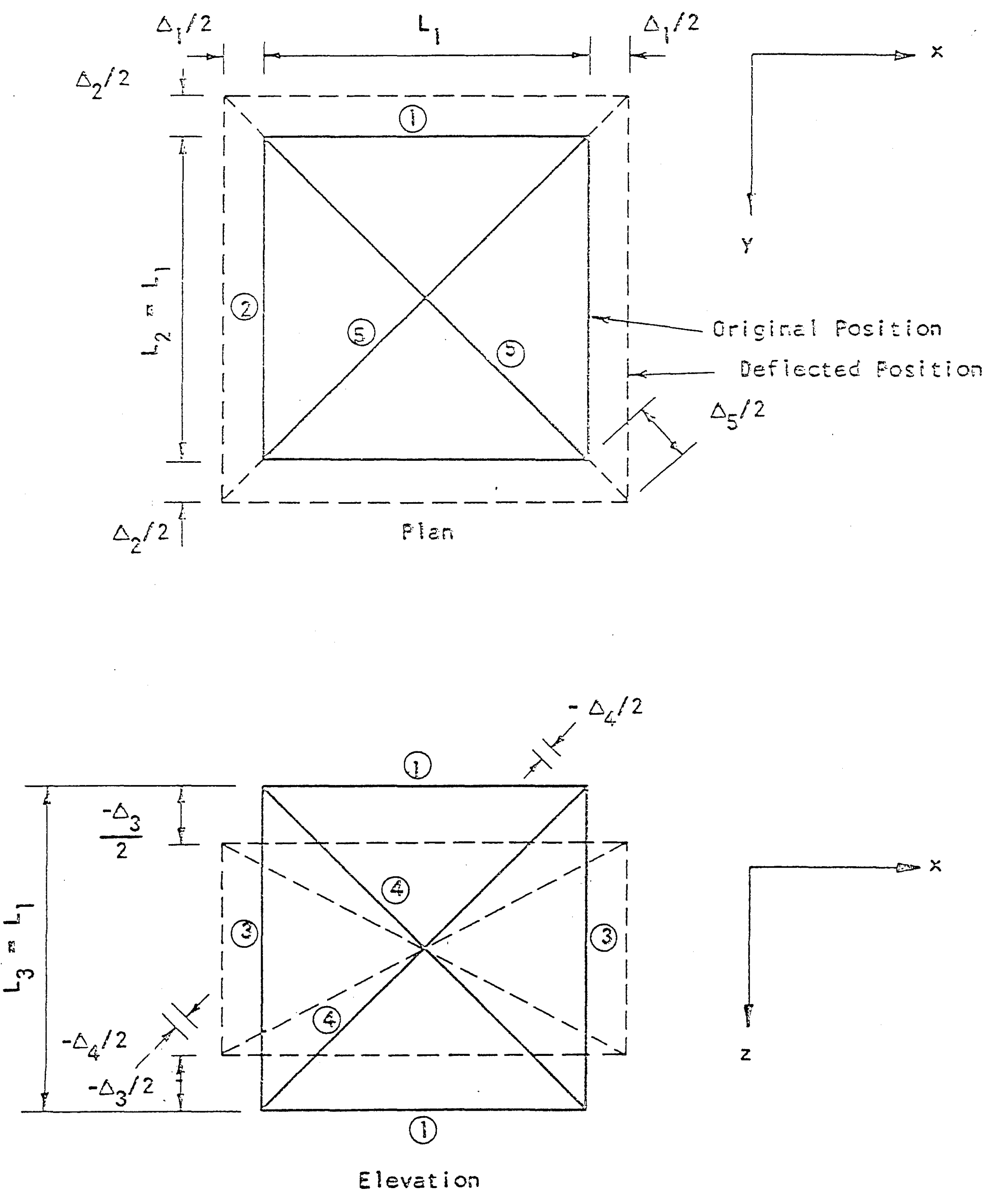

FIG. 3.4 DEFLECTION OF MODEL UNDER UNCONFINED COMPRESSION

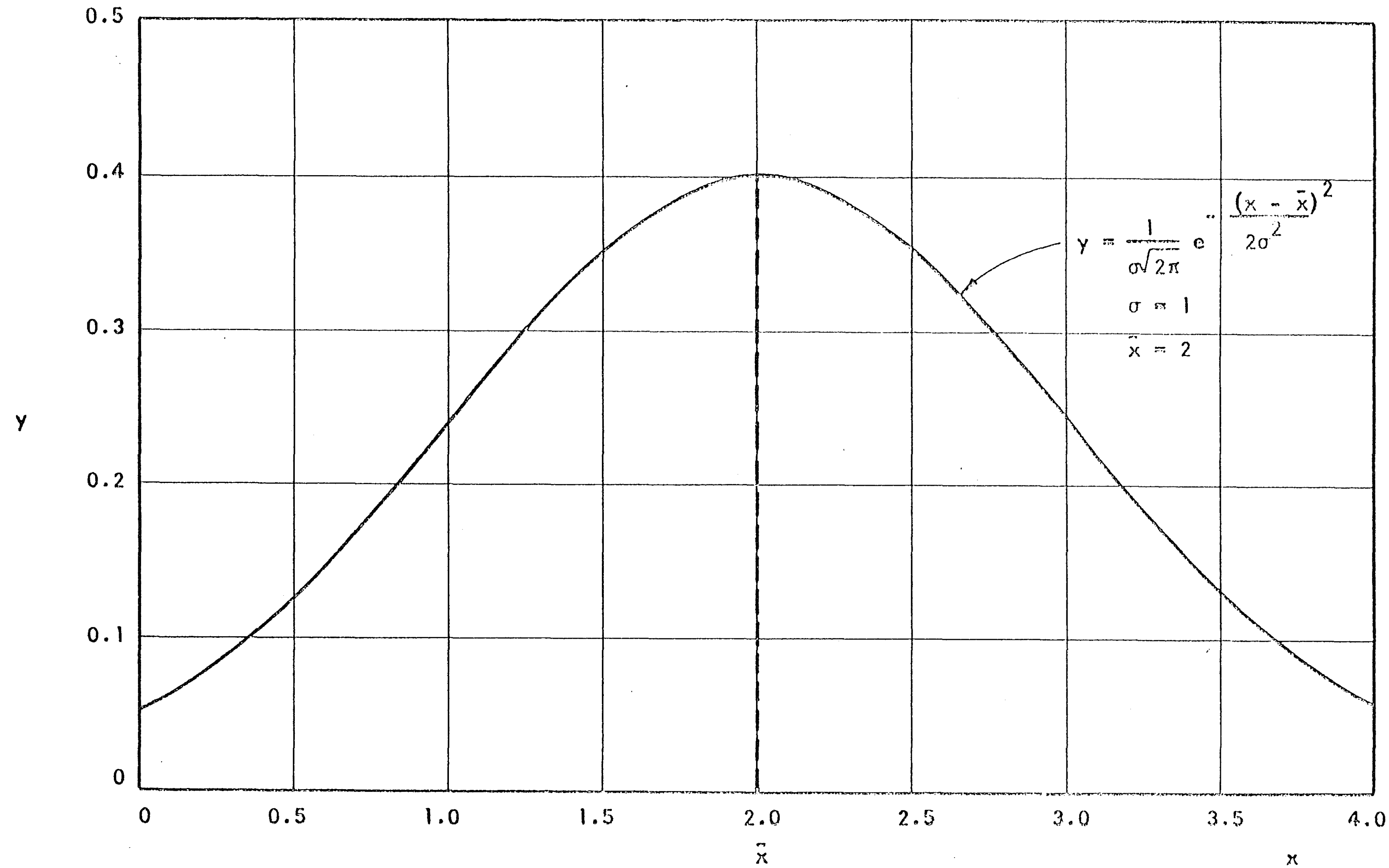

FIG. 3.5 NORMAL DISTRIBUTION CURVE

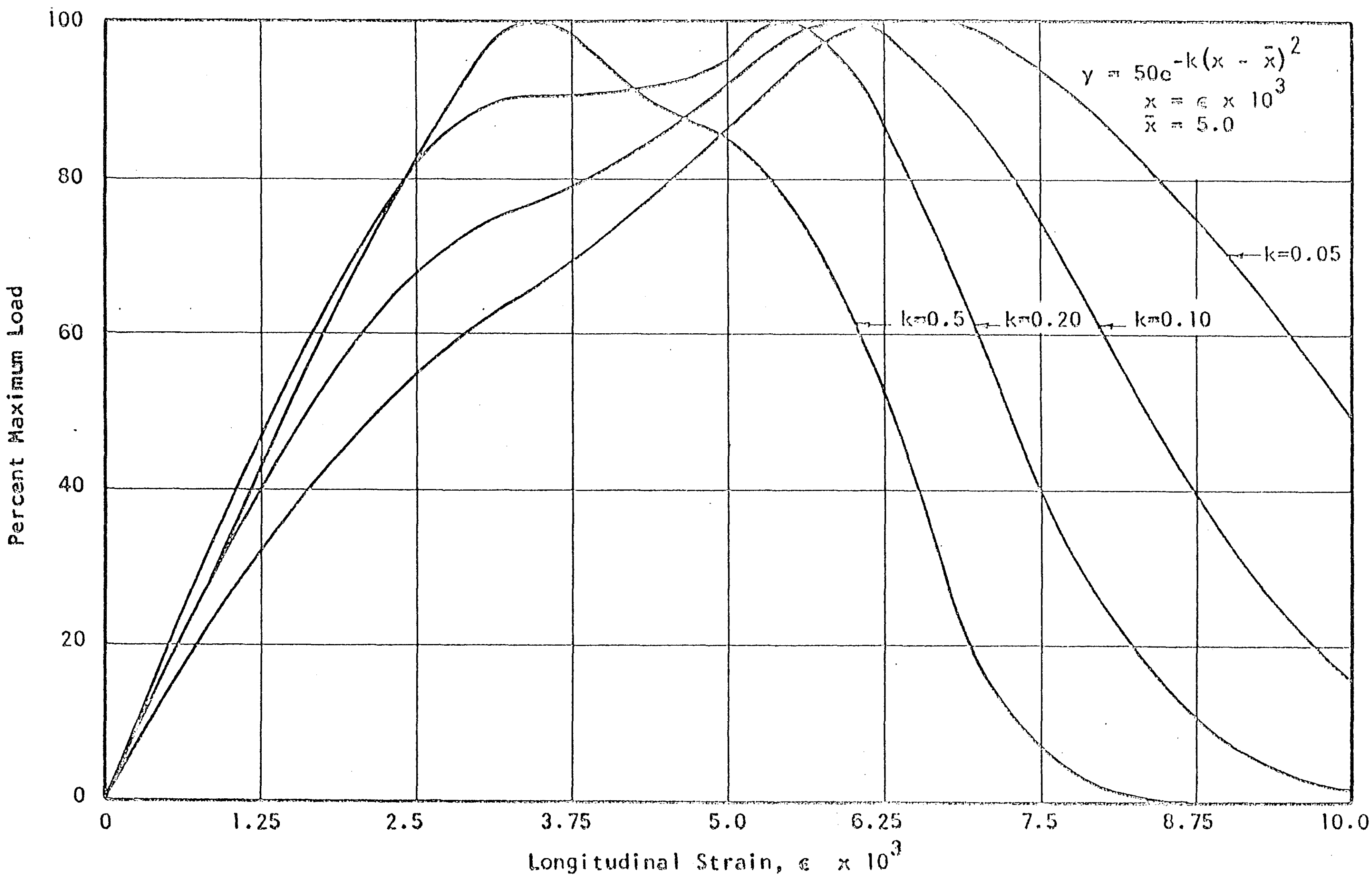

FIG. 3.6 LOAD-STRAIN RELATIONSHIPS FOR A SINGLE COMPRESSION STRUT BASED ON A NORMAL DISTRIBUTION OF EFFECTIVE AREA VS. STRAIN

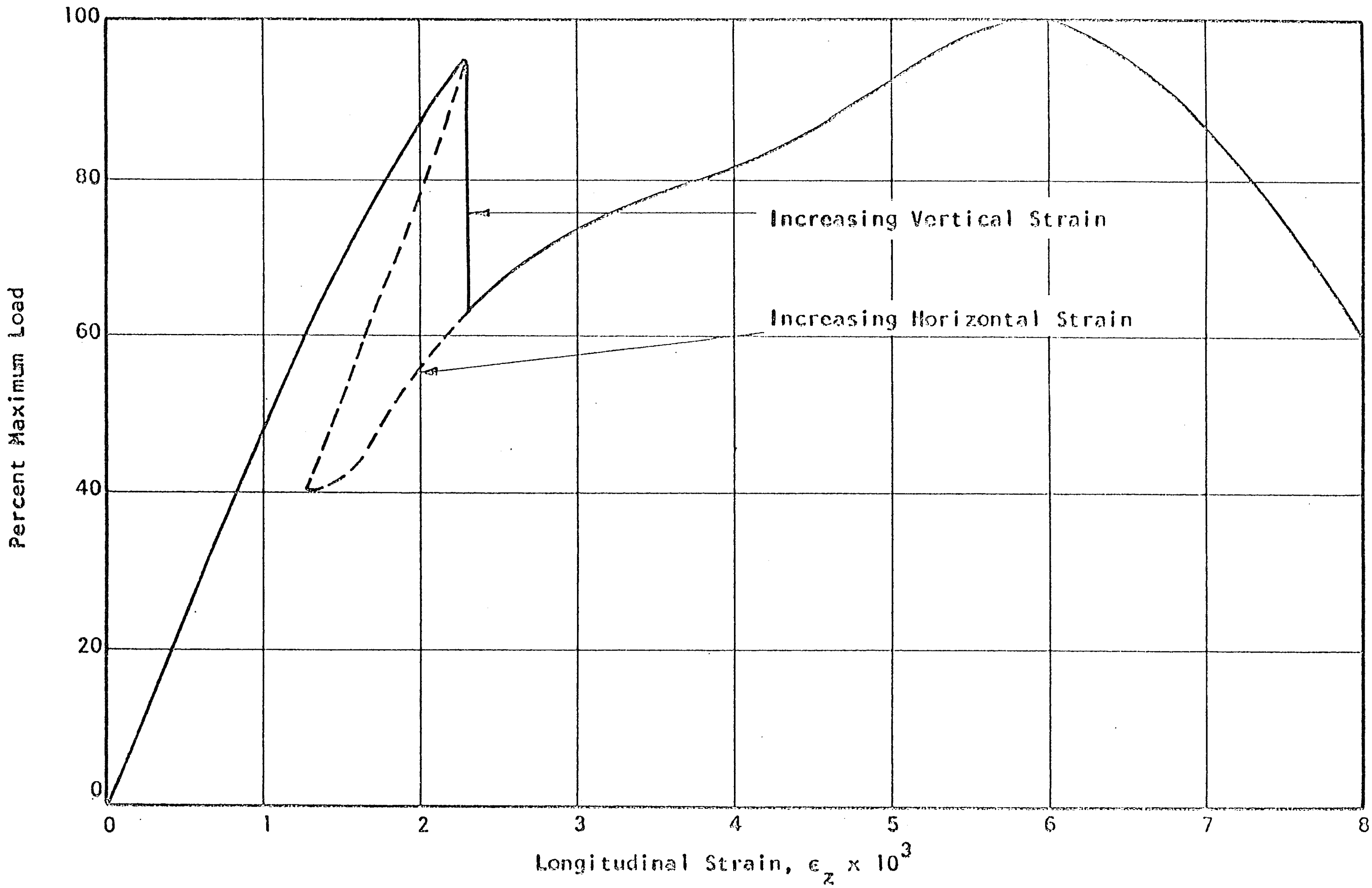

FIG. 3.7 COMPUTED LOAD-STRAIN RELATIONSHIP OF CUBIC MODEL BASED ON A NORMAL DISTRIBUTION OF EFFECTIVE AREA VS. STRAIN

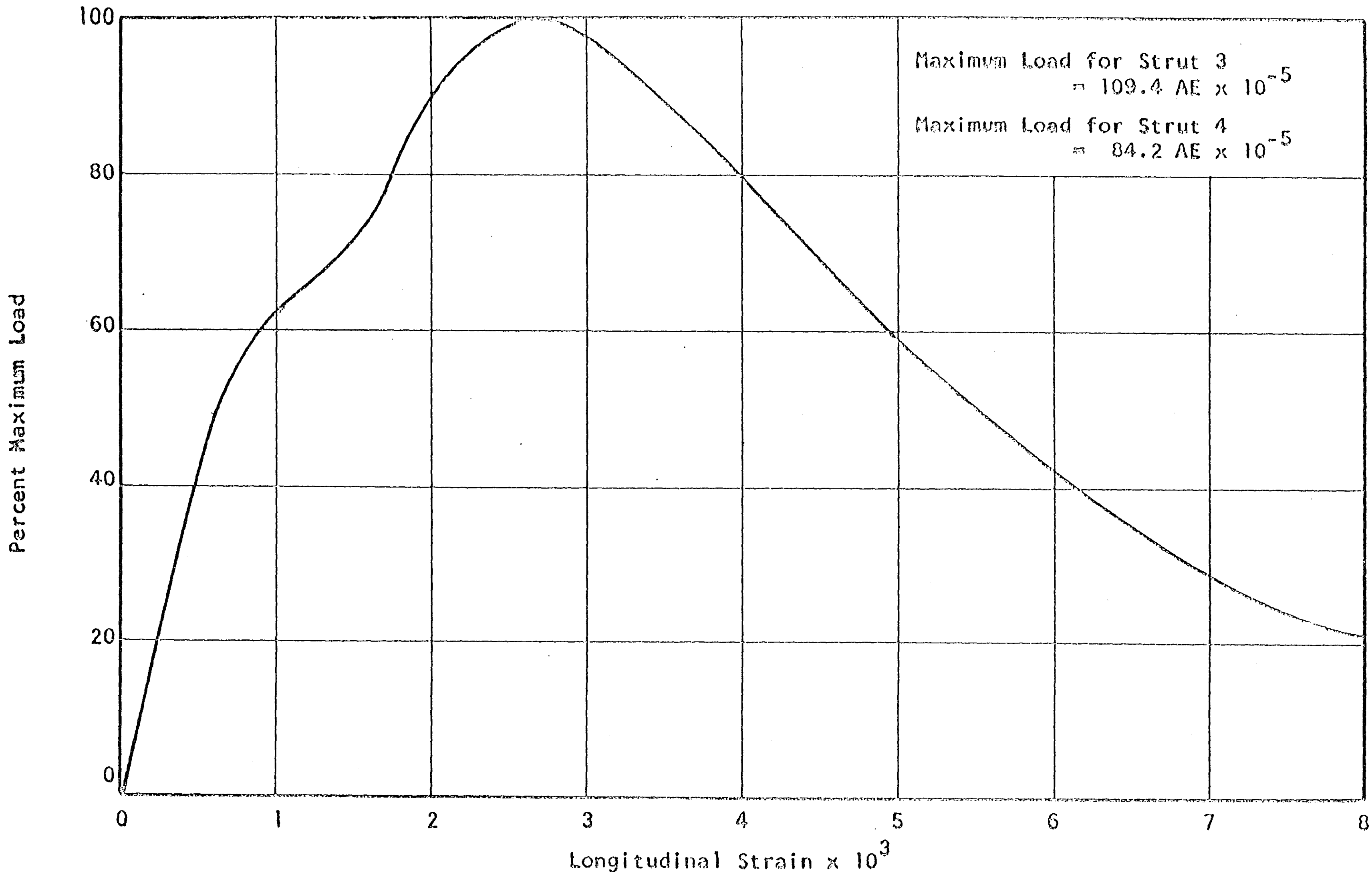

FIG. 3.8 COMPUTED LOAD-STRAIN RELATIONSHIP FOR A SINGLE COMPRESSION STRUT BASED ON A SKEWED DISTRIBUTION OF EFFECTIVE AREA VS. STRAIN

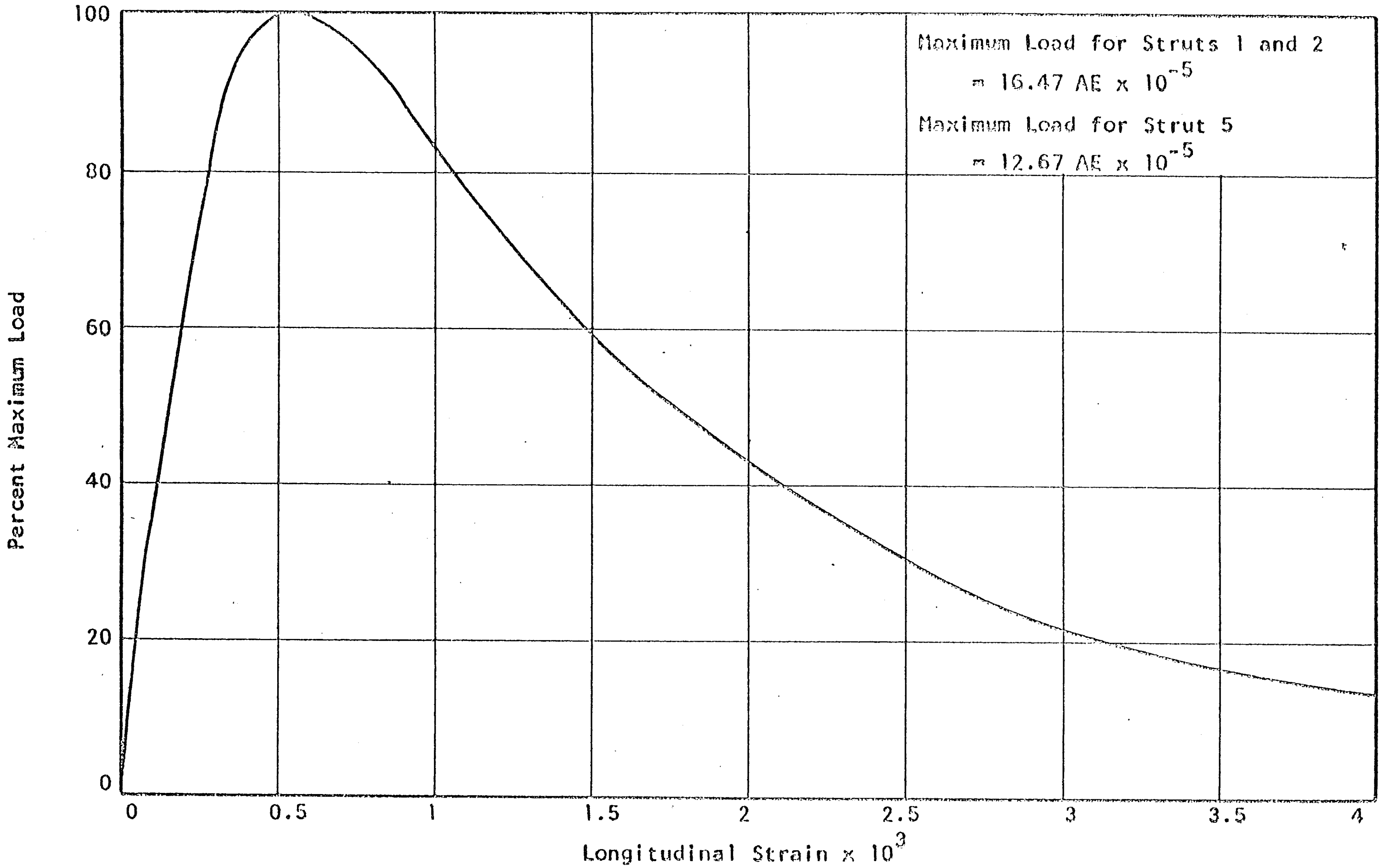

FIG. 3.9 COMPUTED LOAD-STRAIN RELATIONSHIP FOR A SINGLE TENSION STRUT BASED ON A SKEWED DISTRIBUTION OF EFFECTIVE AREA VS. STRAIN

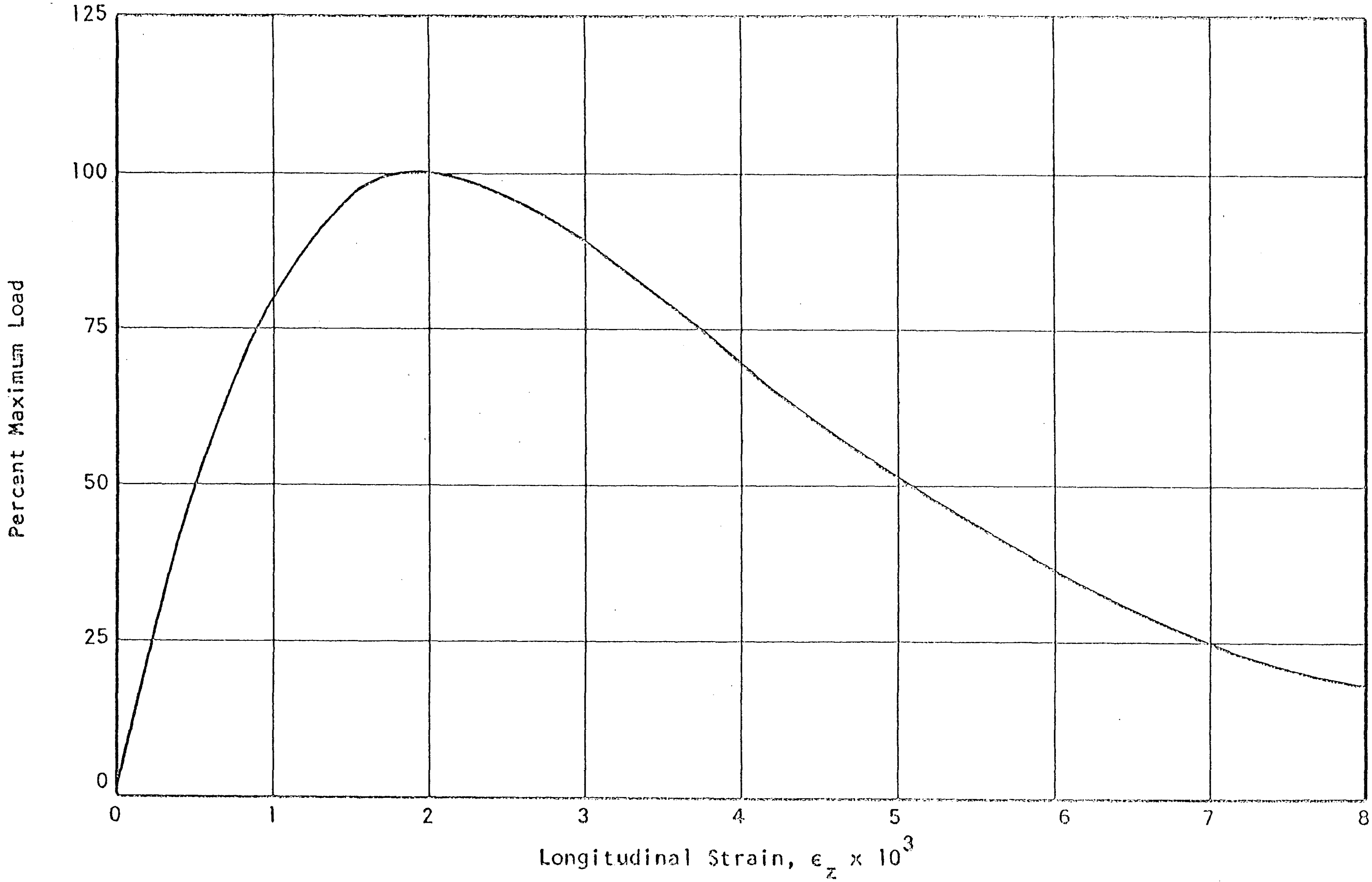

FIG. 4.1 PREDICTED LOAD VS. LONGITUDINAL STRAIN RELATIONSHIP FOR UNCONFINED CONCRETE BASED ON THE CUBIC MODEL

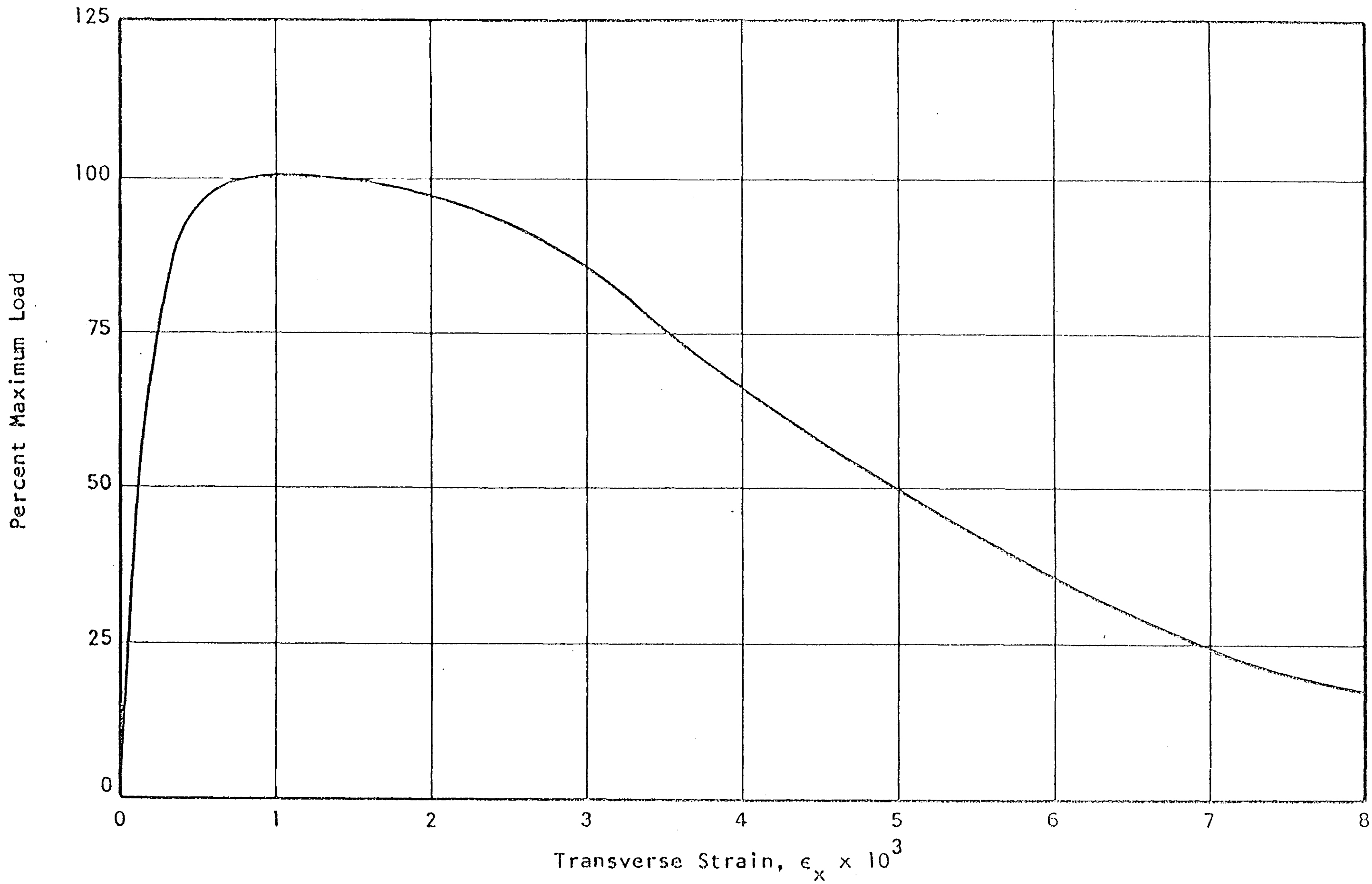

FIG. 4.2 PREDICTED LOAD VS. TRANSVERSE STRAIN RELATIONSHIP FOR UNCONFINED CONCRETE BASED ON THE CUBIC MODEL

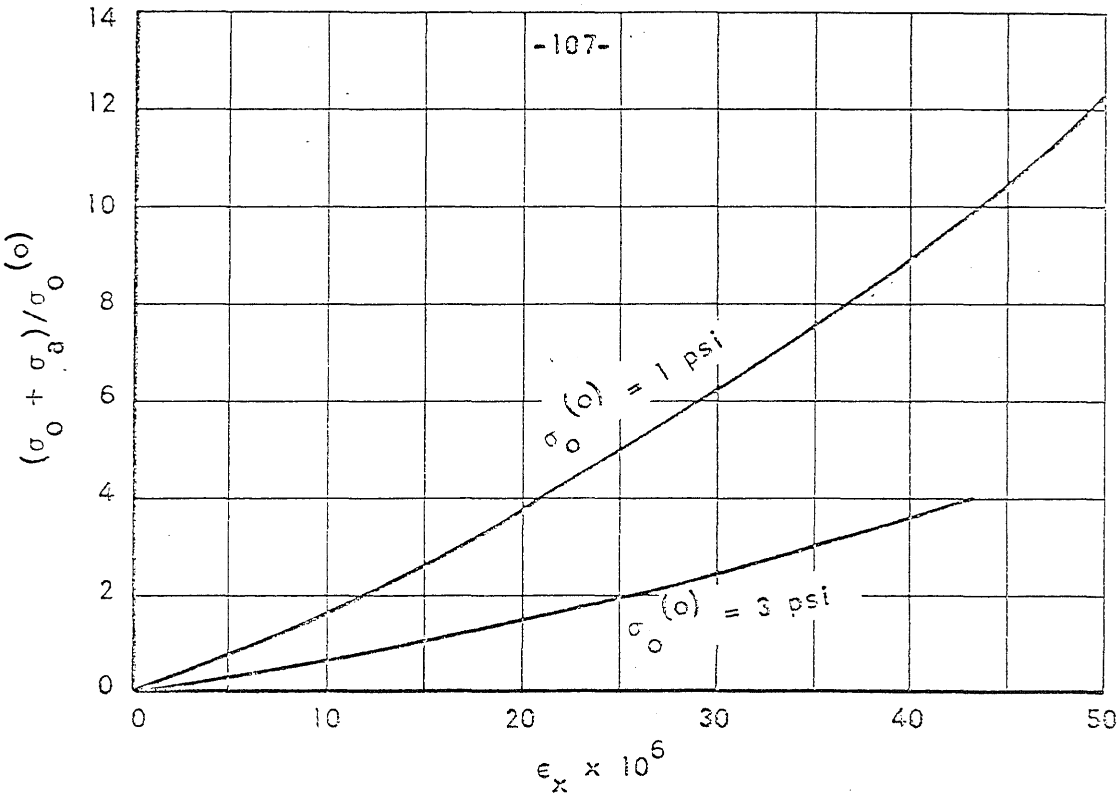

FIG. 5.1 STRESS-STRAIN RELATIONS OF BODY-CENTERED CUBIC ARRAY OF SPHERES (Reference 20)

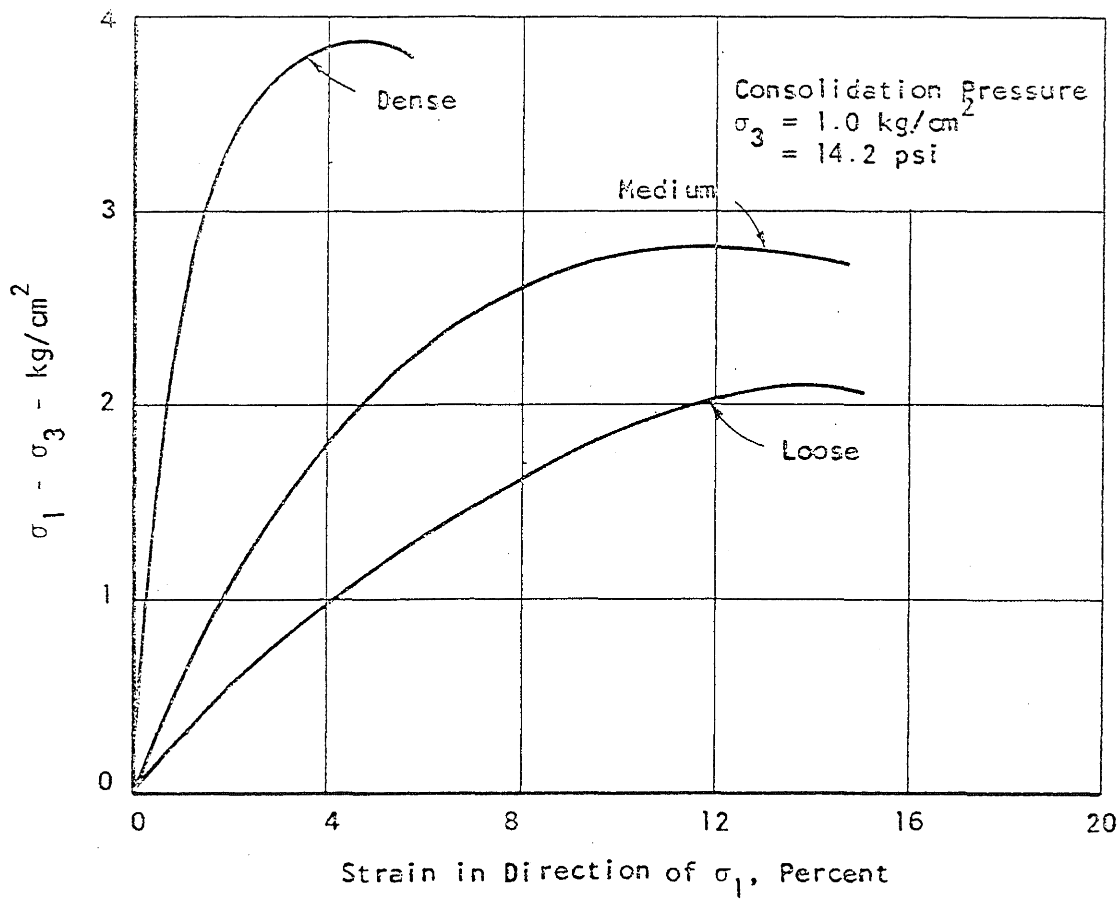

FIG. 5.2 STRESS-STRAIN RELATIONS OF FINE SAND OBTAINED UNDER TRIAXIAL COMPRESSION (Reference 21)

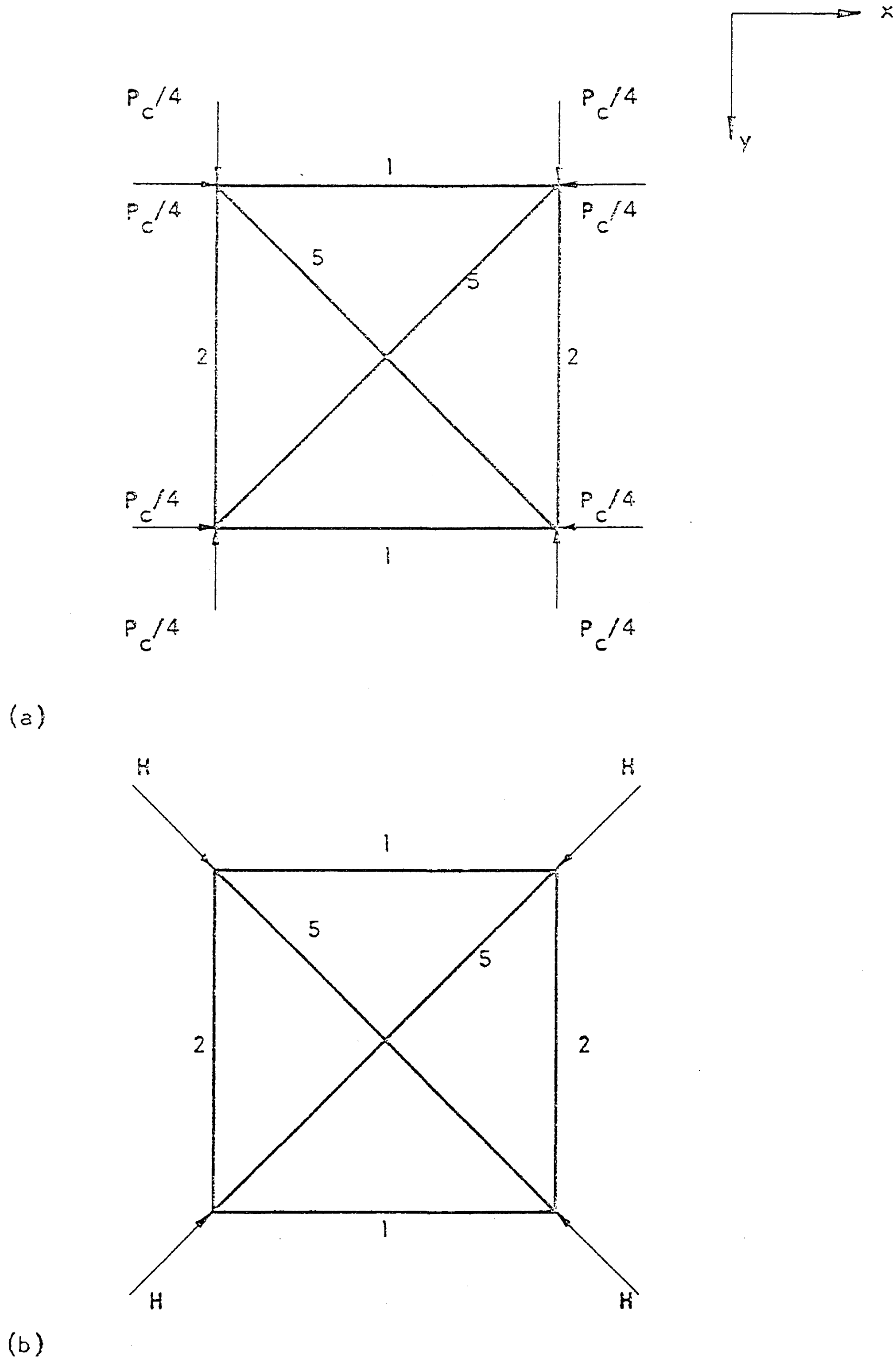

FIG. 5.3 PLAN OF CUBIC MODEL SUBJECTED TO CONFINING PRESSURE

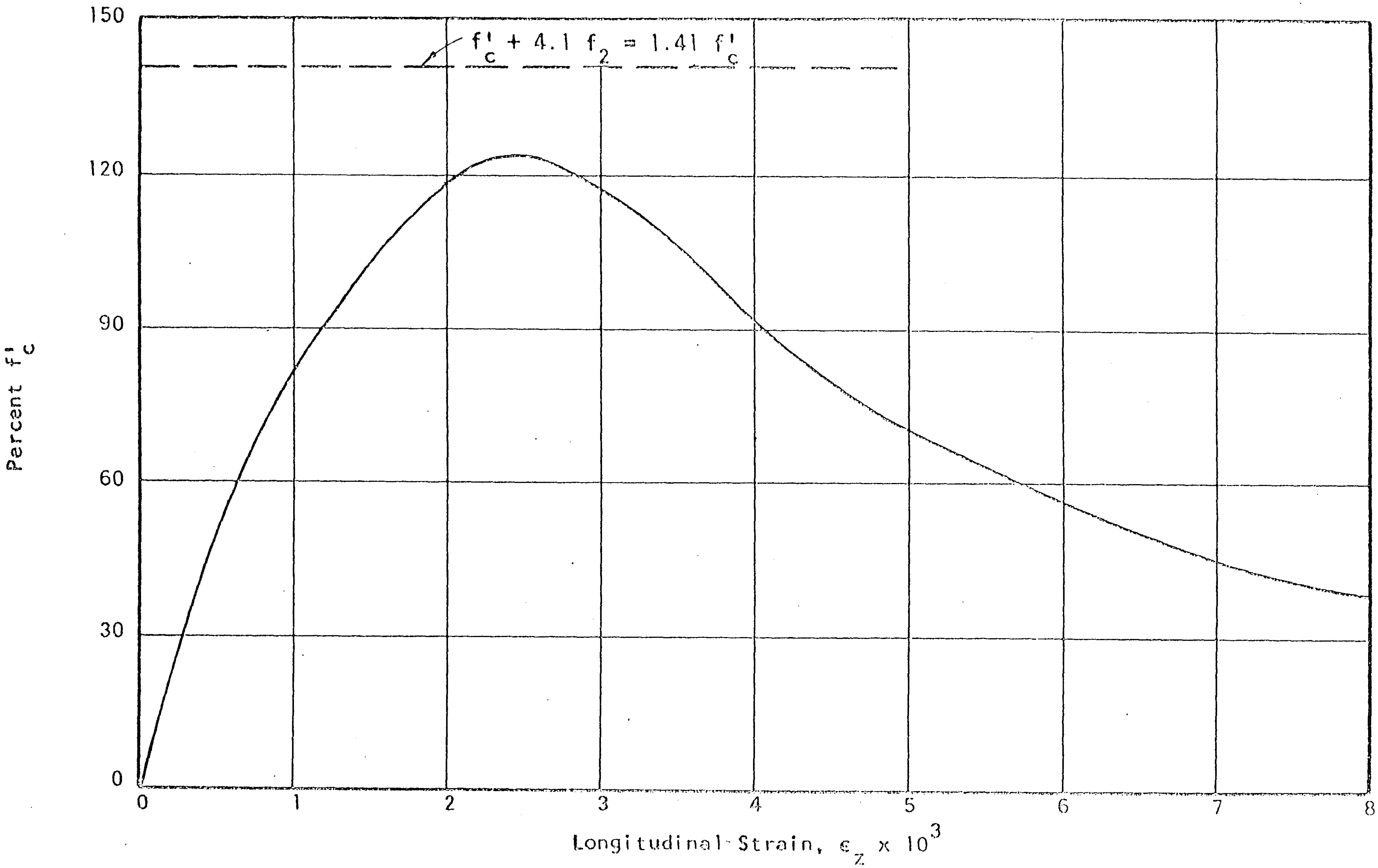

FIG. 5.4 COMPUTED LOAD-STRAIN RELATIONSHIP FOR CONCRETE CONFINED BY SPIRAL REINFORCEMENT

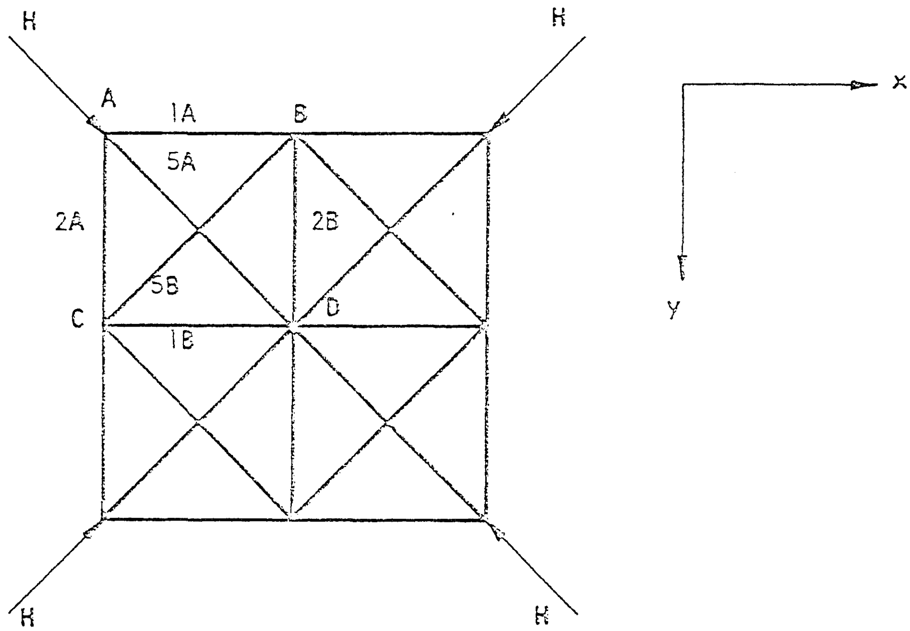

FIG. 5.5 PLAN VIEW OF THE 2 BY 2 GRID

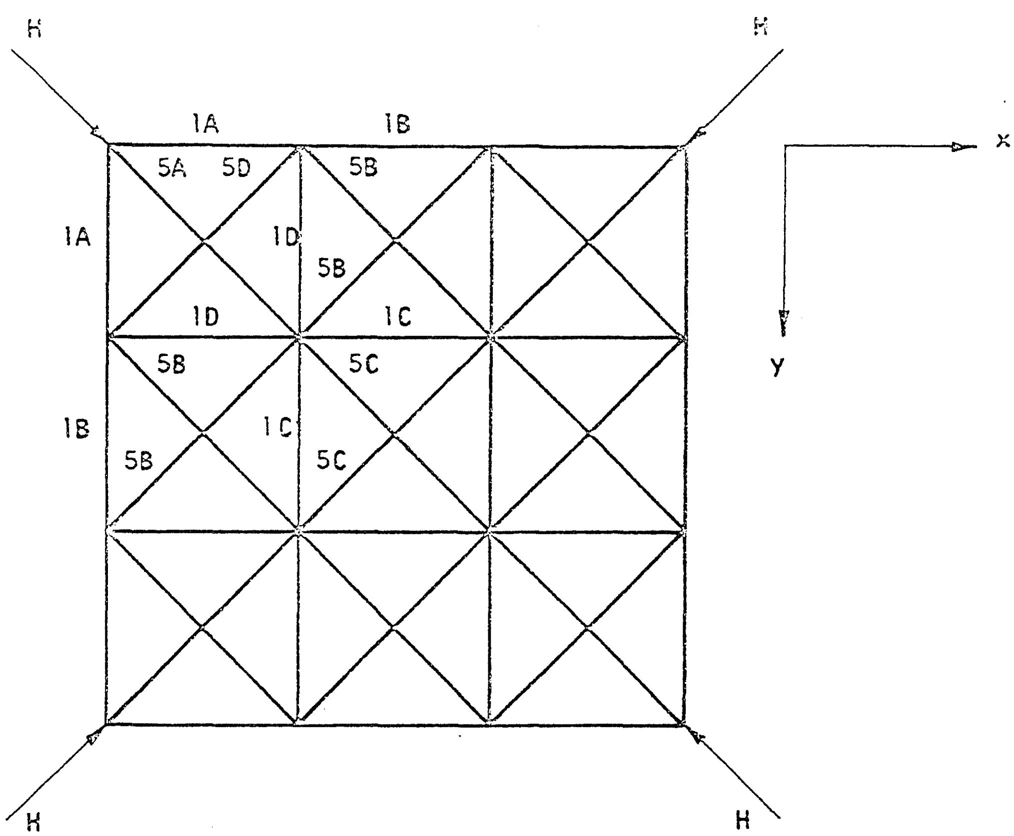

FIG. 5.6 PLAN VIEW OF THE 3 BY 3 GRID

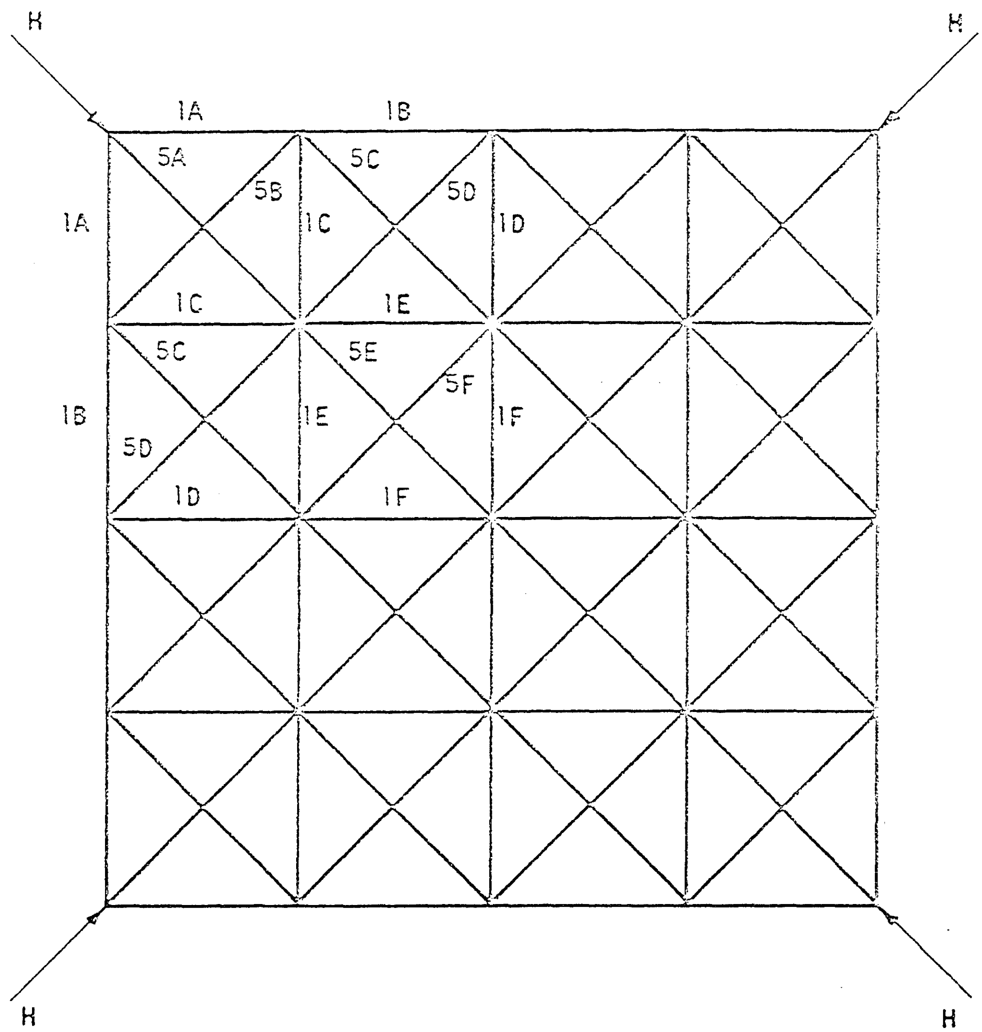

FIG. 5.7 PLAN VIEW OF THE 4 BY 4 GRID

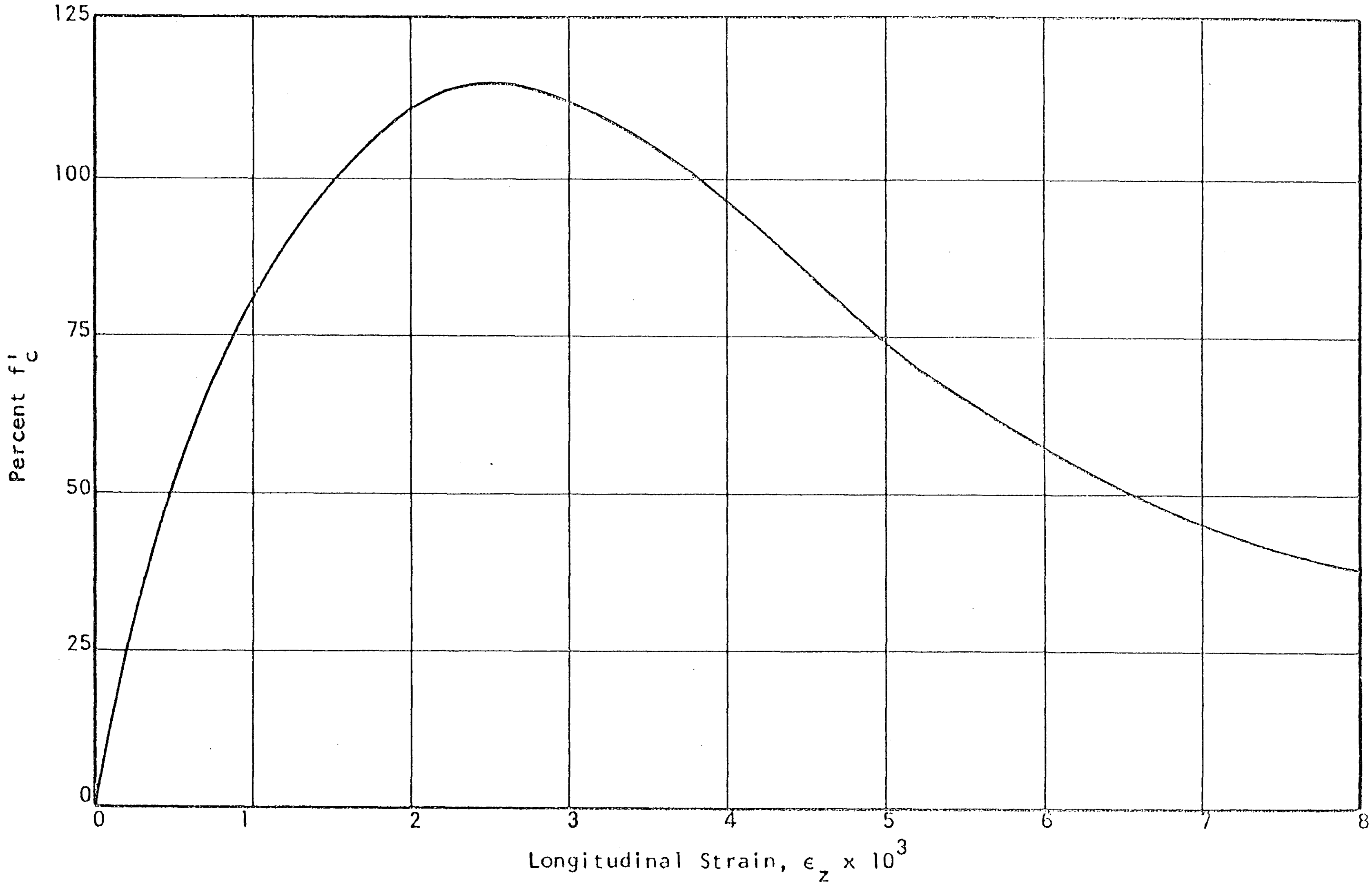

FIG. 5.8 COMPUTED LOAD-STRAIN RELATIONSHIP FOR CONCRETE CONFINED BY RECTANGULAR REINFORCEMENT, 2 BY 2 GRID

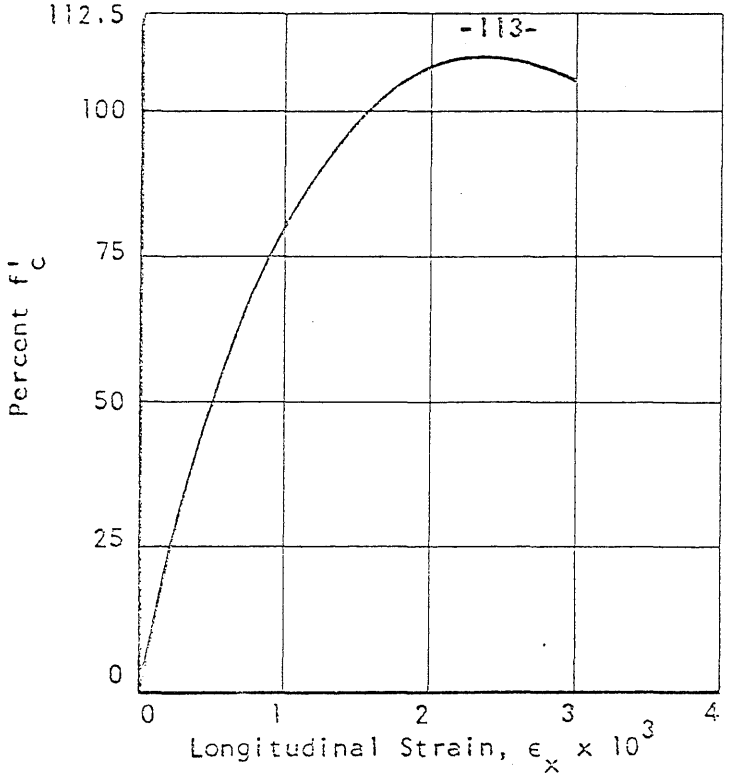

FIG. 5.9 COMPUTED LOAD-STRAIN RELATIONSHIP FOR CONCRETE CONFINED BY RECTANGULAR REINFORCEMENT, 3 BY 3 GRID

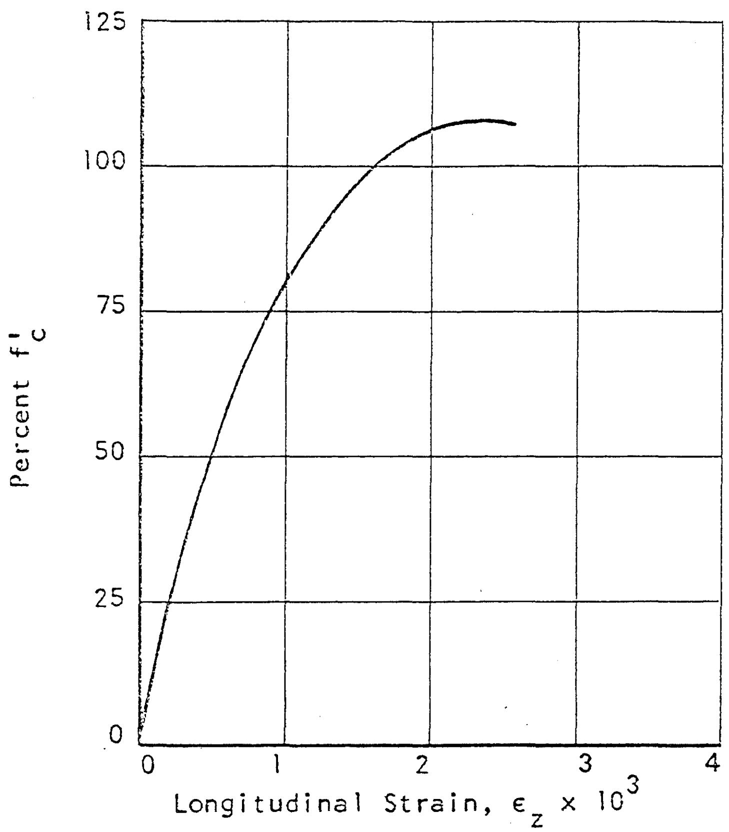

FIG. 5.10 COMPUTED LOAD-STRAIN RELATIONSHIP FOR CONCRETE CONFINED BY RECTANGULAR REINFORCEMENT, 4 BY 4 GRID

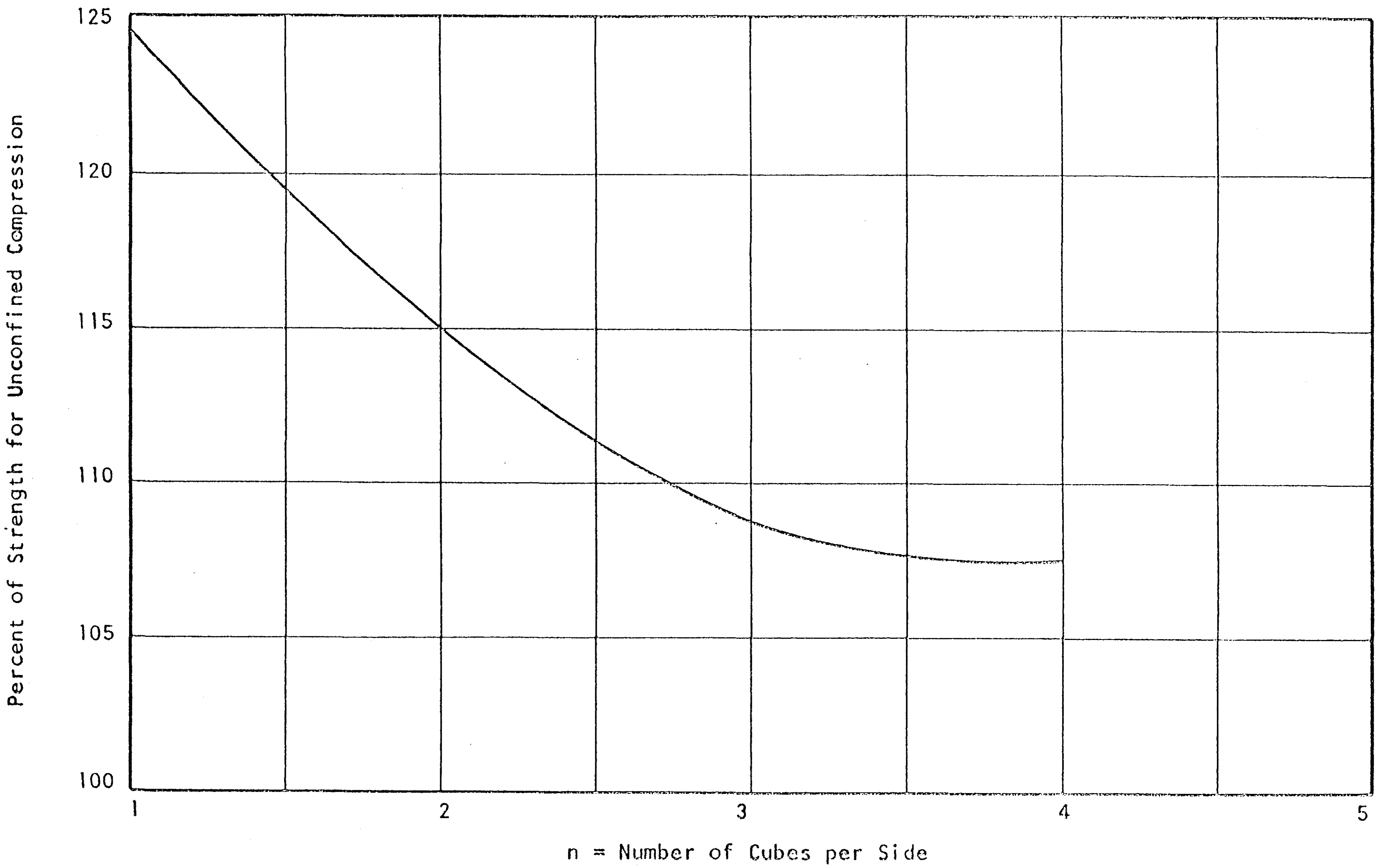

FIG. 5.11 VARIATION OF COMPUTED MAXIMUM LOAD WITH FINENESS OF GRID
RECTANGULAR TRANSVERSE REINFORCEMENT

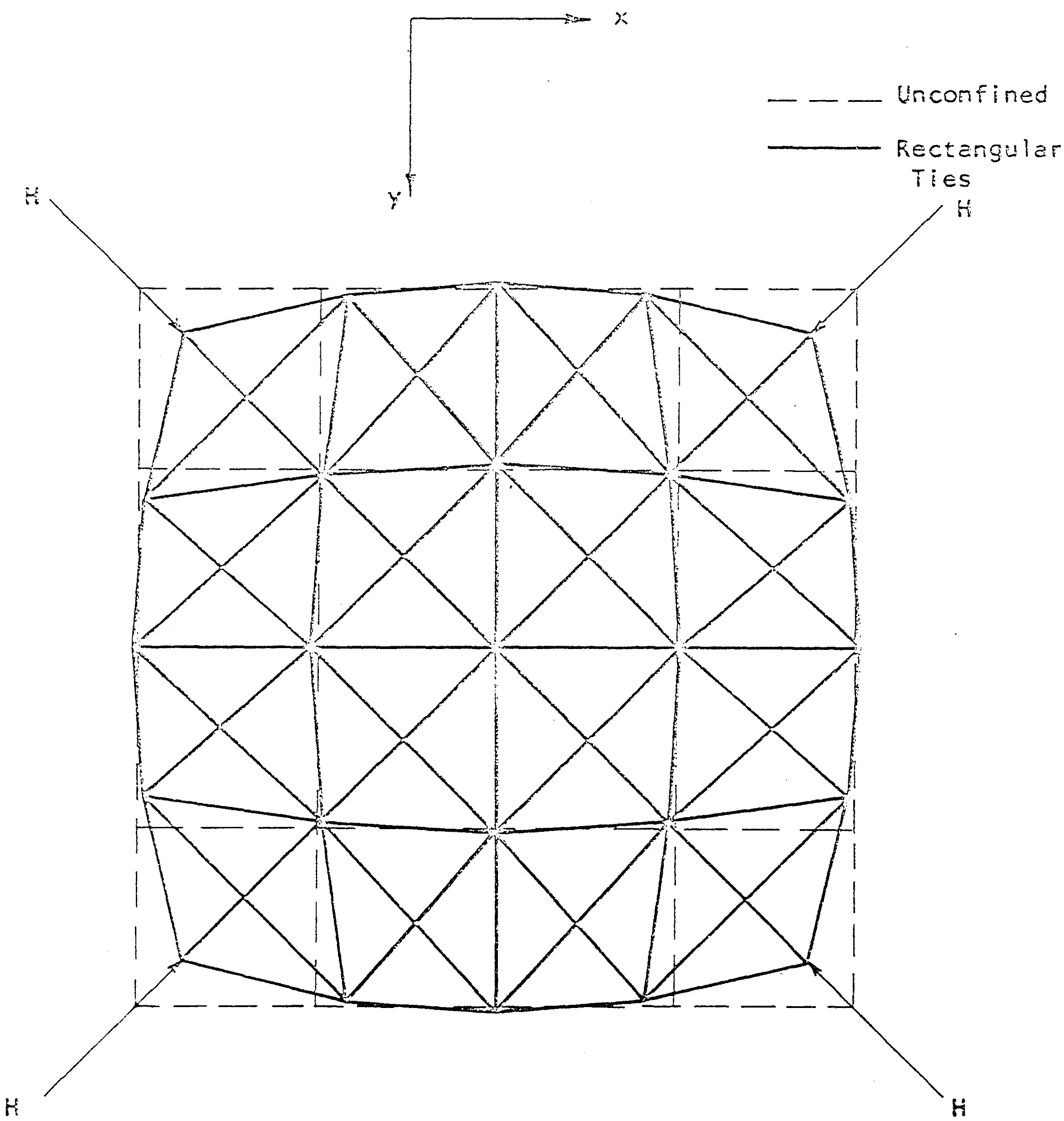

FIG. 5.12 DEFLECTED SHAPE AT MAXIMUM LOAD, 4 BY 4 GRID
Magnification 100 x

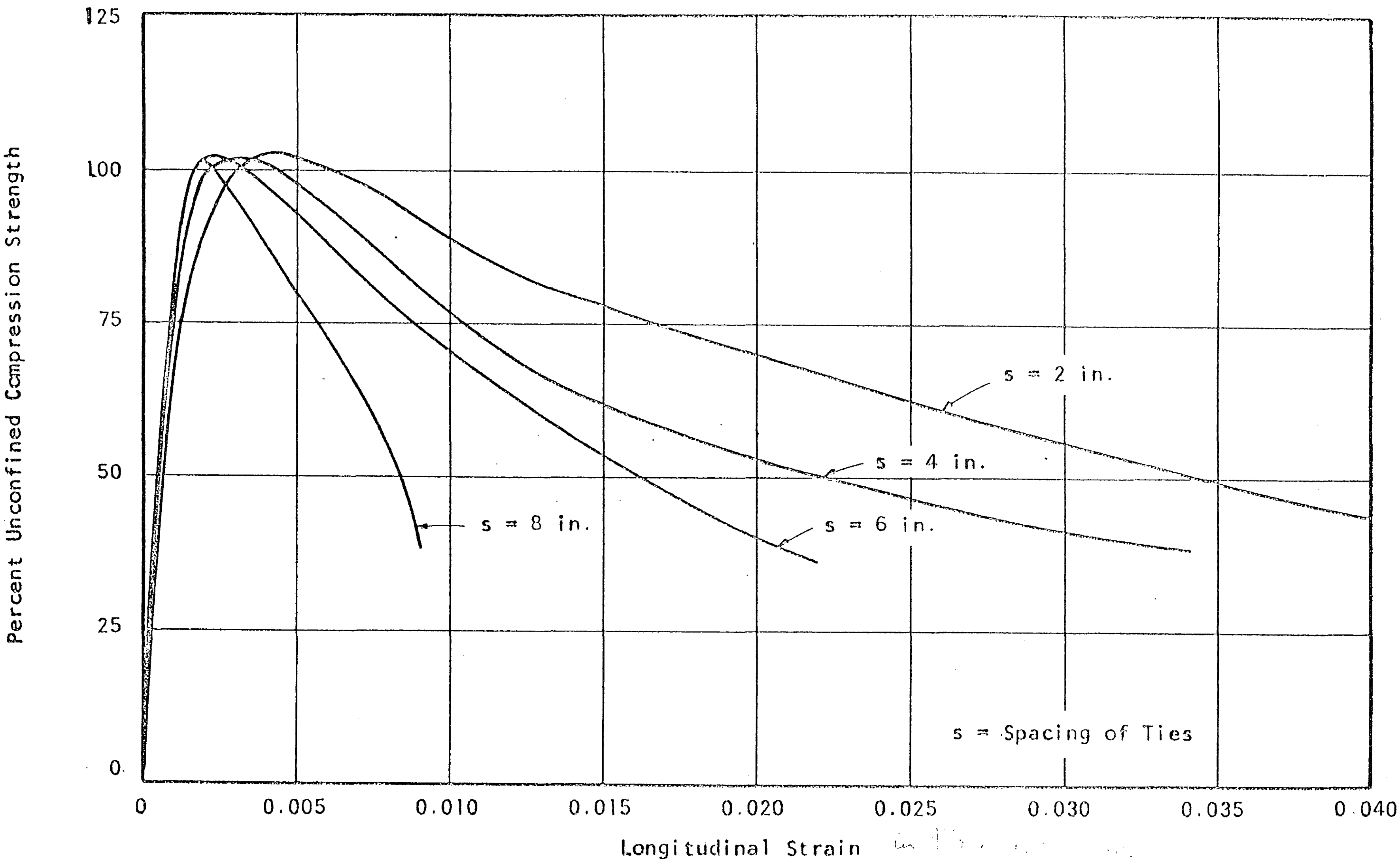

FIG. 6.1 EFFECT OF TIE SPACING ON LOAD-DEFORMATION RELATIONSHIP OF CONCRETE CONFINED BY RECTANGULAR REINFORCEMENT

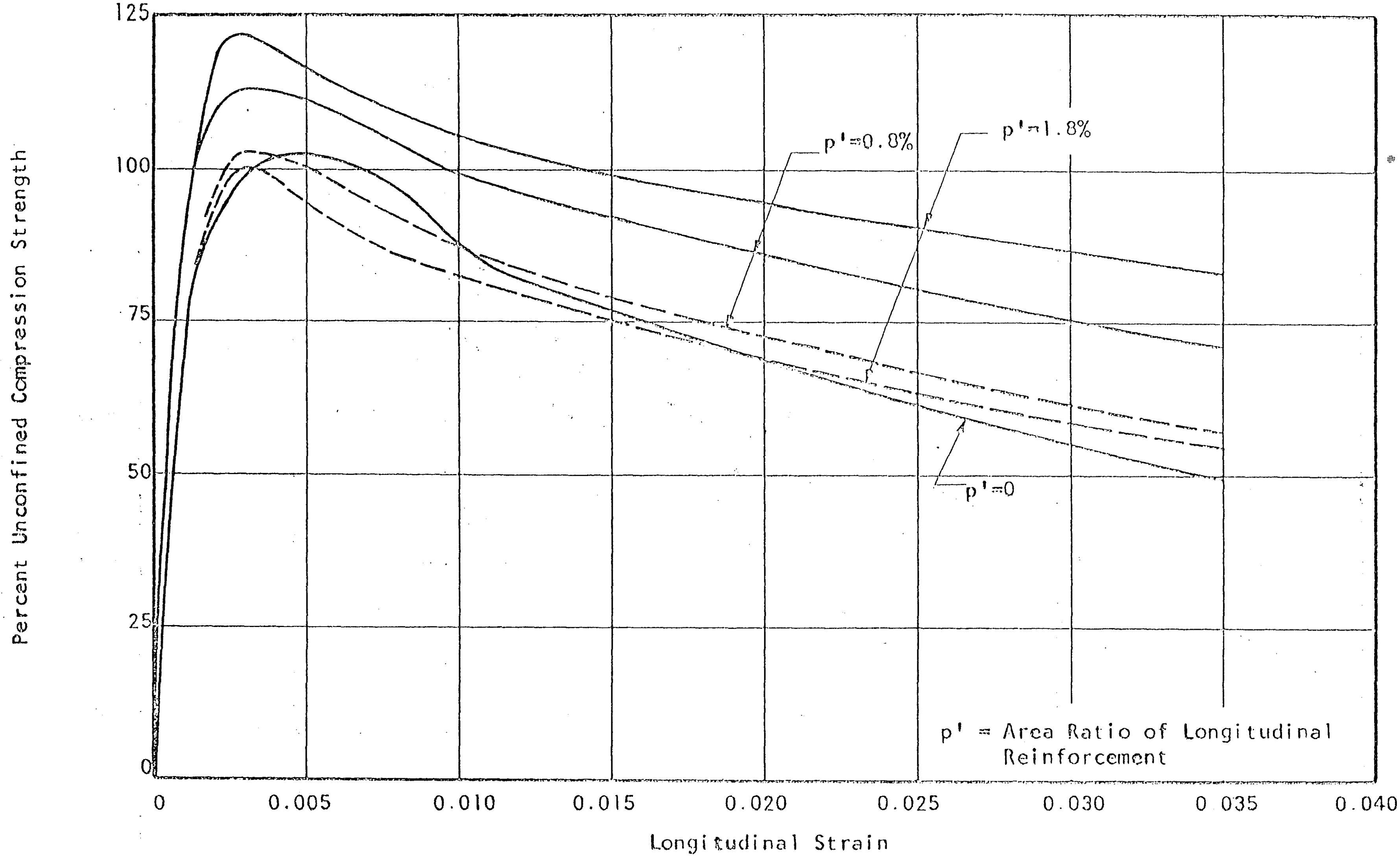

FIG. 6.2 EFFECT OF LONGITUDINAL REINFORCEMENT ON LOAD-DEFORMATION RELATIONSHIP OF CONCRETE CONFINED BY RECTANGULAR REINFORCEMENT

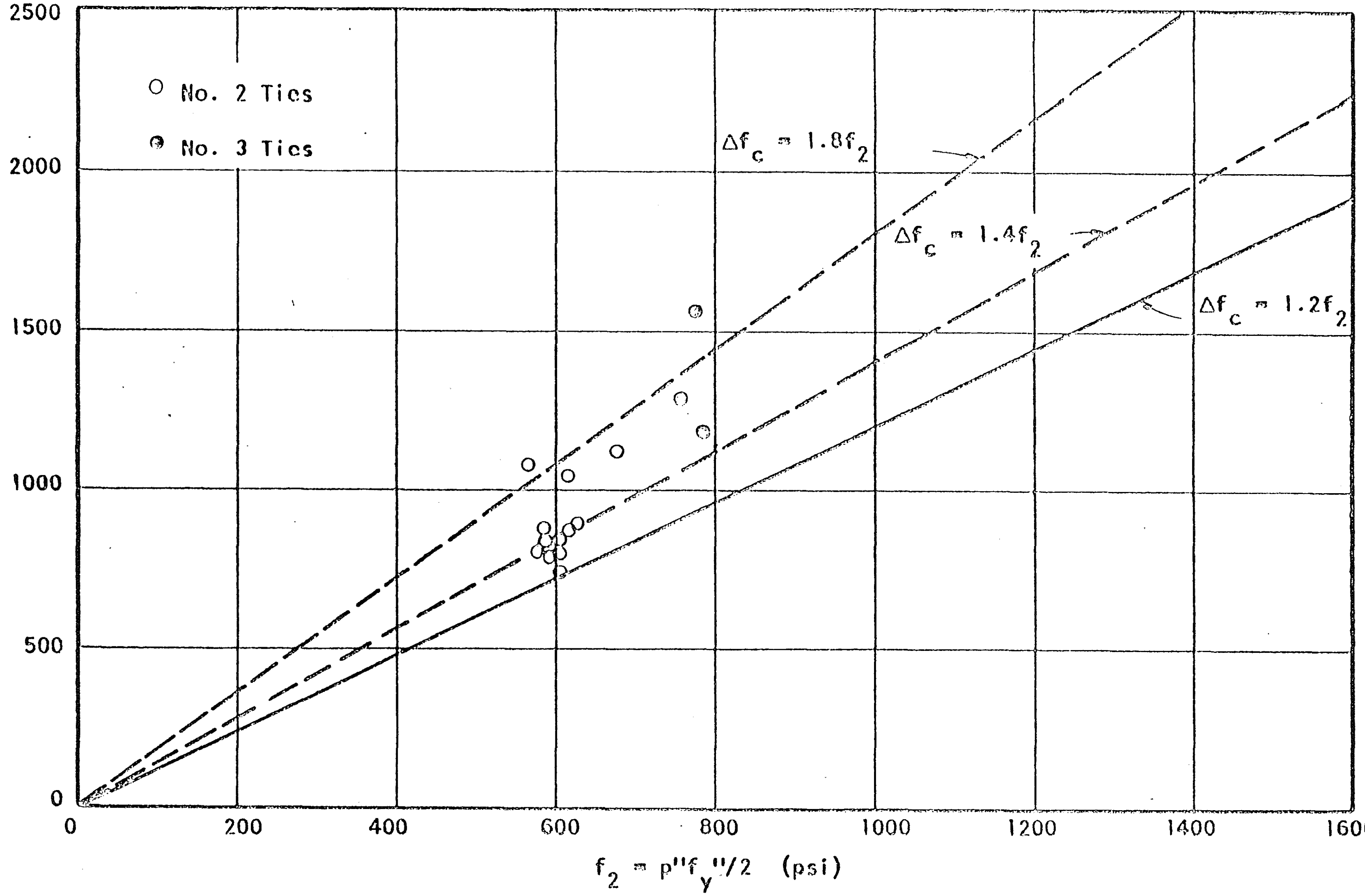

FIG. 6.3 COLUMNS WITH TIES AND NO LONGITUDINAL REINFORCEMENT

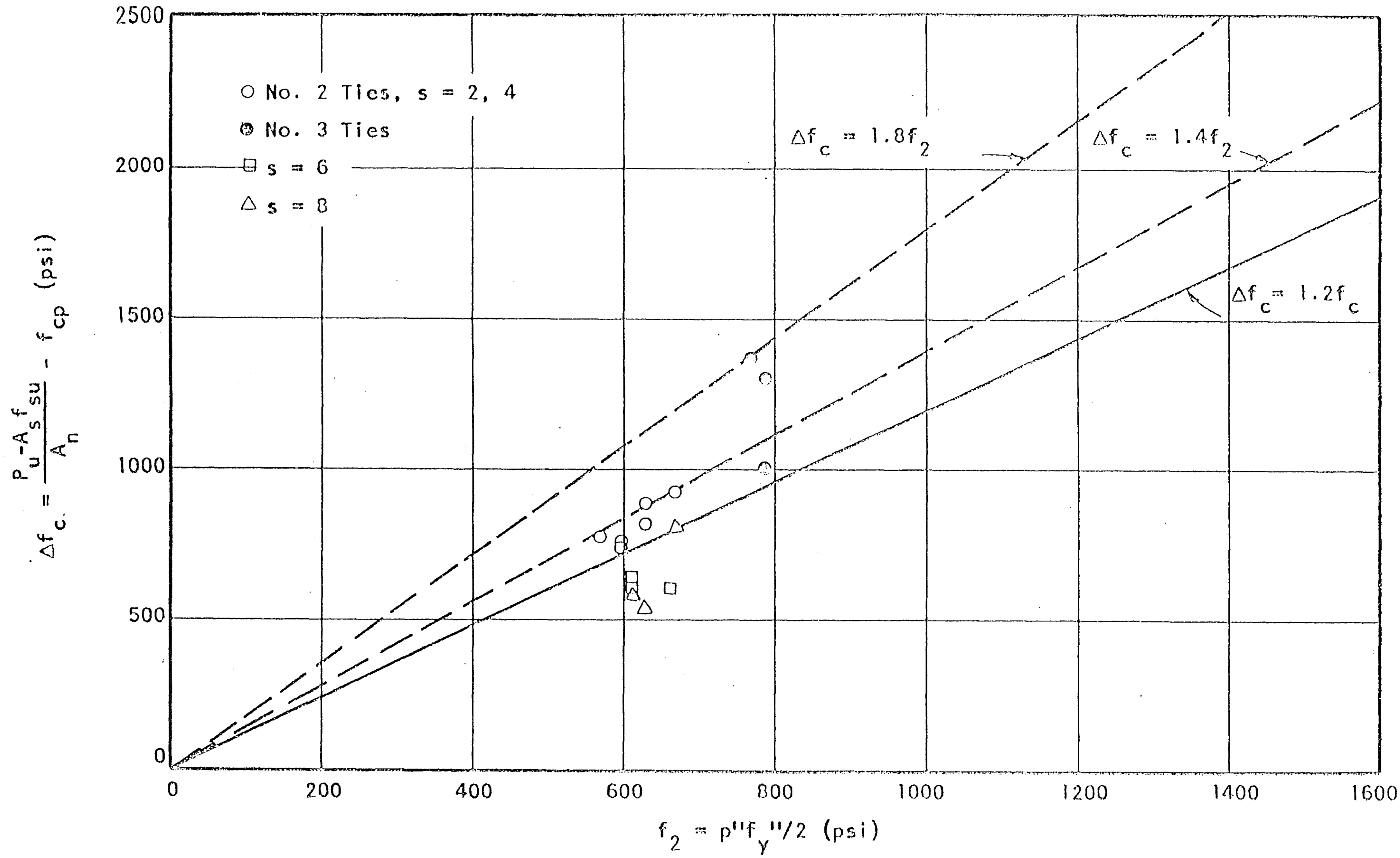

FIG. 6.4 COLUMNS WITH TIES AND 4-NO.2 LONGITUDINAL BARS

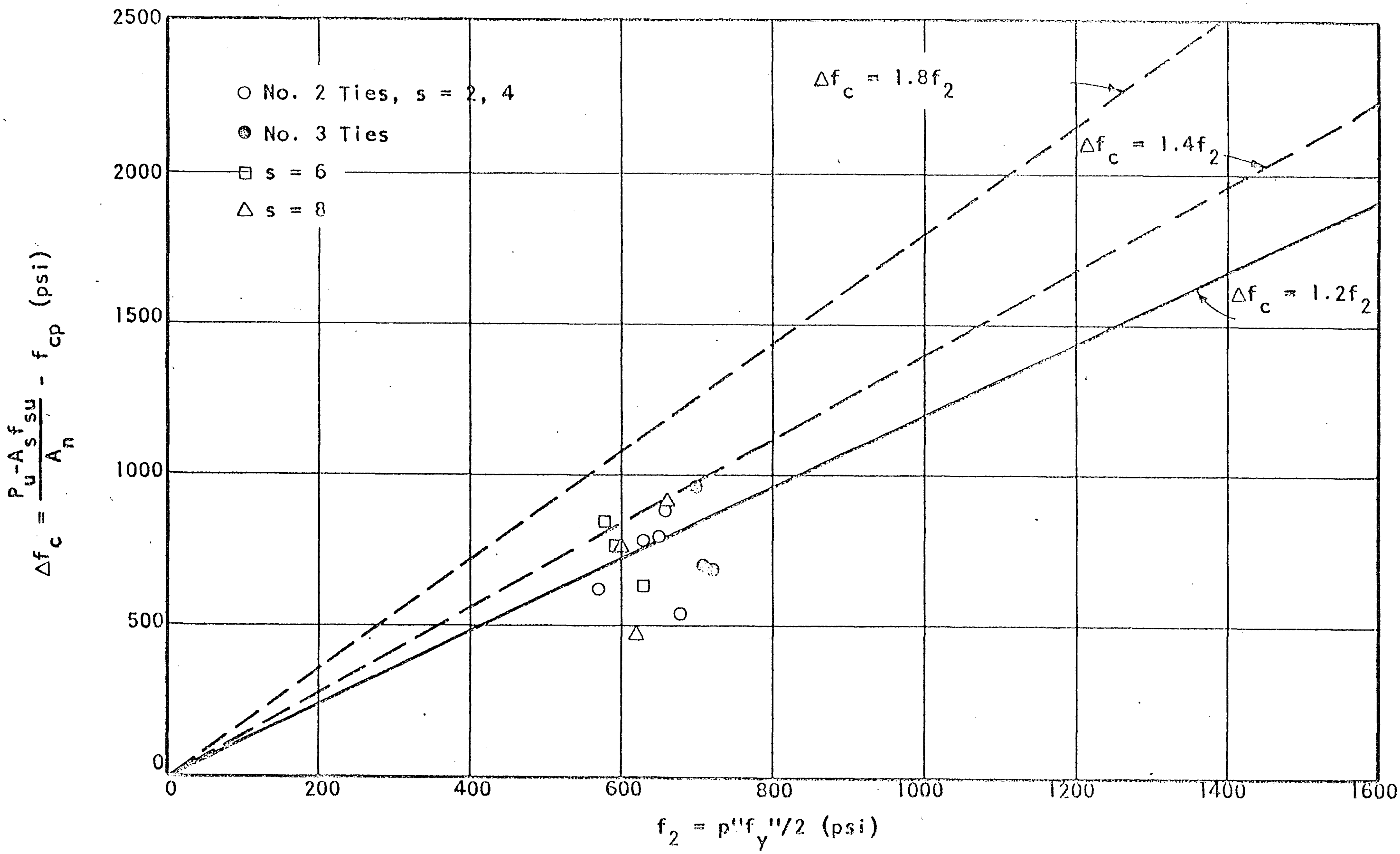

FIG. 6.5 COLUMNS WITH TIES AND 4-NO. 3 LONGITUDINAL BARS

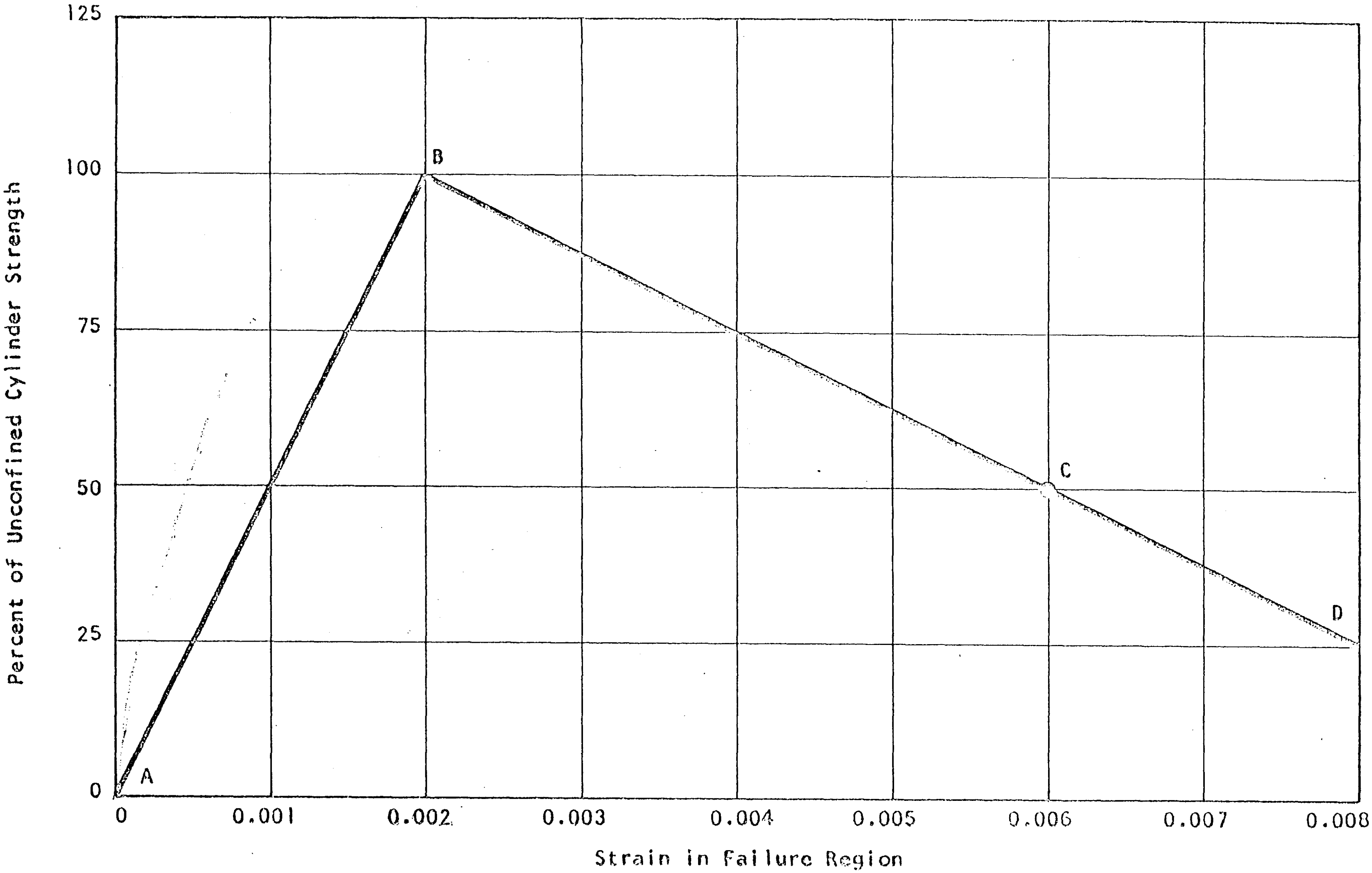

FIG. 6.6 TYPICAL STRESS-STRAIN RELATION FOR CONCRETE CONFINED BY RECTANGULAR TIES

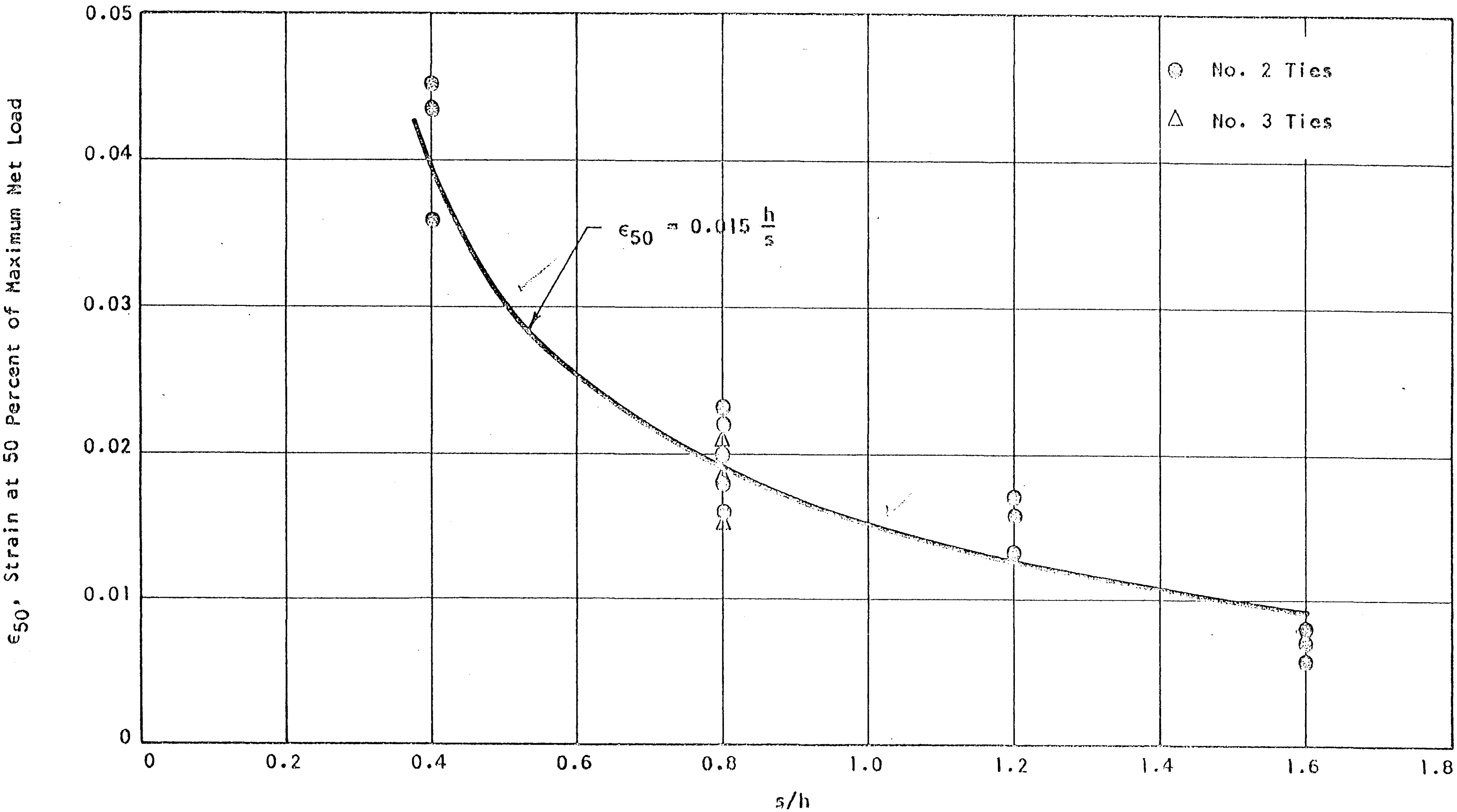

FIG. 6.7 RELATION BETWEEN STRAIN AT 50 PERCENT MAXIMUM NET LOAD AND RELATIVE TIE SPACING

APPENDIX A

EXPERIMENTAL WORK

A.1 Test Specimens

A total of 60 specimens were cast and tested in 15 groups of 4. The specimens measured 5 by 5 by 25 in.

The nominal concrete compressive strength was 3000 psi and the nominal volumetric ratio of the transverse reinforcement was 0.02 for all specimens.

The variables were:

(1) Spacing of transverse reinforcement (2, 4, 6, 8 in.)

(2) Stiffness of transverse reinforcement (No. 2 and No. 3 bars)

(3) Amount of longitudinal reinforcement (area ratio, $p' = 0$, 0.008, 0.018)

(4) Stiffness of longitudinal reinforcement (a secondary variable as a result of the different tie spacings)

Each specimen was assigned a designation consisting of four numerals having the following significance: The specimens were grouped into different series according to size and spacing of transverse reinforcement. The first numeral indicated the test series to which the specimen belonged.

1 : No. 2 ties at 2-in. spacing

2 : 2-No. 2 ties at 4-in. spacing

3 : No. 3 ties at 4-in. spacing

4 : 3-No. 2 ties at 6-in. spacing

5 : 4-No. 2 ties at 8-in. spacing

The second numeral was used to distinguish the specimens having the same variables.

The third numeral described the longitudinal reinforcement.

0 : No longitudinal reinforcement

2 : 4-No. 2 longitudinal bars

3 : 4-No. 3 longitudinal bars

The fourth numeral indicated the size of ties.

2 : No. 2 ties

3 : No. 3 ties

A summary of the properties of all the specimens is given in Table A.1.

A.2 Concrete

(a) Cement

Marquette brand type III portland cement was used for all specimens.

(b) Aggregates

The concrete was manufactured using Wabash River sand and gravel. Because of the close tie spacing used, the maximum size of the gravel was restricted to 3/8 in.

The absorption of the sand was 1.6 percent and that of the gravel was 2 percent by weight of surface-dry aggregate.

(c) Concrete Mix

All aggregates were oven-dried before each batch of concrete was mixed in order to control the strength variation throughout the test series.

The nominal mix proportions were 1:3.6:3.9 (cement:sand:gravel) by weight. The water/cement ratio was 0.76, corrected for absorbed water.

The compressive strength of the concrete was determined by testing 6 by 12-in. cylinders, and the tensile strength was measured by splitting tests on 6 by 6-in. cylinders.

The properties of each concrete mix are summarized in Table A.1.

A.3 Casting, Forms, Reinforcement

(a) Casting

All specimens were cast in a horizontal position, and the concrete was placed using a mechanical hand vibrator. Twenty-four hours after casting, the specimens were removed from the forms and stored for five days in a moist room, maintained at 100 percent relative humidity and 74°F. They were then placed in the laboratory for a minimum of 24 hours before testing.

(b) Forms

The forms were constructed of steel, and were manufactured with extreme care so as to maintain the dimensions of the specimens within a tolerance of 1/32 in. The bottom of each form consisted of a 7-in. steel channel, and the sides and ends were 5-in. steel channels. The sides and ends were bolted to the base to facilitate removal of the specimen.

(c) Reinforcement

Both No. 2 and No. 3 reinforcing bars were used for the ties and longitudinal reinforcement. The No. 2 bars were round, with a diameter of 1/4 in., and the No. 3 bars were deformed, with a nominal diameter of 3/8 in. and a nominal area of 0.11 sq. in.

A 24-in. test sample was cut from each length of reinforcing bar, and tested in tension to failure. The strains during each test were determined using an 8-in. gage length. A summary of the properties of the reinforcing bars is given in Table A.5, and typical stress-strain curves for the No. 2 and No. 3 bars are shown in Figs. A.1 and A.2 respectively. In addition, a histogram of the yield stresses for the No. 2 bars is given in Fig. A.3.

The ties were fabricated by cold bending. The ends of the bar were lapped a distance of approximately 2 in. and welded. The ties were placed in the forms so that the laps occurred on two opposite faces of the specimen only, and on each alternate tie on each face. In the specimens with no longitudinal reinforcement, the ties were held in position during casting by connecting them with No. 14 gage annealed wire. The ties in the specimens with longitudinal bars were positioned by fastening each corner of the tie to the longitudinal bar at that corner by means of No. 19 gage wire.

Each specimen with longitudinal reinforcement contained four bars extending throughout the length of the specimen, one at each corner inside the ties.

A.4 Instrumentation

Since the tests conducted by Szulczynski (5) gave relations between longitudinal and transverse strains, and indicated that yield strain had been reached in the ties at maximum load, it was decided that only the longitudinal strains would be measured during the tests.

The instrumentation which was used in the test program is shown in Fig. A.58.

The over-all deflections of the specimens were determined by measuring the shortening between the upper and lower loading plates of the testing machine. This was accomplished by means of two 0.001-in. dials attached to extensometers and placed at the north and south faces of the specimen.

In order to measure local deformations of the specimen, and if possible the deformation at the failure zone, the deflection of the specimen was also measured over two continuous 2-in. gage lengths located near the mid-height. For this purpose, three square frames with approximate inside dimensions of 5 1/2 by 5 1/2 in. were constructed from 1/4 by 1/2 in. steel bars. The spacing between the frames was maintained by means of spacer plates. The frames were attached to the specimen with pointed machine bolts which were threaded through the bars, and after they were in place the spacer plates were removed. The deflection between the frames was measured using eight 0.001-in. deflection dials, one in each gage length on each face of the specimen. By this means it was also possible to determine whether any bending moment was applied to the specimen during testing.

A.5 Test Procedure

The specimens were tested with a 300,000 lb capacity screw-type testing machine.

A particular effort was made to apply axial load to the specimen. Accordingly, 5 by 5 by 1/2 in. steel plates were attached to each end of the specimen with plaster of Paris. The plates were installed while the specimen was in position on the loading platform of the testing machine, and a carpenter's level was used to ensure that the specimen was vertical and the plates horizontal. The deflection dials were then positioned as described in Section A.4, and the specimen was placed under the center of the loading head. The position of the loading head was fixed, but the use of the level plates at the ends of the specimen caused a geometrically-axial load to be applied.

A load of approximately 10 lbs was applied to the specimen, after which initial readings were made on the dials. The load was increased in 10,000-lb increments up to the maximum. It was necessary to discontinue testing of the plain specimens when the maximum load was reached, because the stiffness of the machine was insufficient to prevent complete fracture at this point. In the tests of the tied specimens, incremental strains were applied beyond maximum load such that the load decrements were approximately 10,000 lb. The tests were discontinued when fracture of one of the ties had taken place, or, if no fracture occurred, when the load had reduced to about 10 percent of its maximum value.

After each load increment (or decrement), readings of the 10 deflection dials were recorded, as well as the time. The latter observation was made to provide a measure of time-dependent effects during the test.

A.6 Measured Load-Deformation Characteristics

The results of the tests on the specimens with ties and no longitudinal reinforcement are summarized in Table A.2, and the test results on the specimens with No. 2 and No. 3 longitudinal bars are summarized in Tables A.3 and A.4 respectively. In Tables A.3 and A.4, the net maximum load of the specimens is included. This has been computed by subtracting from the total load the load carried by the longitudinal bars, in order to give a measure of the effect of confinement on the concrete.

Graphs of load vs. measured strains are given in Figs. A.4 to A.34. In these graphs, curve 1 gives values of average strain over the length of the specimen, computed on the basis of the total shortening of the specimen; curve 2 refers to the average strain over the upper 2-in. gage length of the specimen, obtained as described in Section A.4; and curve 3 refers to the average strain over the lower 2-in. gage length. It should be noted that in Figs. A.4 to A.34, curve 1 indicates an initial strain at zero load. This is caused by the fact that the plaster of Paris at the ends of the specimen compressed during the early stages of each test, after initial readings had been recorded for the two extensometers. Curve 1 has been plotted by extrapolating the lower portion of the curve to intersect the zero load axis. True values of the average over-all strain are therefore obtained by subtracting the initial strain from the values represented in curve 1.

Figures A.35 to A.57 are graphs of load vs. strain in the failure zone, for the specimens with ties. In cases for which failure occurred within the two 4-in. gage lengths on the specimen, the strain in the failure region was obtained directly from the mounted dials. For the specimens in which failure occurred outside this length, the shortening in the failure zone was computed by subtracting from the total deflection the deflection of the uncrushed portion of the specimens.

TABLE A.1

PROPERTIES OF SPECIMENS AND CONCRETE

	Mark	Tie Size	Longitudinal Bar Size	Concrete			
5				Slump in.	Age at Test Days	Compressive Strength* psi	Tensile Strength** psi
	1102	No. 2[a]	-				
5	1122	No. 2	No. 2[a]	2 1/2	10	3080	320
	1132	No. 2	No. 3[b]			(3)	(3)
	1202	No. 2	-				
2	1222	No. 2	No. 2	2 1/2	8	2980	290
	1232	No. 2	No. 3			(4)	(4)
	1302	No. 2	-				
2	1322	No. 2	No. 2	2 1/2	9	3700	310
	1332	No. 2	No. 3			(4)	(4)
	2102	No. 2	-				
4	2122	No. 2	No. 2	2	10	3480	350
	2132	No. 2	No. 3			(4)	(4)
	2202	No. 2	-				
4	2222	No. 2	No. 2	3	8	3480	340
	2232	No. 2	No. 3			(4)	(4)
	2302	No. 2	-				
4	2322	No. 2	No. 2	2 1/4	7	3370	340
	2332	No. 2	No. 3			(4)	(4)
	3103	No. 3	-				
4	3123	No. 3	No. 2	2 1/2	7	3320	360
	3133	No. 3	No. 3			(4)	(4)
	3203	No. 3	-				
4	3223	No. 3	No. 2	2 1/2	7	3440	320
	3233	No. 3	No. 3			(4)	(4)
	3303	No. 3	-				
4	3323	No. 3	No. 2	2 1/4	7	3390	340
	3333	No. 3	No. 3			(4)	(4)

* Based on 6 by 12-in. cylinders. Numeral in parentheses indicates number of cylinders tested.

** Based on splitting tests of 6 by 6-in. cylinders.

a Plain bar, 1/4-in. diameter

b Deformed bar, Nominal Diameter: 3/8 in.
Nominal Area: 0.11 sq. in.

TABLE A.1 (Cont'd)

Mark	Tie Size	Longitudinal Bar Size	Concrete: Slump in.	Concrete: Age at Test Days	Concrete: Compressive Strength* psi	Concrete: Tensile Strength** psi
4102	No. 2	-				
4122	No. 2	No. 2	2 1/2	7	3150	310
4132	No. 2	No. 3			(4)	(4)
4202	No. 2	-				
4222	No. 2	No. 2	3 1/4	7	3200	310
4232	No. 2	No. 3			(4)	(4)
4302	No. 2	-				
4322	No. 2	No. 2	3	7	3380	320
4332	No. 2	No. 3			(4)	(4)
5102	No. 2	-				
5122	No. 2	No. 2	2 1/2	7	3330	320
5132	No. 2	No. 3			(4)	(4)
5202	No. 2	-				
5222	No. 2	No. 2	2 1/2	8	3410	340
5232	No. 2	No. 3			(4)	(4)
5302	No. 2	-				
5322	No. 2	No. 2	2 1/4	7	3460	350
5332	No. 2	No. 3			(4)	(4)

* Based on 6 by 12-in. cylinders. Numeral in parentheses indicates number of cylinders tested.

** Based on splitting tests of 6 by 6-in. cylinders.

a Plain bar, 1/4-in. diameter

b Deformed bar, Nominal Diameter: 3/8 in.
Nominal Area: 0.11 sq. in.

December

TABLE A.2

TEST RESULTS: SPECIMENS WITH TIES ONLY

1	2	3	4	5	6	7	8
Mark	Maximum Load P_u kips	Maximum Stress P_u/A psi	Cylinder Strength f'_c psi	Prism* Strength f_{cp} psi	$\frac{P_u}{A\ f'_c}$	$\frac{P_u}{A\ f_{cp}}$	ϵ_p**
1102	90.0	3600	3080	3560	1.17	1.01	0.034[a]
1202	89.0	3560	2980	3320	1.20	1.07	0.026[a]
1302	102.0	4080	3700	4200	1.10	0.97	0.037
2102	86.0	3440	3480	3400	0.99	1.01	0.022
2202	93.8	3750	3480	3520	1.08	1.06	0.030
2302	89.5	3590	3370	3680	1.06	0.98	0.017
3103	90.0	3600	3320	3430	1.09	1.05	0.016
3203	86.0	3440	3440	3480	1.00	0.99	0.019
3303	91.7	3670	3390	3800	1.08	0.97	0.013
4102	85.0	3400	3150	3400	1.08	1.00	0.020
4202	85.0	3400	3200	3360	1.06	1.01	0.009
4302	85.0	3400	3380	3400	1.00	1.00	0.009
5102	85.0	3400	3330	3370	1.02	1.01	0.006
5202	85.5	3420	3410	3440	1.00	1.00	0.009
5302	90.0	3600	3460	3400	1.04	1.06	0.009

* 5 by 5 by 25-in. unreinforced specimen.

** Average strain at the time the resistance is reduced to 25 percent of maximum.

a Average strain at tie fracture.

TABLE A.3

TEST RESULTS: SPECIMENS WITH TIES AND 4-NO. 2 LONGITUDINAL BARS

1	2	3	4	5	6	7	8
Mark	Maximum Load P_u kips	Load Carried By Bars $A_s f_{su}$ kips	Net Maximum Load $P_u - A_s f_s$ kips	$\frac{P_u - A_s f_{su}}{A}$ psi	Prism* Strength f_{cp} psi	$\frac{P_u - A_s f_{su}}{A f_{cp}}$	ϵ_p**
1122	95.0	8.4	86.6	3460	3560	0.97	0.046[a]
1222	94.5	9.4	85.1	3400	3320	1.02	0.028[a]
1322	108.6	8.9	99.7	3990	4200	0.95	0.042[a]
2122	93.3	8.6	84.7	3390	3400	1.00	0.024
2222	98.8	10.5	88.3	3530	3520	1.00	0.025
2322	99.4	10.6	88.8	3550	3680	0.97	0.026
3123	95.0	9.2	85.8	3430	3430	1.00	0.019
3223	94.5	9.2	85.3	3410	3480	0.98	0.034
3323	96.7	11.0	85.7	3430	3800	0.90	0.015
4122	90.0	9.4	80.6	3220	3400	0.95	0.014
4222	90.0	10.6	79.4	3180	3360	0.95	0.018
4322	90.0	9.9	80.1	3200	3400	0.94	0.013
5122	90.0	10.4	79.6	3190	3370	0.95	0.006
5222	95.0	9.6	85.4	3410	3440	1.00	0.009
5322	89.0	10.1	78.9	3150	3400	0.93	0.007

* 5 by 5 by 25-in. unreinforced specimen.

** Average strain at the time the resistance is reduced to 25 percent of maximum.

a Average strain at tie fracture.

TABLE A.4

TEST RESULTS: SPECIMENS WITH TIES AND 4-NO. 3 LONGITUDINAL BARS

1	2	3	4	5	6	7	8
Mark	Maximum Load P_u kips	Load Carried By Bars $A_s f_{su}$ kips	Net Maximum Load $P_u - A_s f_{su}$ kips	$\frac{P_u - A_s f_{su}}{A}$ psi	Prism* Strength f_{cp} psi	$\frac{P_u - A_s f_{su}}{A f_{cp}}$	ϵ_p**
1132	109.0	20.8	88.2	3530	3560	0.99	0.033[a]
1232	89.0[b]	20.8	68.2	2730	3320	0.82	0.035[a]
1332	118.7	20.0	98.7	3950	4200	0.94	0.025[a]
2132	102.9	24.8	78.1	3120	3400	0.92	0.039[a]
2232	110.0	24.8	85.2	3400	3520	0.97	0.028
2332	110.0	24.8	85.2	3400	3680	0.93	0.038
3133	112.1	24.8	87.3	3490	3430	1.02	0.025
3233	108.0	25.0	83.0	3320	3480	0.96	0.038
3333	114.0	25.2	88.8	3550	3800	0.94	0.047
4132	105.0	25.2	79.8	3190	3400	0.94	0.014
4232	107.8	24.4	83.4	3340	3360	0.99	0.015
4332	106.9	24.4	82.5	3300	3400	0.97	0.013
5132	101.7	25.2	76.5	3060	3370	0.91	0.009
5232	111.3	25.2	86.1	3440	3440	1.00	0.007
5332	106.9	24.4	82.5	3300	3400	0.97	0.007

* 5 by 5 by 25-in. unreinforced specimen.

** Average strain at the time the resistance is reduced to 25 percent of maximum.

a Average strain at tie fracture.

b Local failure at end of specimen.

TABLE A.5

PROPERTIES OF REINFORCING BARS

Mark	Size* No.	Yield Stress f_{sy} ksi	Maximum Stress f'_s ksi	Location (Mark of Concrete Specimen) Ties	Longitudinal
1	2	51.1	79.5	1102	
2	2	48.0	74.6	1122	
3	2	51.9	79.3	1132	
4	2	42.9	66.3		1122
5	3	47.3	69.8		1132, 1232
6	2	54.0	76.3	1222	
7	2	46.0	69.2	1202	
8	2	48.0	70.6	1232	
9	2	49.8	78.4	1302	
10	2	45.5	68.8	1322	
11	2	51.2	76.8	1332	
12	2	47.8	70.4		1222
13	3	45.5	71.1		1332
14	2	45.5	69.6		1322
15	2	47.4	69.5	2102	
16	2	50.6	78.6	2122	
17	2	53.6	78.6	2132	
18	2	54.7	80.9	2202	
19	2	50.6	77.2	2222	
20	2	49.5	70.9	2232	
21	2	49.0	71.6	2302	
22	2	48.0	74.6	2322	
23	2	44.1	67.4		2122
24	3	56.4	91.4		2132, 2232
25	2	53.7	79.4		2222
26	2	54.1	80.5		2322
27	2	44.9	67.4	2332	
28	3	56.4	90.6		2332, 3133
29	3	56.7	90.6	3103	
30	3	55.3	87.0	3123	
31	3	55.3	88.4	3133	
32	2	47.1	68.4		3123
33	2	47.1	70.6		3223
34	3	56.7	90.7		3233
35	3	54.9	88.2	3203	
36	3	56.4	91.0	3223, 3233	
37	3	57.3	93.4	3303	
38	3	56.6	91.2	3323, 3333	

* No. 2 : Plain Bar, 1/4-in. diameter.
No. 3 : Deformed Bar, Nominal Diameter: 3/8 in.
Nominal Area: 0.11 sq. in.

TABLE A.5 (Cont'd)

Mark	Size* No.	Yield Stress f_{sy} ksi	Maximum Stress f'_s ksi	Location (Mark of Concrete Specimen) Ties	Longitudinal
39	2	55.9	81.1		3323
40	3	57.3	93.7		3333, 4132
41	2	47.0	70.2	4102	
42	2	49.2	76.1	4122	
43	2	49.8	79.0	4132	
44	2	48.0	69.6		4122
45	2	47.6	69.9	4202	
46	2	48.8	75.9	4222	
47	2	46.0	69.3	4232	
48	2	54.1	79.3		4222
49	3	55.5	88.5		4232, 4332
50	2	49.0	79.9	4302	
51	2	53.1	81.4	4322	
52	2	46.8	69.9	4332	
53	2	49.2	76.8	5102	
54	2	48.8	71.9	5122	
55	2	49.0	71.6	5132	
56	2	48.2	75.9	5202	
57	2	53.7	80.5	5222	
58	2	52.0	78.8	5232	
59	2	50.5	77.8		4322
60	2	49.9	76.9	5302	
61	2	50.6	77.4	5322	
62	2	47.5	70.5	5332	
63	2	52.9	79.4		5122
64	3	57.3	91.8		5132, 5232
65	2	48.8	70.0		5222
66	2	51.5	76.5		5322
67	3	55.4	87.5		5332

* No. 2 : Plain Bar, 1/4-in. diameter.
No. 3 : Deformed Bar, Nominal Diameter: 3/8 in.
Nominal Area: 0.11 sq. in.

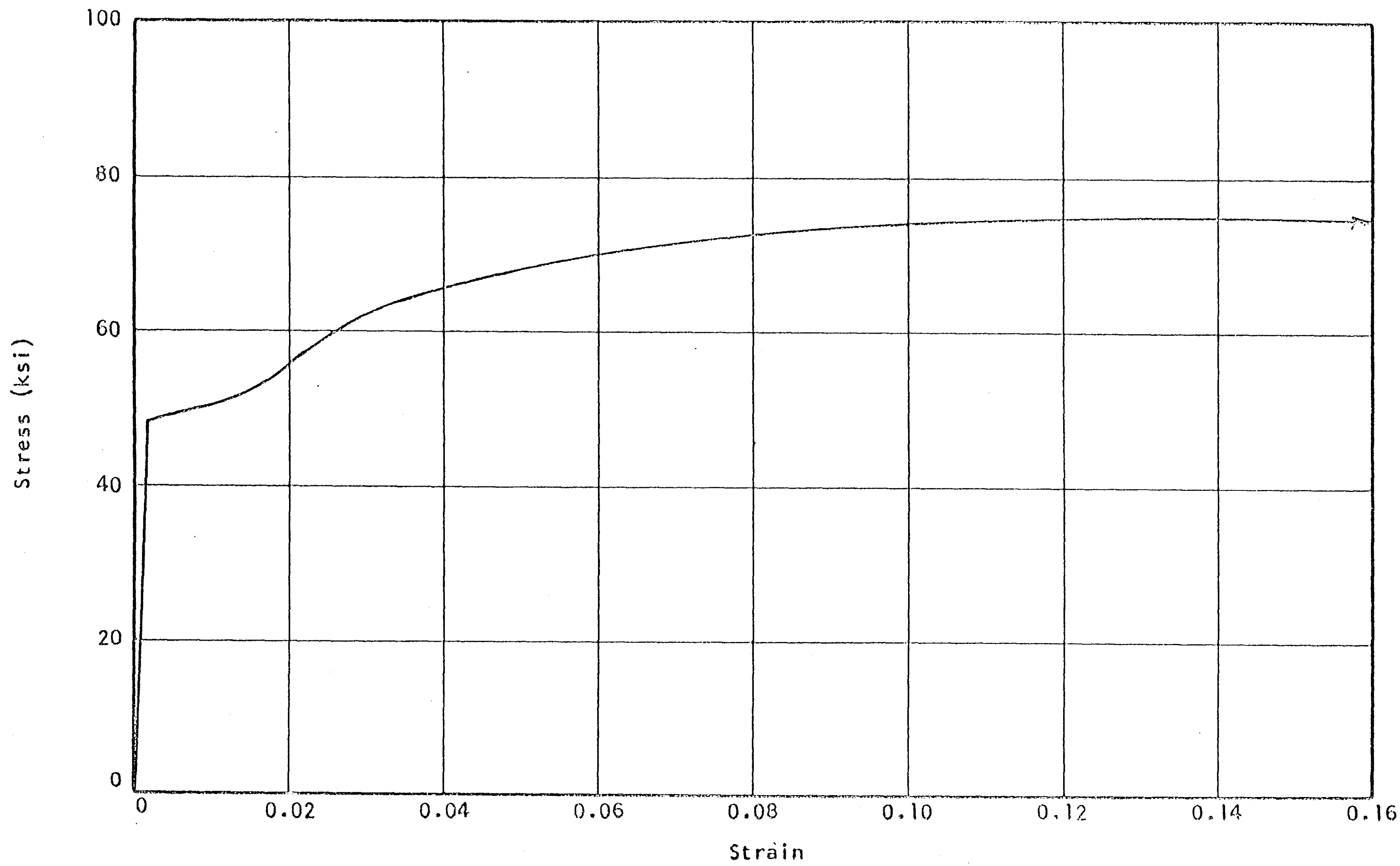

FIG. A.1 TYPICAL STRESS-STRAIN RELATION FOR NO. 2 REINFORCING BARS

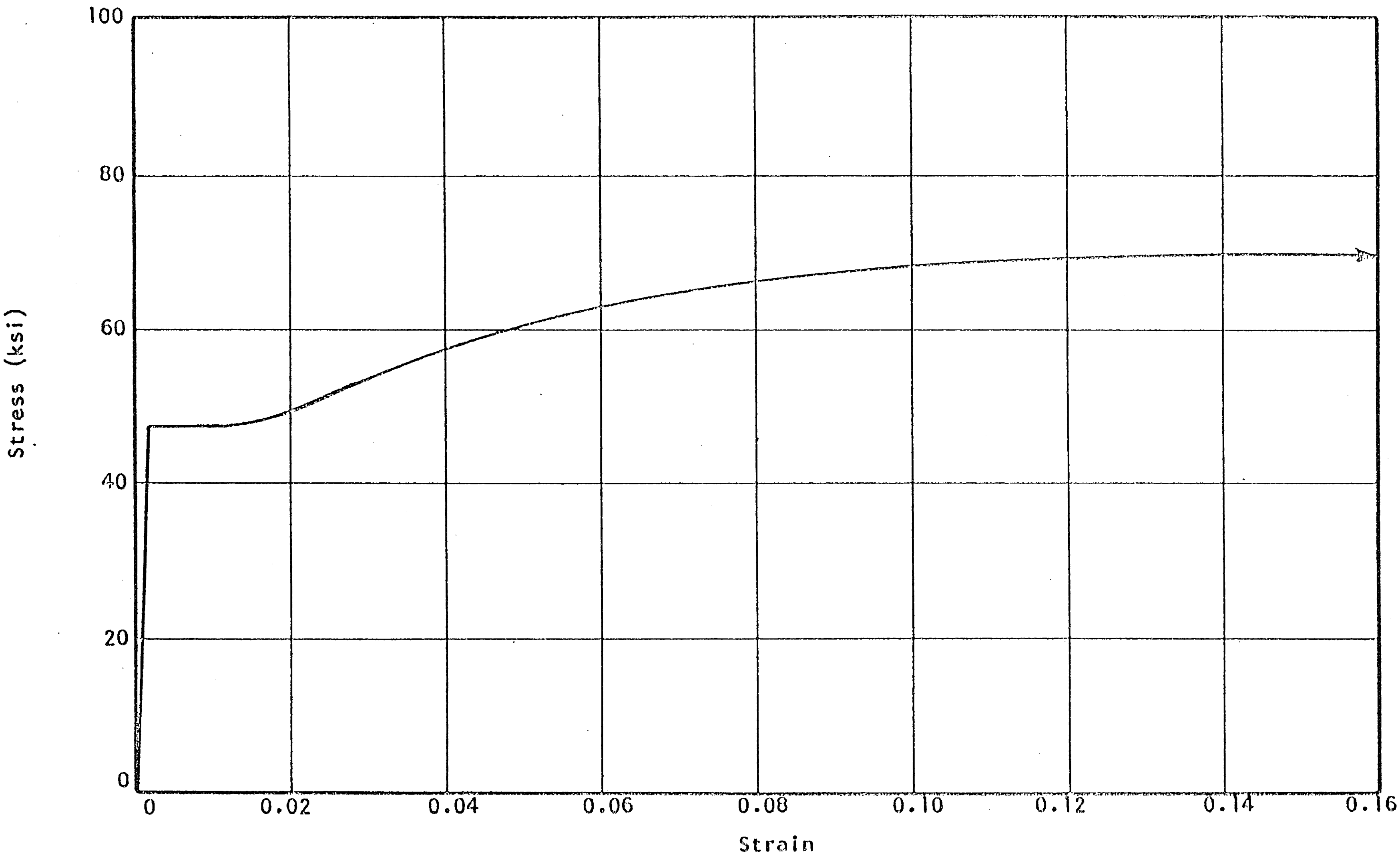

FIG. A.2 TYPICAL STRESS-STRAIN RELATION FOR NO. 3 REINFORCING BARS

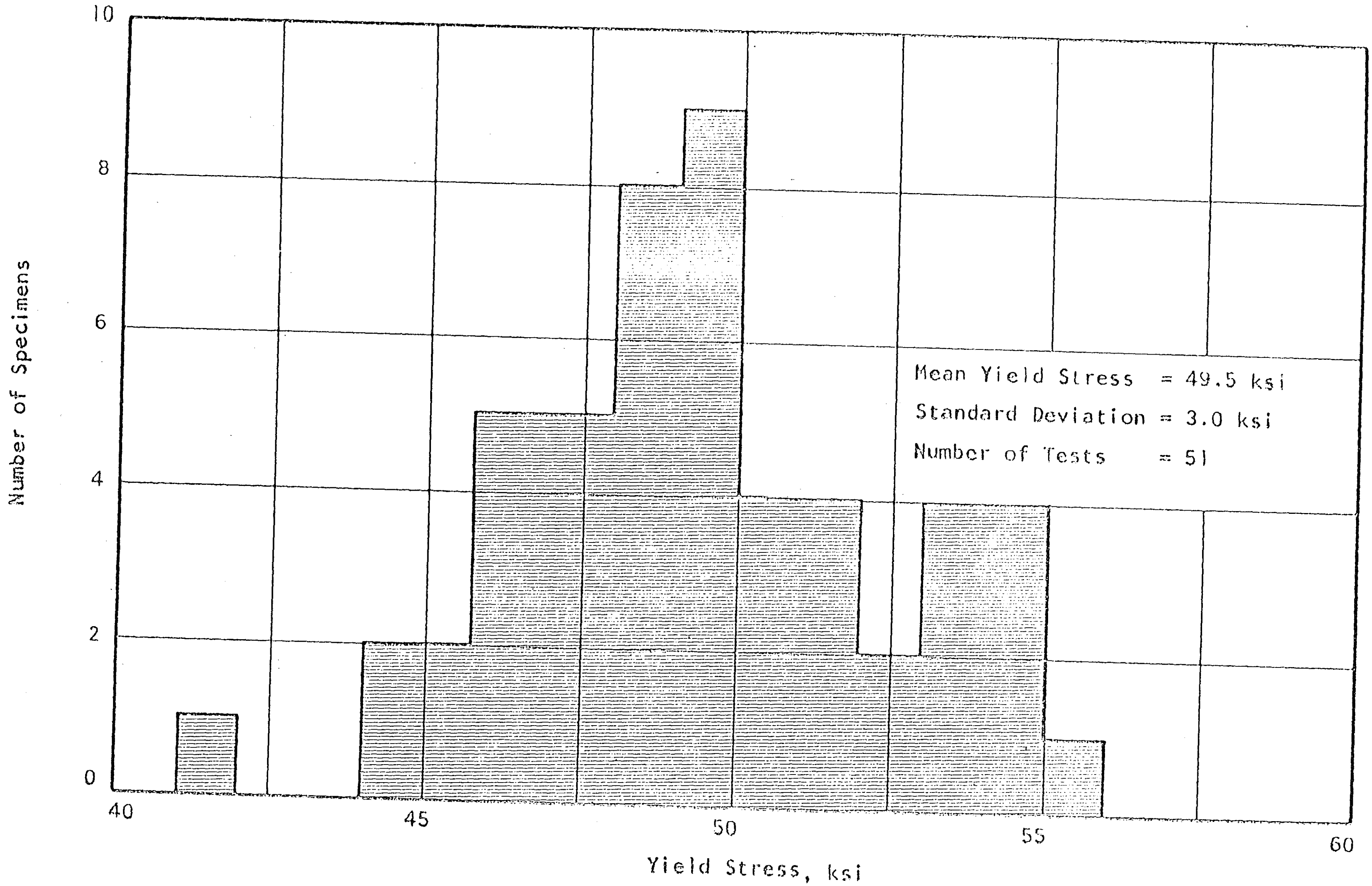

FIG. A.3 HISTOGRAM FOR THE YIELD STRESS OF NO. 2 REINFORCING BARS

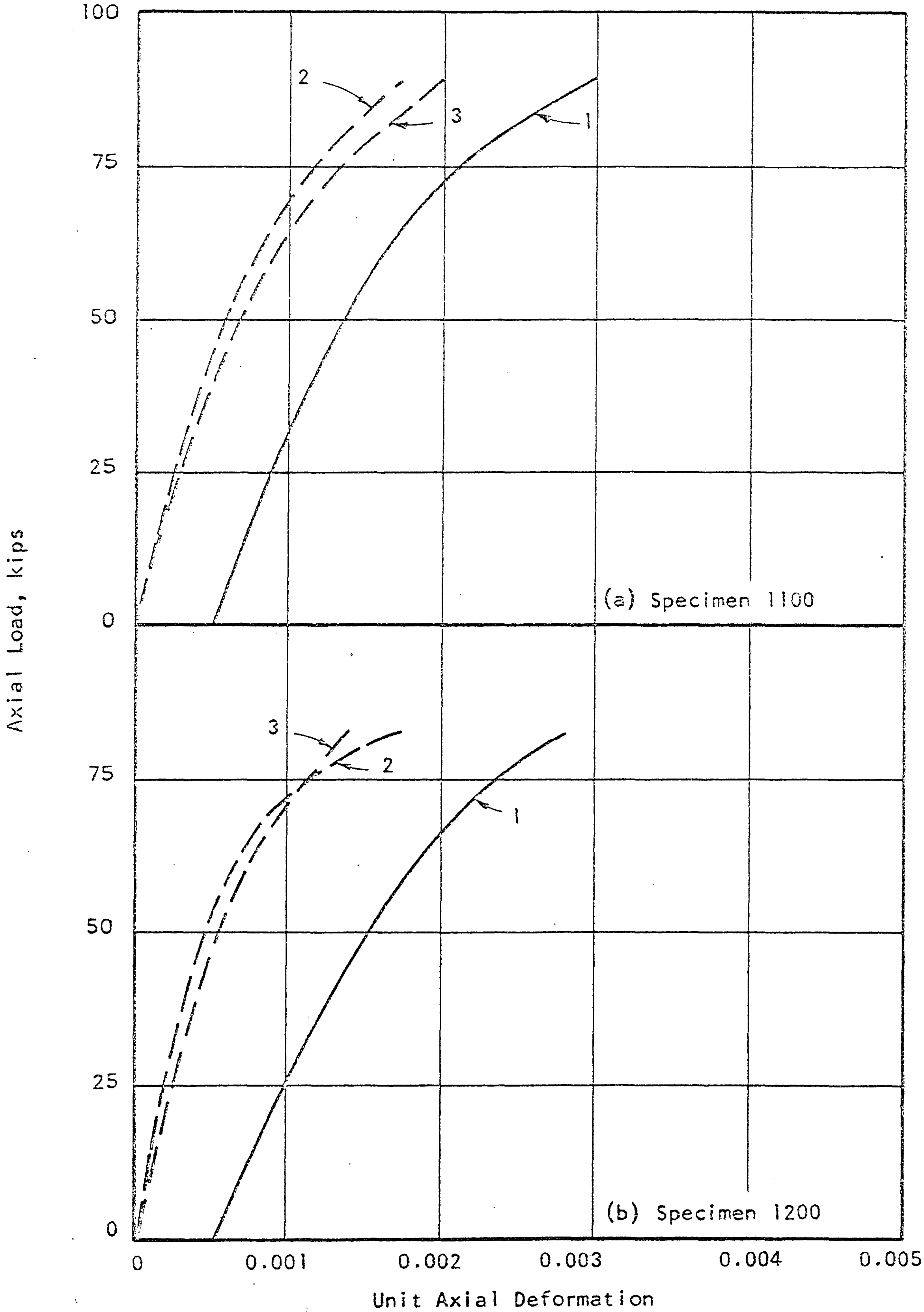

FIG. A-4 MEASURED LOAD-DEFORMATION RELATIONSHIPS FOR SPECIMENS 1100 AND 1200

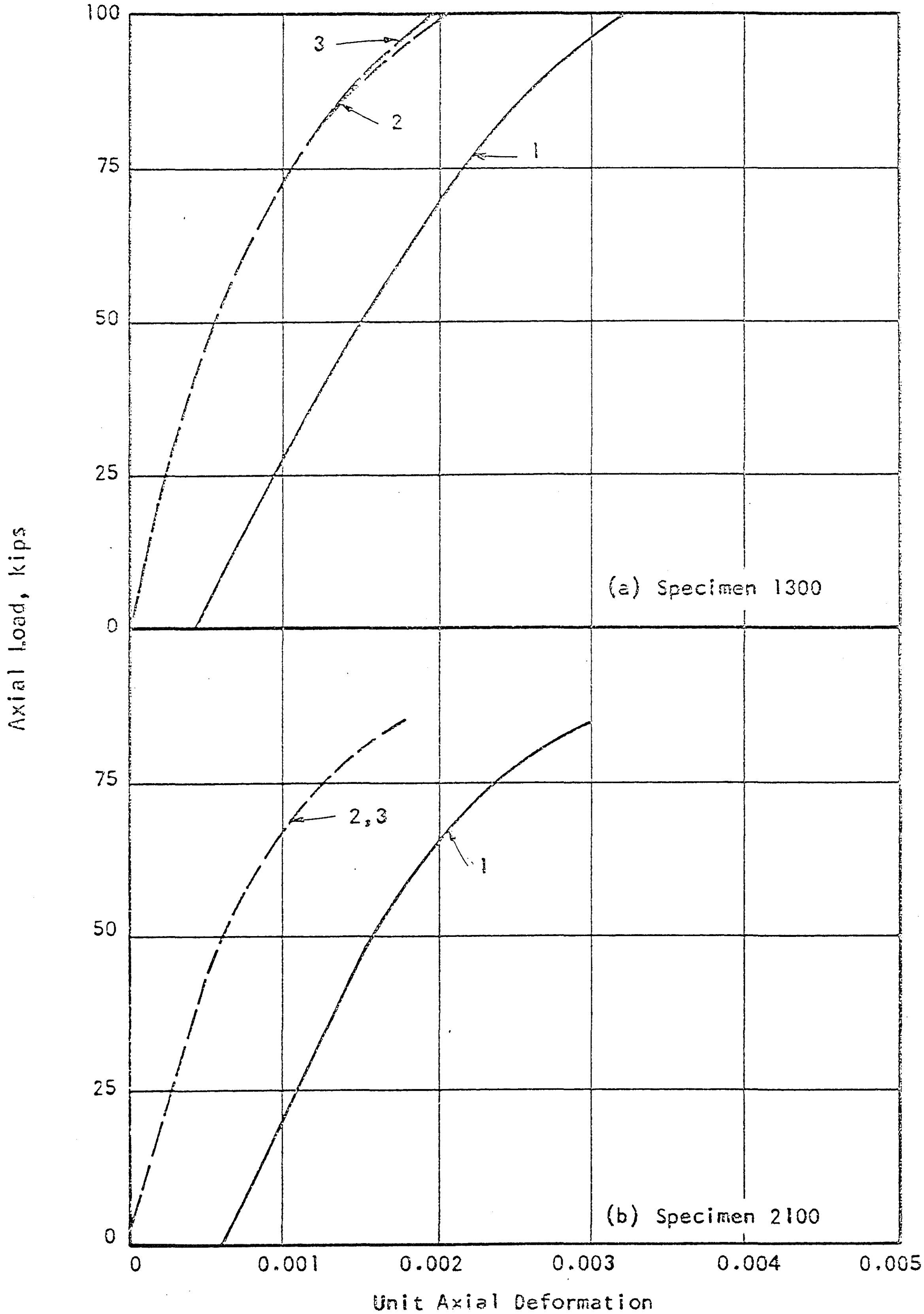

FIG. A.5 MEASURED LOAD-DEFORMATION RELATIONSHIPS FOR SPECIMENS 1300 AND 2100

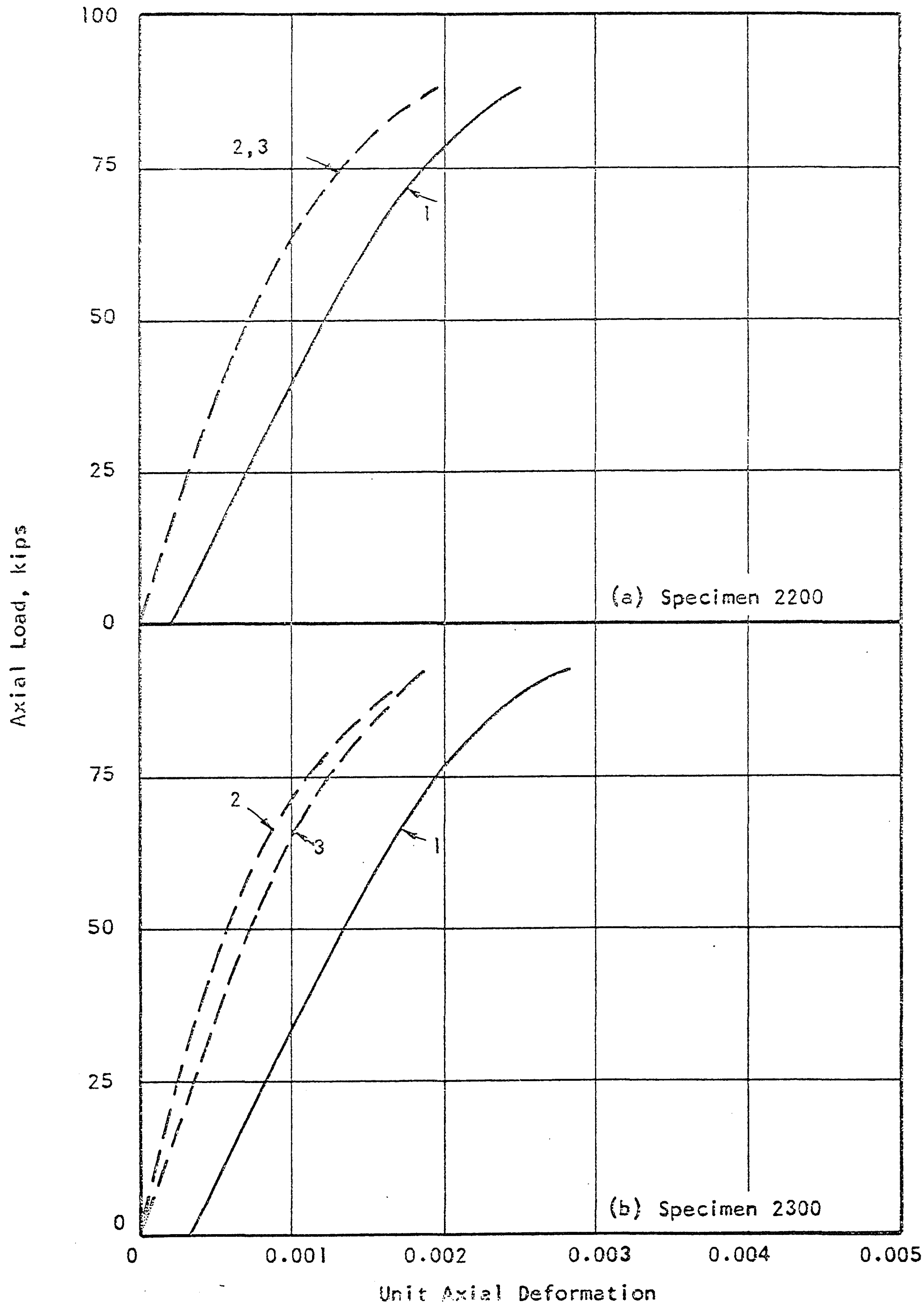

FIG. A.6 MEASURED LOAD-DEFORMATION RELATIONSHIPS FOR SPECIMENS 2200 AND 2300

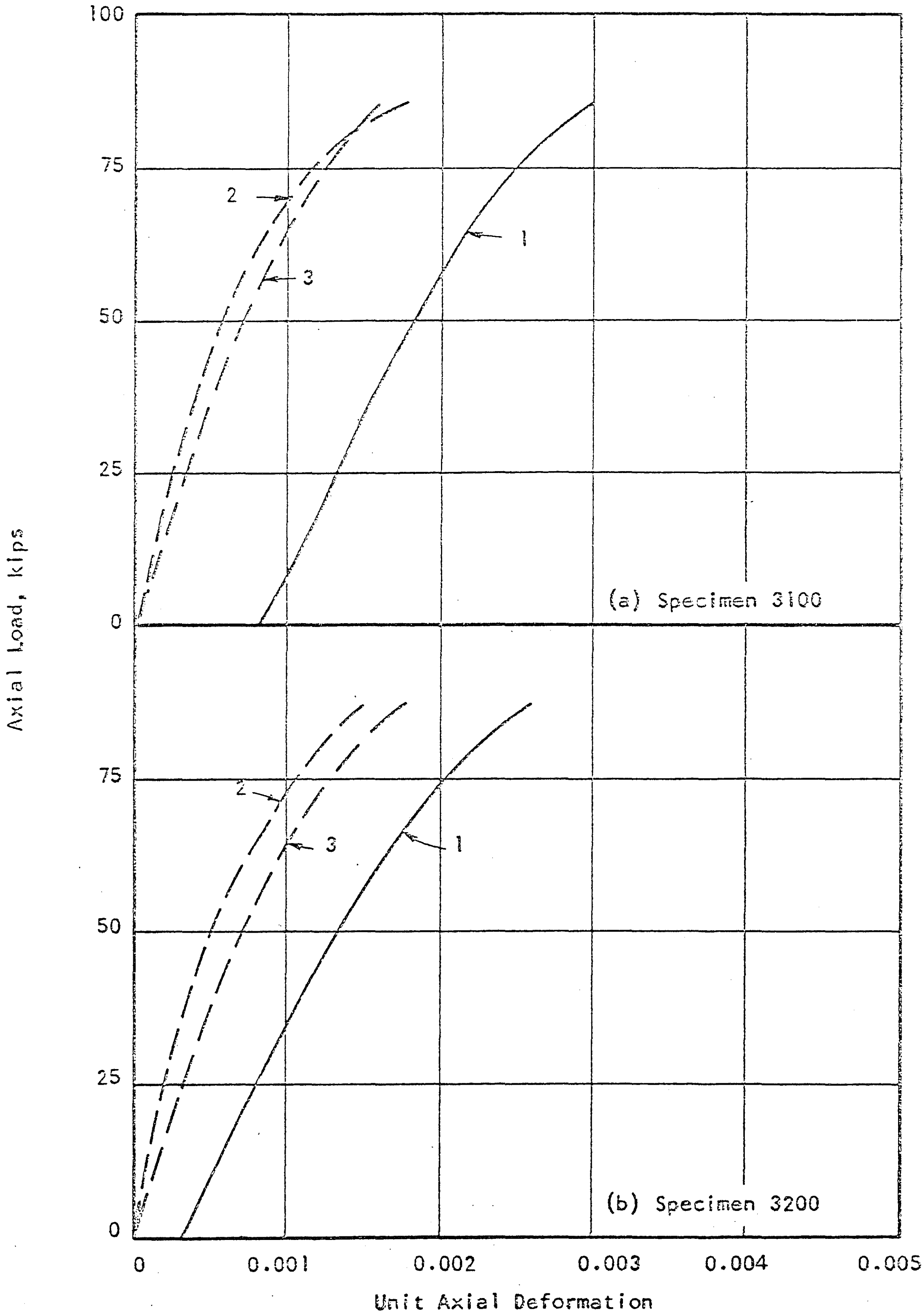

FIG. A.7 MEASURED LOAD-DEFORMATION RELATIONSHIPS
FOR SPECIMENS 3100 AND 3200

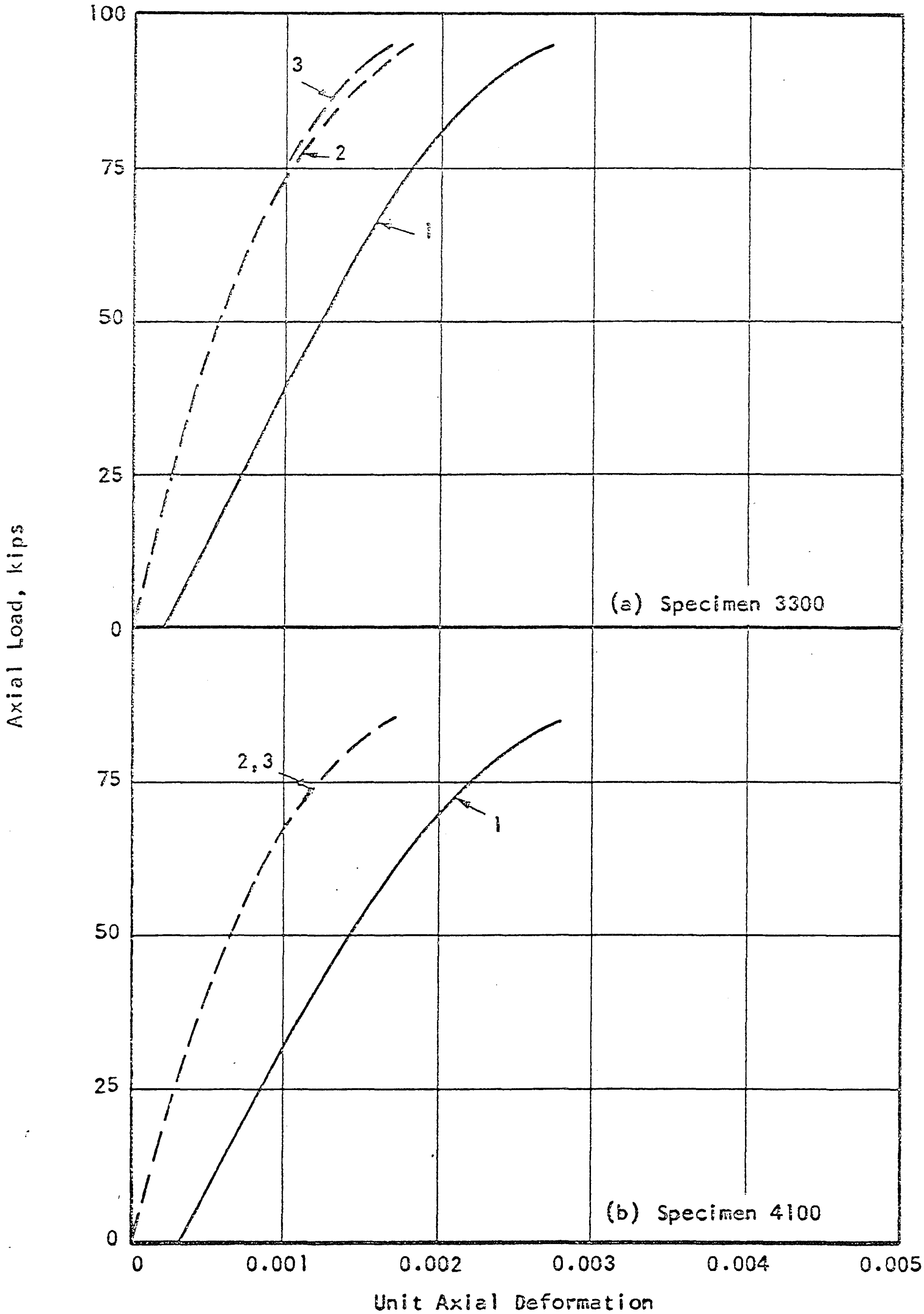

FIG. A.8 MEASURED LOAD-DEFORMATION RELATIONSHIPS FOR SPECIMENS 3300 AND 4100

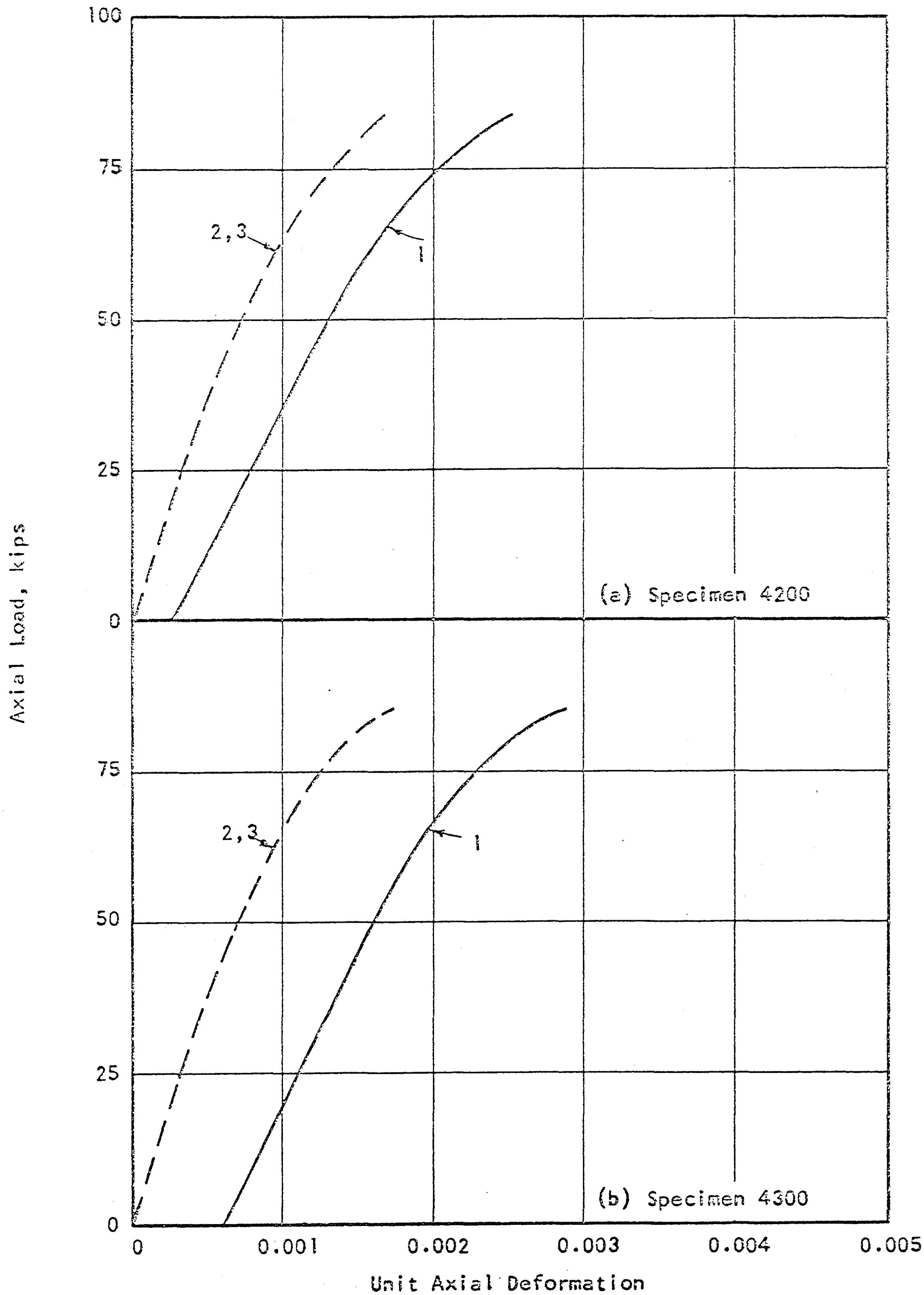

FIG. A.9 MEASURED LOAD-DEFORMATION RELATIONSHIPS FOR SPECIMENS 4200 AND 4300

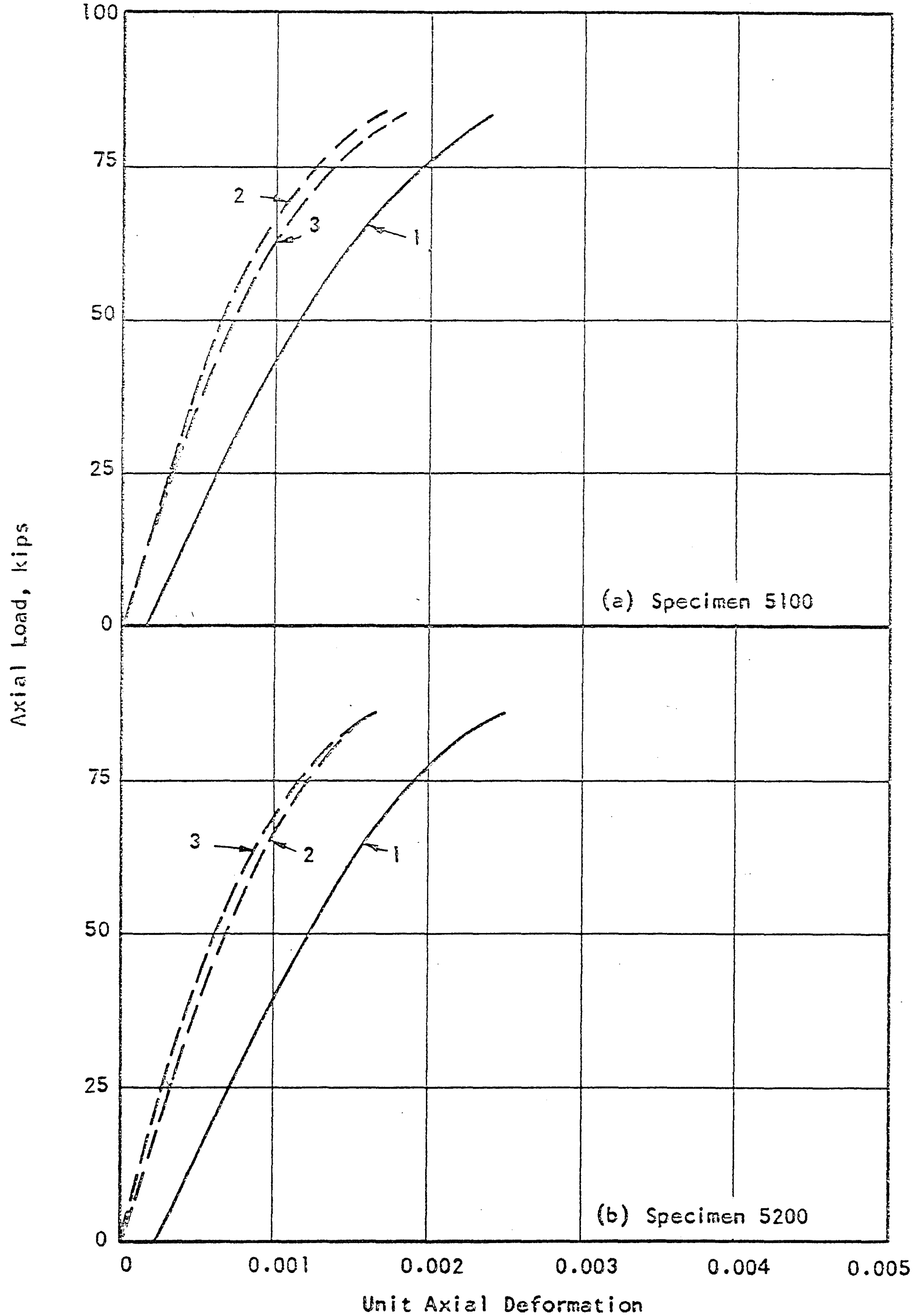

FIG. A.10 MEASURED LOAD-DEFORMATION RELATIONSHIPS FOR SPECIMENS 5100 AND 5200

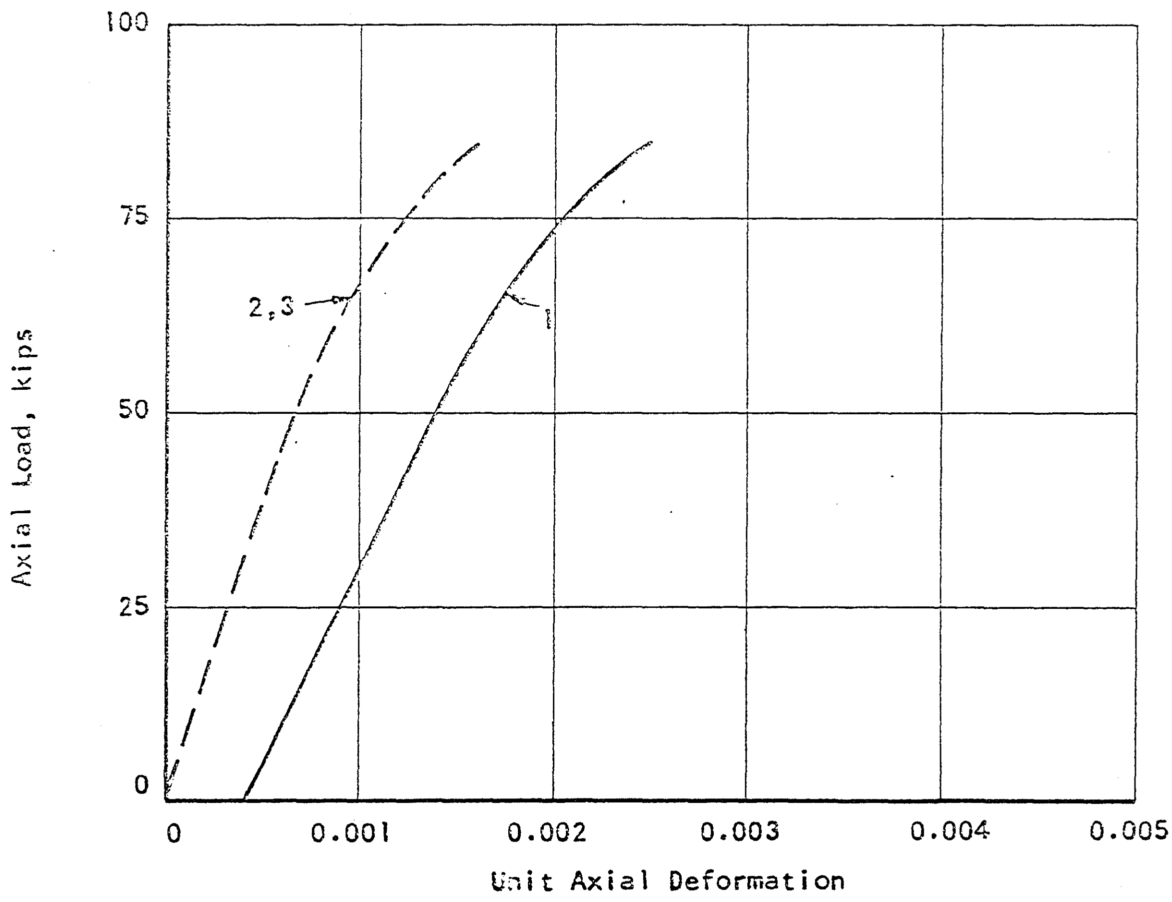

FIG. A.11 MEASURED LOAD-DEFORMATION RELATIONSHIPS FOR SPECIMEN 5300

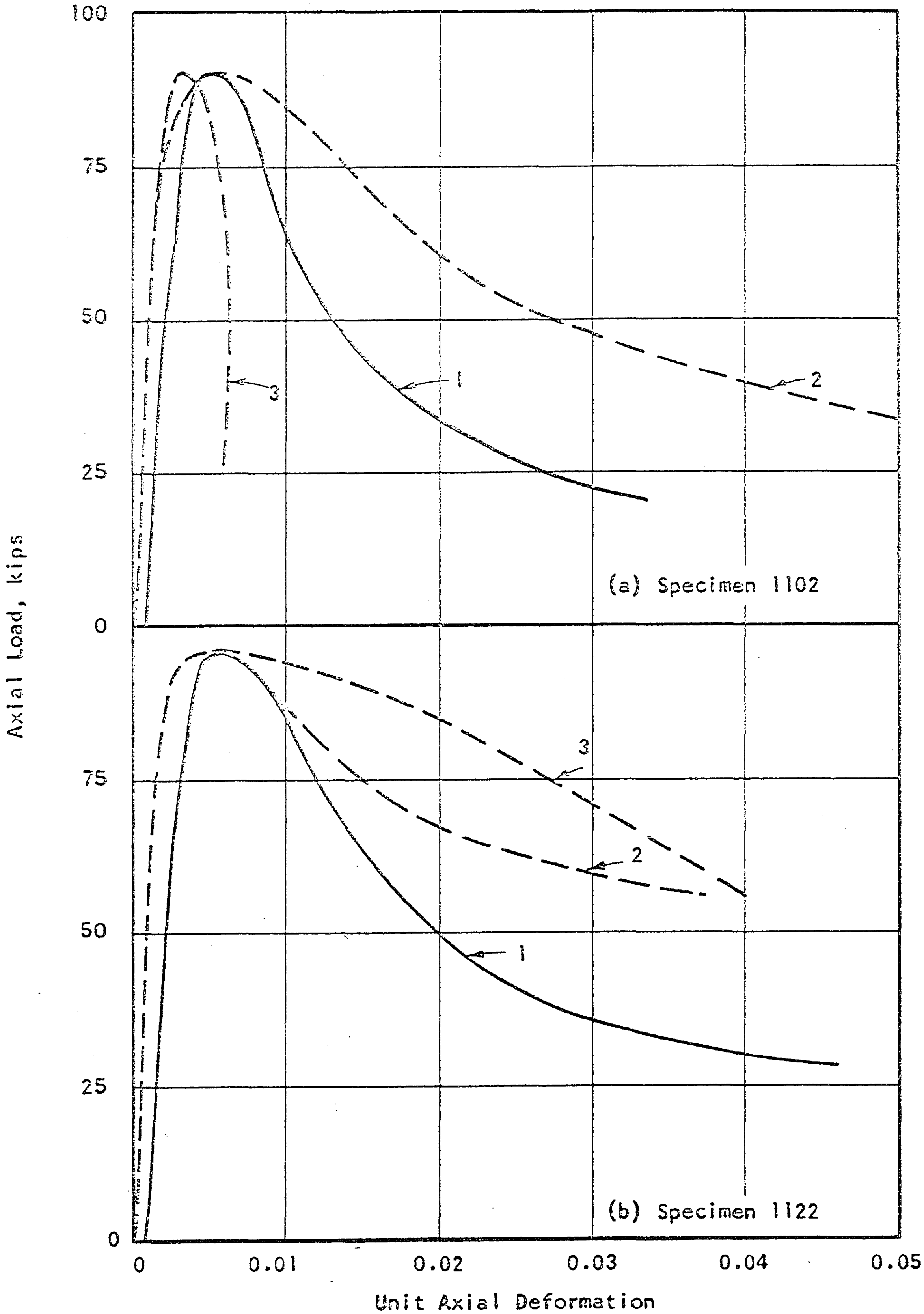

FIG. A.12 MEASURED LOAD-DEFORMATION RELATIONSHIPS FOR SPECIMENS 1102 AND 1122

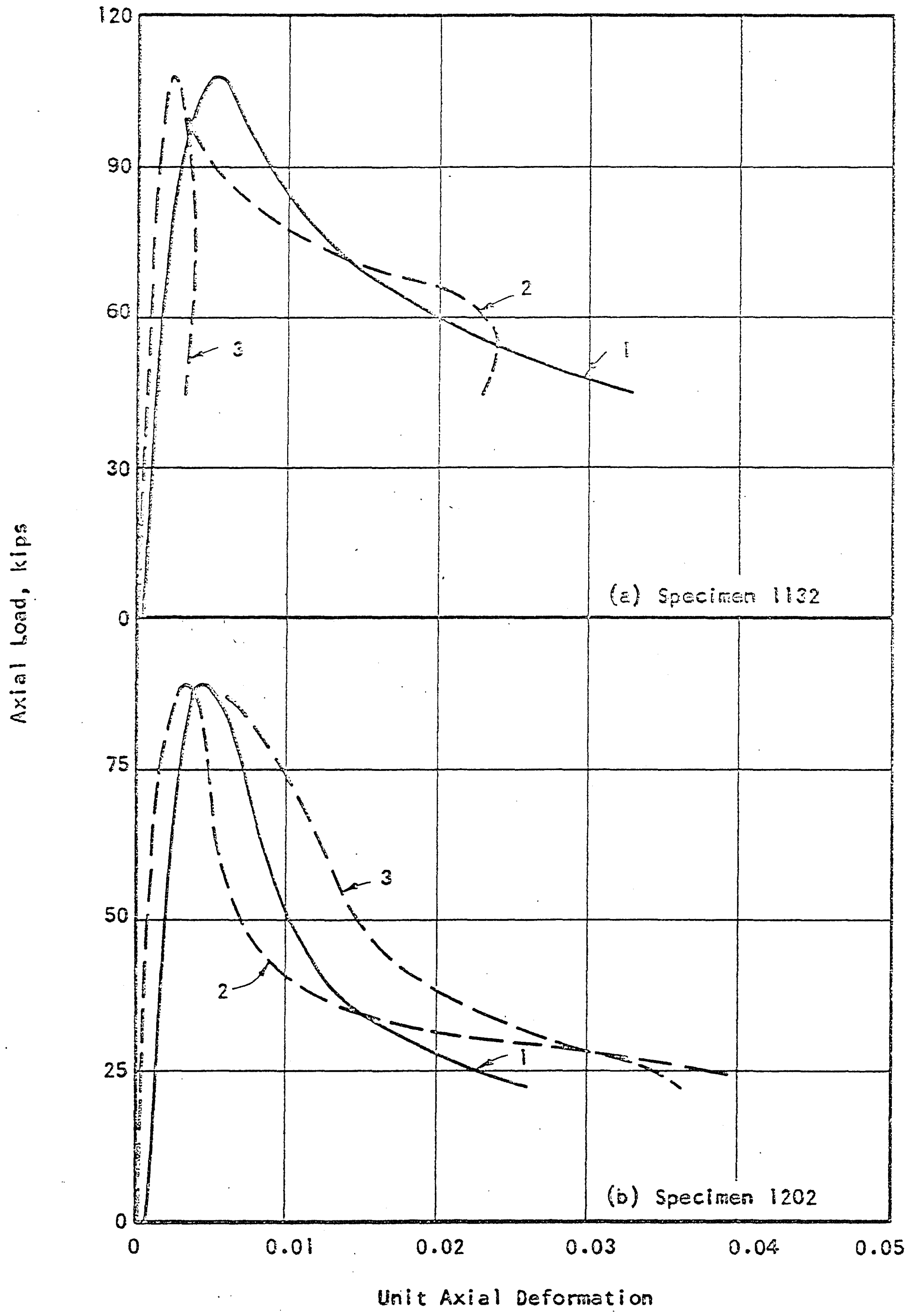

FIG. A.13 MEASURED LOAD-DEFORMATION RELATIONSHIPS FOR SPECIMENS 1132 AND 1202

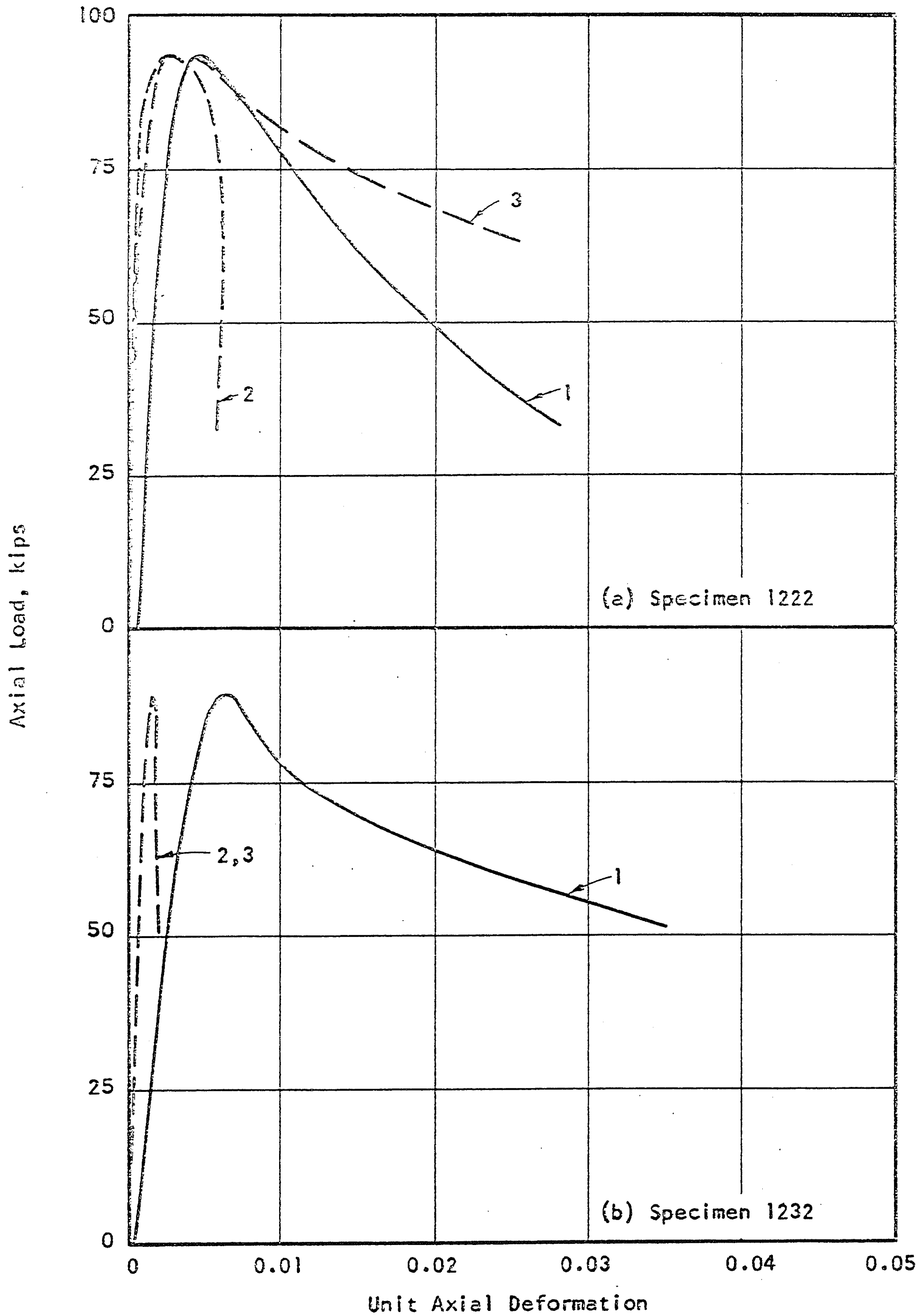

FIG. A.14 MEASURED LOAD-DEFORMATION RELATIONSHIPS FOR SPECIMENS 1222 AND 1232

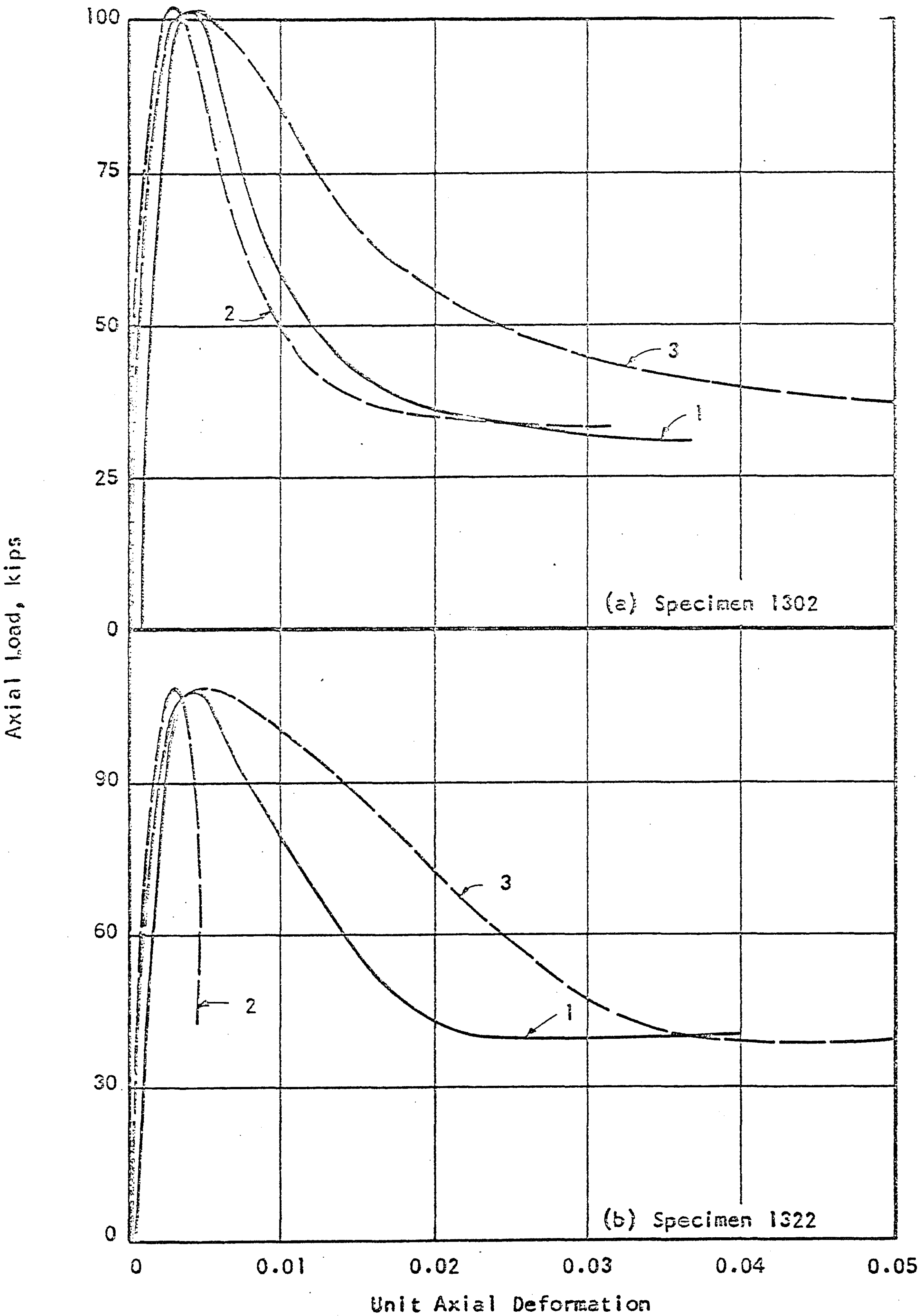

FIG. A.15 MEASURED LOAD-DEFORMATION RELATIONSHIPS FOR SPECIMENS 1302 AND 1322

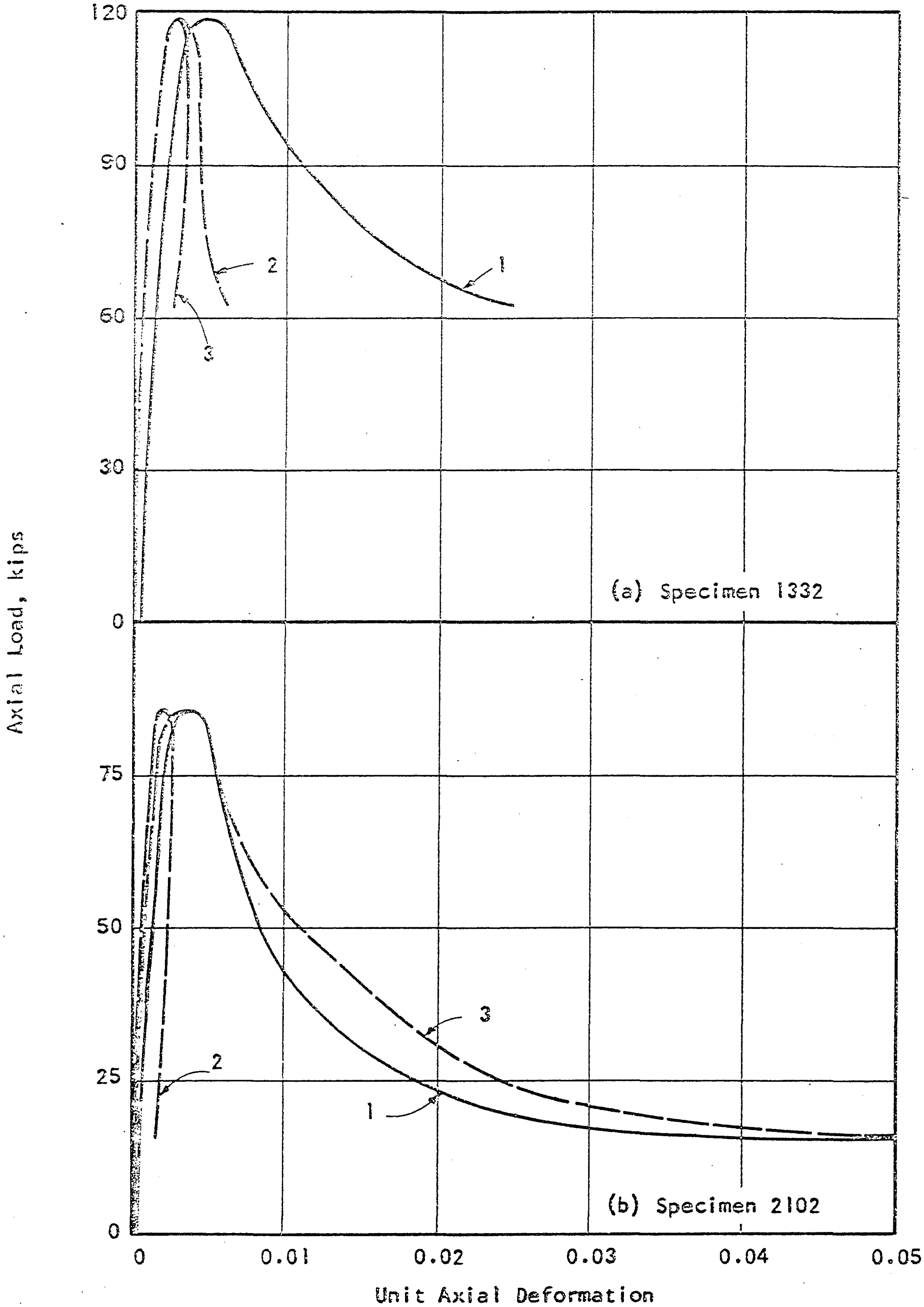

FIG. A.16 MEASURED LOAD-DEFORMATION RELATIONSHIPS FOR SPECIMENS 1332 AND 2102

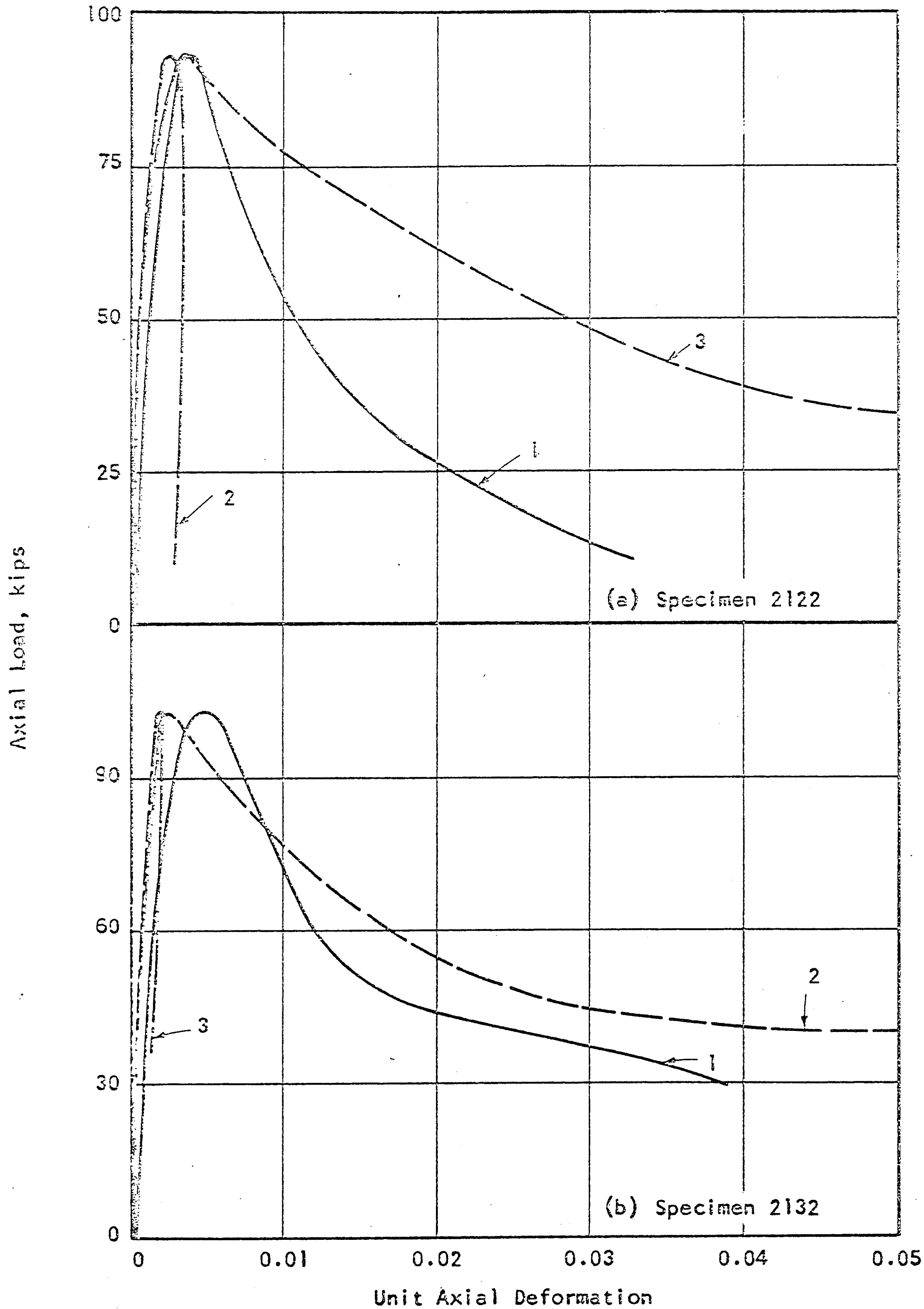

FIG. A.17 MEASURED LOAD-DEFORMATION RELATIONSHIPS FOR SPECIMENS 2122 AND 2132

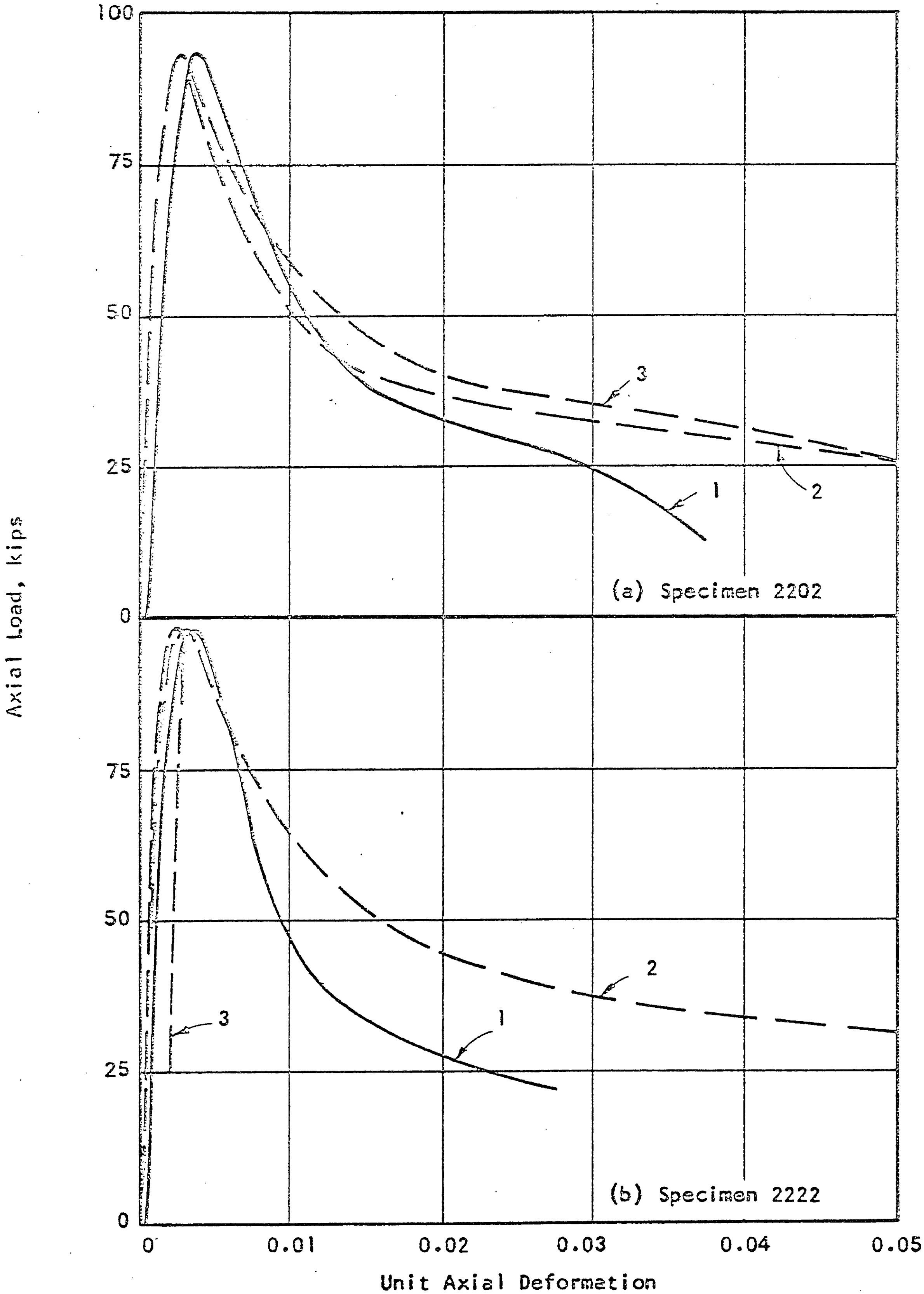

FIG. A.18 MEASURED LOAD-DEFORMATION RELATIONSHIPS FOR SPECIMENS 2202 AND 2222

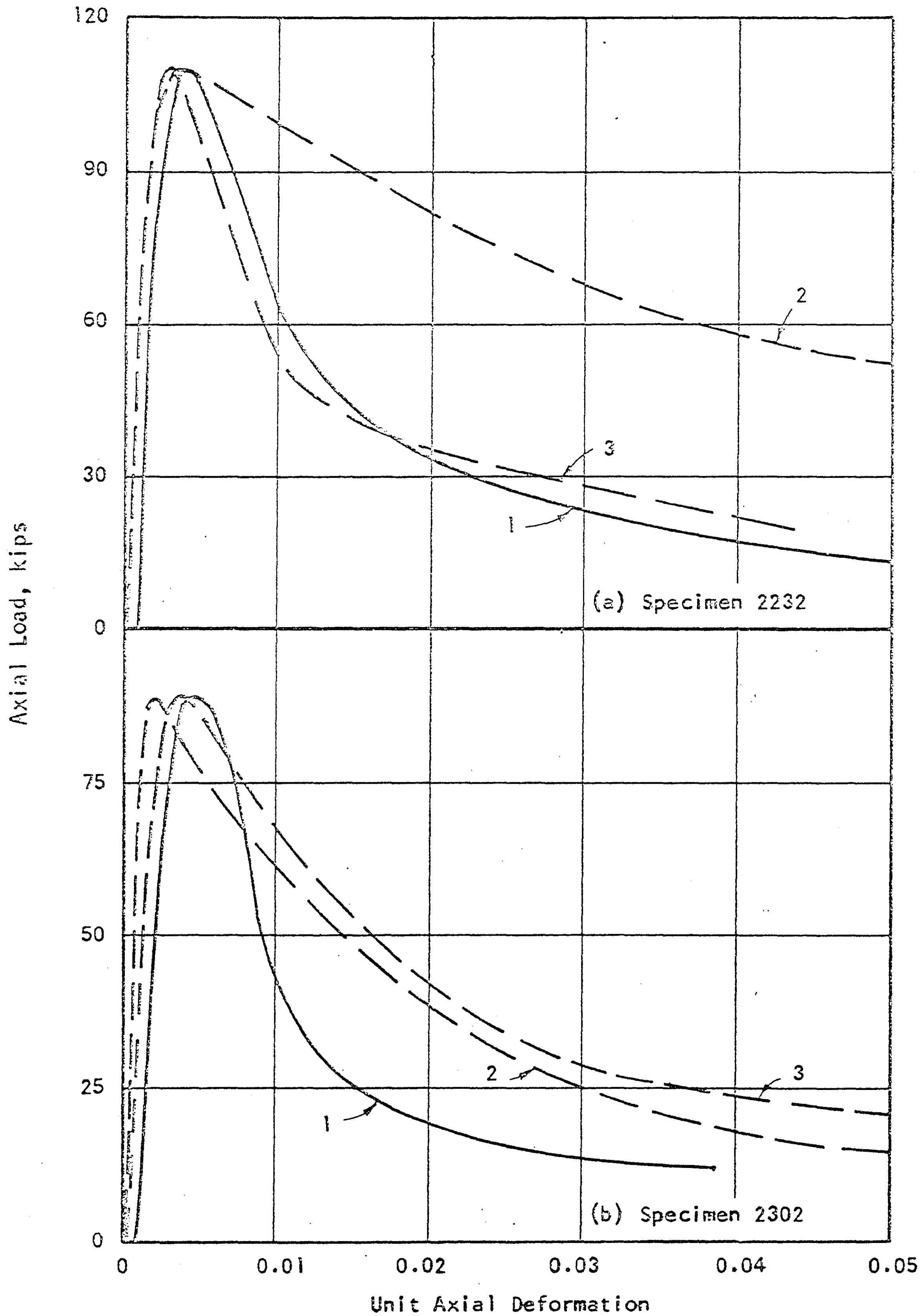

FIG. A.19 MEASURED LOAD-DEFORMATION RELATIONSHIPS FOR SPECIMENS 2232 AND 2302

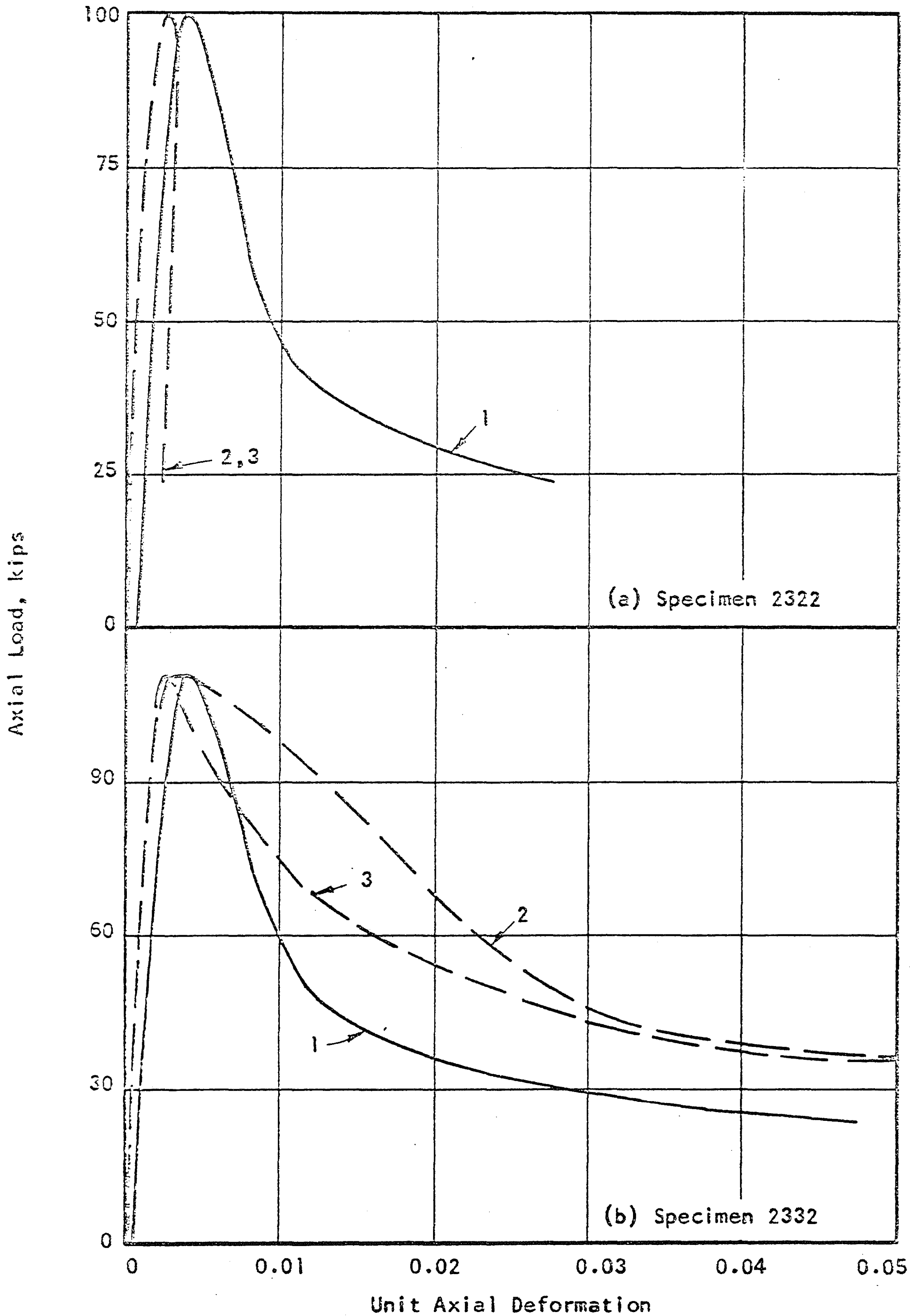

FIG. A.20 MEASURED LOAD-DEFORMATION RELATIONSHIPS
FOR SPECIMENS 2322 AND 2332

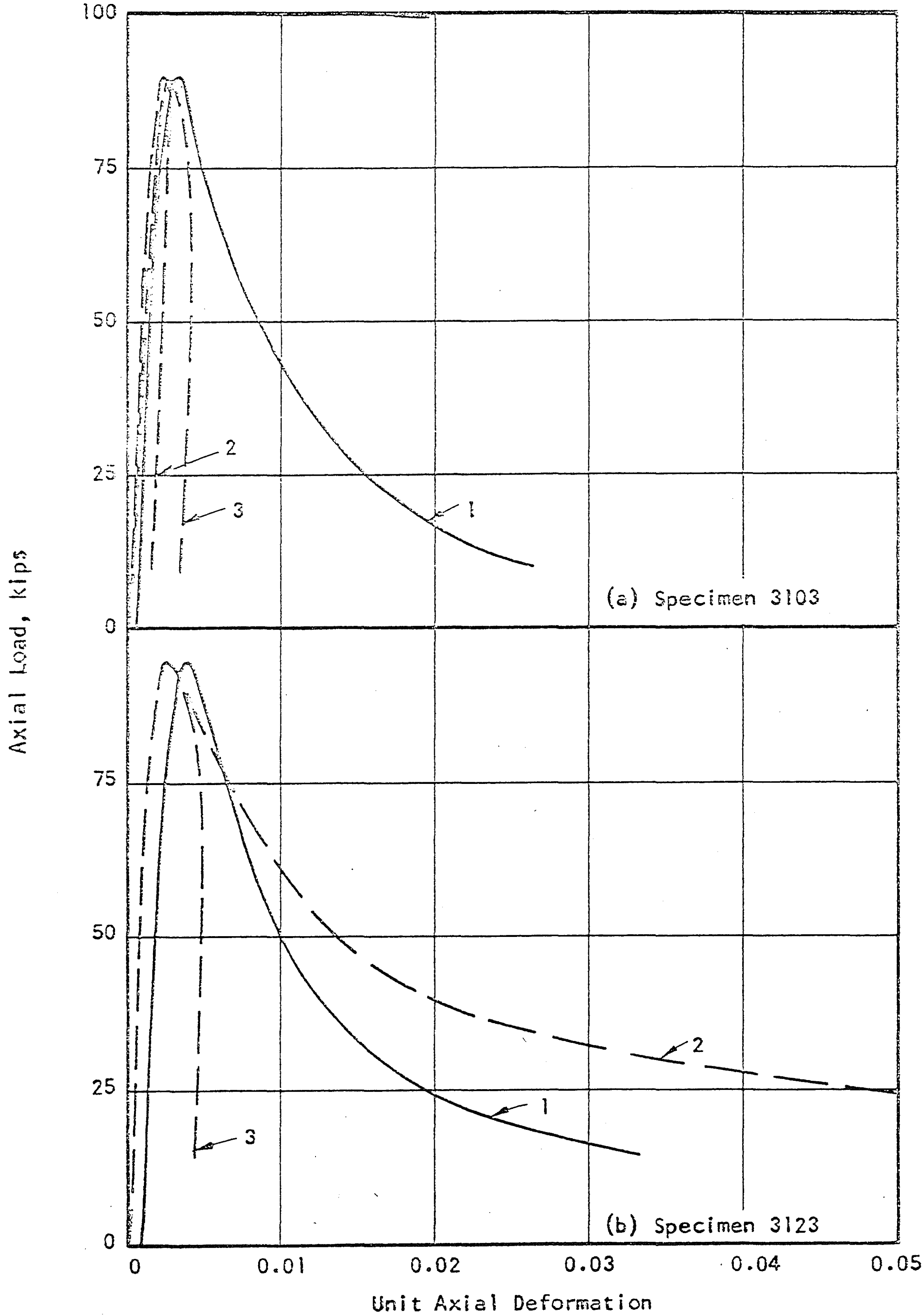

FIG. A.21 MEASURED LOAD-DEFORMATION RELATIONSHIPS FOR SPECIMENS 3103 AND 3123

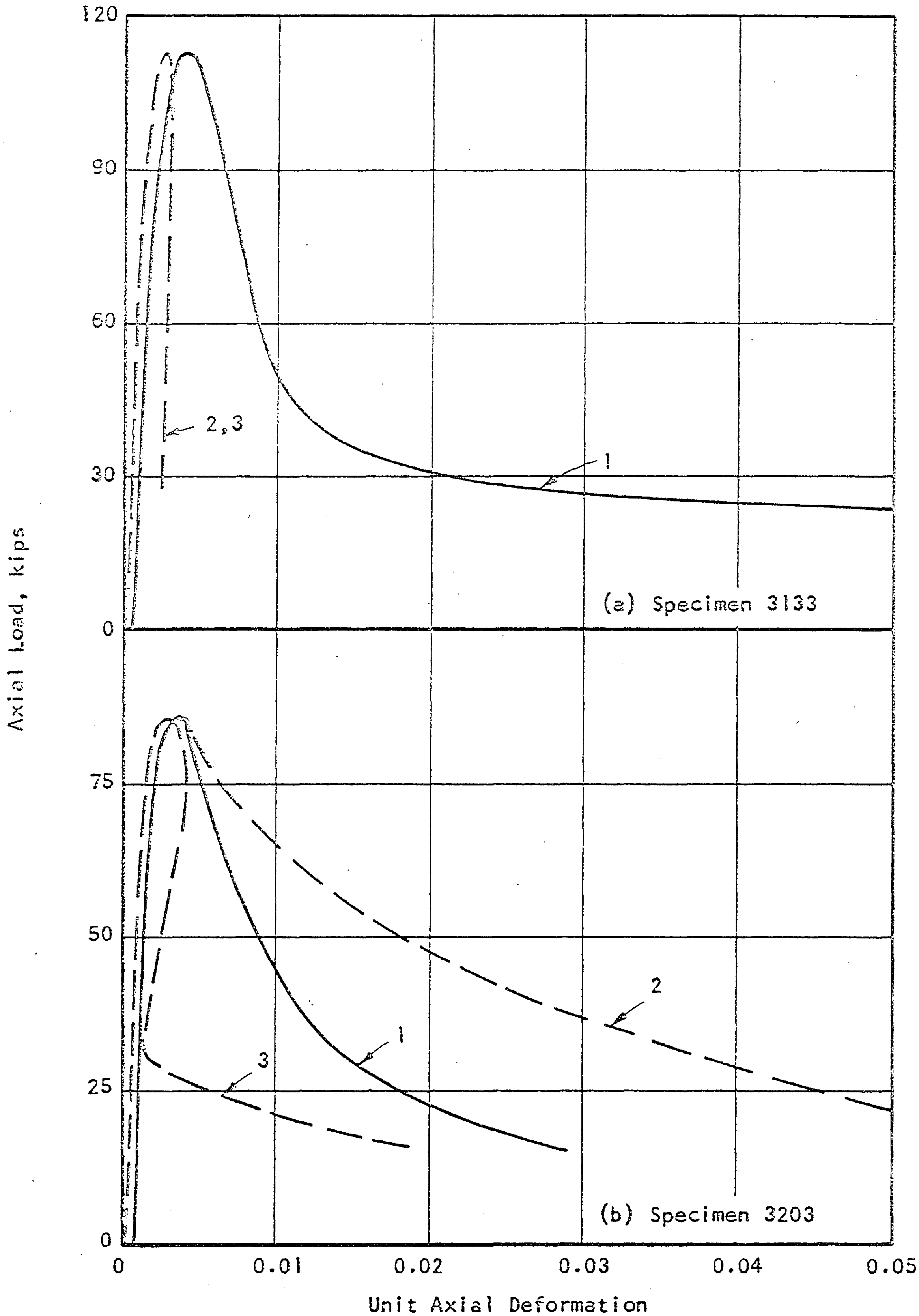

FIG. A.22 MEASURED LOAD-DEFORMATION RELATIONSHIPS FOR SPECIMENS 3133 AND 3203

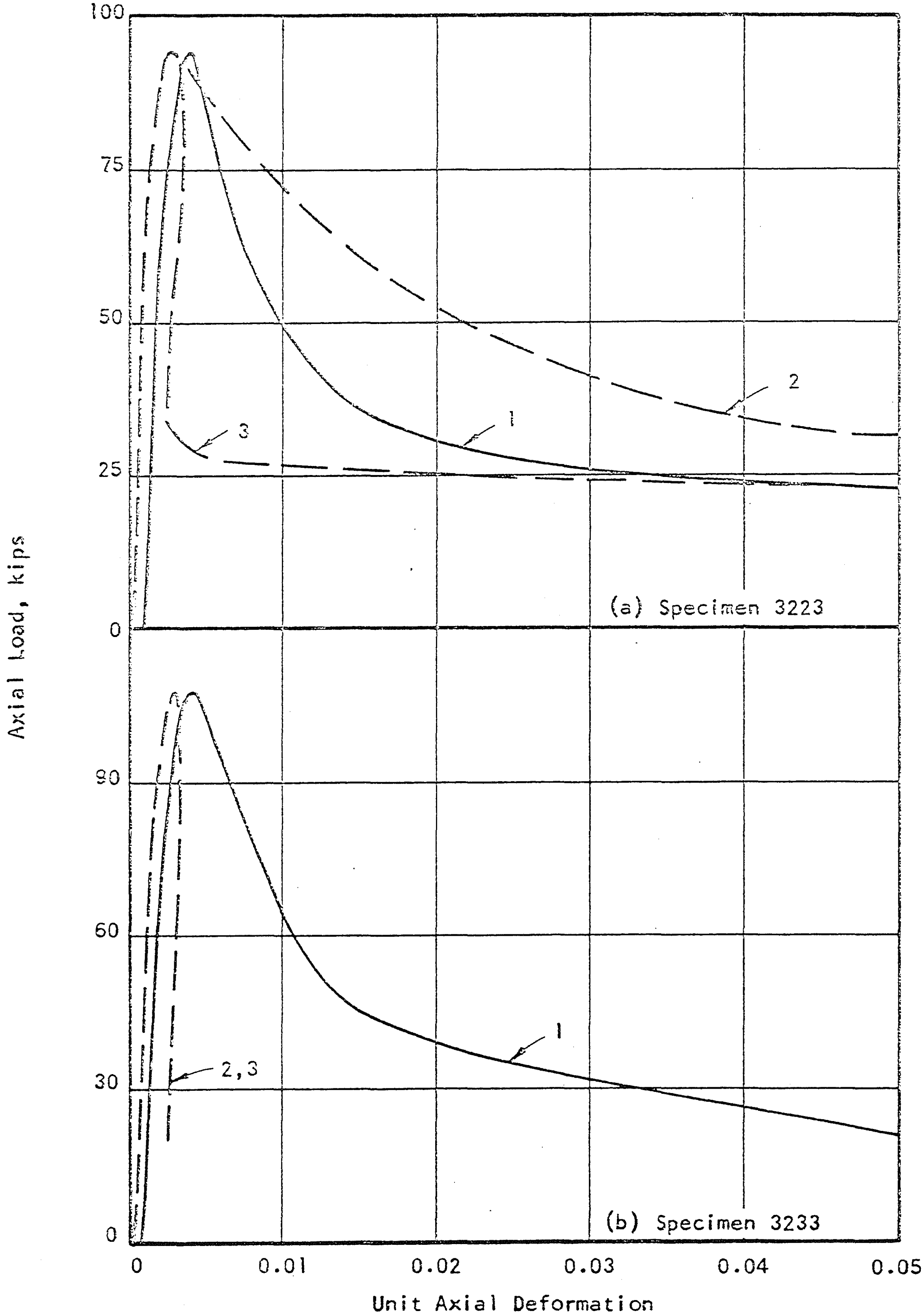

FIG. A.23 MEASURED LOAD-DEFORMATION RELATIONSHIPS
FOR SPECIMENS 3223 AND 3233

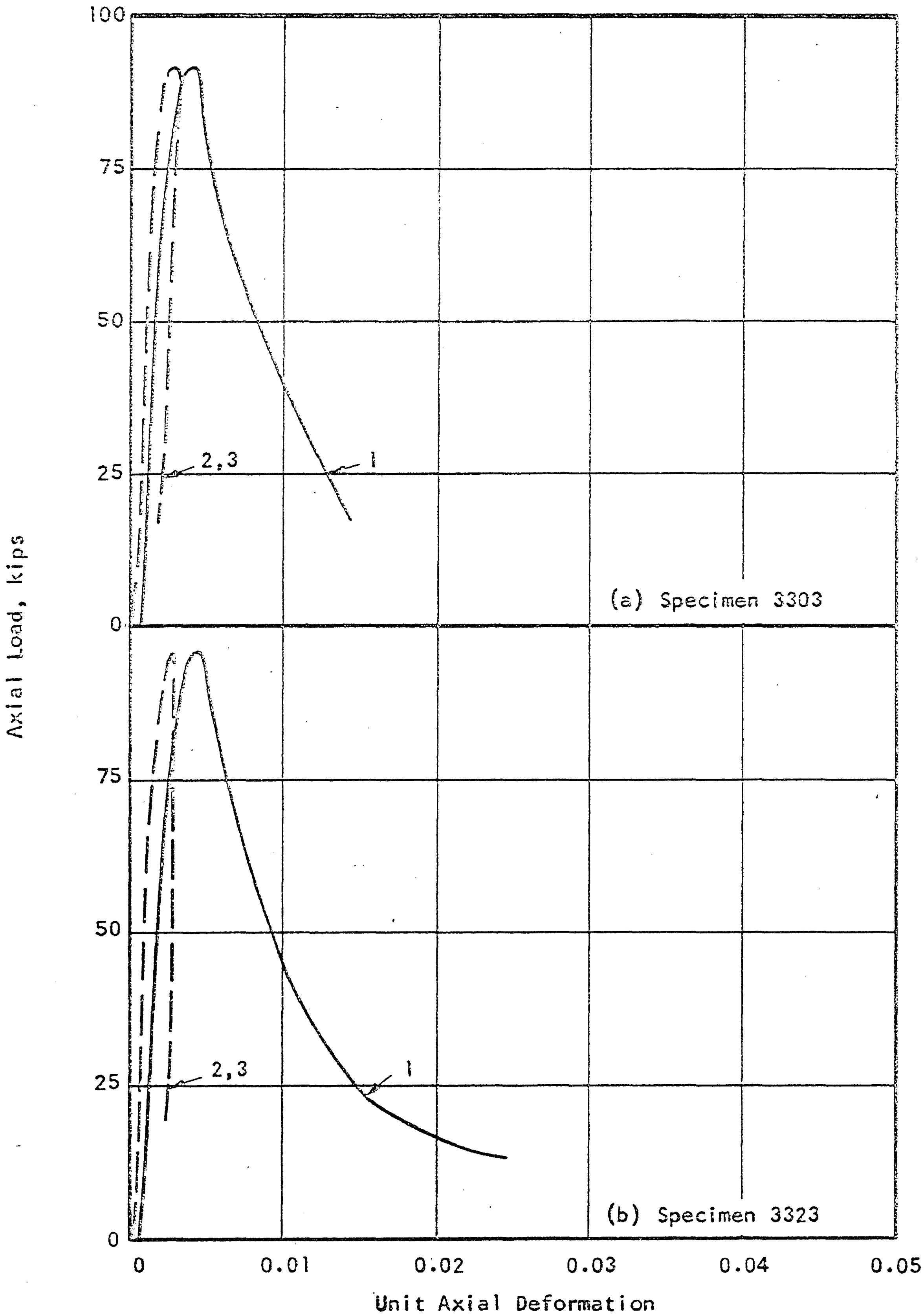

FIG. A.24 MEASURED LOAD-DEFORMATION RELATIONSHIPS FOR SPECIMENS 3303 AND 3323

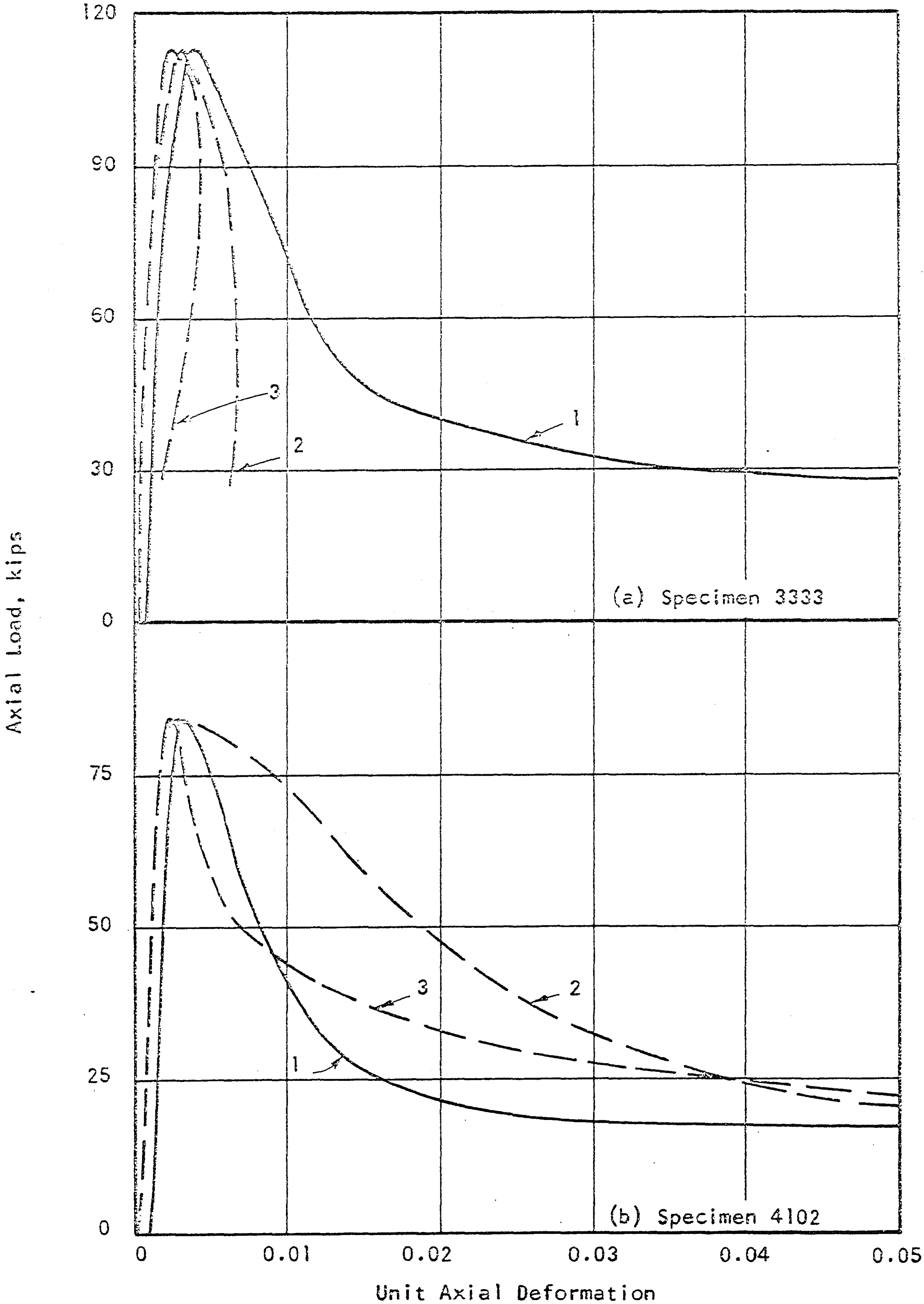

FIG. A.25 MEASURED LOAD-DEFORMATION RELATIONSHIPS FOR SPECIMENS 3333 AND 4102

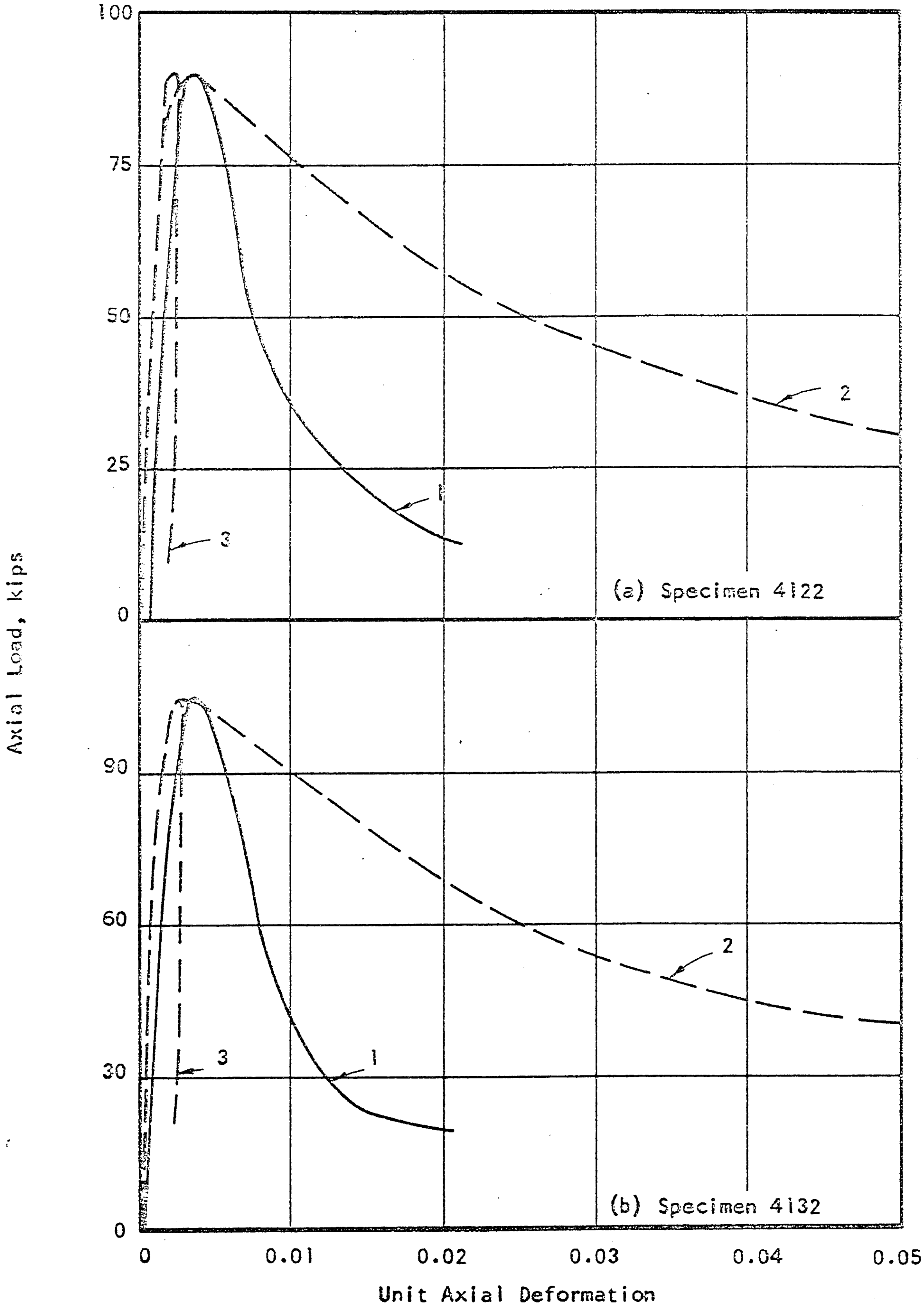

FIG. A.26 MEASURED LOAD-DEFORMATION RELATIONSHIPS FOR SPECIMENS 4122 AND 4132

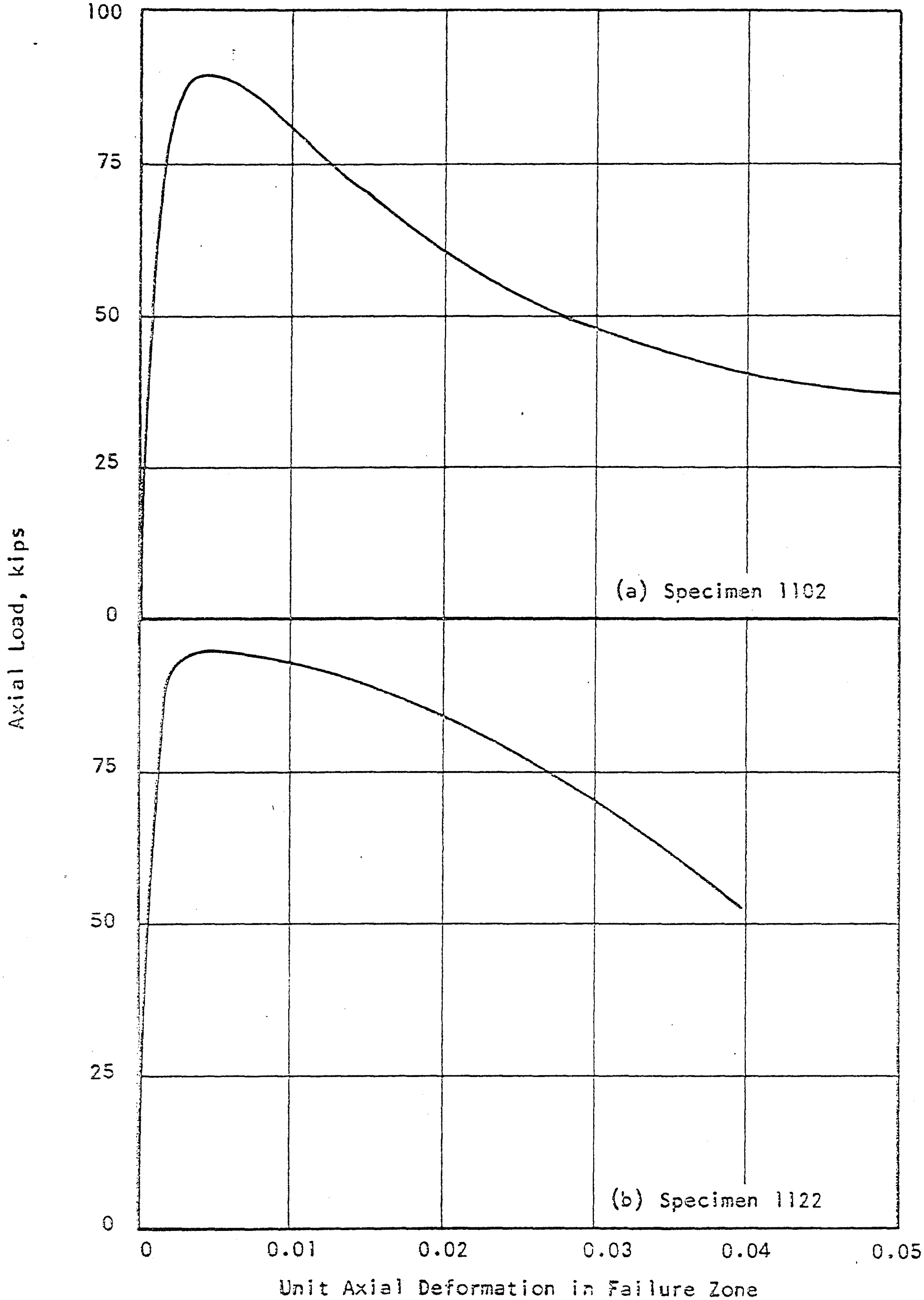

FIG. A.35 RELATIONSHIPS OF LOAD VS. STRAIN IN FAILURE ZONE FOR SPECIMENS 1102 AND 1122

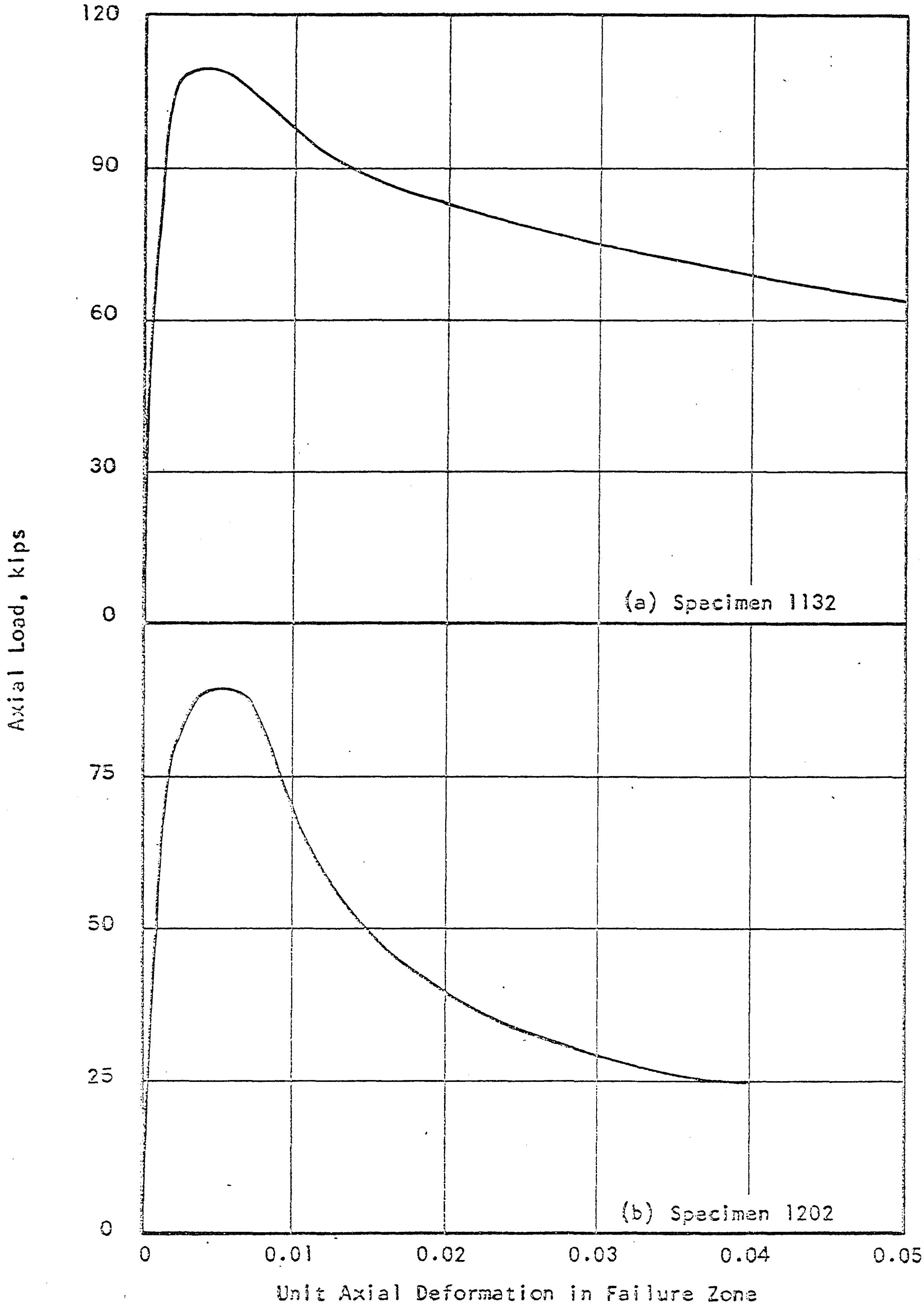

FIG. A.36 RELATIONSHIPS OF LOAD VS. STRAIN IN FAILURE ZONE FOR SPECIMENS 1132 AND 1202

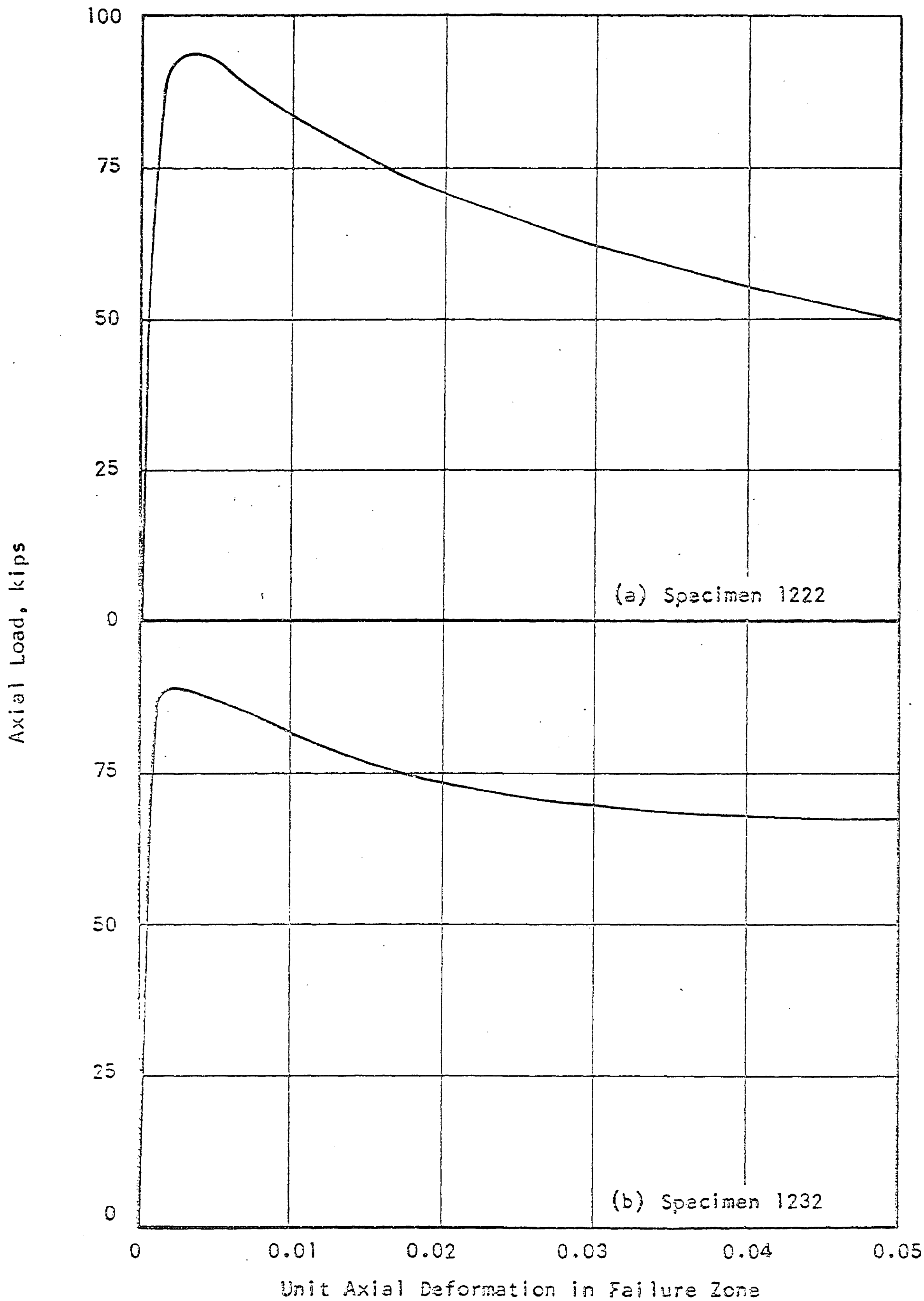

FIG. A.37 RELATIONSHIPS OF LOAD VS. STRAIN IN FAILURE ZONE FOR SPECIMENS 1222 AND 1232

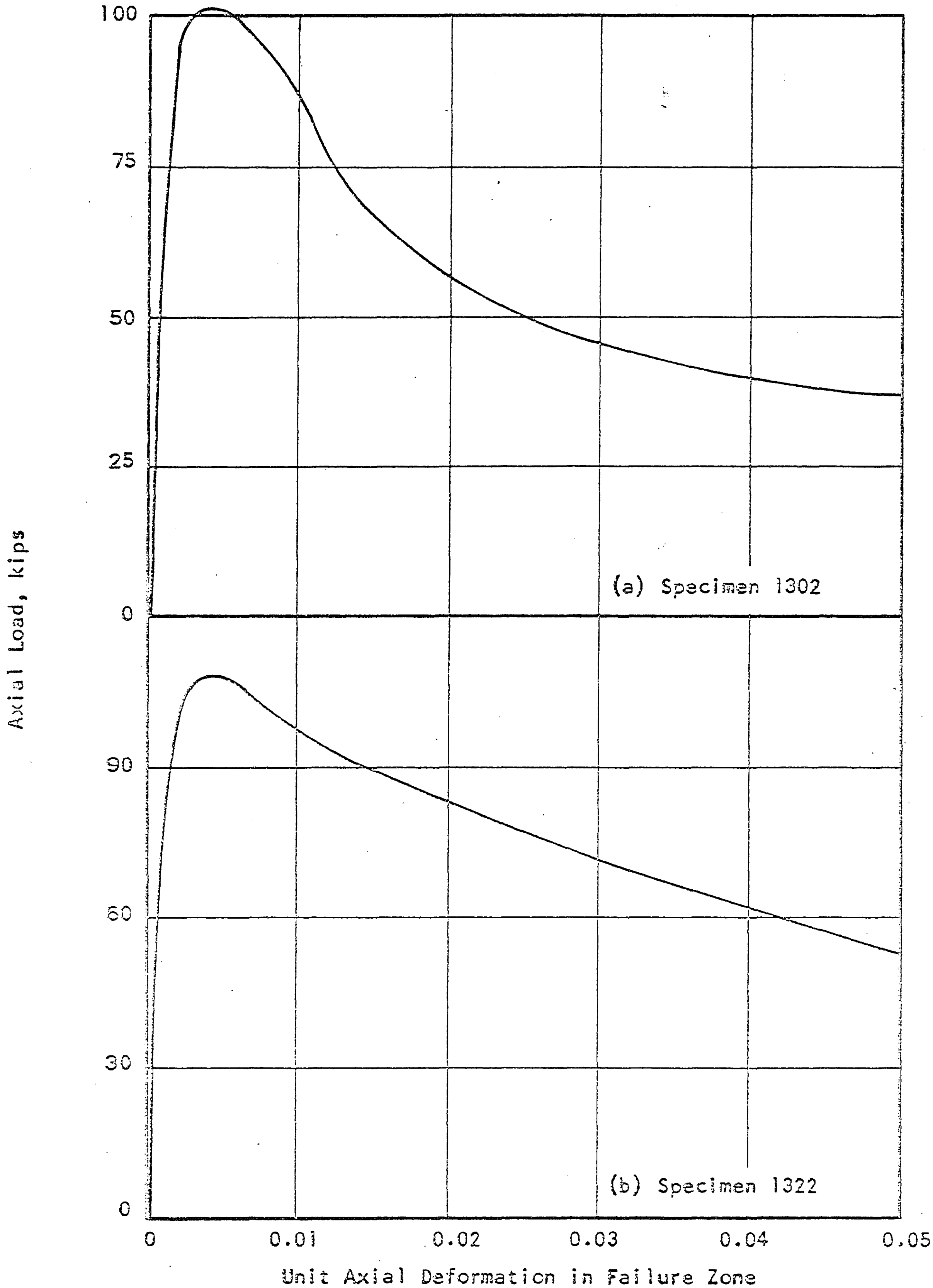

FIG. A.38 RELATIONSHIPS OF LOAD VS. STRAIN IN FAILURE ZONE FOR SPECIMENS 1302 AND 1322

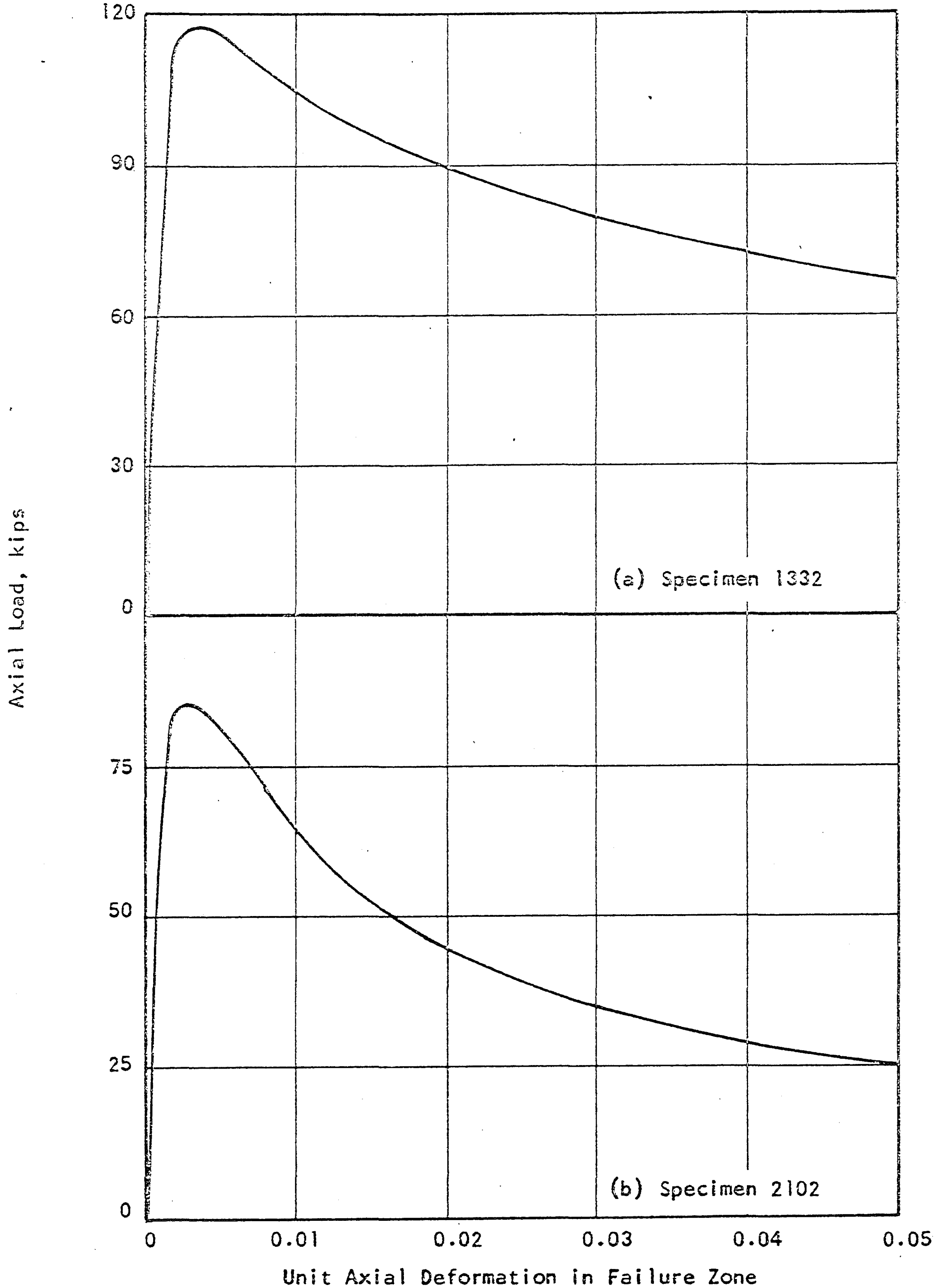

FIG. A.39 RELATIONSHIPS OF LOAD VS. STRAIN IN FAILURE ZONE FOR SPECIMENS 1332 AND 2102

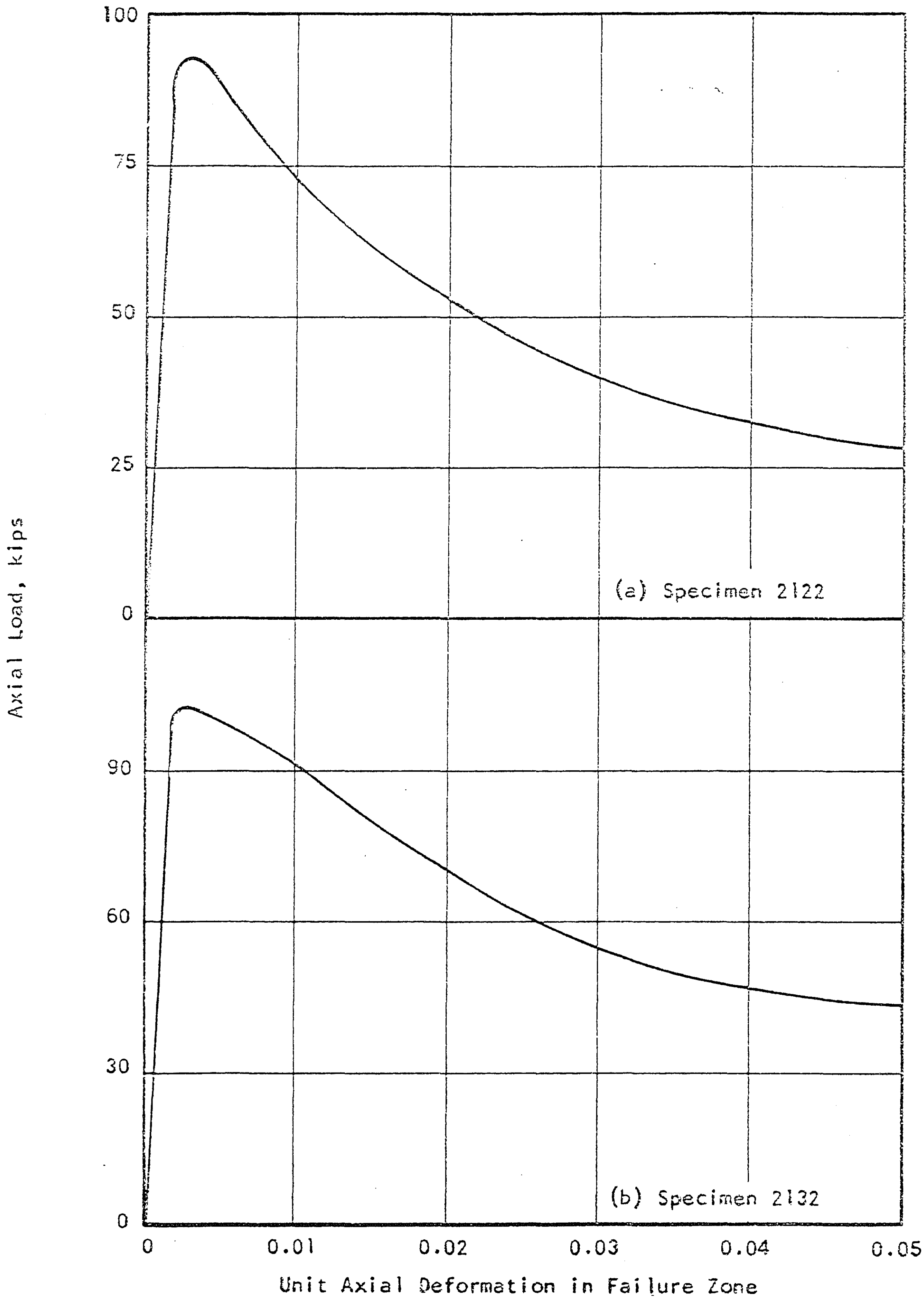

FIG. A.40 RELATIONSHIPS OF LOAD VS. STRAIN IN FAILURE ZONE FOR SPECIMENS 2122 AND 2132

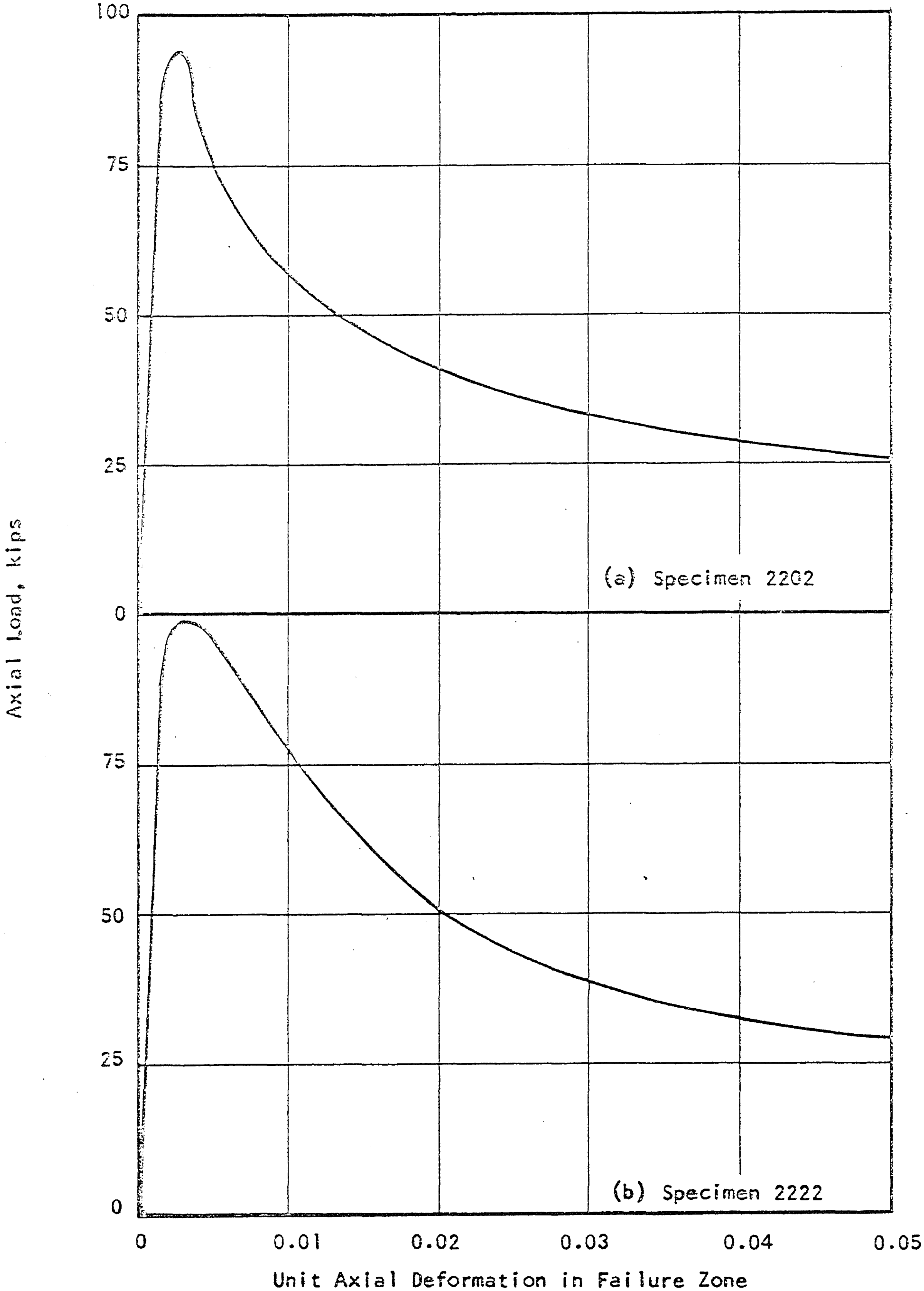

FIG. A.41 RELATIONSHIPS OF LOAD VS. STRAIN IN FAILURE ZONE FOR SPECIMENS 2202 AND 2222

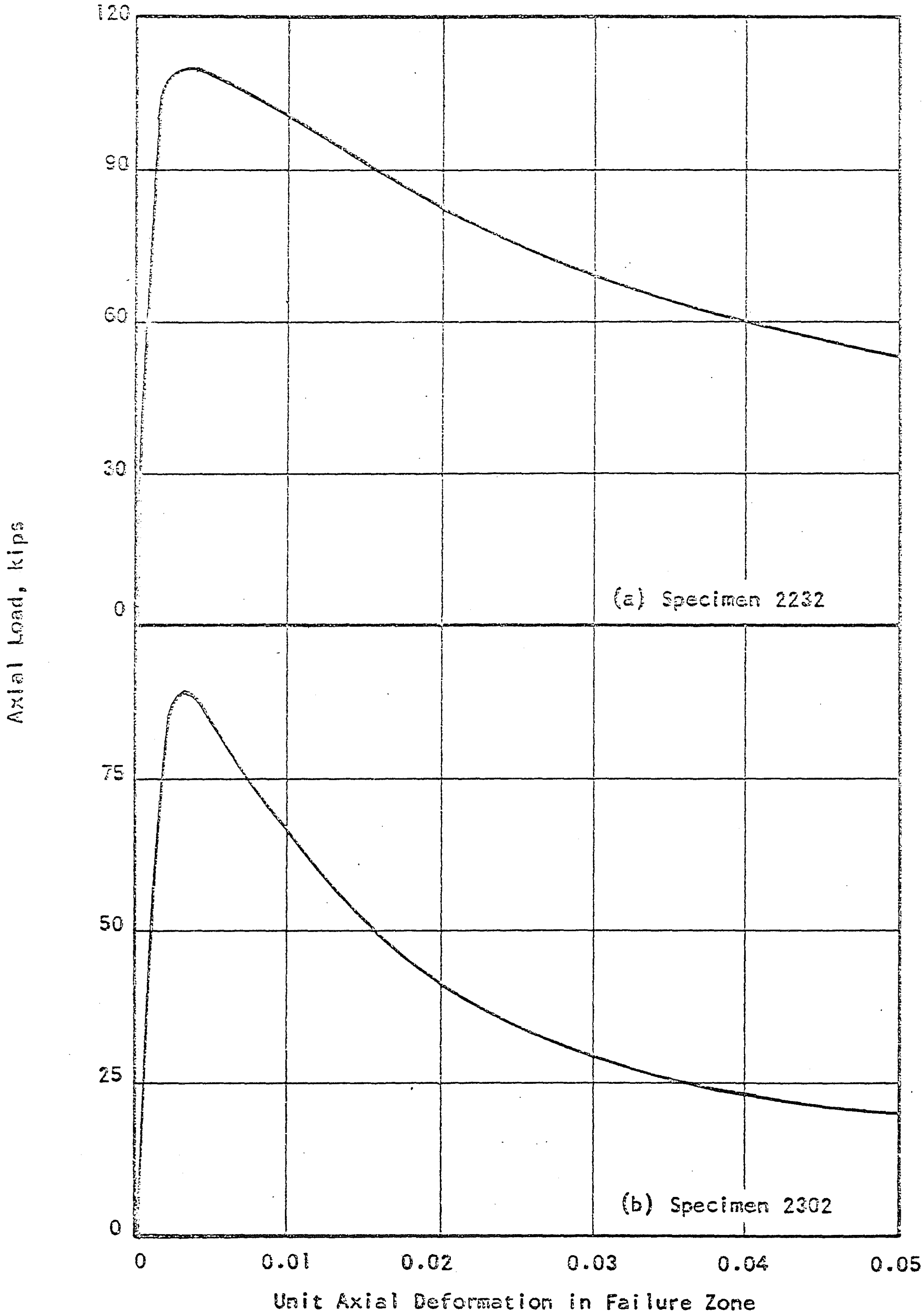

FIG. A.42 RELATIONSHIPS OF LOAD VS. STRAIN IN FAILURE ZONE FOR SPECIMENS 2232 AND 2302

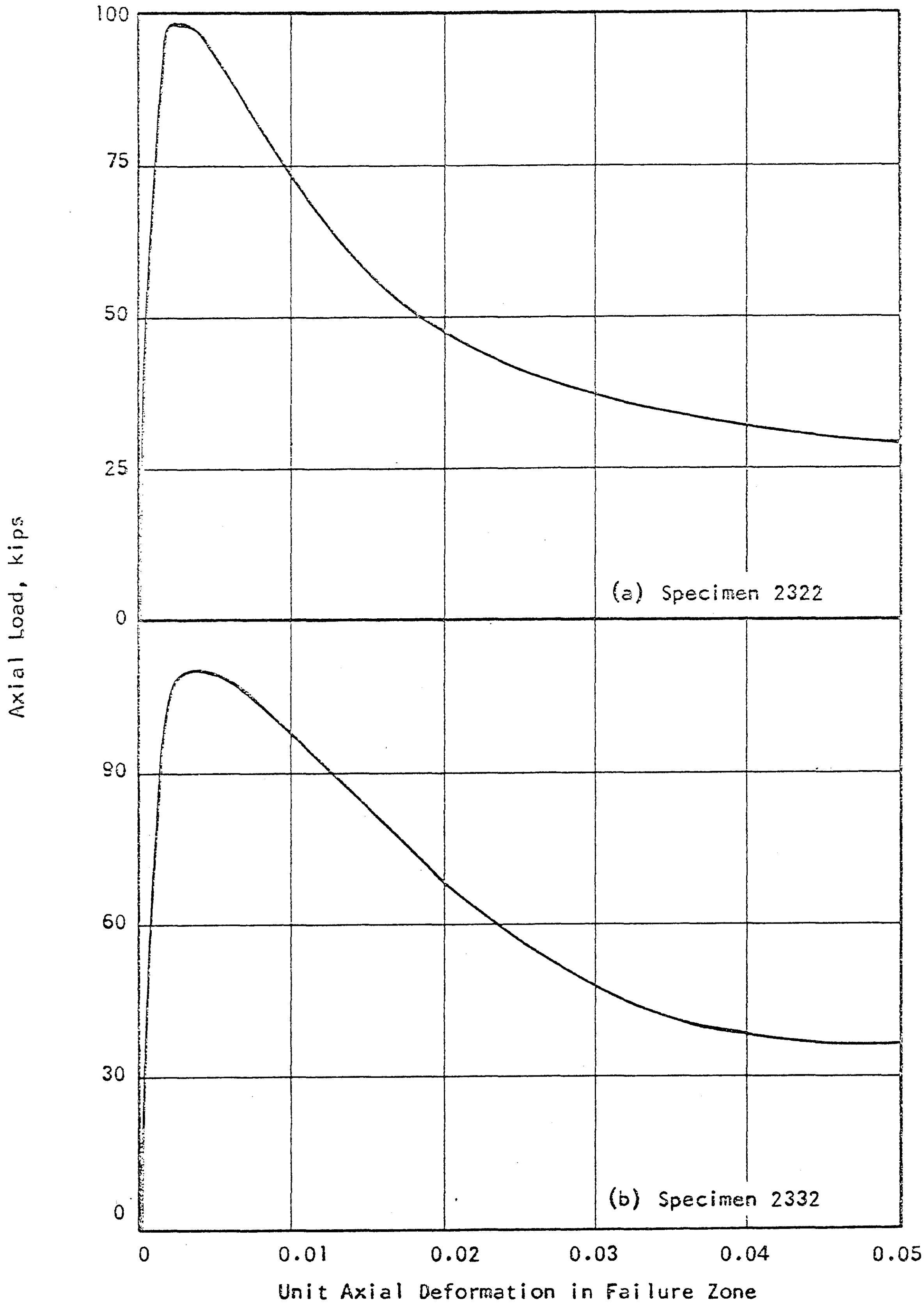

FIG. A.43 RELATIONSHIPS OF LOAD VS. STRAIN IN FAILURE ZONE FOR SPECIMENS 2322 AND 2332

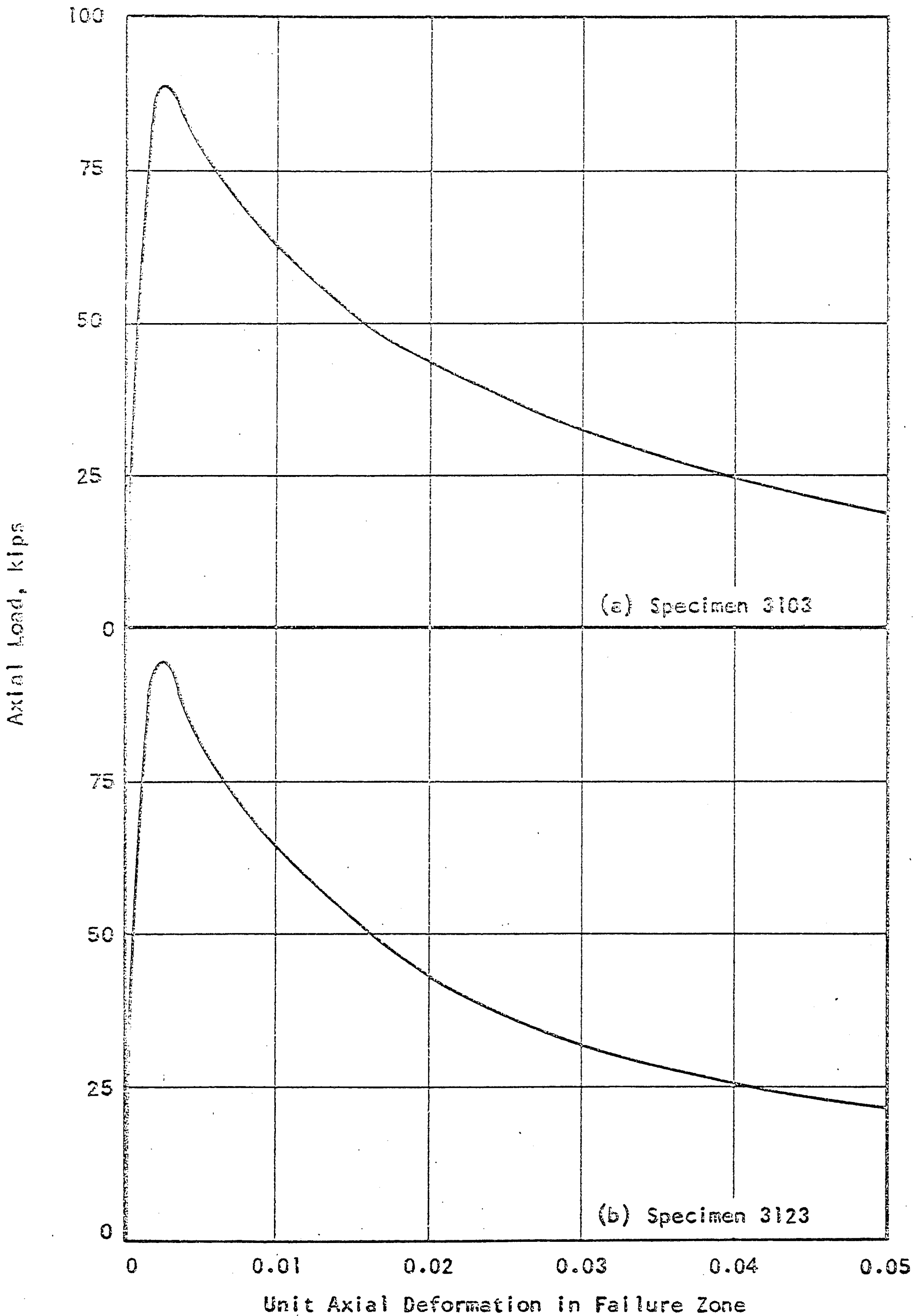

FIG. A.44 RELATIONSHIPS OF LOAD VS. STRAIN IN FAILURE ZONE FOR SPECIMENS 3103 AND 3123

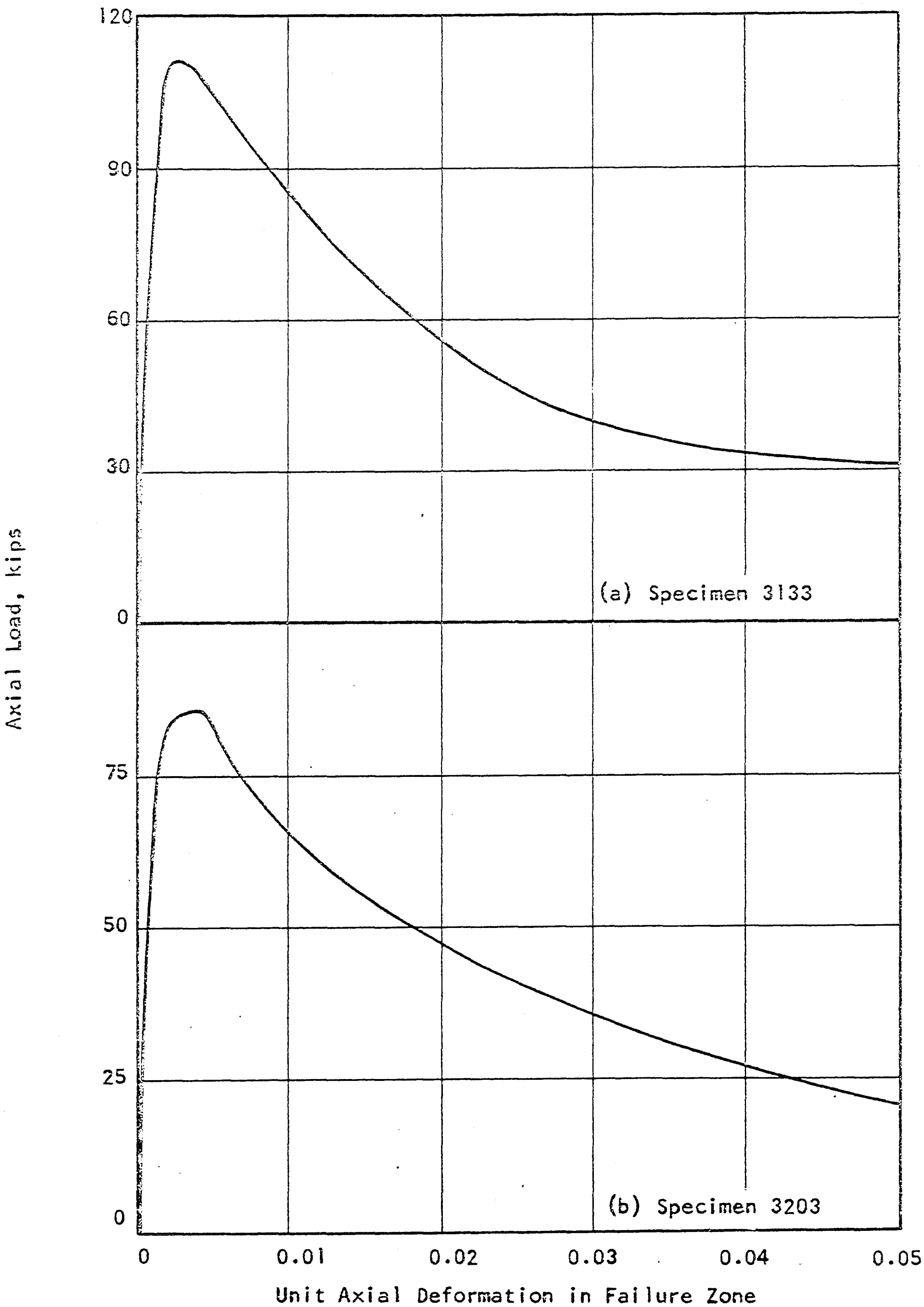

FIG. A.45 RELATIONSHIPS OF LOAD VS. STRAIN IN FAILURE ZONE FOR SPECIMENS 3133 AND 3203

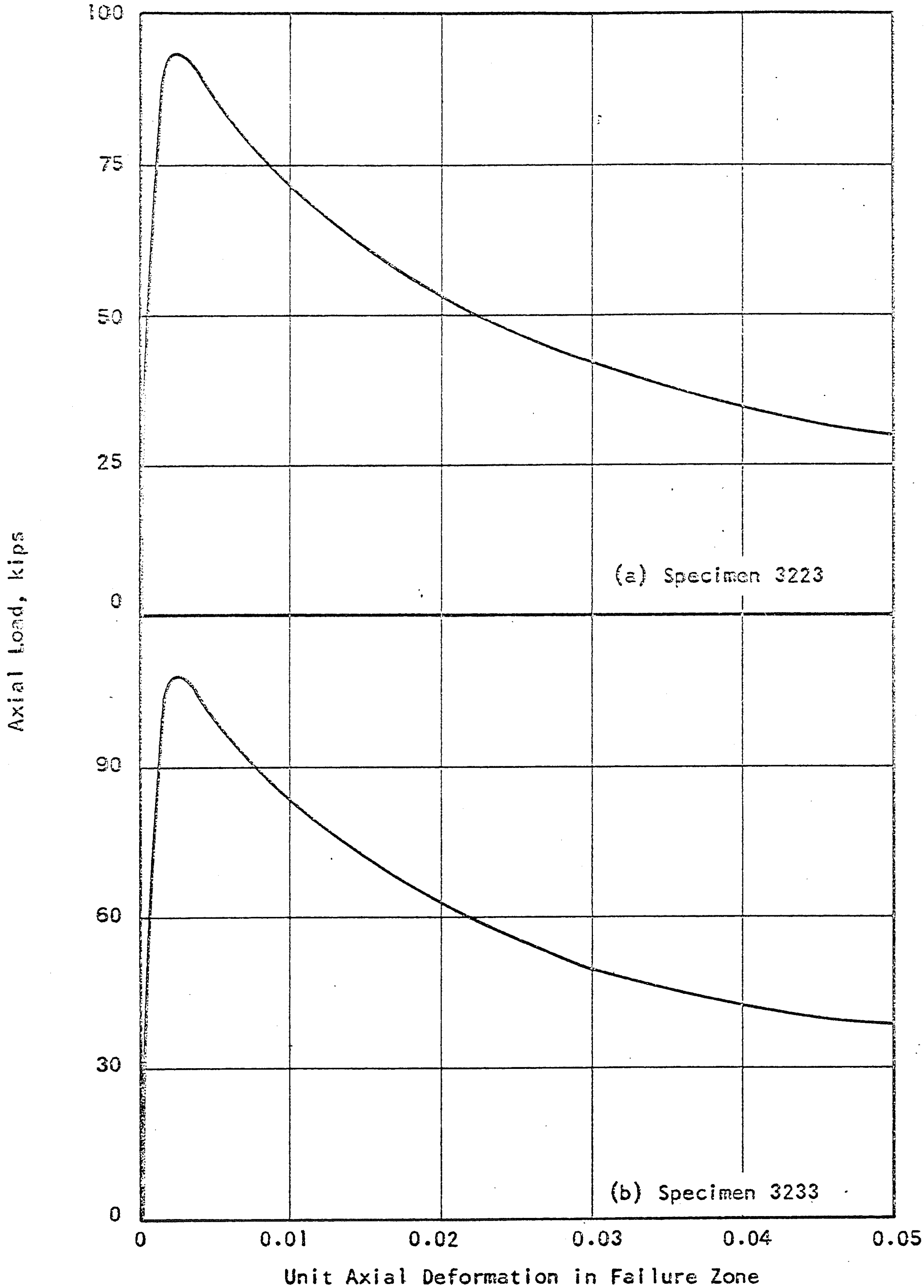

FIG. A.46 RELATIONSHIPS OF LOAD VS. STRAIN IN FAILURE ZONE FOR SPECIMENS 3223 AND 3233

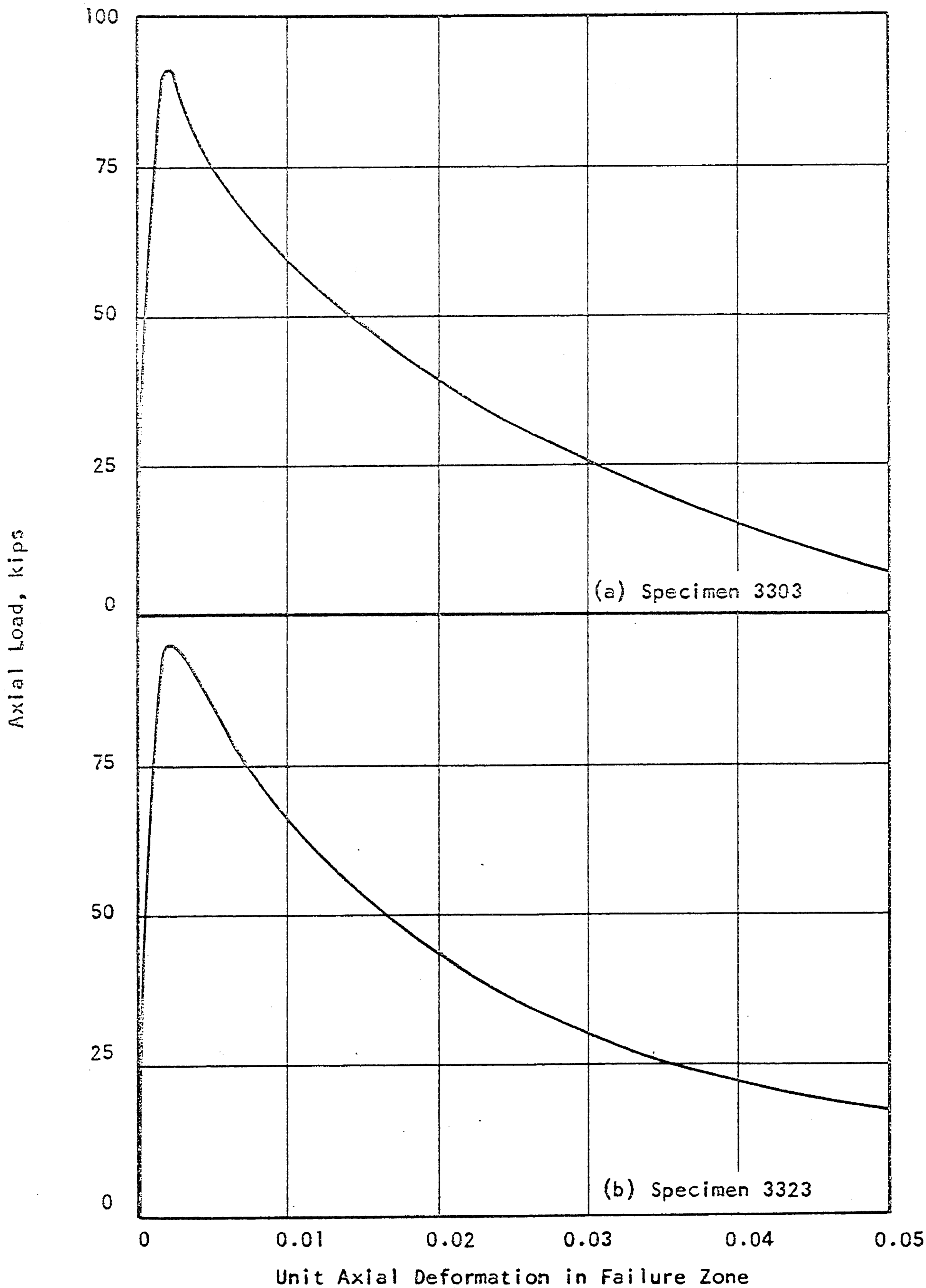

FIG. A.47 RELATIONSHIPS OF LOAD VS. STRAIN IN FAILURE ZONE FOR SPECIMENS 3303 AND 3323

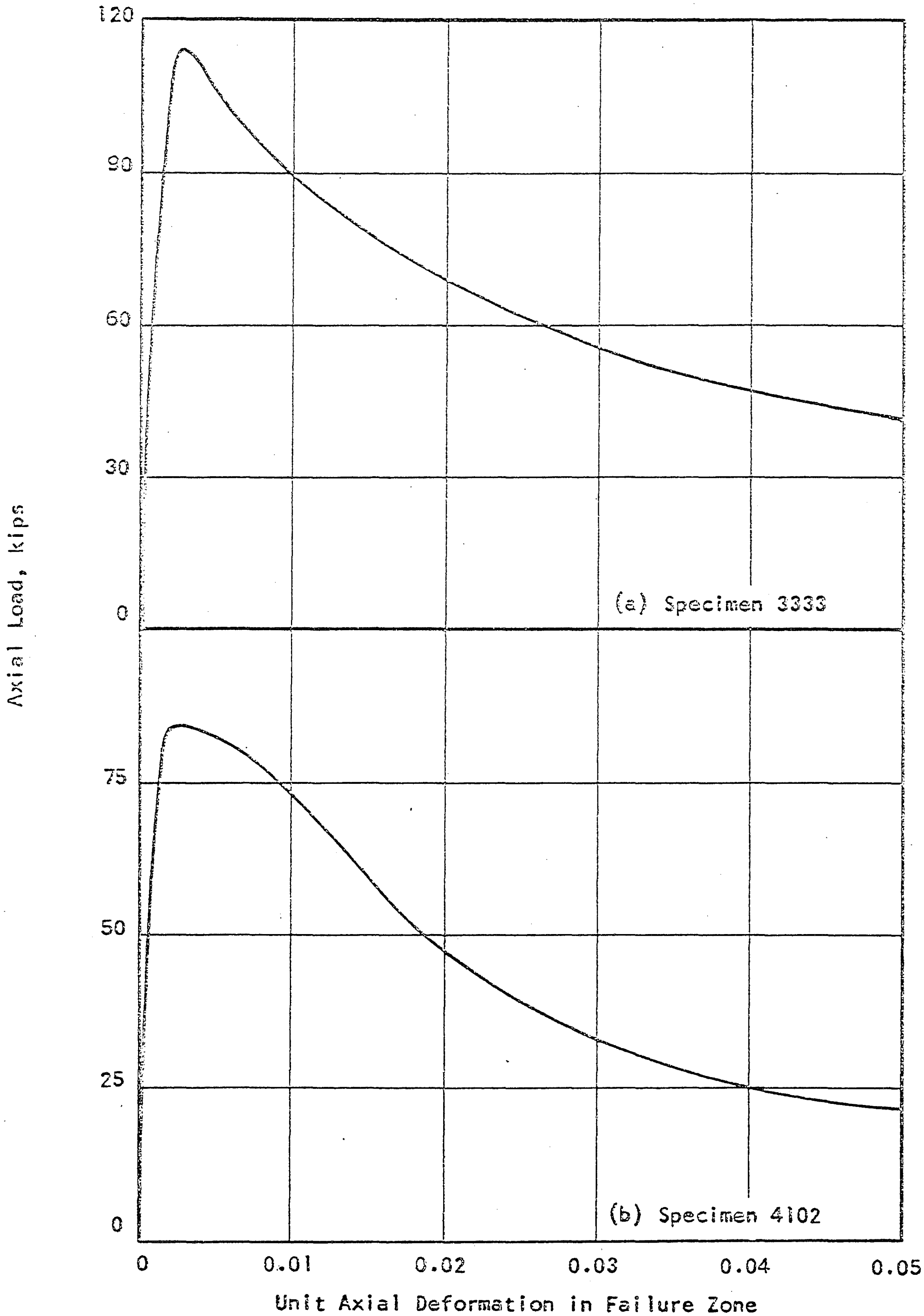

FIG. A.48 RELATIONSHIPS OF LOAD VS. STRAIN IN FAILURE ZONE FOR SPECIMENS 3333 AND 4102

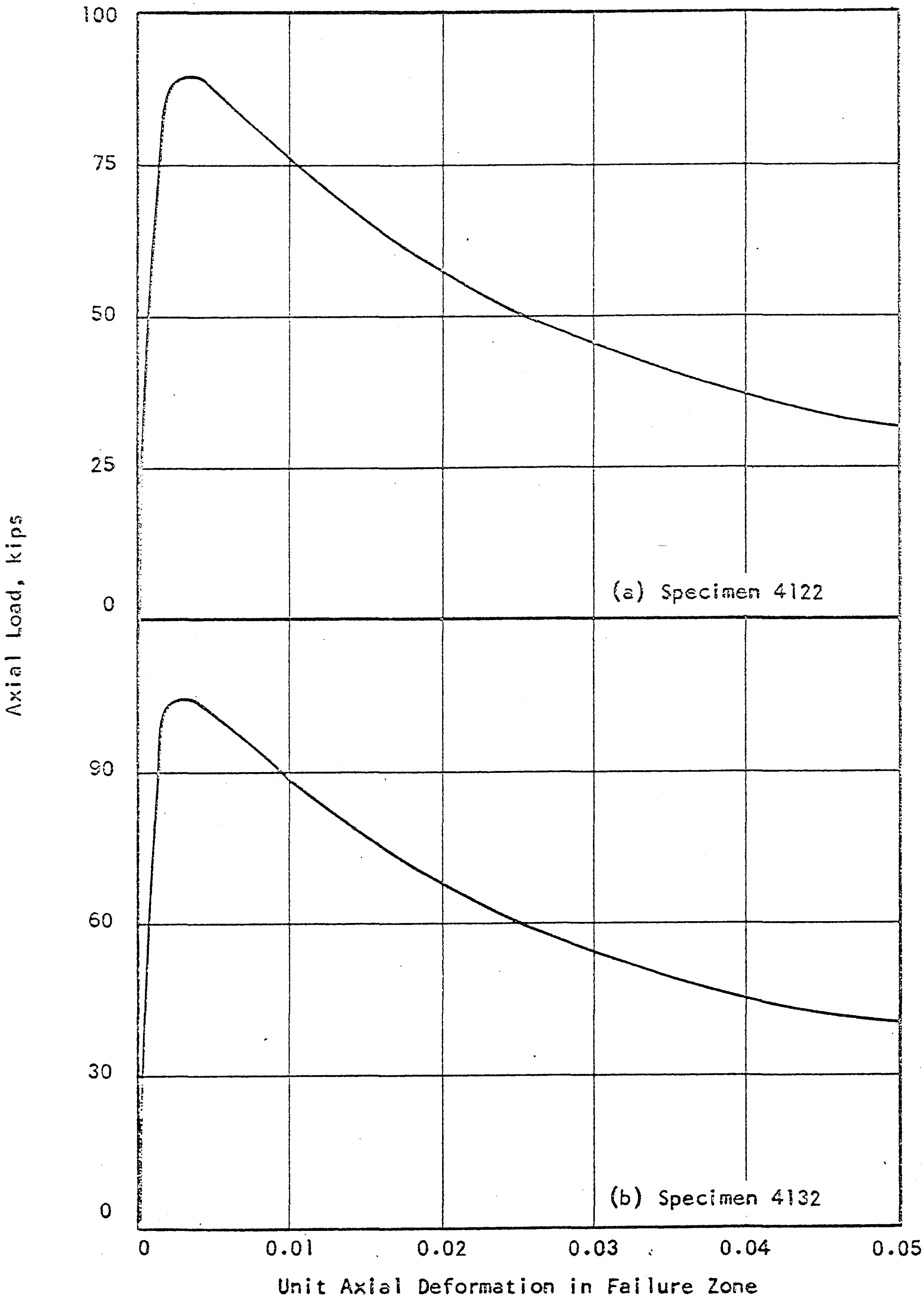

FIG. A.49 RELATIONSHIPS OF LOAD VS. STRAIN IN FAILURE ZONE FOR SPECIMENS 4122 AND 4132

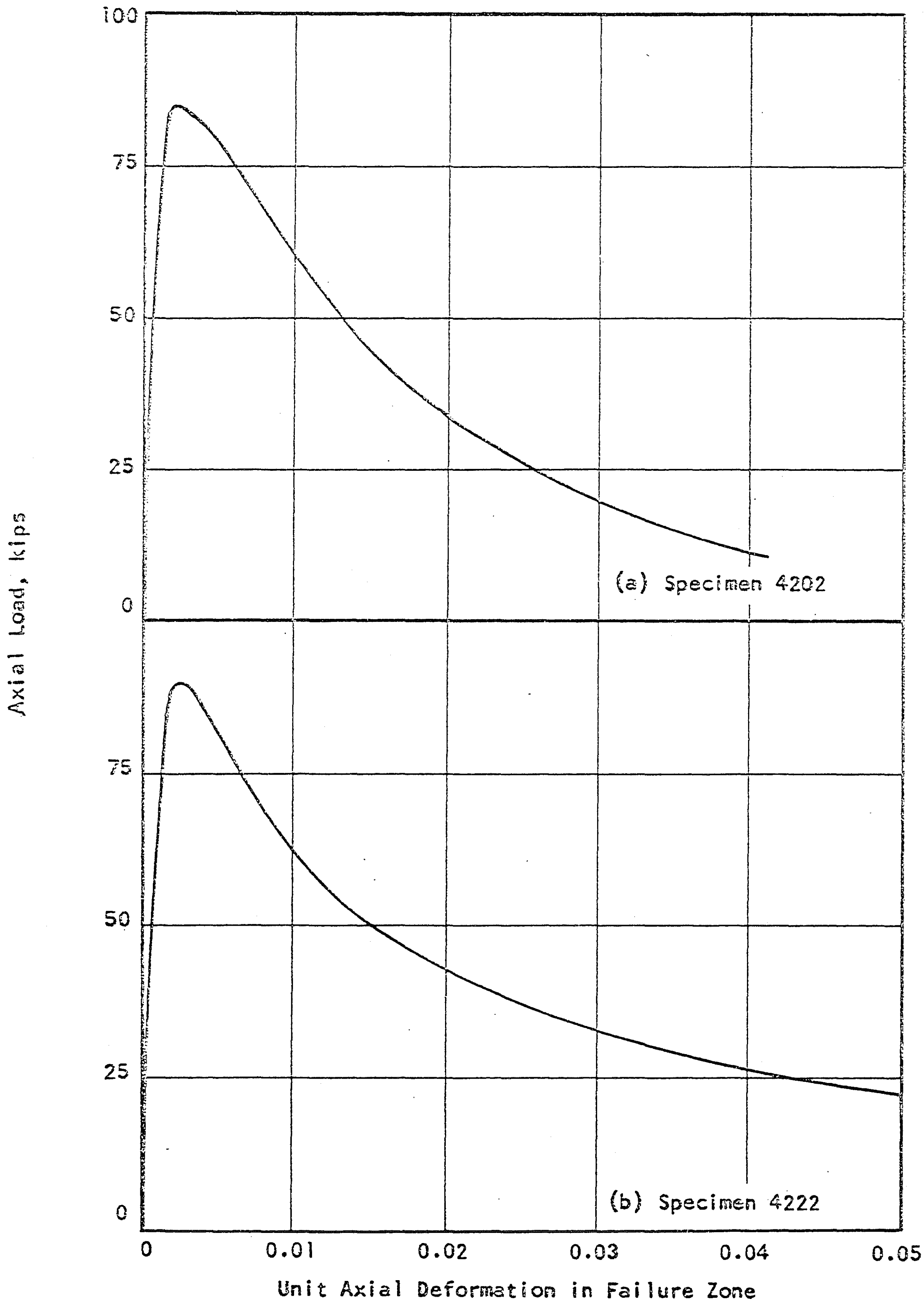

FIG. A.50 RELATIONSHIPS OF LOAD VS. STRAIN IN FAILURE ZONE FOR SPECIMENS 4202 AND 4222

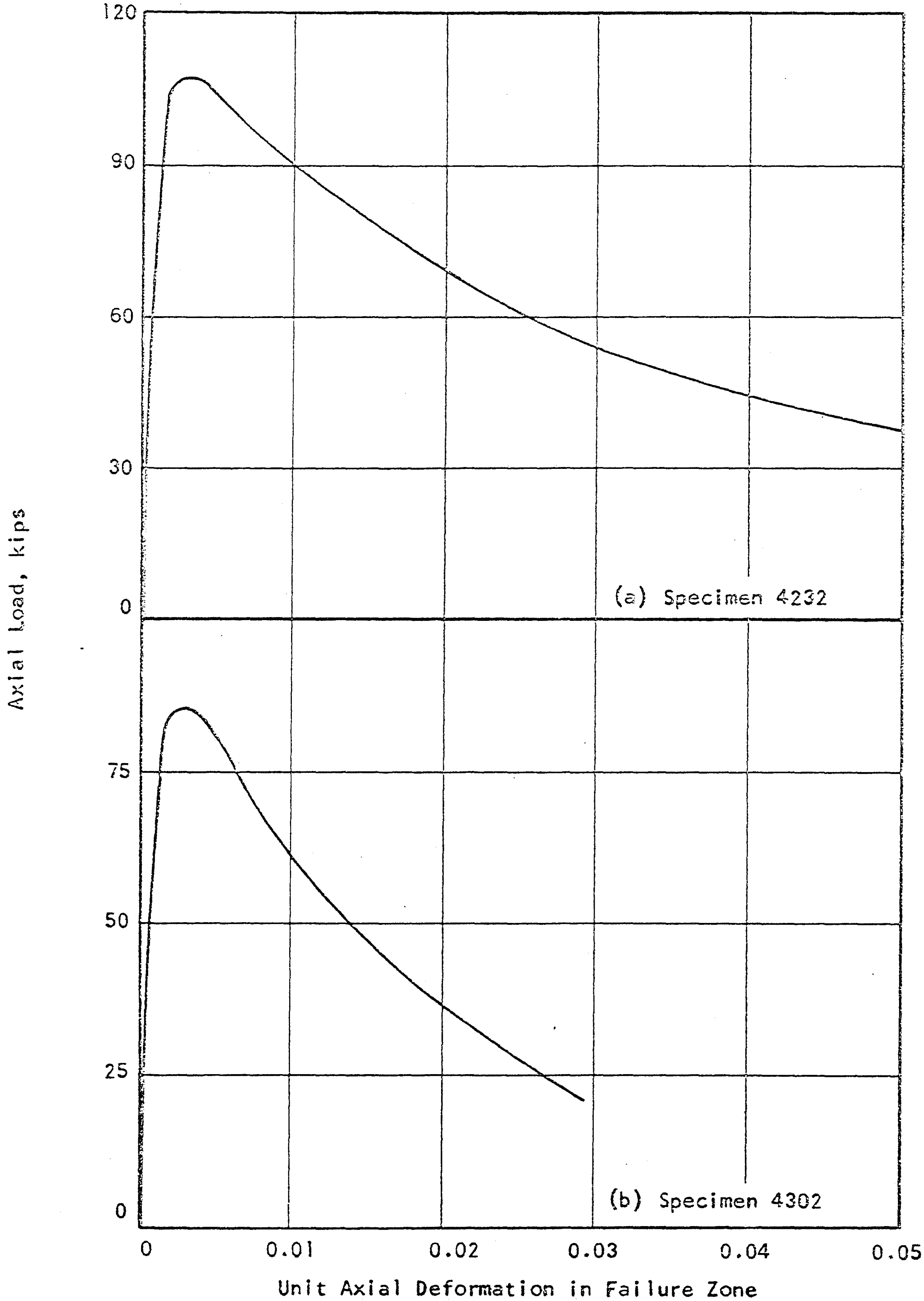

FIG. A.51 RELATIONSHIPS OF LOAD VS. STRAIN IN FAILURE ZONE FOR SPECIMENS 4232 AND 4302

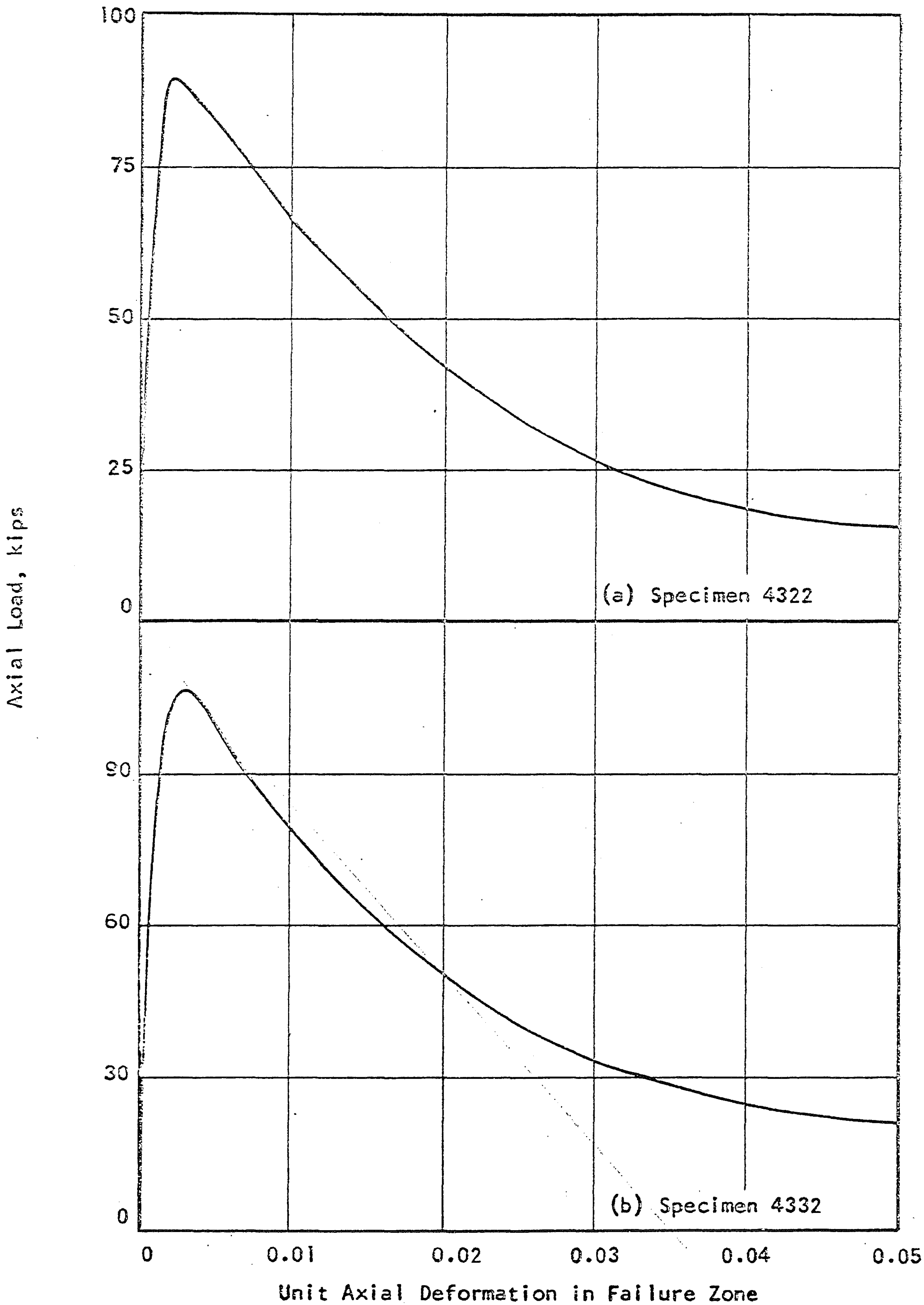

FIG. A.52 RELATIONSHIPS OF LOAD VS. STRAIN IN FAILURE ZONE FOR SPECIMENS 4322 AND 4332

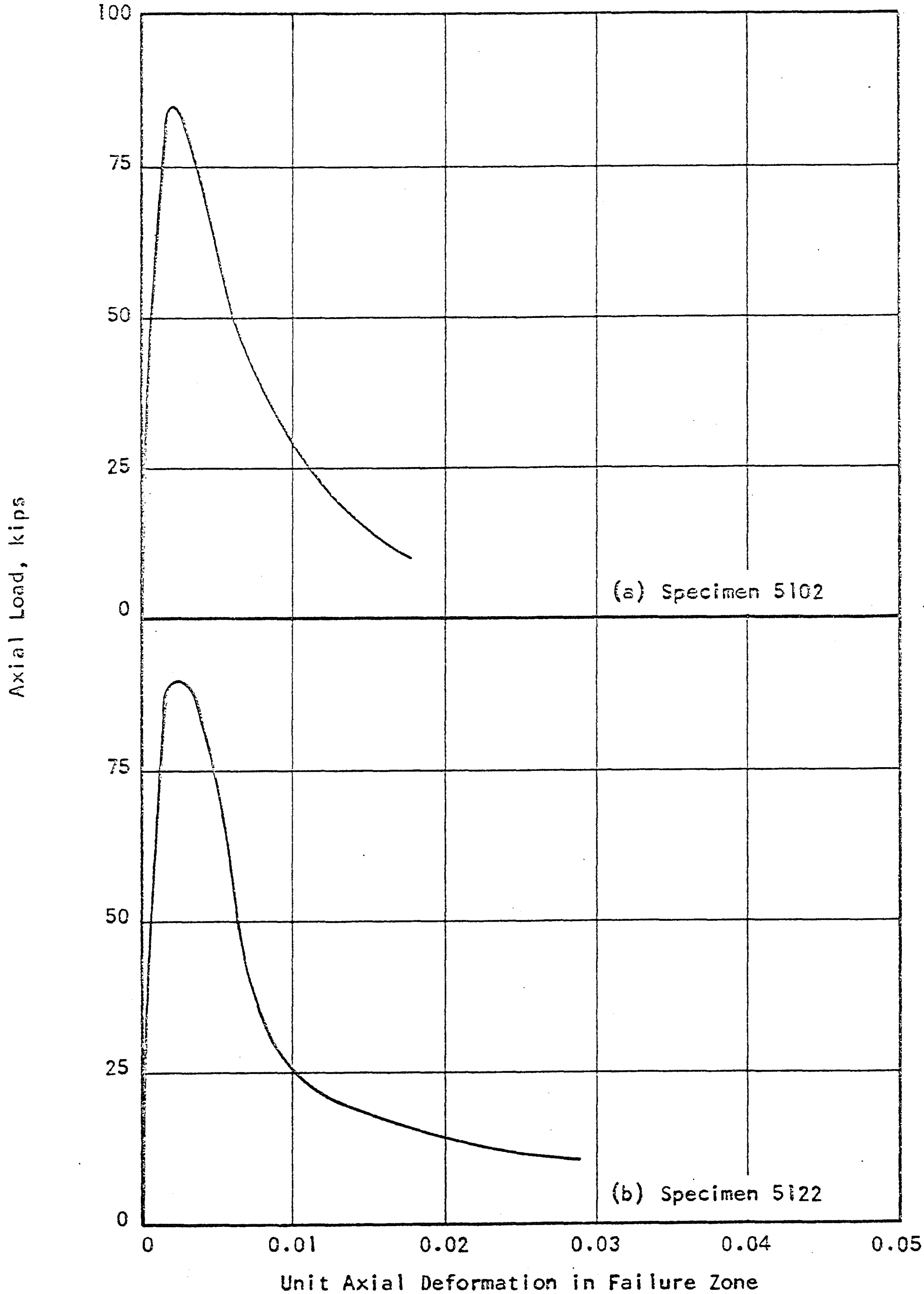

FIG. A.53 RELATIONSHIPS OF LOAD VS. STRAIN IN FAILURE ZONE FOR SPECIMENS 5102 AND 5122

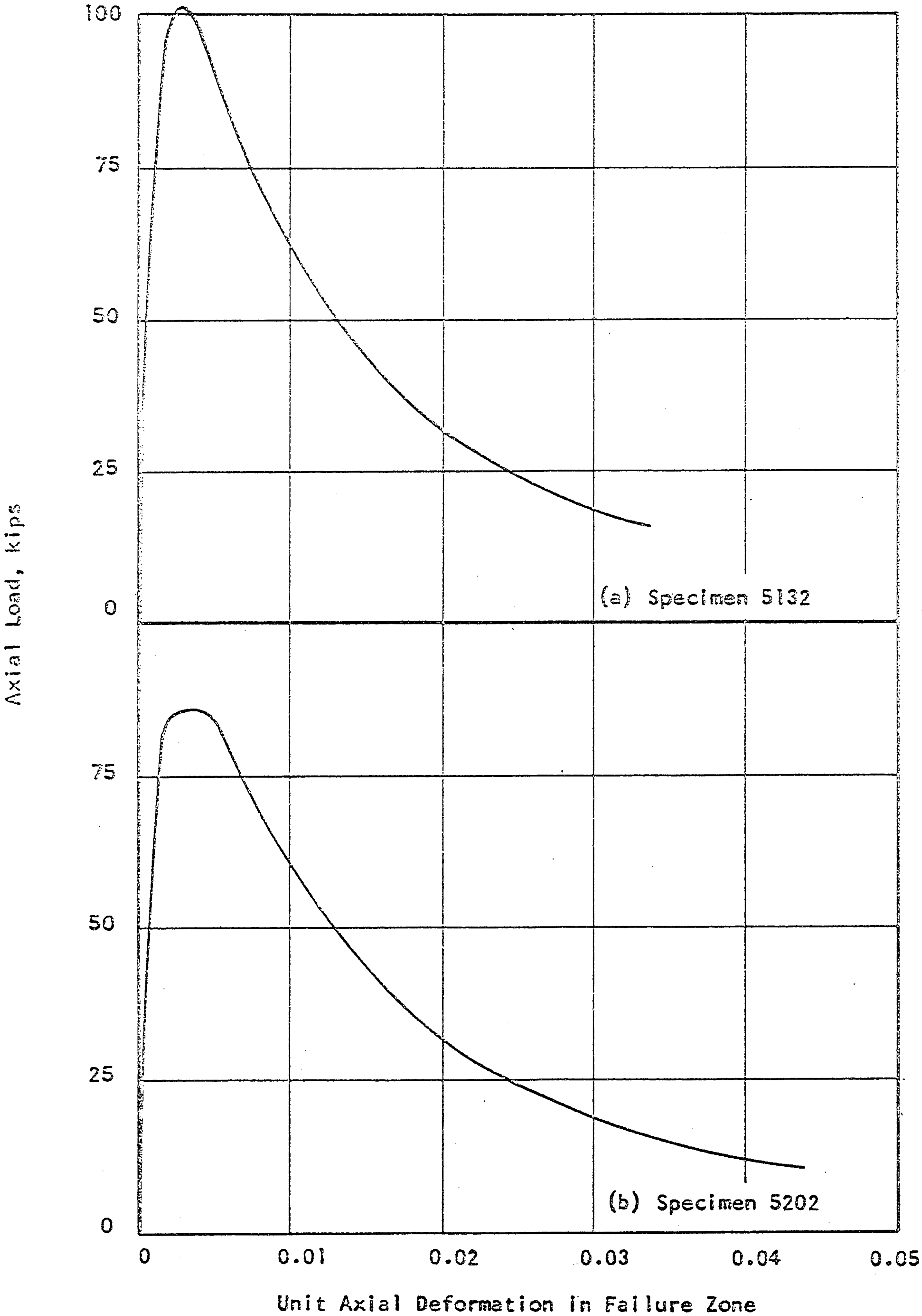

FIG. A.54 RELATIONSHIPS OF LOAD VS. STRAIN IN FAILURE ZONE FOR SPECIMENS 5132 AND 5202

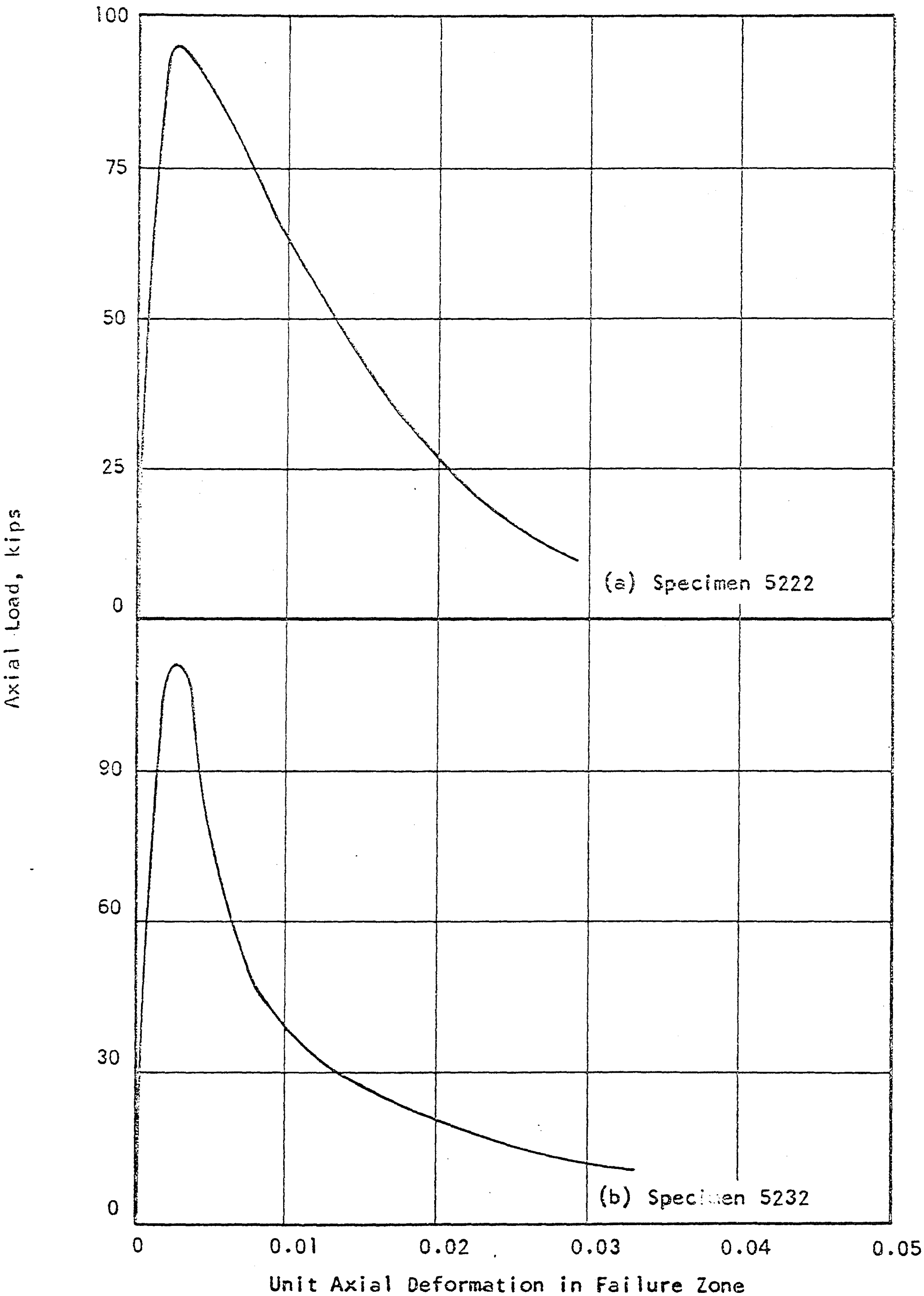

FIG. A.55 RELATIONSHIPS OF LOAD VS. STRAIN IN FAILURE ZONE FOR SPECIMENS 5222 AND 5232

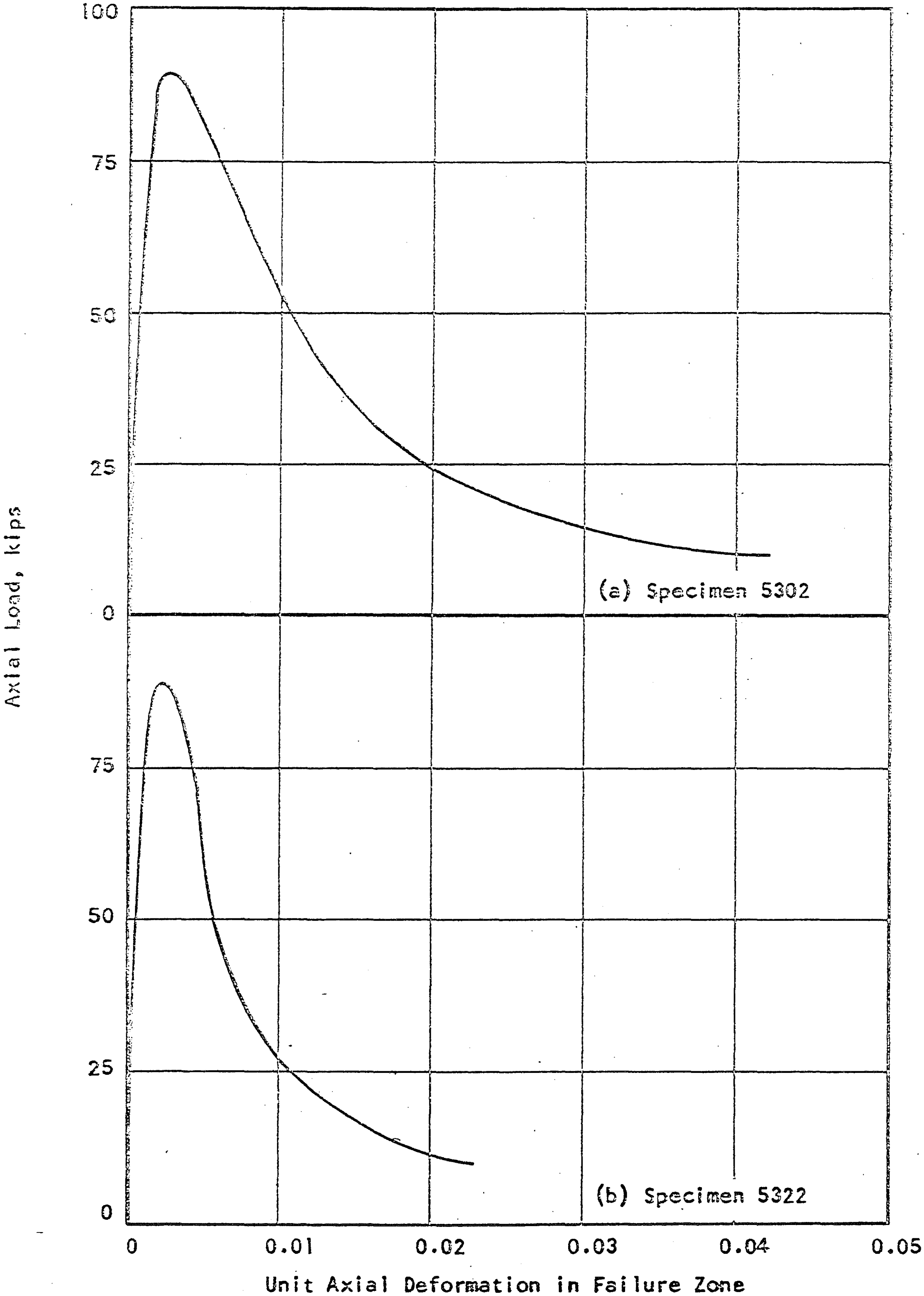

FIG. A.56 RELATIONSHIPS OF LOAD VS. STRAIN IN FAILURE ZONE FOR SPECIMENS 5302 AND 5322

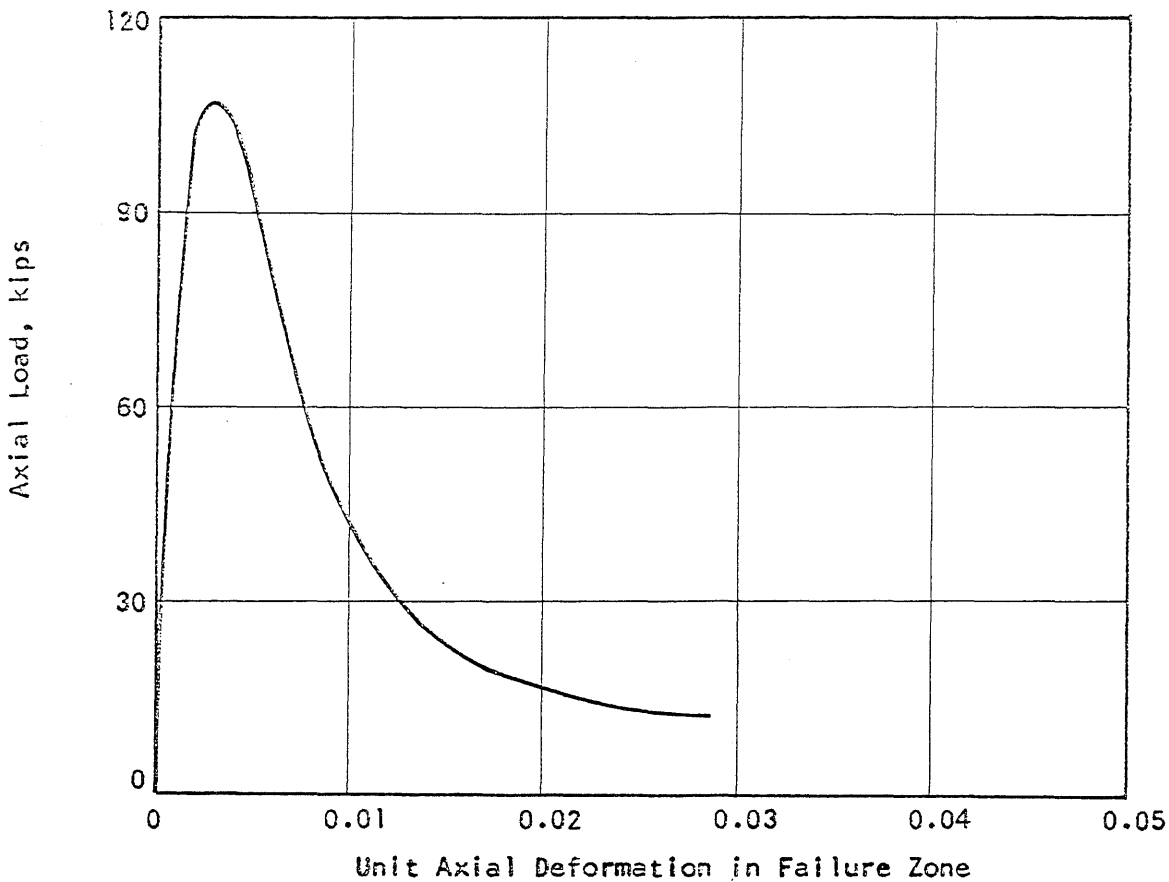

FIG. A.57 RELATIONSHIP OF LOAD VS. STRAIN IN FAILURE ZONE FOR SPECIMEN 5332

FIG. A.59 SPECIMENS OF SERIES 1 AFTER TESTING

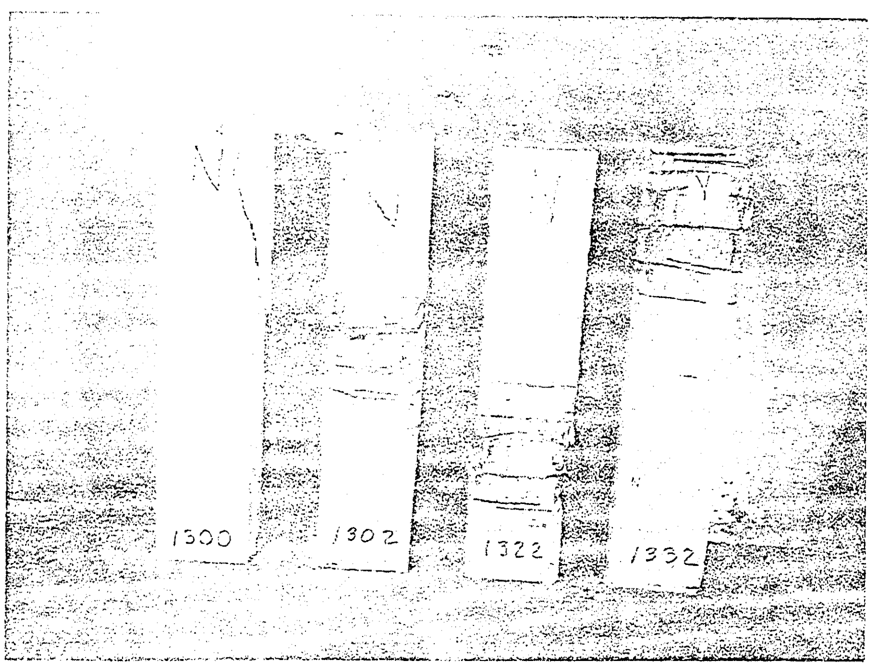

FIG. A.58 PHOTOGRAPH SHOWING INSTRUMENTATION

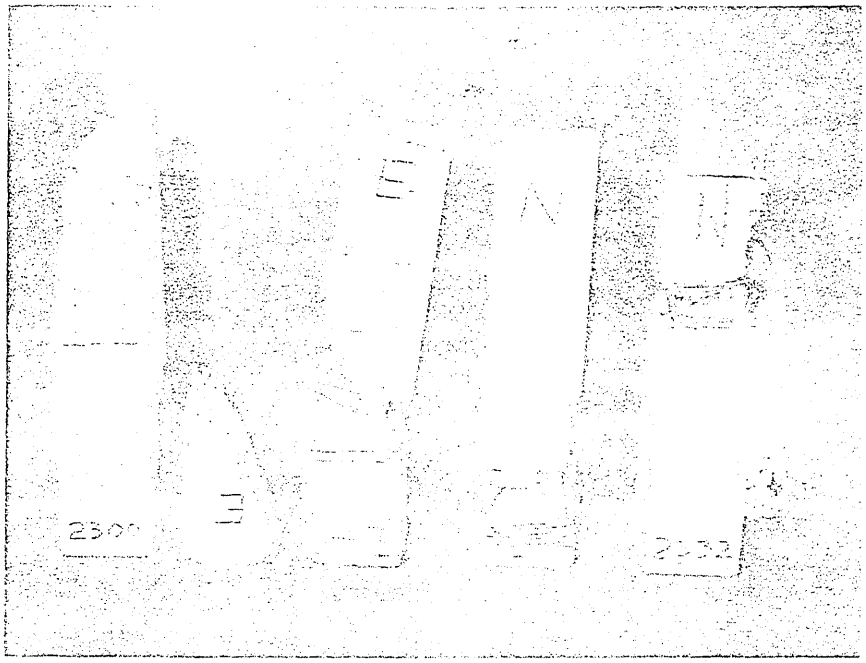

(a) Series 2

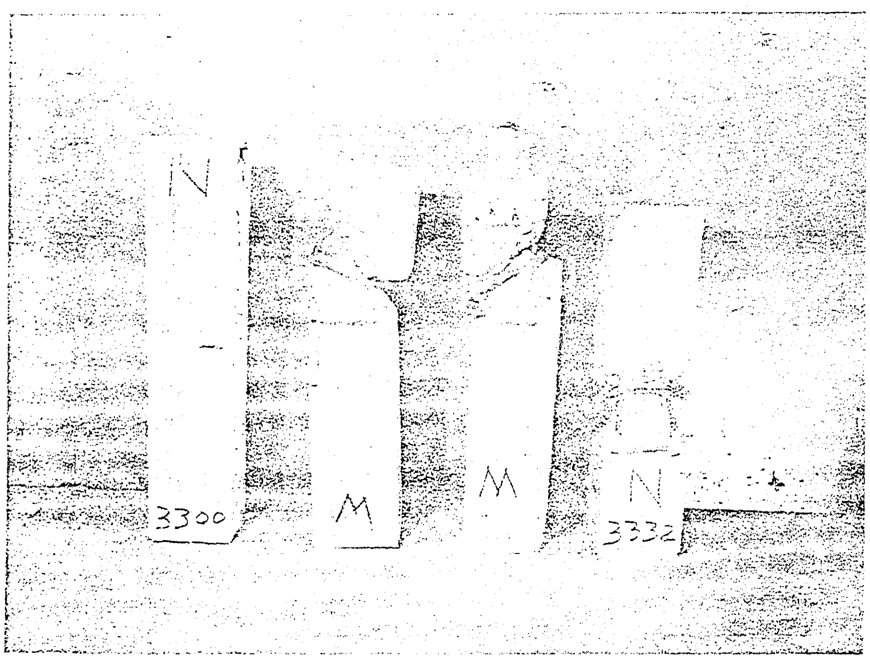

(b) Series 3

FIG. A.60 SPECIMENS OF SERIES 2 AND 3 AFTER TESTING

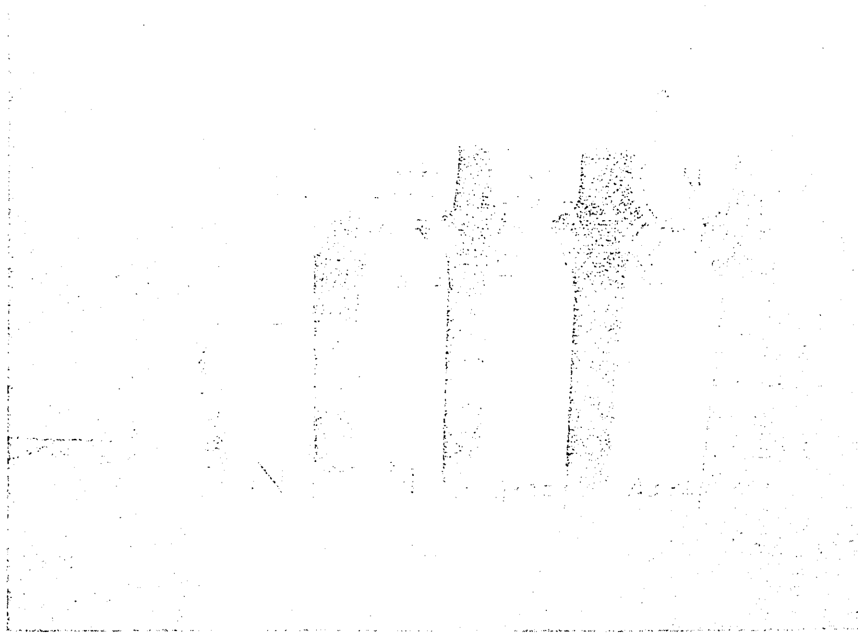

(a) Series 4

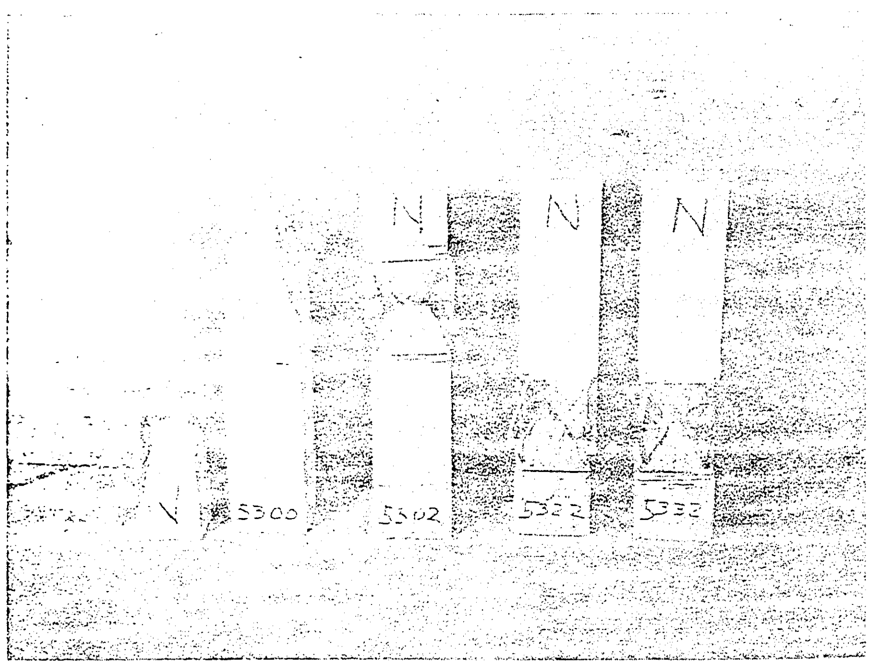

(b) Series 5

FIG. A.61 SPECIMENS OF SERIES 4 AND 5 AFTER TESTING

APPENDIX B

DERIVATIONS

B.1 Models

(a) Tetrahedron

Referring to Fig. 3.1, it can be shown that the angle of inclination of struts AB, AC, and AD with respect to plane BCD is 54.5°. The assumed notation is as follows:

Force in struts AB, AC, and AD	$= P_c$
Force in struts BC, BD, and CD	$= P_T$
Length of struts	$= L$
Area of struts	$= A$
Modulus of elasticity of struts	$= E$

The direction of P indicated in Fig. 3.1 is assumed to be vertical Because of symmetry, the vertical component of P_c must equal P/3 Accordingly,

$$P_c = \frac{P}{3} \csc (54.5^{\circ}) = 0.408 \; P \qquad (B.1)$$

The horizontal component of P_c is equal to $P_c \cos (54.5^{\circ})$. To maintain static equilibrium,

$$2P_T \cos (30^{\circ}) = P_c \cos (54.5^{\circ}) \qquad (B.2a)$$

$$P_T = 0.136 \; P \qquad (B.2b)$$

The axial deformation of struts AB, AC, and AD is given by the equation

$$\Delta_c = \frac{P_c \; L}{AE} = 0.408 \; \frac{PL}{AE} \qquad (B.3)$$

Since point A must move vertically under the action of force P, the vertical component of Δ_c, Δ_v, can be expressed as

$$\Delta_v = \Delta_c \csc (54.5^\circ) = 0.502 \frac{PL}{AE} \tag{B.4}$$

The vertical distance from point A to plane BCD is equal to L sin (54.5°), so that the vertical strain, ϵ_z, is

$$\epsilon_z = \frac{\Delta_v}{L \sin (54.5^\circ)} = 0.618 \frac{P}{AE} \tag{B.5}$$

The horizontal strain, ϵ_x, is

$$\epsilon_x = \frac{P_T}{AE} = 0.136 \frac{P}{AE} \tag{B.6}$$

The value of Poisson's ratio, ν, for the tetrahedron, from Eqs. B.5 and B.6, is

$$\nu = \frac{\epsilon_x}{\epsilon_z} = \frac{0.136}{0.618} = 0.22 \tag{B.7}$$

(b) Body-Centered Cubic Model

The assumed notation for the body-centered cubic model is shown in Fig. 3.2. The length of the diagonal struts, such as AM, is L_4, and the cross-sectional area of each strut is A_4. The area of each cube face is assumed to be unity, and the following equations are derived for the condition of unconfined compression in the z-direction, produced by the action of a single force P_z applied to the exterior of the cube.

The length and area relations for the model may be summarized as follows:

$$L_1 = L_2 = L_3$$

$$L_4 = \frac{\sqrt{3}}{2} L_1 \tag{B.8}$$

$$A_1 = A_2 = A_3$$

The forces in struts 1, 2, 3, and 4 are assumed to be P_1, P_2, P_3 and P_4, respectively.

From symmetry in the horizontal direction

$$P_1 = P_2 \tag{B.9}$$

From equilibrium of forces in the horizontal direction,

$$P_1 = -\frac{2}{\sqrt{3}} P_4 \tag{B.10}$$

In order to determine the compatibility equations for the model, it is assumed that the axial deformations of struts 1, 2, 3, and 4 are Δ_1, Δ_2, Δ_3, and Δ_4 respectively. In addition, it is assumed that strut 4 undergoes a rotation $d\varphi$ in a direction parallel to the z-axis. A positive value of $d\varphi$ is assumed to cause positive values of Δ_1 and Δ_2 and a negative value of Δ_3

The relationship among Δ_1, Δ_4, and $d\varphi$ is given by the equation

$$\Delta_1 = 2\left[\frac{1}{\sqrt{3}} \Delta_4 + \frac{1}{2\sqrt{2}} d\varphi\right] \tag{B.11}$$

and the relationship among Δ_3, Δ_4 and $d\varphi$ may be expressed

$$\Delta_3 = 2\left[\frac{1}{\sqrt{3}}\Delta_4 - \frac{1}{\sqrt{2}}d\varphi\right] \tag{B.12}$$

By combining Eqs. B.11 and B.12

$$\Delta_1 + \frac{1}{2}\Delta_3 = \sqrt{3}\,\Delta_4 \tag{B.13}$$

By means of Eq. 3.6, Eq. B.13 may be rewritten as follows

$$\frac{P_1L_1}{A_1} + \frac{P_3L_3}{2\,A_3} = \frac{\sqrt{3}\,P_4L_4}{A_4} \tag{B.14}$$

Substituting Eqs. B.8 and B.10 into Eq. B.14, the following equation is obtained,

$$P_3 = \frac{3A_3 + 4A_4/\sqrt{3}}{A_4}\,P_4 \tag{B.15}$$

The equation for Poisson's ratio, ν, is

$$\nu = \frac{-\epsilon_x}{\epsilon_z} = \frac{-P_1/A_1}{P_3/A_3} = \frac{-P_1}{P_3} \tag{B.16}$$

By substituting Eqs. B.10 and B.15 into Eq. B.16, ν may be expressed in terms of A_3 and A_4

$$\nu = \frac{2A_4}{3\sqrt{3}A_3 + 4A_4} \tag{B.17}$$

For a value of ν equal to 0.15, Eq. B.17 yields the result

$$A_4 = 0.555\ A_1 \tag{B.18}$$

If it is assumed that the spheres shown in Fig. 3.2 are of finite diameter, the ratio L_4/L_1 is then unknown. In deriving an expression for ν, Eqs. B.9, B.10 and B.13 are still valid, but the resulting equation relating P_3 and P_4 becomes

$$P_3 = \left[2\sqrt{3}\,\frac{A_1}{A_4}\,\frac{L_4}{L_1} + \frac{4}{\sqrt{3}}\right] P_4 \tag{B.19}$$

and the equation for ν is

$$\nu = \frac{1}{\dfrac{3A_1}{A_4}\,\dfrac{L_4}{L_1} + 2} \tag{B.20}$$

Substituting the value $\nu = 0.15$ into Eq. B.20, the relation among the lengths and areas of the struts is

$$\frac{A_1}{A_4}\,\frac{L_4}{L_1} = 1.56 \tag{B.21}$$

B.2 Unconfined Compression

A description of the method used to compute the load-strain relations for unconfined compression of the cubic model (Fig. 3.3) is given in Chapter 4. The corresponding calculations are summarized in Table B.1

The calculations shown in Table B.1 were carried out in the following order:

1. Assume a value of ϵ_x, the transverse strain (Column 1).
2. Determine the proportion of effective area, A_1/A, from Eq. 3.26 (Column 2).
3. Determine the value of P_1/AE corresponding to ϵ_x by multiplying columns 1 and 2 (Column 3).
4. Using Eq. 4.3, determine the value of P_4/AE for the diagonal strut in the vertical plane (Column 4).
5. Enter Fig. 3.8 with the quantity P_4/AE expressed as a percentage of the maximum load for the diagonal strut ($P_4 = 84.2\ AE \times 10^{-5}$) to obtain ϵ_4 (Column 5). For values of ϵ_x greater than that at which the largest value of P_4/AE is reached, determine ϵ_4 by dividing column 4 by column 6 (see step 6).
6. Compute A_4/A from Eq. 3.25 (Column 6). For values of ϵ_x greater than that at which the largest value of P_4/AE is reached, A_4/A remains constant.
7. Evaluate ϵ_z from the compatibility condition expressed by Eq. 3.11 (Column 7).
8. Compute A_3/A from Eq. 3.25 (Column 8).
9. Determine the value of P_3/AE corresponding to ϵ_z by multiplying columns 7 and 8 (Column 9).
10. Calculate the axial load from the equilibrium condition expressed by Eq. 3.5 (Column 10).
11. Express the values of column 10 as a percentage of the maximum value of P_z/AE (Column 11).

B.3 Spiral Reinforcement

The method used to compute the load-strain relations for axial compression of the model confined by spiral transverse reinforcement is described in Section 5.3. The calculations are summarized in Table B.2.

The calculations shown in Table B.2 were carried out in the following order:

1. Assume a value of ϵ_x, the transverse strain (Column 1).
2. Determine the proportion of effective area, A_1/A, from Eq. 3.26 (Column 2).
3. Determine the value of P_1/AE corresponding to ϵ_x by multiplying columns 1 and 2 (Column 3).
4. Using Eq. 5.5, and a value of $H_{max} = 19\ AE \times 10^{-5}$, determine the value of H for the assumed value of ϵ_x (Column 4).
5. Using Eq. 5.4, determine the value of P_4/AE for the diagonal strut in the vertical plane (Column 5).
6. Enter Fig. 3.8 with the quantity P_4/AE expressed as a percentage of the maximum load for the diagonal strut ($P_4 = 84.2\ AE \times 10^{-5}$) to obtain ϵ_4 (Column 6). For values of ϵ_x greater than that at which the largest value of P_4/AE is reached, determine ϵ_4 by means of the equation $\epsilon_4 = P_4/P_4' \times \epsilon_4'$ where P_4' is the largest value of P_4, and ϵ_4' is the corresponding value of ϵ_4.
7. Evaluate ϵ_z from the compatibility condition expressed by Eq. 3.11 (Column 7).
8. Compute A_3/A from Eq. 3.25 (Column 8).

9. Determine the value of P_3/AE corresponding to ϵ_z by multiplying columns 7 and 8 (Column 9).

10. Calculate the axial load from the equilibrium condition expressed by Eq. 3.5 (Column 10).

11. Express the values of column 10 as a percentage of the maximum value of P_z/AE for unconfined compression, $P_z = 537\ AE \times 10^{-5}$ (Column 11).

It can be seen that the calculations required to determine the quantitites in columns 4, 5 and 6 are the only ones which differ from the procedure followed in Table B.1.

B.4 Rectangular Transverse Reinforcement

(a) $n = 2$

The procedure which was followed to determine the load-strain relations for the 2 by 2 grid is described in Section 5.4b. This procedure involved the relation between P_{4A} and ϵ_z for the condition of spiral reinforcement, with $p_c = 0.2\ f'_c$. Accordingly, the calculations of the load-strain relations for this condition are given in Table B.3. The quantities shown in Table B.3 were derived by the same procedure that was followed to obtain Table B.2. The only difference between these two tables is that the value of H, shown in column 4 of Table B.3, was determined by substituting the value $H_{max} = 38\ AE \times 10^{-5}$ into Eq. 5.5. The relation between P_{4A} and ϵ_z, obtained from Table B.3, is shown in Fig. B.1. The relation between P_{4B} and ϵ_z for unconfined compression of the model, obtained from Table B.1, is shown in Fig. B.2. The calculations of the load-strain relations for the 2 by 2 grid are summarized in Table B.4. The calculations shown in Table B.4 were carried out in the following order:

1. Assume a value of ϵ_z, the longitudinal strain (Column 1).
2. Determine the proportion of effective area, A_3/A, from Eq. 3.25 (Column 2).
3. Determine the value of P_3/AE corresponding to ϵ_z by multiplying columns 1 and 2 (Column 3).
4. Enter Fig. B.1 with the assumed value of ϵ_z to obtain the quantity P_{4A}/AE (Column 4).
5. Enter Fig. B.2 with the assumed value of ϵ_z to obtain the quantity P_{4B}/AE (Column 5).
6. Compute the axial load from the equilibrium condition expressed by Eq. 5.6 (Column 6).
7. Express the values of column 6 as a percentage of the maximum value of P_z/AE for unconfined compression, $P_z = 537\ AE \times 10^{-5}$ (Column 7).

(b) n = 3

A diagram of the 3 by 3 grid model is shown in Fig. 5.6. A single quadrant of the model is shown in Fig. B.3, including the assumed deflected positions of points A, B, C, and D. The components of deflection, Δ_1, Δ_2, Δ_3, and Δ_4 have been indicated in their positive directions.

In determining the equilibrium equations for the model, the portions of the structure to the left of lines 1-1, 2-2, 3-3, and 4-4 in Fig. B.3 were considered as free body diagrams, and the equations were determined for equilibrium of forces in the x-direction. The structure was assumed to be one cube in height (in the z-direction), so that struts 1C, 1D, 4C and 4D are doubled because of the corresponding members of the adjoining cube.

For equilibrium of forces to the left of line 1-1

$$\frac{1}{\sqrt{2}} H + P_{1A} + \frac{1}{\sqrt{2}} P_{4A} + \frac{1}{\sqrt{2}} P_{5A} = 0 \tag{B.22}$$

For equilibrium of forces to the left of line 2-2,

$$\frac{1}{\sqrt{2}} H + P_{1B} + \frac{1}{\sqrt{2}} P_{4B} + \frac{2}{\sqrt{2}} P_{5B} + \frac{1}{\sqrt{2}} P_{5A} + 2\ P_{1D} + \frac{2}{\sqrt{2}} P_{4D} = 0 \tag{B.23}$$

For equilibrium of forces to the left of line 3-3,

$$\frac{1}{\sqrt{2}} H + P_{1B} + \frac{1}{\sqrt{2}} P_{4B} + \frac{2}{\sqrt{2}} P_{5B} + 2\ P_{1C} + \frac{2}{\sqrt{2}} P_{4C} + \frac{1}{\sqrt{2}} P_{5C} = 0 \tag{B.24}$$

The equation for equilibrium of forces to the left of line 4-4 was combined with Eq. B.22, which is equivalent to considering equilibrium of joint C in the x-direction

$$\frac{1}{\sqrt{2}} P_{5D} + 2\ P_{1D} + \frac{2}{\sqrt{2}} P_{4D} + \frac{1}{\sqrt{2}} P_{5B} = 0 \tag{B.25}$$

For equilibrium of forces in the z-direction

$$2.25\ P_z = 9P_3 + \frac{4}{\sqrt{2}} P_{4A} + \frac{2}{\sqrt{2}} P_{4B} + \frac{4}{\sqrt{2}} P_{4C} + \frac{8}{\sqrt{2}} P_{4D} \tag{B.26a}$$

$$P_z = 4P_3 + 1.257\ P_{4A} + 0.628\ P_{4B} + 1.257\ P_{4C} + 2.514\ P_{4D} \tag{B.26b}$$

Four equations of compatibility were derived which related the strains of the struts parallel to the x-y plane. These equations were determined by means of the assumed deflections Δ_1, Δ_2, Δ_3, and Δ_4, as described below

$$\Delta_1 = \sqrt{2}L_1 \; (\epsilon_{xA} + 0.5 \; \epsilon_{xB}) \qquad (B.27a)$$

$$\Delta_2 = \sqrt{2}L_1 \; (0.5 \; \epsilon_{xC}) \qquad (B.27b)$$

$$\Delta_3 = 0.5L_1 \; \epsilon_{xB} \qquad (B.27c)$$

$$\Delta_4 = L_1 \; (\epsilon_{xD} + 0.5 \; \epsilon_{xC}) \qquad (B.27d)$$

The strains in struts 5A, 5B, 5C, and 5D may be expressed in terms of Δ_1, Δ_2, Δ_3, and Δ_4 as follows:

$$\epsilon_{5A} = \frac{1}{\sqrt{2}\;L_1} \; (\Delta_1 - \Delta_2) \qquad (B.28a)$$

$$\epsilon_{5B} = \frac{1}{\sqrt{2}\;L_1} \; (\frac{1}{\sqrt{2}} \Delta_3 + \frac{1}{\sqrt{2}} \Delta_4) \qquad (B.28b)$$

$$\epsilon_{5C} = \frac{1}{\sqrt{2}\;L_1} \; (2 \; \Delta_2) \qquad (B.28c)$$

$$\epsilon_{5D} = \frac{1}{\sqrt{2}\;L_1} \; (\sqrt{2} \; \Delta_4 - \sqrt{2} \; \Delta_3) \qquad (B.28d)$$

By combining equations B.27 and B.28, strains ϵ_{5A}, ϵ_{5B}, ϵ_{5C}, and ϵ_{5D} may be expressed in terms of ϵ_{xA}, ϵ_{xB}, ϵ_{xC}, and ϵ_{xD}. The resulting equations are

$$\epsilon_{5A} = \epsilon_{xA} + 0.5\ (\epsilon_{xB} - \epsilon_{xC}) \qquad (B.29a)$$

$$\epsilon_{5B} = 0.25\ \epsilon_{xB} + 0.25\ \epsilon_{xC} + 0.5\ \epsilon_{xD} \qquad (B.29b)$$

$$\epsilon_{5C} = \epsilon_{xC} \qquad (B.29c)$$

$$\epsilon_{5D} = \epsilon_{xD} + 0.5\ (\epsilon_{xC} - \epsilon_{xB}) \qquad (B.29d)$$

Four additional compatibility equations were determined in a manner similar to the derivation of Eq. 3.11. These equations are as follows:

$$\epsilon_{4A} = 0.5\ (\epsilon_{xA} + \epsilon_z) \qquad (B.30a)$$

$$\epsilon_{4B} = 0.5\ (\epsilon_{xB} + \epsilon_z) \qquad (B.30b)$$

$$\epsilon_{4C} = 0.5\ (\epsilon_{xC} + \epsilon_z) \qquad (B.30c)$$

$$\epsilon_{4D} = 0.5\ (\epsilon_{xD} + \epsilon_z) \qquad (B.30d)$$

The force in any strut may be expressed

$$P_i = A_i \epsilon_i E \qquad (B.31)$$

Using Eq. B.31, together with compatibility Eqs. B.29 and B.30, the equilibrium equations (B.22, B.23, B.24 and B.25) were expressed in terms of ϵ_{xA}, ϵ_{xB}, ϵ_{xC} and ϵ_{xD} as independent unknowns. The resulting equations are

$$(\sqrt{2}\, A_{1A} + 0.5\, A_{4A} + A_{5A})\epsilon_{xA} + (0.5\, A_{5A})\epsilon_{xB} - (0.5A_{5A})\epsilon_{xC} +$$

$$+ (0.5\, A_{4A})\epsilon_z + H = 0 \qquad \text{(B.32a)}$$

$$(A_{5A})\epsilon_{xA} + (\sqrt{2}\, A_{1B} + 0.5\, A_{4B} + 0.5\, A_{5A} + 0.5\, A_{5B})\epsilon_{xB} +$$

$$+ (0.5\, A_{5B} - 0.5A_{5A})\epsilon_{xc} + (2\sqrt{2}\, A_{1D} + A_{4D} + A_{5B})\epsilon_{xD} +$$

$$+ (0.5\, A_{4B} + A_{4D})\epsilon_z + H = 0 \qquad \text{(B.32b)}$$

$$(\sqrt{2}\, A_{1B} + 0.5\, A_{4B} + 0.5\, A_{5B})\epsilon_{xB} + (2\sqrt{2}\, A_{1C} + A_{4C} + 0.5A_{5B} + A_{5C})\epsilon_{xC} +$$

$$+ (A_{5B})\epsilon_{xD} + (0.5\, A_{4B} + A_{4C})\epsilon_z + H = 0 \qquad \text{(B.32c)}$$

$$(0.25\, A_{5B} - 0.5\, A_{5D})\epsilon_{xB} + (0.25\, A_{5B} + 0.5\, A_{5D})\epsilon_{xC} +$$

$$+ (2\sqrt{2}\, A_{1D} + A_{4D} + 0.5\, A_{5B} + A_{5D})\epsilon_{xD} + (A_{4D})\epsilon_z = 0 \qquad \text{(B.32d)}$$

The value of H, determined from Eq. 5.5, is

$$H = 22.6\, \epsilon_{xA} + 11.3\, \epsilon_{xB} \qquad \text{(B.33)}$$

$$H_{max} = 57\ AE \times 10^{-5}$$

Equations B.32 were then solved by the procedure described in Section 5.4c. The resulting strains are given in Table B.5, and the corresponding strut areas, determined from Eqs. 3.25 and 3.26, are given in Table B.6.

The value of P_z for each incremental vertical strain, ϵ_z, was computed by means of Eq. B.26. The results of these calculations are summarized in Table B.7. The quantities given in Table B.7 were derived by the following procedure.

1. Assume a value of axial strain, ϵ_z, of the same magnitude as that used in solving Eqs. B.32, and indicated in Tables B.5 and B.6 (Column 1).
2. From column 3 of Table B.4, obtain the value of P_3/AE corresponding to ϵ_z. Multiply the value of P_3/AE by 4 (Column 2).
3. Determine the quantity P_{4A}/AE by multiplying the appropriate values of ϵ_{4A} and A_{4A}/A given in Tables B.5 and B.6 respectively. Multiply this value of P_{4A}/AE by 1.257 (Column 3).
4. Repeat the procedure followed in step 3 to determine the appropriate multiples of P_{4B}, P_{4C}, and P_{4D} shown in Table B.7 (Columns 4, 5, and 6, respectively).
5. Determine the value of P_z corresponding to the assumed value of ϵ_z from the equilibrium relation expressed by Eq. B.26 (Column 7)
6. Express the values of column 7 as a percentage of the maximum value of P_z/AE for unconfined compression, $P_z = 537\ AE \times 10^{-5}$ (Column 8).

(c) <u>n = 4</u>

Figure B.4 is a diagram of one quadrant of the 4 by 4 grid model. The assumed deflection components of the horizontal deformations are Δ_1, Δ_2,

Δ_3, Δ_4, Δ_5, and Δ_6. The method of solution was similar to that described in Section B.4b.

The relations among the forces in the struts were expressed by means of six equilibrium equations. These equations were derived by considering equilibrium of joints L, M, N, P, and Q in the x and y directions.

For $\Sigma F_x = 0$ at joint L

$$\sqrt{2}\ P_{xA} + P_{4A} + P_{5A} + H = 0 \tag{B.34}$$

For $\Sigma F_x = 0$ at joint M

$$\sqrt{2}\ P_{xA} - \sqrt{2}\ P_{xB} + P_{4A} - P_{4B} + P_{5B} - P_{5C} = 0 \tag{B.35}$$

For $\Sigma F_y = 0$ at joint M

$$2\sqrt{2}\ P_{xC} + 2\ P_{4C} + P_{5B} + P_{5C} = 0 \tag{B.36}$$

For $\Sigma F_y = 0$ at joint N

$$\sqrt{2}\ P_{xD} + P_{4D} + P_{5D} = 0 \tag{B.37}$$

For $\Sigma F_x = 0$ at joint P

$$2\sqrt{2}\ P_{xC} - 2\sqrt{2}\ P_{xE} + 2\ P_{4C} - 2\ P_{4E} + P_{5A} - P_{5E} = 0 \tag{B.38}$$

For $\Sigma F_y = 0$ at joint Q

$$\sqrt{2}\ P_{xD} - \sqrt{2}\ P_{xF} + P_{4D} - P_{4F} + P_{5C} - P_{5F} = 0 \tag{B.39}$$

For equilibrium in the z-direction

$$P_z = 4\ P_3 + 0.707\ (P_{4A} + P_{4B} + P_{4D} + P_{4F}) + + 1.414\ (P_{4C} + P_{4E}) \tag{B.40}$$

The compatibility equations relating the strains in struts parallel to the x-y plane were derived in a manner similar to that described in Section B.4b. The resulting equations are as follows:

$$\epsilon_{5A} = \epsilon_{xA} + \epsilon_{xB} - \epsilon_{xE} \tag{B.41a}$$

$$\epsilon_{5B} = \epsilon_{xC} + \epsilon_{xE} - \epsilon_{xB} \tag{B.41b}$$

$$\epsilon_{5C} = 0.5\ (\epsilon_{xB} + \epsilon_{xC} + \epsilon_{xE} - \epsilon_{xF}) \tag{B.41c}$$

$$\epsilon_{5D} = 0.5\ (\epsilon_{xD} + \epsilon_{xF}) \tag{B.41d}$$

$$\epsilon_{5E} = \epsilon_{xE} \tag{B.41e}$$

$$\epsilon_{5F} = \epsilon_{xF} \tag{B.41f}$$

In addition, six compatibility equations were derived by means of Eq. 3.11

$$\epsilon_{4A} = 0.5\ (\epsilon_{xA} + \epsilon_{z}) \tag{B.42a}$$

$$\epsilon_{4B} = 0.5\ (\epsilon_{xB} + \epsilon_{z}) \tag{B.42b}$$

$$\epsilon_{4C} = 0.5\ (\epsilon_{xC} + \epsilon_{z}) \tag{B.42c}$$

$$\epsilon_{4D} = 0.5\ (\epsilon_{xD} + \epsilon_{z}) \tag{B.42d}$$

$$\epsilon_{5E} = 0.5\ (\epsilon_{xE} + \epsilon_{z}) \tag{B.42e}$$

$$\epsilon_{xF} = 0.5\ (\epsilon_{xF} + \epsilon_{z}) \tag{B.42f}$$

The final equilibrium equations, expressed in terms of strut areas and strain, are,

$$(\sqrt{2}\ A_{1A} + 0.5\ A_{4A} + A_{5A})\epsilon_{xA} + (A_{5A})\epsilon_{xB} - (A_{5A})\epsilon_{xE} +$$

$$+ (0.5\ A_{4A})\epsilon_z + H = 0 \qquad \text{(B.43a)}$$

$$(\sqrt{2}\ A_{1A} + 0.5\ A_{4A})\epsilon_{xA} - (\sqrt{2}\ A_{1B} + 0.5\ A_{4B} + A_{5B} + 0.5\ A_{5C})\epsilon_{xB} +$$

$$+ (A_{5B} - 0.5\ A_{5C})\epsilon_{xC} + (A_{5B} - 0.5\ A_{5C})\epsilon_{xE} + (0.5\ A_{5C})\epsilon_{xF} +$$

$$+ (0.5\ A_{4A} - 0.5\ A_{4B})\epsilon_z = 0 \qquad \text{(B.43b)}$$

$$(0.5\ A_{5C} - A_{5B})\epsilon_{xB} + (2\sqrt{2}\ A_{1C} + A_{4C} + A_{5B} + 0.5\ A_{5C})\epsilon_{xC} +$$

$$+ (A_{5B} + 0.5\ A_{5C})\epsilon_{xE} - (0.5\ A_{5C})\epsilon_{xF} + (A_{4C})\epsilon_z = 0 \qquad \text{(B.43c)}$$

$$(\sqrt{2}\ A_{1D} + 0.5\ A_{4D} + 0.5\ A_{5D})\epsilon_{xD} + (0.5\ A_{5D})\epsilon_{xF} + (0.5\ A_{4D})\epsilon_z = 0 \qquad \text{(B.43d)}$$

$$(A_{5A})\epsilon_{xA} + (A_{5A})\epsilon_{xB} + (2\sqrt{2}\ A_{1C} + A_{4C})\epsilon_{xC} +$$

$$- (2\sqrt{2}\ A_{1E} + A_{4E} + A_{5A} + A_{5E})\epsilon_{xE} + (A_{4C} - A_{4E})\epsilon_z = 0 \qquad \text{(B.43e)}$$

$$(0.5\ A_{5C})\epsilon_{xB} + (0.5\ A_{5C})\epsilon_{xC} + (\sqrt{2}\ A_{1D} + 0.5\ A_{4D})\epsilon_{xD} +$$

$$+ (0.5\ A_{5C})\epsilon_{xE} - (\sqrt{2}\ A_{1F} + 0.5\ A_{4F} + 0.5\ A_{5C} + A_{5F})\epsilon_{xF} +$$

$$+ (0.5\ A_{4D} - 0.5\ A_{4F})\epsilon_z = 0 \qquad \text{(B.43f)}$$

The value of H is

$$H = 22.6\ \epsilon_{xA} + 22.6\ \epsilon_{xB} \tag{B.44}$$

$$H_{max} = 76\ AE \times 10^{-5}$$

Equations B.43 were solved by the trial and error procedure described in Section 5.4c. The resulting strains are summarized in Table B.8, and the corresponding areas are given in Table B.9. For the sake of simplicity, only the results for struts 1 and 4 are given in Tables B.8 and B.9. The strains in struts 5 may be determined by Eqs. B.41, and the corresponding areas may be obtained from Eq. 3.26.

The load-strain relations, calculated from Eq. B.40, and using a procedure similar to that followed in deriving the quantities in Table B.7, are summarized in Table B.10.

TABLE B.1

CALCULATION OF THEORETICAL LOAD-STRAIN RELATIONS FOR UNCONFINED COMPRESSION

(1)	(2)	(3)	(4)	(5)	(6)	(7)	(8)	(9)	(10)	(11)
$\epsilon_x \times 10^3$	A_1/A (%)	$\frac{P_1}{AE} \times 10^5$ = (1)x(2)	$\frac{P_4}{AE} \times 10^5$ =-2.18(3)	$\epsilon_4 \times 10^3$	A_4/A (%)	$\epsilon_z \times 10^3$ =2(5)-(1)	A_3/A (%)	$\frac{P_3}{AE} \times 10^5$ = (7)x(8)	$\frac{P_z}{AE} \times 10^5$ =4(9)+5.66(4)	Percent Maximum Load
0.001	100	0.10	- 0.22	-0.003	76.9	-0.007	100	- 0.7	- 4	0.7
0.04	86.4	3.46	- 7.54	-0.097	76.9	-0.234	98.8	- 23.1	-135	25.2
0.08	67.0	5.36	-11.7	-0.152	76.9	-0.384	97.8	- 37.6	-216	40.2
0.12	56.1	6.73	-14.7	-0.191	76.9	-0.502	94	- 47.2	-272	50.7
0.17	50.7	8.61	-18.75	-0.245	76.5	-0.660	86.5	- 57.1	-334	62.2
0.23	49.5	11.4	-24.9	-0.328	75.9	-0.886	74	- 65.5	-403	75.1
0.30	46.0	13.8	-30.1	-0.402	74.8	-1.104	63.4	- 70.0	-450	83.8
0.40	39.4	15.75	-34.4	-0.470	73.2	-1.34	55.4	- 74.2	-491	91.5
0.57	28.9	16.5	-36.0	-0.499	72.2	-1.568	51.2	- 80.3	-525	97.8
0.90	16.2	14.6	-31.8	-0.441	72.2	-1.782	50	- 89.1	-537	100
1.50	6.5	9.75	-21.2	-0.294	72.2	-2.088	48.6	-103	-532	99.1
2.25	2.7	6.08	-13.2	-0.183	72.2	-2.62	41.6	-109	-511	95.2
3.0	1.2	3.6	- 7.85	-0.109	72.2	-3.22	32.2	-103.8	-459	85.5
4.5	0.4	1.8	- 3.93	-0.055	72.2	-4.61	15.8	- 72.8	-313	58.3
6.0	0.15	0.9	- 1.96	-0.027	72.2	-6.05	7.5	- 45.4	-193	36.0
8.0	0.06	0.48	- 1.05	-0.015	72.2	-8.03	2.8	- 22.5	- 96	17.9

TABLE B.2

CALCULATION OF THEORETICAL LOAD-STRAIN RELATIONS FOR MODEL CONFINED BY SPIRAL REINFORCEMENT ($P_c = 0.1\ f'_c$)

(1)	(2)	(3)	(4)	(5)	(6)	(7)	(8)	(9)	(10)	(11)
$\epsilon_x \times 10^3$	A_1/A (%)	$\frac{P_1}{AE} \times 10^5$ $=(1)\times(2)$	$\frac{H}{AE} \times 10^5$ $=11.4(1)$	$\frac{P_4}{AE} \times 10^5$ $=-[(4)+2.18(3)]$	$\epsilon_4 \times 10^3$	$\epsilon_z \times 10^3$ $=2(6)-(1)$	A_3/A (%)	$\frac{P_3}{AE} \times 10^5$ $=(7)\times(8)$	$\frac{P_z}{AE} \times 10^5$ $=4(9)+5.66(5)$	Percent Unconfined Compression Maximum Load
0.001	100	0.10	0.01	- 0.23	-0.003	-0.007	100	- 0.7	- 4	0.75
0.04	86.4	3.46	0.45	8.0	-0.104	-0.24	99.8	- 24	-141	26.3
0.08	67.0	5.36	0.9	12.6	-0.166	-0.41	97.1	- 39.8	-230	42.8
0.12	56.1	6.73	1.4	16.1	-0.212	-0.54	92.4	- 50	-291	54.2
0.17	50.7	8.61	1.9	20.7	-0.27	-0.71	83.8	- 59.5	-355	66.1
0.30	46.0	13.8	3.4	33.4	-0.46	-1.22	59.0	- 72	-477	88.8
0.40	39.4	15.75	4.6	38.9	-0.56	-1.52	51.8	- 78.8	-535	99.6
0.57	28.9	16.45	6.5	42.3	-0.62	-1.81	50	- 90.5	-601	112
0.90	16.2	14.6	10.2	42.0	-0.62	-2.14	48.1	-103	-650	121
1.50	6.5	9.75	17.1	38.2	-0.56	-2.62	41.6	-109	-652	121.4
2.25	2.7	6.07	19.0	32.2	-0.47	-3.19	32.7	-104.2	-599	111.5
3.0	1.2	3.6	19.0	26.8	-0.39	-3.78	24.1	- 91	-516	96
4.5	0.4	1.8	19.0	22.9	-0.34	-5.18	11.6	- 60	-370	69
6.0	0.15	0.9	19.0	21.0	-0.31	-6.62	5.5	- 36.4	-264	49
8.0	0.06	0.48	19.0	20.0	-0.29	-8.58	2.1	- 18.0	-185	34.5

TABLE B.3

CALCULATION OF THEORETICAL LOAD-STRAIN RELATIONS FOR MODEL CONFINED BY SPIRAL REINFORCEMENT ($P_c = 0.2 f'_c$)

(1)	(2)	(3)	(4)	(5)	(6)	(7)	(8)	(9)	(10)	(11)
$\epsilon_x \times 10^3$	A_1/A (%)	$\frac{P_1}{AE} \times 10^5$ $=(1)\times(2)$	$\frac{H}{AE} \times 10^5$ $=22.8(1)$	$\frac{P_4}{AE} \times 10^5$ $=1[(4)+2.18(3)]$	$\epsilon_4/10^3$	$\epsilon_z \times 10^3$ $=2(6)-(1)$	A_3/A (%)	$\frac{P_3}{AE} \times 10^5$ $=(7)\times(8)$	$\frac{P_z}{AE} \times 10^5$ $=4(9)+5.66(5)$	Percent Unconfined Compression Maximum Load
0.001	100	0.10	0.02	- 0.24	0.003	0.007	100	0.7	4	0.7
0.04	86.4	3.46	0.91	8.46	0.11	0.26	99.6	25.9	152	28.3
0.08	67.0	5.36	1.8	13.5	0.18	0.44	96.2	42.3	245	45.7
0.12	56.1	6.73	2.7	17.4	0.23	0.58	90.6	52.5	308	57.4
0.17	50.7	8.61	3.9	22.7	0.30	0.77	80.5	62.0	377	70.2
0.30	46.0	13.8	6.8	36.8	0.51	1.32	55.9	73.8	503	93.7
0.40	39.4	15.75	9.1	43.5	0.65	1.70	50.2	85.3	587	109.3
0.57	28.9	16.45	13.0	48.9	0.82	2.21	47.3	104.8	694	129
0.90	16.2	14.6	20.5	52.3	0.97	2.84	38.3	109	732	136
1.50	6.5	9.75	34.2	55.4	1.20	3.90	23.1	90	673	125
2.25	2.7	6.07	38	51.2	1.11	4.47	17.0	76	593	110
3.0	1.2	3.6	38	45.9	1.00	5.00	12.9	64.5	518	96.5
4.5	0.4	1.8	38	41.9	0.91	6.32	6.3	39.8	396	73.8
6.0	0.15	0.9	38	39.9	0.87	7.74	3.3	25.6	330	61.5
8.0	0.06	0.48	38	39.0	0.85	9.70	1.3	12.6	271	50.5

TABLE B.4

CALCULATION OF THEORETICAL LOAD-STRAIN RELATIONS FOR MODEL CONFINED BY RECTANGULAR TRANSVERSE REINFORCEMENT, 2 BY 2 GRID

(1)	(2)	(3)	(4)	(5)	(6)	(7)
$\epsilon_z \times 10^3$	$\frac{A_3}{A}$ (%)	$\frac{P_3}{AE} \times 10^5$ $= (1) \times (2)$	$\frac{P_{4A}}{AE} \times 10^5$	$\frac{P_{4B}}{AE} \times 10^5$	$\frac{P_z}{AE} \times 10^5$ $= 4(3) + 2.83[(4)+(5)]$	Percent Unconfined Compression Maximum Load
-0.5	94.1	- 47.0	-15.6	-15.3	-275	51.3
-1.0	68.2	- 68.2	-28.8	-28.2	-434	80.8
-1.5	52.1	- 78.1	-40.6	-35.5	-528	98.5
-2.0	49.3	- 98.6	-47.3	-23.5	-594	110.5
-2.5	43.4	-108.5	-51.0	-14.5	-619	115.0
-3.0	35.6	-106.8	-53.3	- 9.3	-603	112.3
-3.5	28.2	- 98.7	-55.0	- 6.2	-568	105.8
-4.0	21.7	- 86.8	-55.2	- 5.0	-517	96.3
-5.0	12.9	- 64.5	-45.9	- 3.4	-398	74.2
-6.0	7.7	- 46.2	-42.7	- 2.0	-312	58.2
-8.0	2.8	- 22.4	-39.5	- 1.2	-205	38.2

TABLE B.5

STRAIN RELATIONS FOR MODEL CONFINED BY RECTANGULAR REINFORCEMENT
3 BY 3 GRID

(1)	(2)	(3)	(4)	(5)	(6)	(7)	(8)	(9)	(10)	(11)	(12)	(13)	(14)
ϵ_z $\times 10^3$	$\frac{H}{AE} \times 10^5$	ϵ_{xA} $\times 10^3$	ϵ_{4A} $\times 10^3$	ϵ_{5A} $\times 10^3$	ϵ_{xB} $\times 10^3$	ϵ_{4B} $\times 10^3$	ϵ_{5B} $\times 10^3$	ϵ_{xC} $\times 10^3$	ϵ_{4C} $\times 10^3$	ϵ_{5C} $\times 10^3$	ϵ_{xD} $\times 10^3$	ϵ_{4D} $\times 10^3$	ϵ_{5D} $\times 10^3$
-0.5	3.25	0.094	-0.203	0.087	0.100	-0.200	0.113	0.114	-0.193	0.114	0.119	-0.191	0.126
-1.0	7.28	0.212	-0.394	0.196	0.220	-0.340	0.251	0.253	-0.373	0.253	0.266	-0.367	0.282
-1.5	11.04	0.320	-0.590	0.256	0.338	-0.581	0.452	0.465	-0.518	0.465	0.502	-0.499	0.592
-2.0	17.53	0.579	-0.711	0.139	0.393	-0.804	1.092	1.272	-0.364	1.272	1.353	-0.324	1.798
-2.5	25.03	0.914	-0.793	0.076	0.387	-1.057	1.664	2.062	-0.219	2.062	2.105	-0.197	2.943
-3.0	31.24	1.132	-0.934	0.031	0.501	-1.249	2.170	2.702	-0.149	2.702	2.740	-0.130	3.841

TABLE B.8

STRAIN RELATIONS FOR MODEL CONFINED BY RECTANGULAR REINFORCEMENT
4 BY 4 GRID

(1)	(2)	(3)	(4)	(5)	(6)	(7)	(8)	(9)	(10)	(11)	(12)	(13)	(14)
ϵ_z	$\frac{H}{AE} \times 10^5$	ϵ_{xA} $\times 10^3$	ϵ_{4A} $\times 10^3$	ϵ_{xB} $\times 10^3$	ϵ_{4B} $\times 10^3$	ϵ_{xC} $\times 10^3$	ϵ_{4C} $\times 10^3$	ϵ_{xD} $\times 10^3$	ϵ_{4D} $\times 10^3$	ϵ_{xE} $\times 10^3$	ϵ_{4E} $\times 10^3$	ϵ_{xF} $\times 10^3$	ϵ_{4F} $\times 10^3$
-1.0	9.36	0.200	-0.400	0.214	-0.393	0.264	-0.368	0.264	-0.368	0.248	-0.376	0.258	-0.371
-1.5	14.13	0.315	-0.593	0.310	-0.595	0.517	-0.491	0.504	-0.498	0.447	-0.526	0.485	-0.508
-2.0	23.55	0.666	-0.667	0.376	-0.812	1.345	-0.328	1.335	-0.333	1.101	-0.450	1.438	-0.281
-2.5	35.93	1.245	-0.627	0.345	-1.077	2.063	-0.219	2.115	-0.192	1.744	-0.378	2.313	-0.094

TABLE B.9

AREA RELATIONS FOR MODEL CONFINED BY RECTANGULAR REINFORCEMENT
4 BY 4 GRID

(1)	(2)	(3)	(4)	(5)	(6)	(7)	(8)	(9)	(10)	(11)	(12)	(13)
ϵ_z $\times 10^3$	A_{1A}/A (%)	A_{4A}/A (%)	A_{1B}/A (%)	A_{4B}/A (%)	A_{1C}/A (%)	A_{4C}/A (%)	A_{1D}/A (%)	A_{4D}/A (%)	A_{1E}/A (%)	A_{4E}/A (%)	A_{1F}/A (%)	A_{4F}/A (%)
-1.0	50.0	74.9	49.8	74.8	48.0	75.4	48.0	75.4	48.7	75.3	48.2	75.4
-1.5	45.0	69.2	45.5	69.1	31.9	72.6	32.5	72.4	36.2	71.5	33.8	72.1
-2.0	24.0	66.3	41.0	60.0	8.15	72.6	8.25	72.4	11.4	71.5	7.13	72.1
-2.5	9.5	67.9	41.0	49.7	3.25	72.6	3.10	72.4	4.72	71.5	2.45	72.1

TABLE B.7

LOAD-STRAIN RELATIONS FOR MODEL CONFINED BY RECTANGULAR REINFORCEMENT
3 BY 3 GRID

(1)	(2)	(3)	(4)	(5)	(6)	(7)	(8)
$\epsilon_z \times 10^3$	$\frac{4P_3}{AE} \times 10^5$	$1.257 \times \frac{P_{4A}}{AE} \times 10^5$	$0.628 \times \frac{P_{4B}}{AE} \times 10^5$	$1.257 \times \frac{P_{4C}}{AE} \times 10^5$	$2.514 \times \frac{P_{4D}}{AE} \times 10^5$	$\frac{P_z}{AE} \times 10^5$ $= (2)+(3)+(4)+(5)+(6)$	Percent Unconfined Compression Maximum Load
-0.5	-188	-19.6	- 9.7	-18.6	-23.1	-259	48.3
-1.0	-272.4	-37.2	-16.0	-35.3	-69.6	-431	80.3
-1.5	-312.8	-51.4	-25.4	-46.9	-91.0	-528	98.5
-2.0	-394.4	-57.6	-30.5	-32.9	-59.0	-574	107.0
-2.5	-434	-60.7	-33.5	-19.9	-36.0	-584	108.8
-3.0	-427.2	-64.6	-35.0	-13.4	-23.6	-563	105.0

TABLE B.6

AREA RELATIONS FOR MODEL CONFINED BY RECTANGULAR REINFORCEMENT
3 BY 3 GRID

(1)	(2)	(3)	(4)	(5)	(6)	(7)	(8)	(9)	(10)	(11)	(12)	(13)
ϵ_z $\times 10^3$	A_{1A}/A (%)	A_{4A}/A (%)	A_{5A}/A (%)	A_{1B}/A (%)	A_{4B}/A (%)	A_{5B}/A (%)	A_{1C}/A (%)	A_{4C}/A (%)	A_{5C}/A (%)	A_{1D}/A (%)	A_{4D}/A (%)	A_{5D}/A (%)
-0.5	62.0	76.9	49.6	60.5	76.9	44.2	57.2	76.9	44.0	56.5	76.9	42.3
-1.0	49.8	75.0	38.5	49.7	75.0	37.3	48.5	75.4	37.1	47.9	75.5	36.2
-1.5	45.0	69.4	37.0	43.5	69.7	27.5	35.0	72.0	27.0	33.0	72.5	23.1
-2.0	28.2	64.4	37.0	39.8	60.4	8.15	9.1	72.0	7.0	8.05	72.5	3.42
-2.5	15.6	60.9	37.0	39.8	50.4	3.73	3.6	72.0	2.53	3.13	72.5	1.03
-3.0	11.0	55.0	37.0	32.5	44.6	2.23	1.68	72.0	1.29	1.60	72.5	0.46

TABLE B.10

LOAD-STRAIN RELATIONS FOR MODEL CONFINED BY RECTANGULAR REINFORCEMENT
4 BY 4 GRID

(1)	(2)	(3)	(4)	(5)	(6)	(7)	(8)	(9)	(10)
ϵ_z $\times 10^3$	$\frac{4P_z}{AE} \times 10^5$	$0.707 \times \frac{P_{4A}}{AE} \times 10^5$	$0.707 \times \frac{P_{4B}}{AE} \times 10^5$	$1.414 \times \frac{P_{4C}}{AE} \times 10^5$	$0.707 \times \frac{P_{4D}}{AE} \times 10^5$	$1.414 \times \frac{P_{4E}}{AE} \times 10^5$	$0.707 \times \frac{P_{4F}}{AE} \times 10^5$	$\frac{P_z}{AE} \times 10^5$ = (2)+(3)+(4)+(5) +(6)+(7)+(8)	Percent Unconfined Compression Maximum Load
-1.0	-272.4	-21.2	-20.8	-39.3	-19.7	-40.0	-19.8	-433.2	80.6
-1.5	-312.8	-29.0	-29.1	-50.5	-25.5	-53.2	-25.9	-526.0	97.8
-2.0	-394.4	-31.2	-34.4	-33.7	-17.0	-45.5	-14.4	-570.6	106.1
-2.5	-434.0	-30.1	-37.8	-22.5	-19.8	-38.2	- 4.8	-577.2	107.5

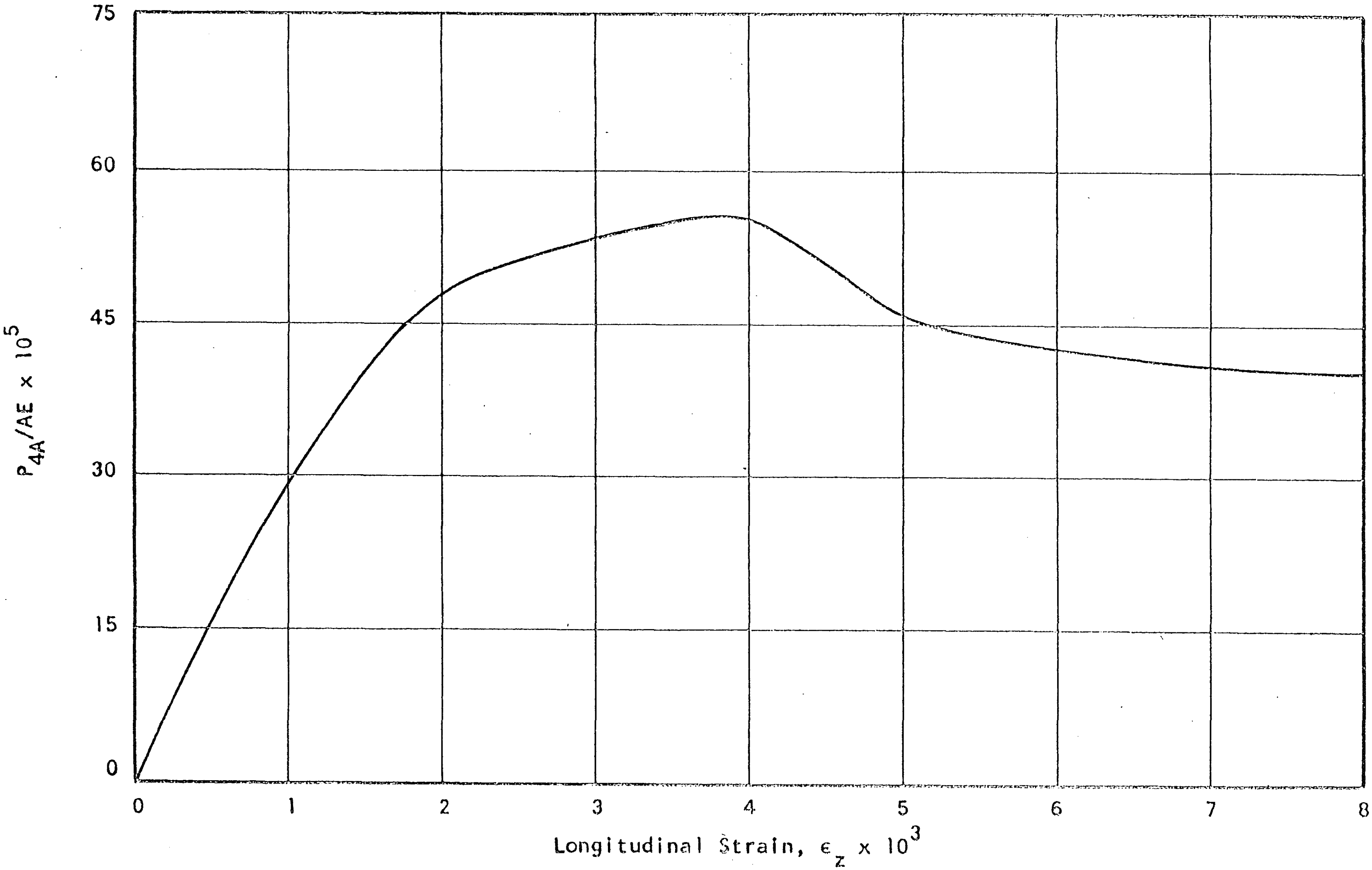

FIG. B.1 THEORETICAL RELATION BETWEEN P_{4A} AND ϵ_z FOR AXIAL COMPRESSION WITH CONFINEMENT PROVIDED BY SPIRAL REINFORCEMENT ($p_c = 0.2\ f'_c$)

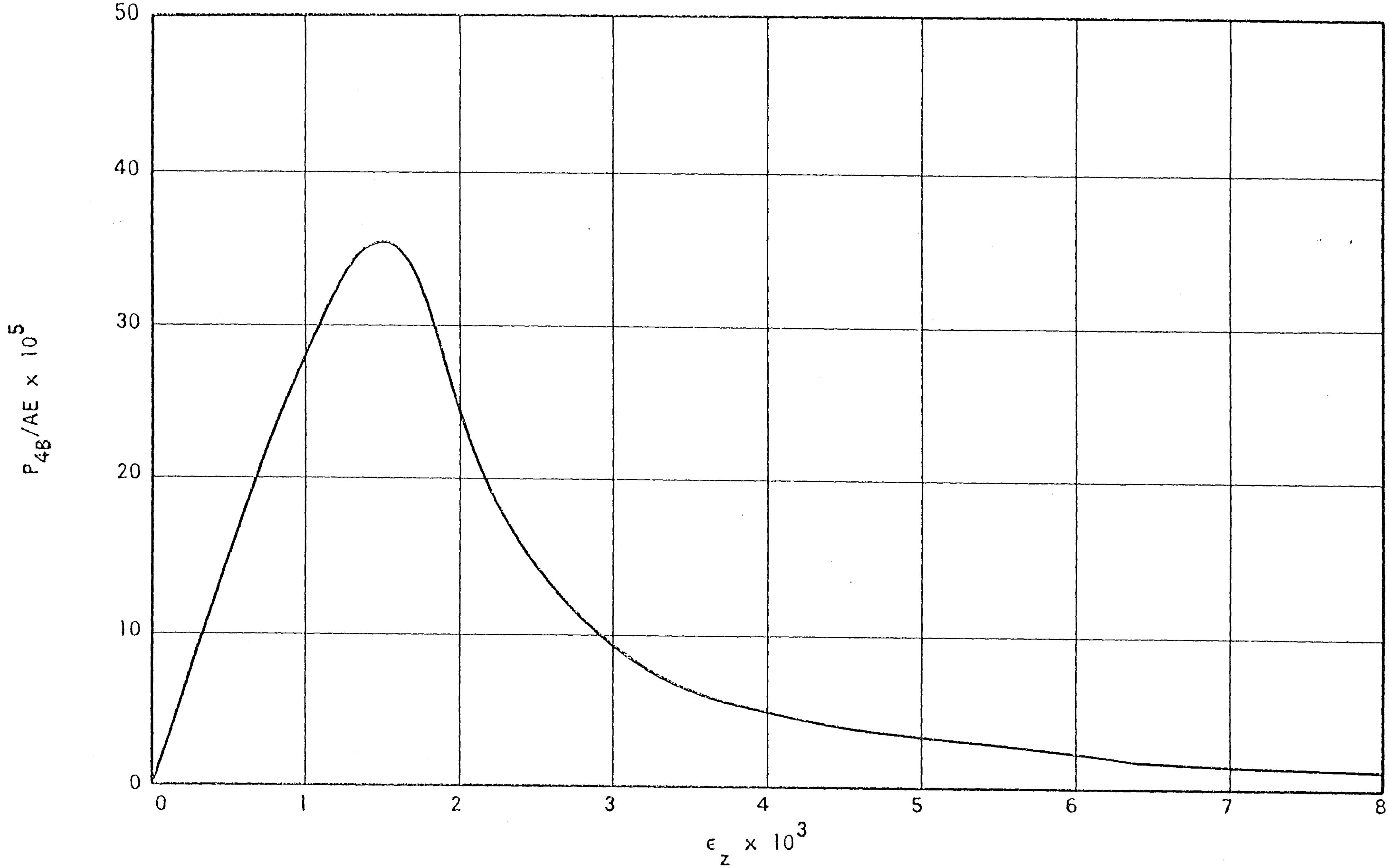

FIG. B.2 THEORETICAL RELATION BETWEEN P_{4B} AND ϵ_z FOR UNCONFINED COMPRESSION

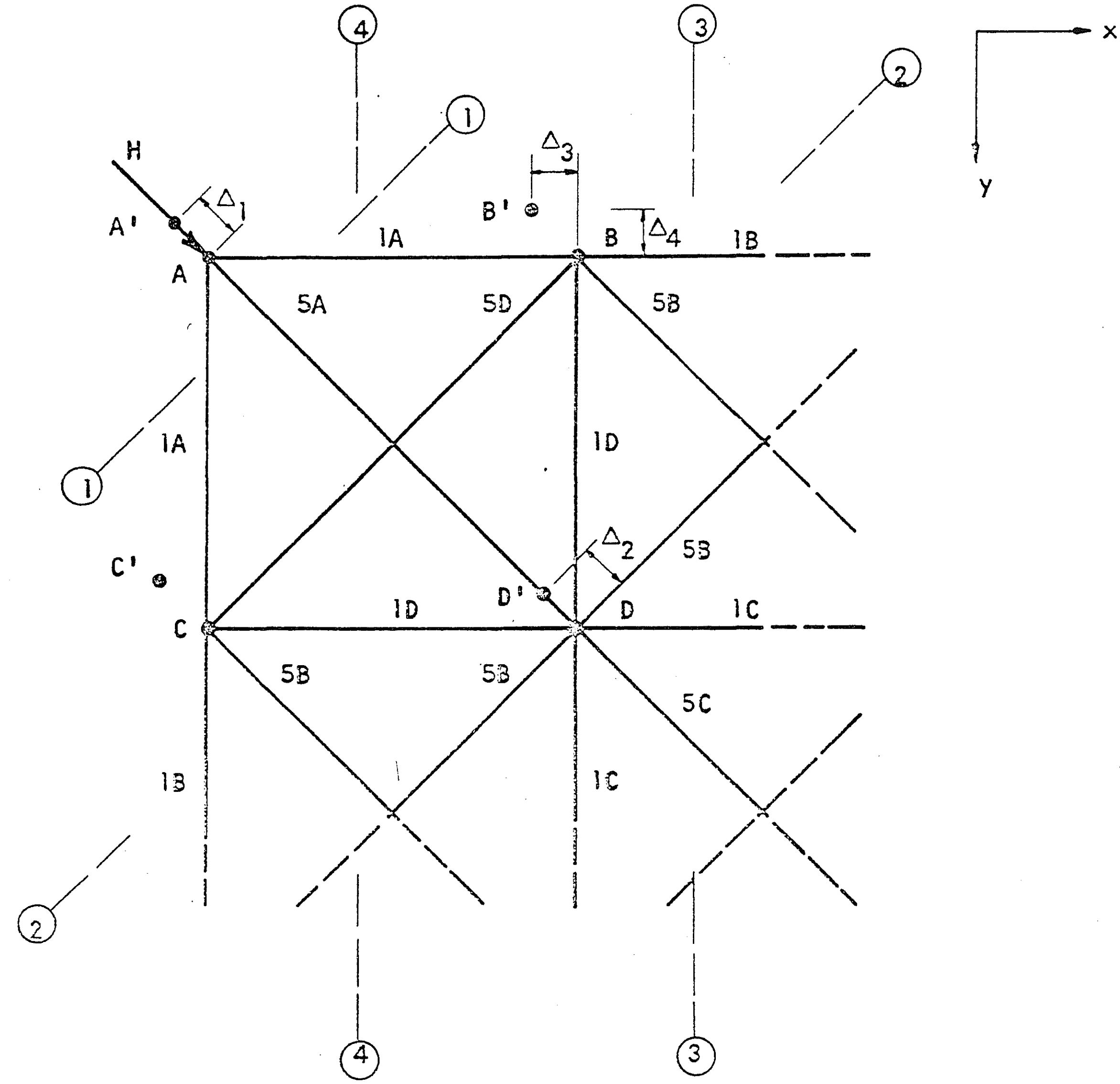

A, B, C, D : Original Positions

A',B',C',D' : Assumed Deflected Positions

FIG. B.3 QUADRANT OF 3 BY 3 GRID MODEL SHOWING ASSUMED DEFLECTIONS

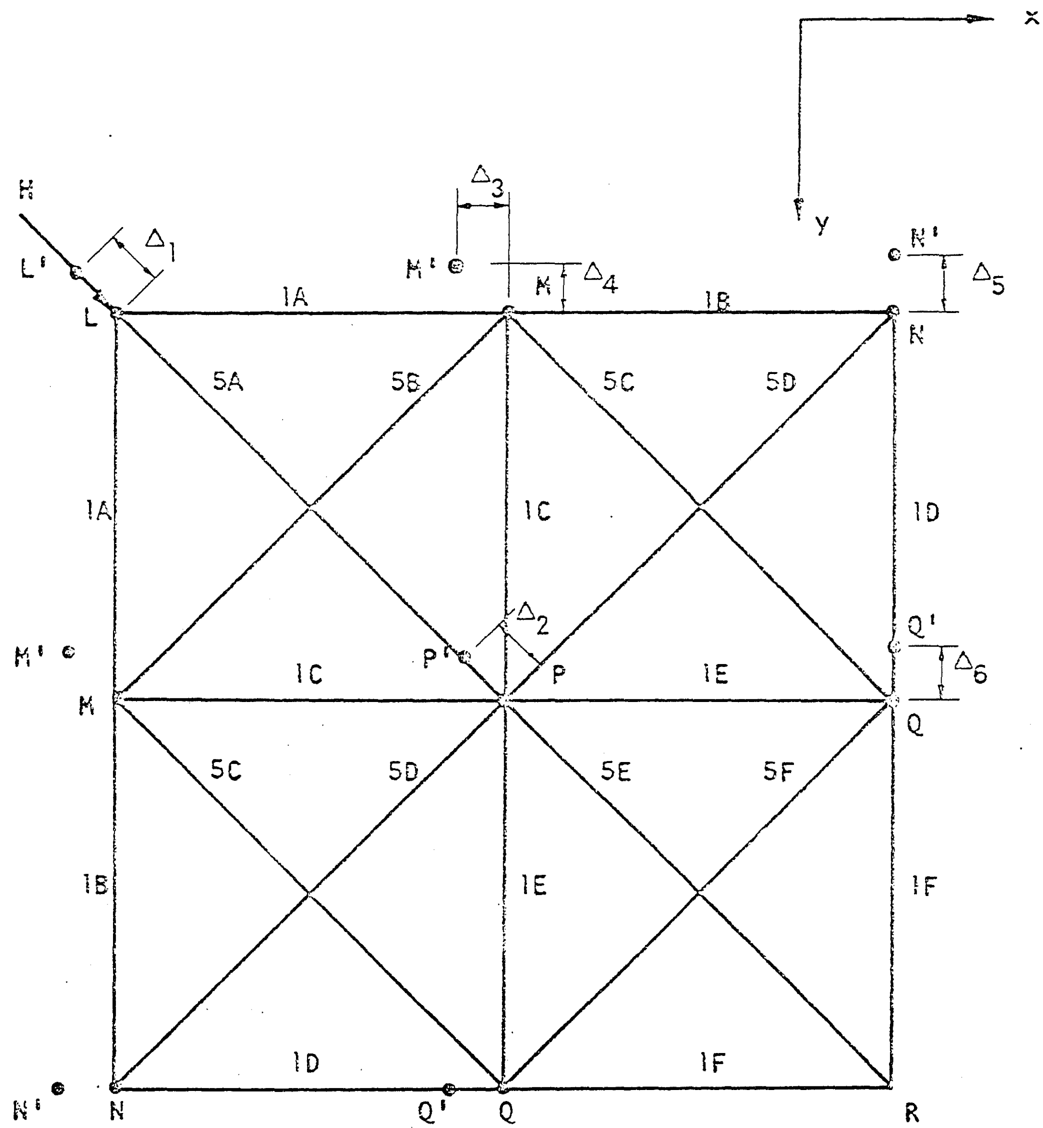

L, M, N, P, Q, : Original Positions
L',M',N',P',Q' : Assumed Deflected Positions

FIG. B.4 QUADRANT OF 4 BY 4 GRID MODEL SHOWING ASSUMED DEFLECTIONS